PhD-FSTC-2016-28
The Faculty of Sciences, Technology and Communication

# DISSERTATION

Presented on 05/07/2016 in Luxembourg

to obtain the degree of

## DOCTEUR DE L'UNIVERSITÉ DU LUXEMBOURG

## EN SCIENCES DE L'INGÉNIEUR

by

Robert PYTLIK
Born on 15 May 1986 in Raciborz (Poland)

# SOIL FATIGUE DUE TO CYCLICALLY LOADED FOUNDATIONS

This thesis was supervised by:

| | |
|---|---|
| Prof. Dr. Ir. Stefan van Baars, | University of Luxembourg |
| Prof. Dr. Ing. Stefan Maas, | University of Luxembourg |
| Prof. Dr. Ir. Alain Holeyman, | Université catholique de Louvain |

Members of the jury:

| | |
|---|---|
| Prof. Dr. Ing. Christoph Odenbreit | University of Luxembourg |
| Prof. Dr. Ing. Stefan Maas | University of Luxembourg |
| Prof. Dr. Ir. Stefan Van Baars | University of Luxembourg |
| Prof. Dr. Ir. Alain Holeyman | Université catholique de Louvain |
| A-Prof. Dr. Ir. Dominique Ngan-Tillard | Delft University of Technology |

# ACKNOWLEDGEMENTS

I would like to express my special appreciation and thanks to my supervisor Professor Stefan Van Baars for supporting me during these past four years. I would like to thank him for encouraging my research and for allowing me to grow as a research scientist. I am also very grateful to my dissertation committee members, Professor Alain Holeyman and Professor Stefan Maas, for their scientific advice and knowledge and insightful discussions and suggestions. I am also thankful to Darius Macijauskas for his help with experiments and interesting talks. I thank all the technical support staff members: Gilbert Klein, Claude Collé, Ed Weyer, Ralph Reiter and Vicente Reis Adonis for their support and assistance in the laboratory. At the end I would like to thank all my friends and colleagues in Luxembourg for their encouragement, support and good time during my stay here.

# ABSTRACT

Cyclic loading on civil structures can lead to a reduction of strength of the used materials. A literature study showed that, in contrast to steel structures and material engineering, there are no design codes or standards for fatigue of foundations and the surrounding ground masses in terms of shear strength reduction. Scientific efforts to study the fatigue behaviour of geomaterials are mainly focused on strain accumulation, while the reduction of shear strength of geomaterials has not been fully investigated. It has to be mentioned that a number of laboratory investigation have been done and some models have been already proposed for strain accumulation and pore pressure increase which can lead to liquefaction.

Laboratory triaxial tests have been performed in order to evaluate the fatigue of soils and rocks by comparing the shear strength parameters obtained in cyclic triaxial tests with the static one. Correlations of fatigue with both, the number of cycles and cyclic stress ratio have been given. In order to apply cyclic movements in a triaxial apparatus, a machine setup and configuration was made. A special program was written in LabVIEW to control the applied stresses and the speed of loading, which allowed simulating the natural loading frequencies. Matlab scripts were also written to reduce the time required for the data processing.

Both cohesive and cohesionless geomaterials were tested: artificial gypsum and mortar as cohesive geomaterials, and sedimentary limestone, and different sands, as cohesionless and low-cohesive natural materials. The artificial gypsum, mortar and natural limestone exhibit mostly brittle behaviour, where the crumbled limestone and other sand typical ductile one. All the sands as well as the crumbled limestone were slightly densified before testing therefore; they can be treated as dense sands. The UCS for the crumbled limestone is 0.17 MPa and standard error of estimate $\sigma_{est}$ = 0.021 MPa, where for mortar UCS = 9.11 MPa with $\sigma_{est}$ = 0.18 MPa and for gypsum UCS = 6.02 MPa with standard deviation = 0.53.

All triaxial tests were conducted on dry samples in the natural state, without presence of water (no pore pressure). The range of the confining pressure was between 0 MPa and 0.5 MPa. The cyclic tests carried out were typical multiple loading tests with constant displacement ratio up to a certain stress level. The frequency was kept low to allow for precise application of cyclic load and accurate readings. What is more, the frequency of the cyclic loading corresponds to the natural loading of waves and winds. The number of applied cycles was from few cycles up to few hundred thousand (max number of applied cycles was 370 000).

Due to the complex behaviour of materials and high scatter of the results, many tests were required. Two different strategies were used to investigate fatigue of geomaterials:

1) the remaining shear strength curve; after a given number of cycles, a final single load test was done until failure in order to measure the remaining shear strength of the sample.
2) the typical S-N curve (Wöhler curves); there is simply a constant loading until failure.

The remaining shear strength (or strength reduction) curve has been compared with the standard S-N curve, and is found to be very similar because the cyclic stress ratio has little influence. The cyclic loading on geomaterials, being an assemblage of different sizes and shapes of grains with voids etc., showed different types of effects. Cohesionless materials show a shear strength increase during the cyclic loading, while cohesive ones show a shear strength decrease. For the cohesive materials the assumption was made that the friction angle remains constant; so, the fatigue of geomaterials can be seen as a reduction of the cohesion. In this way, the fatigue of a cohesive geomaterial can be described by a remaining cohesion.

The imperfections in the artificial gypsum have a significant impact on the results of the (especially cyclic) strength tests. Therefore another man made materials was used – a mixture of sand and cement (mortar). As the first static test results were very promising, mortar was used in further tests. The cyclic tests, however, presented similar, high scatter of results as for artificial gypsum. An unexpected observation for both materials was a lack of dependency of the remaining shear strength on the cyclic stress ratio.

The strain-stress relationship in cyclic loading shows that the fatigue life of the geomaterials can be divided into three stages, just as for creep. The last phase with a fast increase in plastic strains could be an indicator of an incoming failure. The accumulation of strains and increase of internal energy could be good indicators too, but no strong correlation, has been found. Similar to the shear strength, the stiffness changes during cyclic loading; for cohesive materials the stiffness increase, while for cohesionless it decreases. This could help to predict the remaining shear strength of a geomaterial by using a non-destructive method.

Keywords: Geomaterials, Cyclic loading, Fatigue, Cyclically loaded foundations, Shear strength reduction, Cohesion reduction, Life prediction of geomaterials in cyclic loading.

# CONTENTS

# 1. GEOTECHNICAL STRUCTURES UNDER CYCLIC LOADING

## 1.1. Introduction

The life span of many structures such as wind turbines, high-speed trains or bridges etc., strongly depends on the foundation and its surrounding ground. The analysis of these structures requires careful planning and good evaluation of the aging process. The impact of the natural forces, both constant and variable, must be taken into account to describe the strength and stability of the whole construction over the entire life time. The variable forces, due to the quite regular, fairly rhythmic nature, are known as cyclic loading, and can significantly reduce the strength. This aspect of ground strength weakening caused by cyclic loading is an important factor in foundation design.

The role of foundations, which consists of both the ground and foundation, is to transfer the static, live and cyclic forces to deeper layers. Within time, these forces can not only damage the foundations, but probably also the surrounding soil or rock.

The main areas in geotechnical engineering, where foundations and surrounded rock and soil masses are subjected to cyclic loading, are (see Figure 1.1):

- offshore structures subjected to waves, and/or ice,
- foundations of structure subjected to wind load,
- foundations of structure in seismic regions,
- foundations of road, railway and tunnel, airport, subjected to traffic loading,
- water table changes (sluices, embankments, dams, storage pounds),
- industrial cyclic loading, under crane rails, and large machines foundations,
- foundations of storage facilities such as grain silos, oil tanks,
- emptying and refilling underground caverns and storage facilities (water or air under high pressure, as well as nuclear waste disposal),
- mining operations (excavation, cutting, blasting).

One of the most noticeable examples of structures, for which cyclic loads have a very high value compared to the static loads, are wind farm towers and offshore oil platforms (Figure 1.2). The wind farms can be placed on both land and an offshore site. In both cases the soil masses will be cyclically loaded with high cyclic forces caused by the wind. For an offshore windmill and oil platform there are additionally tidal water movements, sudden wind gusts,

and/or ice floating on the see surface. These forces can cause structural micro damages in both, the construction and the foundation. After accumulation of thousands of these microcracks the structure may fail; this is known as a fatigue. A proper design and evaluation method already exists for structural failure, like fatigue of a tower such as the international standard IEC 61400-1 (2005-2008), but this does not exist yet for geotechnical failure. To ensure safety and stability of wind farms and other structures subjected to cyclic loading, a proper design tool for cyclic behaviour and fatigue must be proposed.

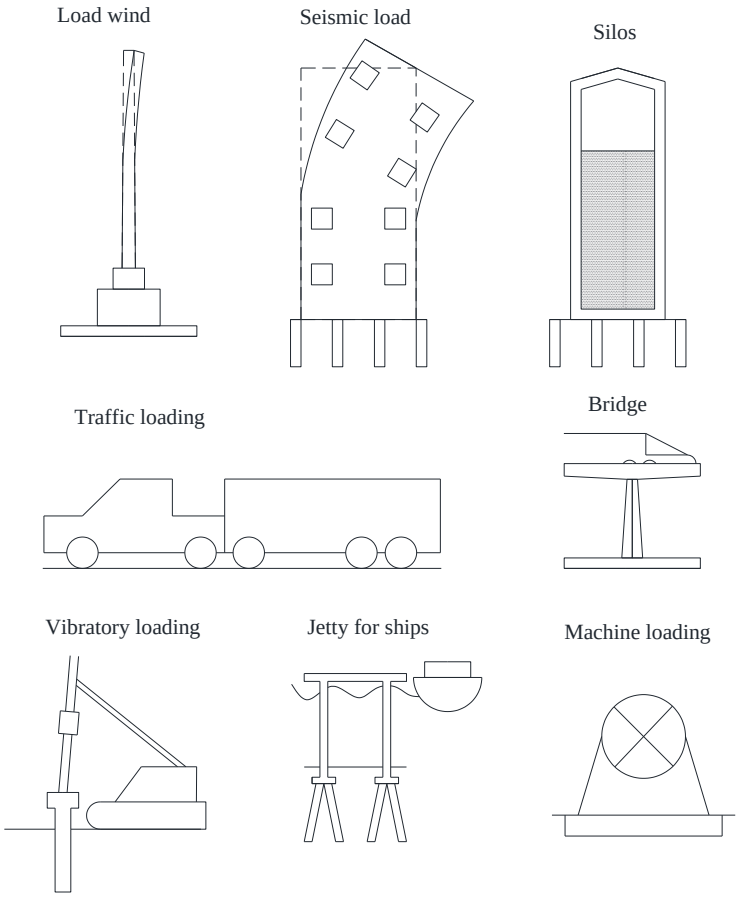


*Figure 1.1. Common situations in which soils experience significant cyclic loading*

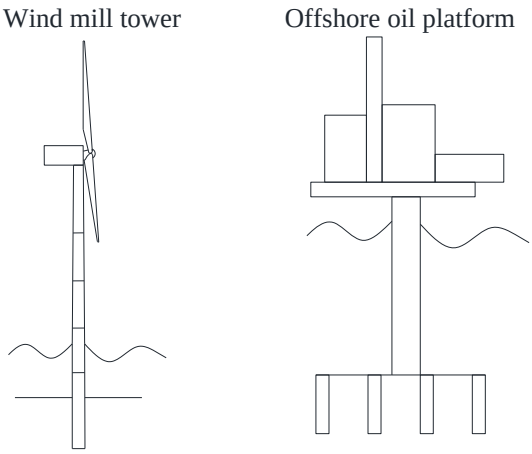


*Figure 1.2. Cyclically loaded foundations of wind mill and offshore oil platform*

## 1.2. Goals of this work

The aim of this research is to investigate the remaining shear strength after a number of cyclic loads, to improve fatigue life prediction for geomaterials subjected to cyclic loading and to propose a simple design tool which could be incorporated into geotechnical guidelines and standards. This also means that by decreasing the uncertainties in fatigue calculations for geomaterials, the safety factors, that deal with the uncertainties, can be decreased which reduces the total cost of a foundation or/and extend the life of already built foundation.

In order to describe the loss of strength due to cyclic loading and to determine the design values of the soil strength parameters, strength tests and a proper constitutive soil model must be obtained. Such a model should predict the loss of strength in number of cycles under cyclic loading including a probability analysis in case a correct evaluation of the remaining shear strength and fatigue life is required. This model should be able to describe the fatigue behaviour of all geomaterials including rocks and soils.

There is unfortunately no model which characterises the fatigue of geomaterials and not enough available laboratory data to study the behaviour of geomaterials for fatigue in terms of shear strength (models for sand and clay for e.g. earthquakes, however, have been already proposed). The reason for such a limited experimental data is simple: the creation of such of data base is very expensive in terms of both testing time and actual financial cost. Therefore, the proposed model should be simple to use and its parameters easy to obtain from laboratory tests.

Other main objectives of the thesis are:

- To gain a better understating of behaviour of geomaterials under cyclic loading,
- To describe the reduction of the shear strength parameters $c$ and $\phi$ due to cyclic loading,
- To produce a simple and easily parameterised shear strength model, which can be used in geotechnical design standards for cyclic loading,
- To predict the remaining shear strength based on only a few cyclic and static strength tests if possible,
- To predict the fatigue life of a material in cyclic loading,
- To investigate which factors affect shear strength reduction of geomaterials,
- To check if other parameters of geomaterials (e.g. stiffness, density etc.) are correlated to fatigue, because this could improve the prediction of the loss of strength.

## 1.3. Investigation method

Natural and manmade materials influenced by cyclic loading, lose in each cycle a part of their strength and can fail prematurely after a certain number of cycles. Probably the same mechanism can be found in geomaterials as well. The only available models that exist in geotechnical engineering for cyclic loads focus on other aspects: the stress-strain behaviour of a soil, the increase in pore water pressure and shaft friction reduction. So far, a limited

amount of scientific research was done by others in order to investigate the soil and rock shear strength reduction in cyclic loading. One of the methods for predicting shear fatigue of geomaterials is to use available classical theoretical models, which are based on metal fatigue.

The classical fatigue analysis (e.g. of metals) uses the Palmgren-Miner rule, S-N curves and constant fatigue life diagram (Goodman diagram). A similar approach will be applied here, however, some modification are introduced into the standard methodology, in order to give more proper description of fatigue for geomaterials.

A remaining shear strength curve will be proposed and compared with the standard S-N curve. Both curves are similar and can give detailed description of fatigue of materials. The question is if the fatigue life and strength be predicted with reasonable effort and cost. The investigation of remaining shear strength curve application could help answer these questions.

The laboratory tests are standard static triaxial tests. To be able to conduct cyclic triaxial tests, a special LabVIEW program was written. This program allows to control and to apply cyclic loading on geomaterials and to acquire all necessary data. After conducting the triaxial tests, the shear strength parameters based on the Mohr-Coulomb failure criterion obtained from the cyclic tests will be compared with the ones from the static tests. Correlations between them will be investigated and a mathematical description of the remaining shear strength will be given. The impact of other parameter (cyclic stress ratio, impact of confining pressure, etc.) will also be investigated.

### 1.4. Thesis organisation

This thesis is composed of 10 chapters. The second chapter is an introduction into to cyclic loading on foundations. In the third chapter a description of fatigue is presented. In chapter 4 a model describing the remaining shear strength of geomaterials is proposed. In chapters 5 to 7 laboratory tests and their results are presented. Chapter 8 give remarks to the tests results as well as a comparison between the S-N curve and the proposed remaining shear strength curve. Final conclusions and recommendations are given in chapter 9.

# 2. CYCLICALLY LOADED FOUNDATIONS & GEOMATERIALS

## 2.1. Cyclically loaded foundations

Foundations are a very important part of a building, assuring stability of the whole structure by supporting the weight and transmitting the static and cyclic loads to underlying soils and rocks. The static (also sometimes denoted as a monotonic) and cyclic loads from buildings or other structures are first transmitted into their foundations to be later dispersed in the surrounding rock and soil masses. Therefore the way how the loads are transferred from the foundations into the soil and rock masses is very important for the stability of the structure.

The decision which type of foundation can be used is based on a number of factors:

- depth (to prevent frost damage),
- bearing capacity (the foundation must be safe against a bearing capacity failure),
- settlement (the foundation must not settle to an extent that it damages the structure),
- type of material used for the foundation (wood, steel, concrete),
- level of ground water table,
- loads (seismic forces, environmental forces).

Usually foundations are divided in two main categories: 1) shallow foundations and 2) deep foundations (Figure 2.1). In the next two subchapters a bearing capacity for shallow and deep foundations will be shortly described.

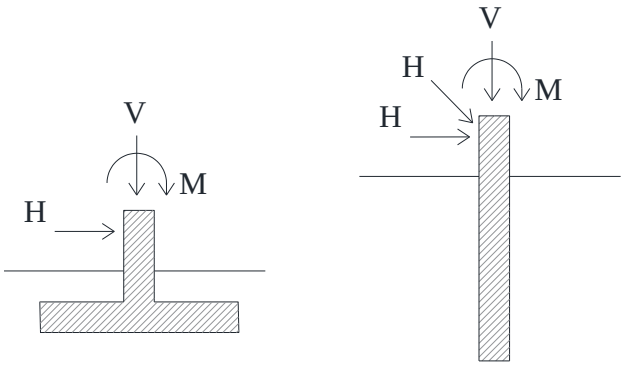


*Figure 2.1. Generalised cyclic forces and cyclic moments on shallow and deep foundation*

### 2.1.1. Shallow foundations subjected to cyclic loading

Shallow foundations (spread footing, strip footing, slab-on-grade footings, etc.) are foundation, which spread loads at shallow depths. When the loads are small and the ground conditions are good enough, shallow foundations are in most cases more appropriate and much cheaper than deep foundation; therefore shallow foundations rarely are carrying high cyclic loads.

*Bearing capacity of shallow foundations*

The parameter which is used for the design of foundations is the bearing capacity. The bearing capacity is the intensity of pressure transmitted by foundation at which the supporting ground is expected to fail.

The bearing capacity formulation for shallow foundation was introduced by Prandtl (1920) and Reissner (1924) for the simplest case, a strip of infinite length, on weightless soil:

$$p = cN_c + qN_q \qquad 2\text{-}1$$

where $p$ is the ultimate bearing capacity, $q$ is a side load, and $c$ is the cohesion. $N_c$ and $N_q$, are the dimensionless bearing capacity factors depending on the internal friction angle $\phi$.

Prandtl's formula has been extended by e.g. Keverling Buisman (1940), Terzaghi (1943), Caquot & Kérisel (1953) and Brinch Hansen (1970) with a term for the soil self-weight $N_\gamma$. The formula for the remaining bearing capacity coefficient is written in the form given by Terzaghi (1943):

$$p = cN_c + qN_q + \frac{1}{2}\gamma BN_\gamma \qquad 2\text{-}2$$

where $B$ is the total width of the loaded strip; $\gamma$ is the volumetric weight of the soil. The $N_\gamma$ also depends on the internal friction angle $\phi$. Formula in Eq. (2-2) is for a strip footing, and when it is used to calculate the bearing capacity of square or rectangular footings, shape factors $s_c$, $s_q$, $s_\gamma$ must be used as in Eq. (2-3):

$$p = s_c cN_c + s_q qN_q + s_\gamma \frac{1}{2}\gamma BN_\gamma \qquad 2\text{-}3$$

The Equation (2-3) can be extended with coefficients $i_c$ $i_q$, $i_\gamma$ which are the correction factors for a possible inclination of the load (so called inclination factors). The inclination factors were proposed first by Meyerhof (1953) and (1963) he gave the formula with both shape and inclination factors:

$$p = i_c s_c cN_c + i_q s_q qN_q + i_\gamma s_\gamma \frac{1}{2}\gamma BN_\gamma \qquad 2\text{-}4$$

The two most commonly cited proposals for the shape factors are those given by Meyerhof (1963) and De Beer (1970). These proposals, however, show large discrepancies. Zhu & Michalowski (2005) examined the shape factors and proposed new values for factor $s_\gamma$ based on finite element analysis. The new proposal depends on the internal friction angle $\phi$, and it

yields values lower than those suggested by Meyerhof but larger than those suggested by de Beer. Zhu & Michalowski concluded that proposals of Meyerhof and De Beer for factors $s_c$ and $s_q$ are conservative estimates, and they are acceptable in design.

In Eurocode 7 (2007) no detailed description of cyclic loading is given and it suggests only: "very cautious design values for the material properties should be used". Some description of foundation subjected to an earthquake is given in Eurocode 8 (2004). Eurocode 8 suggests giving attention to sensitive clays which may suffer shear strength reduction, and to cohesionless materials which are susceptible to dynamic pore pressure build-up under cyclic loading during an earthquake.

The subject of fatigue also receives attention in other areas like: Eurocode 1 (2003) for actions on structures, Eurocode 3 (2006) for steel structures and Eurocode 9 (2011) for aluminium structures. Eurocode 7 (2007) gives a list of actions and design situations which shall be taken into account. The list of design situations describes dynamic loads (e.g. traffic loads; movements and accelerations caused by earthquakes, explosions, vibrations and dynamic loads) but it does not include cyclic loads caused by e.g. wave and wind cyclic actions.

*Settlements of shallow foundations*

Cyclic stresses on shallow foundations usually are much lower than the stresses which could cause a ground failure due to loss of strength (ultimate limit state according Eurocode 7). The accumulated strains (Figure 2.2), however, can exceed the serviceability criteria ($q_a$), which should be prevented. Thus, the concern of the researchers is mainly focused on the accumulation of settlements, especially of cohesionless geomaterials.

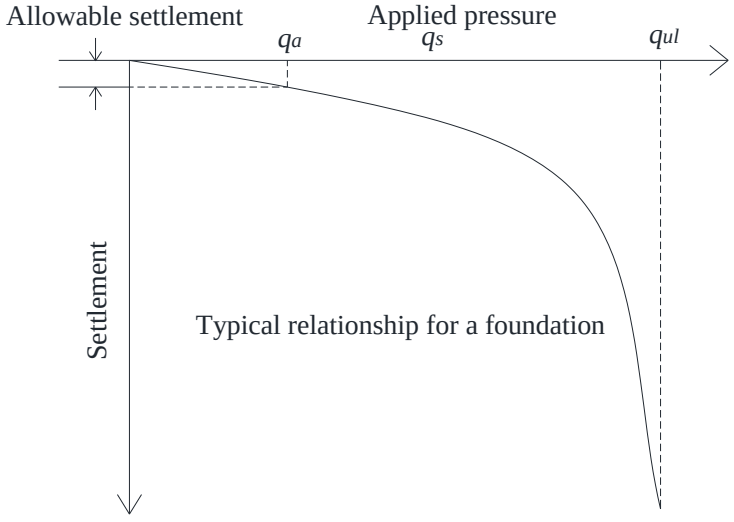


*Figure 2.2. Settlements related to applied pressure ($q_a$ is a applied pressure for maximum allowable settlement, $q_s$ applied pressure, and $q_{ul}$ is an ultimate applied pressure)*

For static loading the allowable settlement is typically solved using empirical or semi-empirical approaches (Poulos, Carter, & Small, 2001). A range of mathematical models,

based on plasticity theory to estimate the strains changes in static loading, already exists e.g. Byrne et al. (2002). These concepts have their roots in the work of Roscoe & Schofield (1957), further extended for clay (Martin C. , 1994) and for dense sand (Cassidy, 1999). The models describing the strain changes for dense sand have been given by e.g.: Butterfield & Gottardi (1994), Collins & Houlsby (1997), for overconsolidated clays by e.g. Martin & Houlsby (2001) and for loose carbonate sands by Byrne & Houslby (2001).

Some work has been done to investigate cyclic loading on shallow foundation e.g. Byrne (2000), Byrne et al. (2002), Byrne & Houlsby (2002) and Houlsby et al. (2005). Some analytical models were proposed for displacement accumulation of cyclically loaded shallow foundations. They are based mainly on: multiple yield surface theory (Houlsby, 1999), hypoplasticity theory (Salciarini & Tamagnini, 2009), contact interface model (Gajan & Kutter, 2009) or empirically derived properties (Bye, Erbrich, Rognlien, & Tjelta, 1995). These models, however, may not be transferable to other sites or conditions and usually require many parameters to be specified.

### 2.1.2. Deep foundations subjected to cyclic loading

The most common type of deep foundation is a pile foundation. Pile foundations are basically used to transfer the load of a structure down through the upper weak soil layer to a stronger layer below. Pile foundations are then used when the expected settlement is excessive to prevent ground surface damage of the structure, or to prevent a bearing capacity failure.

Historically, the first piles were made from wood, later steel. Reinforced concrete, and pre-tensioned concrete piles became widespread in last century as these new technologies and higher buildings were developed. The recent most challenging area of pile foundation research is piles subjected to high cyclic loads in the offshore oil and wind energy industry.

For a structure which is subjected to cyclic loading, especially for offshore structures, usually a deep foundation is required to be able to transmit high cyclic stresses and moments deep in to the ground. The two most common methods to describe the safety of pile foundations are the Limit State Design (LSD) and the Allowable Stress Design (ASD).

*Bearing capacity of pile foundations - base resistance $R_b$ and shaft resistance $R_s$*

The ultimate bearing capacity of a compression pile can be given as a sum of the base resistance $R_b$, and the shaft resistance $R_s$:

$$R_{c;k} = R_{b;k} + R_{s;k} \qquad 2\text{-}5$$

The base resistance $R_b$ is based on the general equation for the bearing capacity given by e.g. Brinch Hansen (1970), Prandtl (1920) and Meyerhof (1963), and it may be written as:

$$R_b = \left(cN_c + qN_q + \frac{1}{2}\gamma d N_\gamma\right) A_b \qquad 2\text{-}6$$

where $d$ is the diameter of the shaft at base level, $q$ is overburden pressure at the base level, $A_b$ base area of pile, $c$ – cohesion of soil, $\gamma$ – effective unit weight of soil, $N_c$, $N_q$, $N_\gamma$ are bearing capacity factors which take into account the shape factor. Because the piles foundations are deep and the diameter $d$ of a pile is relatively small, the term $½\gamma dN_\gamma$ becomes insignificant and it may be dropped. One of the proposed method of determining the bearing capacity factors $N_c$ and $N_q$ as a function of $\phi$ was given by Meyerhof (1976).

The formula for the ultimate skin resistance of a single pile in cohesionless soil is given as:

$$R_s = A_s q_0 K_s \tan\delta \qquad 2\text{-}7$$

where $A_s$ is surface area of the embedded length of the pile, $q_0$ is the average effective overburden pressure over the embedded depth of the pile, $K_s$ is the average lateral earth pressure coefficient and $\delta$ refers to the angle of the wall friction. Broms (1966) has related the values of $K_s$ and $\delta$ to the effective friction angle $\phi$ of cohesionless soils.

Other methods which can be used to derive the skin friction and base resistance based on CPT sounding were summarised by e.g. Niazi & Mayne (2013). These methods can be divided for direct methods (mainly for onshore foundations); and rational method (offshore foundations). The rational methods can also be divided for: alpha approach (total stress): API RP2A-WSD (2007); and beta approach (effective stress): NGI (2005), ICP (2005), UWA (2005), Fugro (2004).

*Limit State Design*

In Europe, the main guideline in geotechnical engineering is Eurocode 7 (2007), and it is based on the limit state design method (LSD). Eurocode 7 defines failure of a foundation as a state in which the foundation reaches any of its limit states, like bearing failure, sliding, overturning, tilting, pile pull-out, large settlements or displacements.

The ultimate resistance of a pile foundation is given in Eurocode 7 (2007) as:

$$R_{c;k} = min\left\{\frac{(R_{c;m})_{mean}}{\xi_1}; \frac{(R_{c;m})_{min}}{\xi_2}\right\} \qquad 2\text{-}8$$

where $\xi_1$ and $\xi_2$ are correlation factors related to the number of piles tested and are applied to the mean $(R_{c;m})_{\text{mean}}$ and the lowest $(R_{c;m})_{\text{min}}$ of $R_{c;m}$ respectively.

The characteristic compressive resistance of the ground, $R_{c;k}$, may be derived from the characteristic values of the base resistance, $R_{b;k}$, and of the shaft resistance, $R_{s;k}$, such that:

$$R_{c;k} = R_{b;k} + R_{s;k} \qquad 2\text{-}9$$

These components can be derived directly from static load test results, or estimated on the basis of the test results or dynamic load tests. The design resistance, $R_{c;d}$ shall be derived from:

$$R_{c;d} = R_{c;k}/\gamma_t \qquad 2\text{-}10$$

or

$$R_{c;d} = R_{b;k}/\gamma_b + R_{s;k}/\gamma_s \qquad 2\text{-}11$$

where the partial factors, $\gamma$, are given by Eurocode 7 (2007) or may be specified by a National Annex of the Eurocode.

*Allowable Stress Design*

According to the allowable stress design method (ASD, also denoted as a working stress design WSD or Permissible stress design PSD) the allowable load on piles is governed by the tolerable settlement at the working load. The working load for all pile types in all types of soil may be taken as equal to the sum of the base resistance $R_b$ and ultimate friction load or skin friction $R_s$ divided by a suitable total factor of safety which in most cases is equal $n$ = 2.5 (Murthy, 2002) (this value should ensure acceptable settlements), so the working load $R_a$ can be written as:

$$R_a = \frac{R_b + R_s}{2.5} \qquad 2\text{-}12$$

In the case where values of $R_b$ and $R_s$ can be obtained independently the formula is given as:

$$R_a = \frac{R_b}{3} + \frac{R_s}{1.5} \qquad 2\text{-}13$$

A smaller value of 2.7 or 2.8 is taken as a design working load (Murthy, 2002).

API RP2A-WSD (2007) suggests using the following factors of safety for the specific failure modes: Failure Mode: bearing failure 2.0, and sliding failure 1.5. These safety factor values should be used after cyclic loading effects have been taken into account.

*Cyclically loaded piles*

For cyclically loaded pile foundations, Eurocode 7 (2007) has the same scarce description as for shallow foundations. Other standards e.g. DIN 1054:2005-01 (2005) also do not propose for calculations of bearing capacity of cyclically loaded piles. Some updated information about cyclic loading was given by Appendix D.2. Later DIN 1054:2010 gave a formulation for pulsating and/or variable loads on cyclic axially loaded piles, including safety factors. In DIN 1054:2010-12 a reference is made to the recommendations of the special working group on piles EA-Pfähle (2012), where chapter 13 refers to cyclic loading. API RP2A-WSD (2007) mentioned a several analytical models (discrete and continuum) which describes the cyclic axial response of piles. The guideline DNV-OS-J101 (2013), states that the non-linear response of soil shall be accounted for, including the effects of cyclic loading. The recommendations given in the guideline BSH (2007) for wind mill foundations are based mainly on published studies and results by Schwarz (2002), Mittag & Richter (2005), and Kempfert (2009).

To predict the pile static load displacement behaviour a range of methods has been developed. To the most common methods belongs:

- elasticity method e.g. Poulos & Davis (1974), Randolph & Wroth (1978) for soft clays, non-linear elastic methods e.g. Coyle & Reese (1966) for clays,
- limit state method e.g. Eurocodes,
- finite element methods,
- subgrade reaction method - known as the *p-y* method e.g. Reese et al. (1974) and O'Neil & Murchinson (1983) for sands.

Many authors have proposed various types of design graphs for displacements caused by cyclic loading, they all took the cyclic shear stress into account e.g.; Andersen & Lauritzsen (1988) for overconsolidated Drammen clay, Yoshida et al. (1994) for medium to dense saturated sand, Jardine & Standing (2000) for dense and very dense sand, Randolph (2009) for medium dense sand and normally consolidated and light overconsolidated Drammen clay, Randolph & Gouvernec (2011), Mao (2000), Shajarati et al. (2012) for , Andersen (2009) for sand, clay and silt, Andersen et al. (2013). Some of them gave diagrams including combinations of pore pressure, average and cyclic load ratio e.g. Nielsen et al. (2012) for a very dense sand (relative density 80%) or liquefaction e.g. Ibsen (1999). A simple scheme for including cyclic load amplitudes was proposed by e.g. Tsuha et al. (2012) for sand with relative density 72%. Matlock et al., (1978), PMB Engineering, (1988) Grashuis et al., (1990) and Rajashree & Sundaravadivelu (1996) for soft clay, developed equations which model the stiffness and/or remaining strength of soil-pile load-transfer curves. Numerical analysis on effects of cyclic loading was run by e.g. Boulon et al. (1980), Vahdatirad et al. (2012). One of the last big projects for cyclically loaded pile design standardisation SOLCYP (2013) resulted in a list of publications summarising studies of forty years of practice in design of offshore structure subjected to cyclic loading.

*Cyclically loaded piles in clay*

Usually piles are founded in cohesionless soils, and piles only pass through cohesive soils. Because of that, there is a lack of available data results for piles founded in clay even for static loading. Randolph et al. (1979) investigated the behaviour of driven piles in overconsolidated clay. He found that under static conditions the bearing capacity increased. Kraft et al. (1981), conducted tests in which the combined effects of one-way cycling and rapid loading rate in clay resulted in a load capacity which exceed the static value by up to 20%. Karlsrud et al. (2014), confirmed by tests on piles in sand (loose and medium dense) and clay (normally and overconsolidated) that the axial bearing capacity of driven tubular steel piles increase in time and repeated load testing to failure of the same pile can give both a lower and a higher capacity than for first time testing. Liu & Huang (2013) proposed a modified undrained elastic-plastic model considering the cyclic degradation of clay soil.

*Skin friction degradation in sand*

Degradation of the bearing capacity at the pile shaft in sand due to cyclic loading was described e.g. by Jardine & Chow (1996), in dense sand - White & Lehane (2004), Kirsch & Richter (2010), dense sand - Jardine & Standing, (2012). Schwarz (2002), for medium dense sand and Gavin et al. (2015) for medium dense and dense sand, stated that for cyclic loading in sand above a certain combinations of cyclic loads no pile capacity reduction is to be expected. Randolph et al. (1994), proposed a reduction in lateral stress toward active earth pressure conditions in proportion to pile diameter and empirical degradation factor for pile in medium to dense sand.

*Horizontal loading*

The behaviour of piles under cyclic horizontal loading in sand was subject of research of Gudehus & Hettler (1981), Poulos et al. (2001), Rücker (2007), Peralta & Achmus (2010) for dry sand, LeBlanc et al. (2010) for drained loose and dense sand and Rimoy et al. (2013) for a dense sand, etc. Cyclic shakedown, described in book e.g. Yu (2006), of piles subjected to lateral loading was studied by e.g. Swane & Poulos (1985) in stiff clay, Levy et al. (2009) in normally consolidated clay. Methods for laterally loaded piles were also proposed by Long & Vanneste (1994) for different sand densities, Grabe & Dührk (2008) and Achmus (2008) in medium dense sand.

*Field and laboratory tests*

Experiments involving field-scale instrumented piles carried out by e.g. Van Weele (1979), Lehane (1992) in loose to medium dense sand, Chow (1997) in dense sand, Jardine (1998) in very dense sand, Jardine & Standing (2012) in dense Dunkerque marine sand, Puech et al. (2013) have successfully reduced the level of uncertainties associated with the prediction of the axial capacity of piles in dense sand. This led to the development of improved approaches such as those proposed by Lehane & Jardine (1994), Randolph et al. (1994) for medium and dense sands, Poulos (1987) for medium dense sand and soft and stiff clays. Additionally, centrifuge tests e.g. Garnier (2013) can also be conducted to investigate pile head displacements, bending moments and soil reaction in dry sand and overconsolidated clay due to lateral cyclic loads. Kempfert et al. (2010) conducted cyclic tests on a small-scale model pile tests in medium dense dry sand and found that the pile and soil behaviour depends mainly on the mode of the cyclic load. Puech (2013) for dense sand and stiff overconsolidated clay and Poulos (1982) for medium sand and remoulded clay investigated the significance of group effects. Bjerrum (1973) and Bea et al. (1980) confirmed that the rate has a significant effect on the pile capacity in clays and the more rapid the cycling loading rate, the greater the pile capacity is.

*Two way cyclic loading*

Holmquist & Matlock (1976), and Steenfelt et al. (1981), stated that two–way cyclic loading in normally consolidated clays results in a much higher reduction in pile capacity than the one way. Matlock & Foo (1979) developed a reduction model in which cyclic reduction of

stiff clay only occurs if plastic reversal of strain occurs. Poulos (1981) presented model tests, which revealed that one–way cyclic loading will also cause a reduction in skin friction. He concluded that result tests of Ireland (1957) on piles driven into fine sand suggested that the average skin friction for tensile loading is equal to that for compressional loading, but data summarised by Sowa (1970) for loose and medium sand and clay and Downs & Chieruzzi (1966) indicated considerable variations in average skin friction between different tests. A verification method of the side friction on the piles under cyclic loading was suggested by Begemann (1969).

## 2.2. Cyclically loaded geomaterials

The cyclic loads and moments transferred from the foundations to the surrounding geomaterials can cause several effects on the geomaterials. These effects of the cyclic loading on the geomaterials can be described by different physical phenomena, such as:

- Cyclic strain accumulation
- Liquefaction
- Stiffness reduction
- Crack propagation
- Particle breaking
- Compaction of granular materials
- Shear strength reduction

These phenomena are different for different types of geomaterials (Table 2-1). By measuring the changes of these phenomena it is possible to evaluate the material damage in number of cycles.

*Table 2-1. Cyclic loading effects on sand and rock*

| Damage measurement | Sand | Rock |
|---|---|---|
| Shear Strength reduction | Not fully investigated | Not fully investigated |
| Settlements | Large | Small |
| Water pore pressure | Liquefaction | None or negligible |
| Stiffness changes | Increase or decrease | Significant decrease |
| Cracks and microcracks | Already crushed, eventually crush of the grains | Cracks and microcraks development like for other brittle materials |

### 2.2.1. Cyclic strain accumulation

The accumulation of strains in cyclic loading can cause large and/or uneven settlements (Ibsen & Liingaard, 2005). Eurocode 7 (2007) defines deformations equals to 10% of the pile diameter as the failure criterion excessive settlements of pile foundations, and settlements equal to $s$ =50 mm as failure criterion for spread foundations.

The stress-strain behaviour (Figure 2.3) of geomaterials has been investigated by many researchers, to mention a few of them: Matlock et al. (1978), Poulos (1979), O'Reilly (1991), Ibsen (1999) for very dense sand, Niemunis et al. (2005), (2006) for dense sand and Andersen et al. (2013). Masing (1926) is one of the first, who described the one-dimensional non-linear

cyclic strain development. The existence of the fatigue strain limit has been proved for and brittle rocks, Haimson & Kim (1972) and Brown & Hudson (1974). The impact of soil composition (type of soil, grain size) initial state (void ratio), structure, loading conditions, and stress history can significantly affect the irreversible stress-strain relationship Poulos & Jansen (1989).

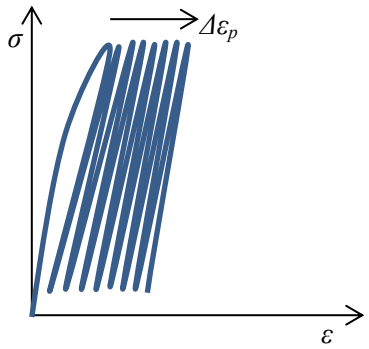


*Figure 2.3. Strain accumulation in cyclic loading*

*Stress-strain models*

Several mathematical models are used to predict the stress-strain response of soils. The two main approaches are based on:

- The elasticity theory: undrained models of soils were described by e.g. Muir Wood (1991) and the drained models by e.g. Kramer (1996),
- The plasticity theory – different plasticity theories have been proposed: bounding surface plasticity e.g. Dafalias & Herrmann (1982), Bardet (1986), kinematic hardening models e.g. Iwan (1967), isotropic hardening models e.g. Mróz (1967), bubble model e.g. Al-Tabbaa & Wood (1989), generalised plasticity models e.g. Zienkiewicz & Mróz (1984), etc. Models which are accounting for the pore water pressure increase was given by e.g. Finn et al. (1977) and Pyke (1979).

Some other stress-strain relationship models proposed in literature are:

- Simple formulas for estimating cumulative plastic strains e.g. Dingqing & Selig (1994),
- Viscoelastic models & viscoplastic models e.g. Pecker (2007), Zambelli et al. (2004) and O'Reilly & Brown (1991),
- Cyclic damage models,
- Fatigue contour diagram model given by e.g. Andersen (2009), Yoshida et al. (1994),
- Degradation index model given by Idriss et al. (1978) further developed by e.g. Allotey & El Naggar (2008), Yasuhara et al. (1997), Matasovic & Vucetic (1995),
- Cyclic fatigue model propsed by Ibsen (1999),
- Extended cam clay model for cyclic loading by e.g. Carter 1982, Pender 1982,
- CASM model (which based on the critical state theory) was extended for cyclic loading Yu et al. (2007).

The above mentioned models are able to describe the accumulation of displacements and to simulate stress-strain during with loading-unloading, but they also have a lot of limitations. The main limitations of these models are the small range of validity and need for many parameters. Some of the models are not correct for higher number of cycles (Wichtmann & Triantafyllidis, 2012), do not consider the effect of the confining stress or cannot be applied for all geomaterials such as model given by Niemunis et al. (2005). Most of the numerical models are very time-demanding and the available stress-strains models also do not take into account the reduction of the soil strength parameters $c$ and $\phi$.

### 2.2.2. Liquefaction

Soil liquefaction is a very important phenomenon in which the strength and stiffness of a soil is reduced by earthquake shaking or other rapid cyclic loading. Liquefaction mainly occurs in saturated undrained cohesionless soils (Duncan & Wright, 2005). Thus the methods applied in the liquefaction, would not be useful in e.g. drained case. In the case of cohesive sediments, the term cyclic softening is used (Idriss & Boulanger, 2008). The liquefaction mechanism is already considered in many standards especially in areas where earthquake induced cyclic loading may occur e.g. ASTM D6066 (2011), EN1998-5:2004 Eurocode 8 (2004) and Japan Road Association (2002).

Soil liquefaction has been observed many times during large earthquakes. Prior to an earthquake, the water pressure is relatively low. However, earthquake shaking can cause the water pressure to increase to the point where the soil particles can easily move with respect to each other. During earthquake, there is not enough time for the water in the pores of the soil to be dissipated. Instead, the water is "trapped" and prevents the soil particles from moving closer together. This is accompanied by an increase in pore water pressure which reduces the contact forces between the individual soil particles. The accumulation of pore pressure (Figure 2.4) is caused by continues rearrangements of the particles after each cycle of loading. The soil can become a grain suspension and loses its solid state - it starts to behave like a fluid. Loss of a solid state inevitable leads to soil strength and stiffness decrease and reduces the ability of a soil to support foundations for buildings, bridges, an off-shore wind power turbine, or costal piers (Figure 2.5 and Figure 2.6).

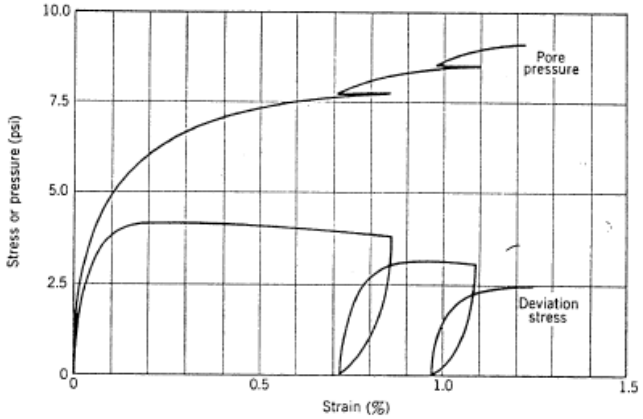


*Figure 2.4. Effect of repeated loading on undrained strength of very loose saturated sand*

*Figure 2.5. Liquefaction induced by earthquake (Kobe 1995)*

*Figure 2.6. Liquefaction induced by earthquake (Venezuela 1967)*

Many liquefaction models have already been proposed by Seed & Lee (1966), Lee & Albesia (1974), Martin et al. (1975), DeAlba et al. (1976), Seed et al. (1976), Finn (1988), Sawicki (1987) and others. A damage extension (Van Eekelen, 1977) of the cam clay model to consider pore pressure increase in cyclic loading was given by Van Eekelen & Potts (1978). Cyclic mobility (or cyclic ratcheting), which is a type of liquefaction triggered by cyclic loading, was described by e.g. Casagrande (1971), Castro (1975) and Castro & Poulos (1977). Laboratory tests by Kitamura & Hidaka (1988), Tavakoli et al. (2008), Erken & Ulker (2006); field investigations by Poulos (1982); and numerical analysis Jostad et al. (2015), have been conducted to investigate the cyclic behaviour of saturated soils.

### 2.2.3. Stiffness reduction in cyclic loading

The cyclic loading can lead to stiffness reduction of soils (Kramer, 1996); (Ishihara, 1996) and rocks (Bagde & Petroš, 2011). The stiffness of a soil is governed by the density, described by the shakedown theory (Yu, 2006). The stiffness reduction of rocks can be associated with a loss of strength caused by a loss of bonds in shear or axial stresses. In general, stiffness reduction in fatigue follows the pattern shown in Figure 2.7 consisting of three stages. At the beginning and near the end of fatigue life, the stiffness reduction is rapid Brown (1974), Galjaard et al. (1996), but for most of the fatigue life, the stiffness reduction is gradual and linear to the fatigue life.

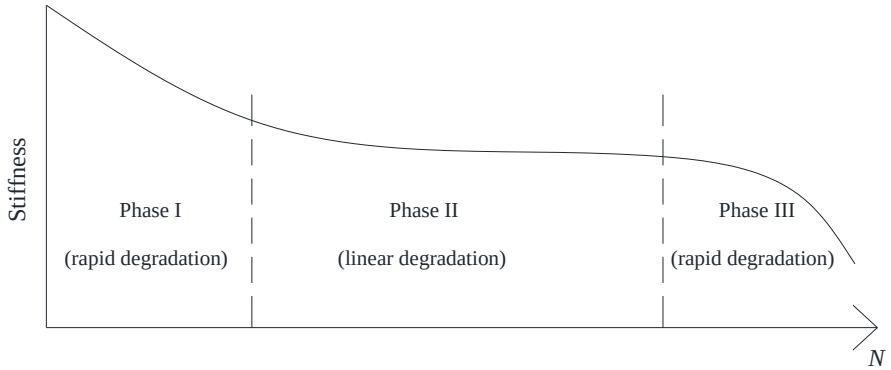


*Figure 2.7. Typical stiffness reduction*

The stiffness reduction can be presented in a similar way for the S-N curve and the fatigue failure is occurring when the stiffness has degraded to a critical level (Hahn & Kim, 1976), (O'Brien & Reifsnider, 1981).

### 2.2.4. Crack propagation

The micromechanical approach of fatigue, stems from fracture mechanics which concerns with the development and propagation of a crack caused by cyclic loading (Figure 2.8 and Figure 2.9). The crack initiates from small flaws or discontinuities which are present internally or on the surface of body. At these flaws stresses are very high due to stress concentration and under cyclic loadings these flaws can grow due to plastic deformations, even if the applied normal stresses are lower than the maximum strength. When the crack length becomes large enough, the undamaged part of a structure cannot sustain the applied load. This results in a very rapid crack growth followed by an abrupt failure of the material.

To describe the crack propagation, several different formulations reference for a variety of materials and processes have been proposed. To the main formulations belong: elastic–brittle, brittle, creep, fatigue and creep-fatigue, etc. These formulations have widened the application range of the continuum damage theory also to non-metallic materials. Still, the crack growth implementation for fatigue by micromechanical modelling is a very challenging task for engineers. Especially the fatigue life estimation based on the crack growth is very complicated.

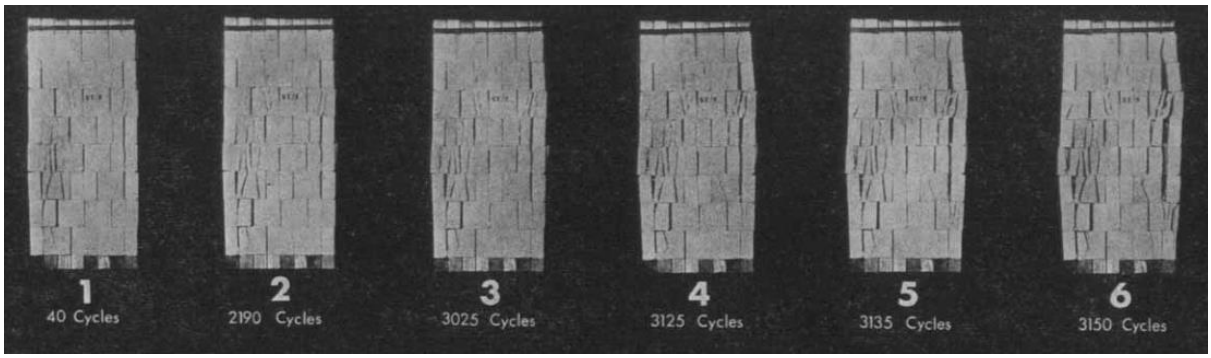


*Figure 2.8. Fatigue failure of jointed rocks (Brown & Hudson, 1974)*

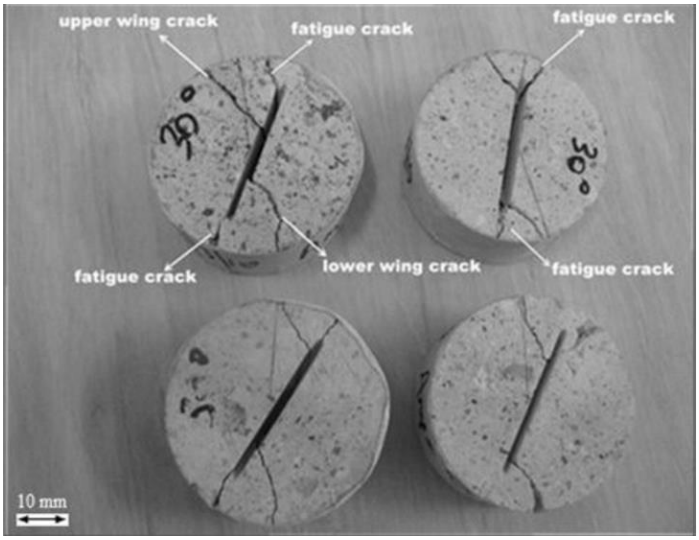


*Figure 2.9. β = 30° inclined notch and newly formed crack patterns on CCNBD specimens tested under diametral compressive cyclic loading (Erarslan & Williams, 2012b)*

In material science, Griffith (1921) and (1924) published first a relation between fracture strength and crack size. He formulated a fracture theory based on the principles of energy balance which stems from the first law of thermodynamics. He postulated that when the strain energy is sufficient enough to overcome the surface energy of the material the flaw becomes unstable and fracture propagation occurs. Other descriptions were given among others by Paris et al. (1961), Manson et al. (1961), Freudenthal & Heller (1959), Haibach (1970), Corten & Dolan (1956), Shanley (1953) and Cornelissen & Reinhardt (1984).

The most common way of describing the crack propagation in material science and fracture mechanics was given by Paris (1961). The Paris law relates the stress intensity factor to crack growth under a fatigue stress and is given as:

$$\frac{da}{dN} = C\Delta K^m \qquad 2\text{-}14$$

where, $a$ is the crack length and $N$ is the number of load cycles. The expression d$a$/d$N$ is known as the crack growth rate in mm per cycle. The $C$ and $m$ are empirically determined materials constants and $\Delta K$ is the range of the stress intensity factor, i.e. the difference between the stress intensity factor at maximum and minimum loading. The constant $C$ has dimension of mm/(cycle·MPa·mm$^{0.5}$) and the $m$ is dimensionless. The $\Delta K$ can be calculated from:

$$\Delta K = K_{max} - K_{min} \qquad 2\text{-}15$$

where $K_{max}$ is the maximum stress intensity factor (MPa·mm$^{0.5}$) and $K_{min}$ is the minimum stress intensity factor. The typical relationship between the crack growth rate and the range of the stress intensity is presented in Figure 2.10 and Figure 2.11. It can be mentioned that many other attempts have been made to establish models for crack growth e.g.: Foreman et al. (1967), McEvily (1988), Dowling & Begley (1976), Anderson (1991).

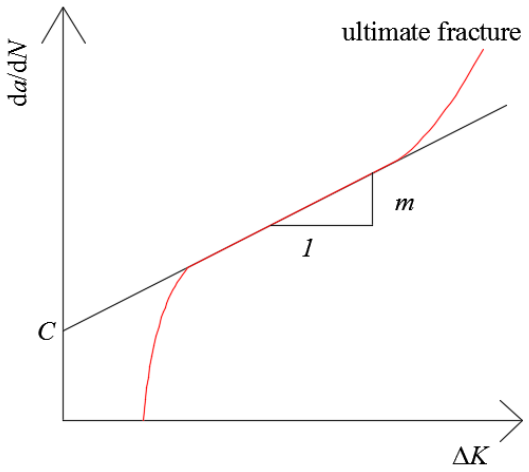


*Figure 2.10. Paris law*

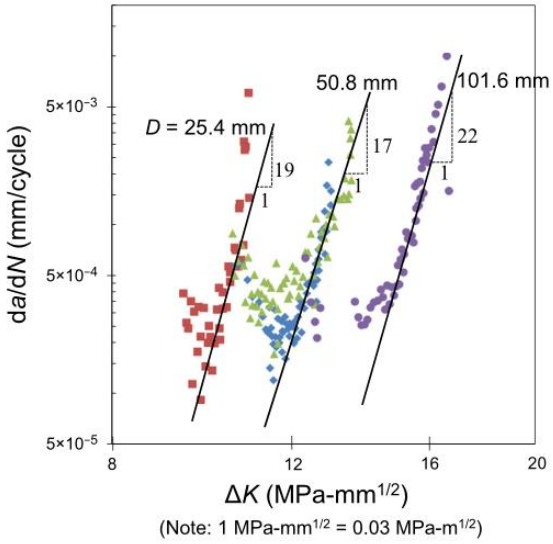


*Figure 2.11. Measured fatigue crack growth rates for different Berea sandstone specimen sizes (Le, Manning, & Labuz, 2014)*

*Crack propagation in geomaterials*

The cracks can occur only in cohesive materials, therefore the crack growth and micromechanical approach can only be applied on rock materials in geomechanics. For sands and other weak cohesive materials no cracks can be created as the materials are already completely fractured or contain a large number of cracks (e.g. very jointed rocks).

The fatigue failure mechanism of metals is different than that of rocks because the rock as a natural material contains cracks and imperfections. The metal fatigue can be described by a dominant single crack growth, where for rock material it is a generalised microcracks growth (Post, Case, & Lesko, 2008). The micromechanical approach to fatigue of rocks can even become further complicated by the anisotropic behaviour (Gatelier, Pellet, & Loret, 2002) which results in a stress redistribution and behaviour of cracks under hydrostatic pressure (Lockner, 1998).

For rocks, the results of studies of the initiation and propagation of a fracture from a single crack in a biaxial compressive stress was proposed e.g. by Hoek & Bieniawski (1965), Aglan and Bayomy (1998) etc. Many authors (Chen & Taylor, 1986), (Bagde & Petroš, 2005), (Peng, Ju, Xie, & Li, 2011), have proposed models based on energy-dependent crack propagation. Attewell & Farmer (1973) found similarities with creep response under constant static loading. Le et al. (2014), showed that the Paris-Erdogan law is applicable for a wide range of amplitudes of the stress intensity factor for Berea sandstone.

The crack propagation in rocks (induced by creep or cyclic loading) has been analysed using laboratory experiments (Gatelier, Pellet, & Loret, 2002), (Bagde & Petroš, 2009), (Xiao, Ding, Jiang, & Xu, 2009), (Erarslan & Williams, 2012a), (Salim & Mohamed, 2012); acoustic emission AE (Labuz & Biolzi, 2007); scanning electron microscope–SEM (Erarslan

& Williams, 2012b) and numerical simulations (Ingraffea & Heuze, 1980), (Kazerani, 2011), (Sukumar, Chopp, & Moran, 2003), (Manouchehrian & Marji, 2012). The cracks are generally characterised for the jointed models of rocks in uniaxial compression tests on rock-like samples (Brown & Hudson, 1974) with artificial flaws (Li, Chen, Zhang, & Swoboda, 2001).

The proper description of crack initiation and development it is not an easy task and no simple constitutive law could probably be given for all geomaterials. This is similar to concrete fatigue (see appendix C), where the application of micromechanics into geomaterials is impractical. It can be concluded that the mechanical approach based on crack development is unsuitable for geomaterials and the empirical and statistical approach seems more appropriate.

### 2.2.5. Particle breaking

High cyclic loading stresses and frequencies on granular materials lead to fracture and crushing of individual soil particles (Goder, Kalman, & Ullmann, 2002), (Datta, Gulhati, & Rao, 1982). This is caused because dilatancy is hindered by a confinement pressure, and grains cannot roll or slide and can only crush.

Cyclic loadings transmitted from piles or shallow foundations to adjacent soil masses can cause skin friction degradation due to the particles cracking (Al-Douri & Poulos, 1991). The particle breakage depends on confining pressure; void ratio as well as the size and shape of the particles and the susceptibility of the soil grains to attrition; the amplitude, number and direction of the load-cycles, i.e. one-way or two-way loading e.g. Yang et al. (2010). Basically, particle breaking can also occur for shallow foundations. The particle breakage, however, may not occur and time effects are negligible in granular materials at very low stresses (Lade & Karimpour, 2015).

### 2.2.6. Compaction of granular materials

The other notable phenomenon that occurs in cyclic loadings on sand is a large decrease in void ratio compared to other static or low frequency cyclic loading. This large volume decrease is sometimes broadly described as compaction of a material (Pyke, 1973), (Youd, 1972) and Airey et al. (1992). Compaction of granular material under repeated shear was also found by Ansell & Brown (1978) and Chan (1990). In general, material compaction may be a result of particle rearrangement, a particle crushing (Al-Douri & Poulos, 1991), or a combination of both mechanisms. This does not necessarily lead to a material failure because the compaction can cause for example an increase in maximum shear strength of a granular material (Suiker, 2002). The compaction of granular material can also be described on the base on the shakedown theory (Yu, 2006).

Silver & Seed (1971) found in their experimental studies that compaction in cyclic simple shear tests is a function of the relative density and previous strain history as well as of the

magnitude of the cyclic shear strain. The compaction per cycle decreases with an increasing number of load cycles. They also found, that for a given cyclic shear strain the amount of compaction was independent of the vertical stress. Similar results were presented by Pyke (1973) who showed the amount of compaction in cyclic triaxial tests increases with an increase in the confining pressure but that it is independent of the vertical stress in cyclic simple shear tests. Youd (1972) additionally showed that the compaction in simple shear tests is independent of frequency for both dry and drained saturated samples and also that cyclic shearing is most effective in causing densification.

### 2.3. Conclusions

For both types of foundations, shallow and deep, the shear strength parameters $\phi$ and $c$ are used to calculate the allowable bearing capacity. It was found out, that for both type of foundations, there is no complete formulation which describes the effect of cyclic loading on these shear strength parameters. There are already solutions proposed for cyclic loading on foundations for the offshore oil and gas industry like API RP2A-WSD (2007) or DNV-OS-J101 (2013); however, these are focusing mainly on the stress-strain relation of a pile foundation. This is because, as is usual for cyclically loaded foundations, the serviceability criteria are dictating the design criteria rather than the ultimate capacity. Therefore no typical civil engineering procedure exists that would describe in details the loss of shear strength on soils and rocks.

Changes in type of materials and its properties as well as boundary conditions can cause big differences in the cyclic behaviour and the corresponding strength parameters of geomaterials. There are already a few methods which try to describe the impact of cyclic loading on geomaterials. For geomaterials, important effects of cyclic loading are the irreversible strain accumulation and liquefaction. These two effects are already quite well described in literature. Another type of physical damage measurement is the shear strength. This will be further investigated.

# 3. FATIGUE OF MATERIALS

## 3.1. Introduction

To be able to describe fatigue of geomaterials near foundations, first cyclic loading must be defined. A proper fatigue life characterisation should contain the following elements: the counting method, formulations for describing S-N curves, constant fatigue life diagrams, damage rules and a statistical description of a probability of failure. This will be first discussed in this chapter. Additionally, at the end of this chapter, a short literature review of fatigue on geomaterials will be presented.

## 3.2. Parameters describing cyclic loading

Cyclic loading is defined as a repeated type of loading which has some regularity both in its magnitude and frequency. Machine man-made loading is often regular and can be described by e.g. a sinusoidal wave (Figure 3.1b). To make data obtained from naturally occurred cyclic loading useful for engineers (Figure 3.1a), the natural cyclic loading must be simplified from an irregular to a regular waveform with constant period and amplitude (Figure 3.1b and Table 3-1). The constant period and amplitude should be the same as the natural one. These two parameters are translated into $\sigma$ and $N$, where $\sigma$ is the cyclic stress amplitude and $N$ is the number of cycles.

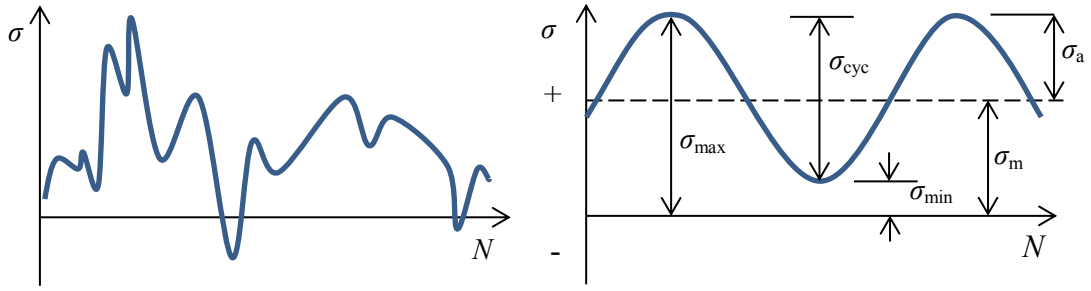


a) Irregular b) Repeated

*Figure 3.1. a) Irregular (or random) stress cycle and b) Repeated stress cycle*

*Table 3-1. Types of cyclic loading*

| | Nature of the loading: | Where occurs: | Description: |
|---|---|---|---|
| Irregular stress cycles | random | natural forces | Very complex |
| Repeated stress cycles | regular | laboratory tests, human induced cyclic loading | By set of values |

The stress cycle is usually sinusoidal (Figure 3.1b) of shape and can be described by the following set of values:

- Maximum cyclic stress $\sigma_{max}$
- Minimum cyclic stress $\sigma_{min}$
- Cyclic stress $\sigma_{cyc} = \sigma_{max} - \sigma_{min}$
- Mean stress $\sigma_m = (\sigma_{max} + \sigma_{min})/2$
- Cyclic stress amplitude $\sigma_a = (\sigma_{max} - \sigma_{min})/2$
- Frequency $f$
- Number of applied cycles $n$
- Number of cycles to failure $N$

The direction, the sign and the type of the cyclic loading play a crucial role in the assessment of fatigue. The type of cyclic loading can significantly change the fatigue life, especially of inhomogeneous materials (e.g. concrete and rocks). These parameters are also very important for the preparation of laboratory tests and for choosing or developing a correct model for the strength loss behaviour.

### 3.3. Counting method

Loads, which are occurring in a natural environment, e.g. wind, traffic, wave and earthquake loads, develop irregularly. Such a type of load is called a random load and is described by means of statistical functions, in particular the probability density function and the energy density spectrum. To correctly evaluate the number of random cycles and the magnitude of the loading, a simple counting method is required.

Many counting methods have been already proposed, e.g. ASTM E1049-85 (2005) includes: level-crossing counting, peak counting, simple-range counting, range-pair counting, and rainflow counting (Figure 3.2). Eurocode 3 (2006) mentions two counting methods: rainflow and reservoir.

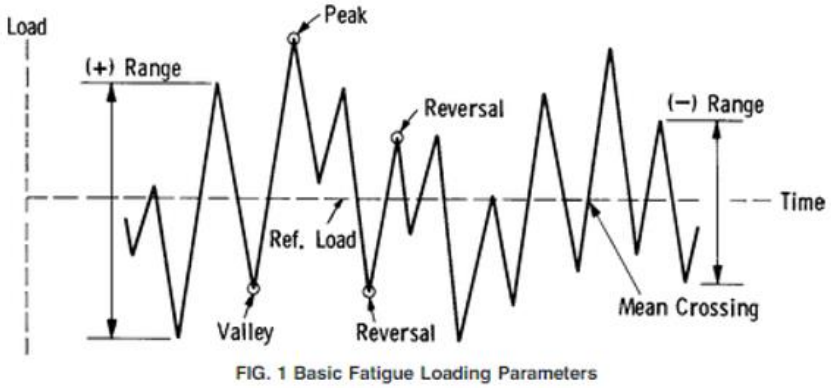


*Figure 3.2. Basic Fatigue Loading Parameters according to ASTM E1049-8 (2005)*

*The rainflow method*

The rainflow counting (Matsuishi & Endo, 1968) belongs to the most often used methods

used in fatigue analysis in order to reduce a spectrum of varying stress into a set of simple stress reversals. The method is very fast, well defined, operator independent, and counts all cycles in the time series according to ASTM E1049-85 (2005). What also makes this method often used is that it allows the application of Miner's rule (see chapter 3.5.4) in order to assess the fatigue life of a structure subjected to complex loading.

The rainflow name is used because this method resembles a flow of a rain drop falling from a pagoda and running down the edges of the roof. The main purpose of the rainflow analysis is to create a histogram of cyclic stress, in order to form a fatigue damage spectrum. The basic algorithm can be described as follows:

- Consider the segment of stress (Figure 3.3, left). Rotate the picture 90° as shown in Figure 3.3, right.
- Imagine each trough has a water source and water flows downward from off of the "roofs".
- The water path is interrupted when the path passes a trough which is more negative (e.g., point 5) than the original (e.g., point 1). This path defines stress range $S_1$ as shown. Note that the mean value of this stress cycle is also defined.
- A path (e.g., starting at point 3) ends when it hits another path as shown. This defines another stress range $S_2$.
- The same process is pursued throughout the length of the available record.
- The process can be repeated by considering the peaks as water sources. The stress cycles generated by the peak process should match the cycles of the trough generated process.

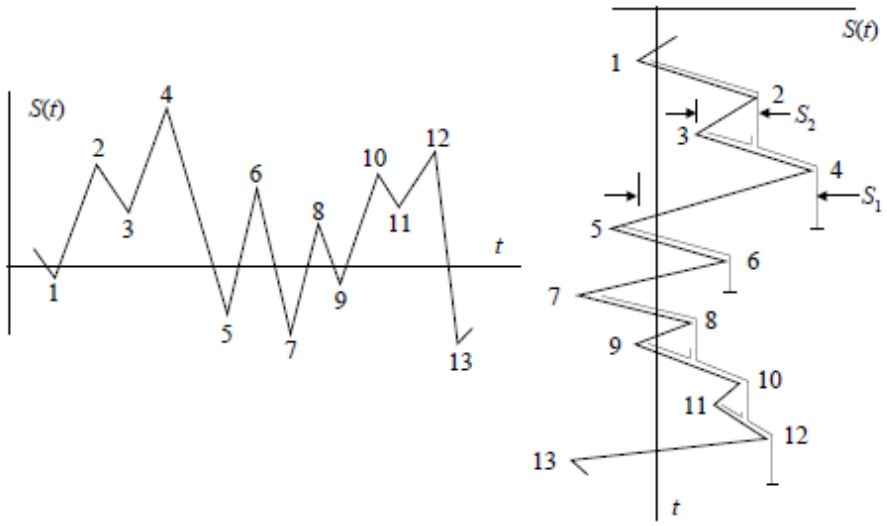


*Figure 3.3 Scheme of rainflow method (ASTM E 1049-85 (Reapproved 2005), 2005)*

In the case of irregular cycles (in terms of maximum stress) a number of equivalent cycles $N_{eq}$ can be introduced. It is used to transform the wave spectrum into equivalent groups of regular uniform waves, assuming that damage can be represented by an equivalent number of uniform waves.

The main limitation of the rainflow method is the loss of cycle order, which means that the high loading at the beginning and low at the end has the same effect as the opposite cyclic loading (low at the beginning and high at the end). Norén-Cosgriff et al. (2015), added that the rainflow method may not be well suited for the determination of the cyclic undrained behaviour of soils because soils are generally highly dependent on the ratio between the average and cyclic stress components.

### 3.4. Definition of fatigue for solid materials

Fatigue is usually defined as a premature failure of materials due to cyclic loading at a stress level lower than its strength under static load conditions. Attention of engineers on the fatigue problems was caused by a loss of 12 Liberty ships during Second World War due to hull and deck cracks. The most significant effect has fatigue in aerospace engineering. Due to the air-craft accidents – De Havilland Comet case from 1954, described by Whitney (2001), which were caused by structural fatigue (e.g. wings cracks), many researchers focused on the metal fatigue and yielded in various methods of its describing and predicting.

Existing fatigue descriptions (in steel fatigue) may be classified under the following groups:

- Fracture mechanics approach (models based on crack growth, see Chapter 2.2.4)
- Empirical relationship - S-N curves, remaining strength curves, etc.
- Low cycle fatigue approach
- Damage models: Palmgren-Miner, Marco & Starkey (1954), Lemaitre brittle damage model (1985), etc.,

In this thesis only the S-N curve and remaining strength curve are employed and will be briefly described in subsequent chapters.

### 3.5. Empirical relationship - S-N curve

Fatigue damage can be presented in various approaches and one of the most common is the empirical approach. The results used in the empirical approach, are based on an experimental characterisation of structures and materials through repetitive loading until a macroscopically observable failure mode occurs: usually fracture, resulting in the inability to carry the applied load.

In the empirical approach, the fatigue data is usually represented by an S-N curve (sometimes called Wöhler's curves or Wöhler's diagrams), where the stress $S$ is plotted against the number of cycles $N$ (Figure 3.4 and Figure 3.5). The $S$ is the magnitude of the cyclic stress $\sigma_{cyc}$ and $N$ is the number of cycles to failure at a specified cyclic stress ratio $S$.

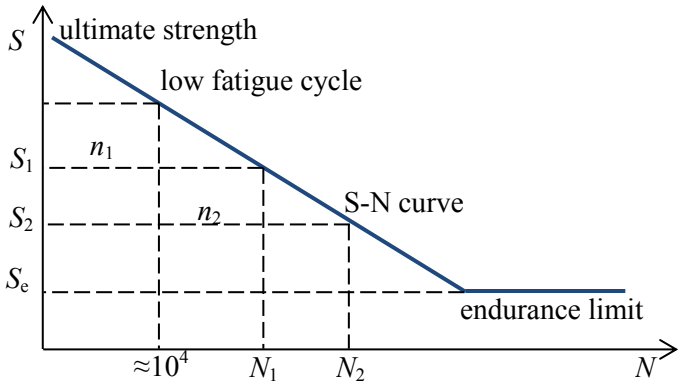


*Figure 3.4. Idealised S-N curve*

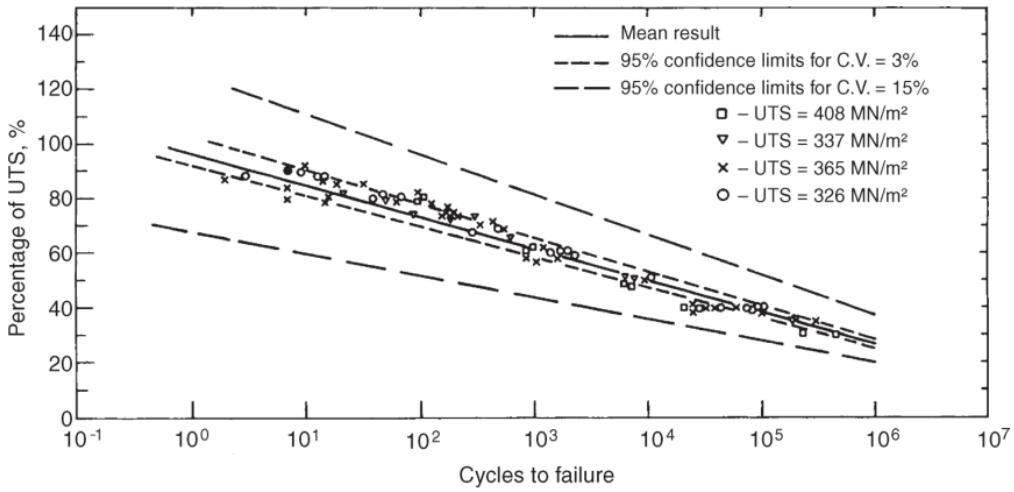


*Figure 3.5. Typical S-N curve for metals (Wikipedia, www.en.wikipedia.org)*

The main purpose of the S-N curve is to count the number of cycles for a given cyclic stress ratios until the sample reaches a failure state. The failure state is observed when the material is not able to reach the applied cyclic stress anymore. This simply states that the static strength $S_0$ is reduced to $\sigma_{cyc}$ for the last cycle $N$. The $N$ is the sought variable denoting the fatigue life of material at given cyclic stress $\sigma_{cyc}$. Thus, one "S-N" curve can be created for various cyclic loads $\sigma_{cyc}$ ($S$ in S-N) and for the corresponding number of cycles to failure $N$. It is usually assumed that the points for $N$ are log-normally distributed (ASTM E739-91, 1998), (EN 1993-1-9:2006 Eurocode 3, 2006).

*Types of S-N diagrams*

Fatigue in the S-N approach can be distinguished in two main ways of how it is described:

- Strain approach - increase in strain due to cyclic loading (ε-N)
- Stress approach - decrease in strength due to cyclic loading (S-N)

A description of both of these approaches can be found in ASTM E739-91 (1998). In the strain approach, the damage parameter is the strain accumulation for given load amplitude

where for the stress approach, the damage parameter is the strength reduction in number of cycles.

In the offshore industry, fatigue assessment in design is based primarily on S-N curves in order to define the strength. Usually the following three standards are the most commonly cited by designers and analysts in the offshore industry: API RP2A-WSD (2007), AWS D1.1:2000 (2000), and UK DEn (1990).

### 3.5.1. Analytical description of S-N curves

*Types of S-N curves*

Since different materials show differences in strength reduction behaviour, it is difficult to establish a unified expression of S-N curve for all materials, therefore different empirical models (parabolic, hyperbolic, linearised, etc.) have been proposed in the literature to fit experimental data. A brief summary was given by e.g. Castillo & Fernandez-Canteli (2009):

| | | |
|---|---|---|
| $log\, N = a - b(S)$ | *(Wöhler, 1870)* | *3-1* |
| $log\, N = a - b(log\, S)$ | *(Basquin, 1910)* | *3-2* |
| $log\, N = a - b(log(S - S_0))$ | *(Strohmeyer, 1914)* | *3-3* |
| $log(N + d) = a - b(log(S - S_0))$ | *(Palmgren, 1924)* | *3-4* |
| $log(N + d) = a - b\, log\big((S - S_0)/(S_{st} - S_0)\big)$ | *(Weibull, 1949)* | *3-5* |
| $log\, N = a - b\, log\big((S - S_0)/(S_{st} - S_0)\big)$ | *(Stüssi, 1955)* | *3-6* |
| $(log\, N - b)(S - S_0) = a\, exp[-c(S - S_0)]$ | *(Bastenaire, 1972)* | *3-7* |

where $a$, $b$, $c$, $d$ are best fit coefficients.

To the most often used models belong this first and the most simple one – the linear S-log$N$ curve (Wöhler, 1870). The biggest advantage of linear formulation is that the log $N = a - b$ ($S$) can be very easily fitted by a statistical linear regression and it gives accurate enough predictions. The Equation 3-1 is also incorporated into main engineering standards ASTM E739-91 (1998) and Eurocode 3 (2006).

*Static strength of materials*

To find the static strength $S_0$, the following two most common failure criterions are used in metal engineering: 1) maximum shear stress – Tresca theory, 2) maximum shear strain energy - Von Mises theory. They are expressed as:

- Maximum shear stress - Tresca:

$$\frac{1}{2} max(|\sigma_1 - \sigma_2|, |\sigma_2 - \sigma_3|, |\sigma_3 - \sigma_1|) = S_{sy} = \frac{1}{2} S_y \qquad 3\text{-}8$$

- Maximum shear-strain energy - Von Mises:

$$(\sigma_1 - \sigma_2)^2 + (\sigma_2 - \sigma_3)^2 + (\sigma_3 - \sigma_1)^2 = 2S_y^2 \qquad 3\text{-}9$$

where $S_y$ is the yield strength in uniaxial tension, $S_{sy}$ is the yield in shear, and $\sigma_1$, $\sigma_2$, $\sigma_3$ are principal stresses.

Both theories (Tresca and Von Mises) are one-parameter theories and therefore these can be very easily applied to the fatigue description of materials in which strength can be described by one parameter (e.g. tensile strength for steel, or unconfined compression strength for concrete).

*Endurance limit and fatigue life of material*

The fatigue S-N curve is commonly associated with a high number of cycles to failure. The endurance limit (Figure 3.4) is also sometimes denoted as a fatigue limit $S_e$ (or $\sigma_e$), which is a stress below which failure would never occur and is in the range of $N = 10^7$ or $10^8$ cycles for metals. Below this limit, the material can endure an infinite number of cycles until failure. Many materials do not have a fatigue limit, thus even a low stress causes damages. The two curves from Figure 3.6 present two different kinds of fatigue in materials. The curve entitled *Aluminium 2014-T6* denotes a material that does not have a fatigue limit, while the 1045 steel presents a typical material with a fatigue limit.

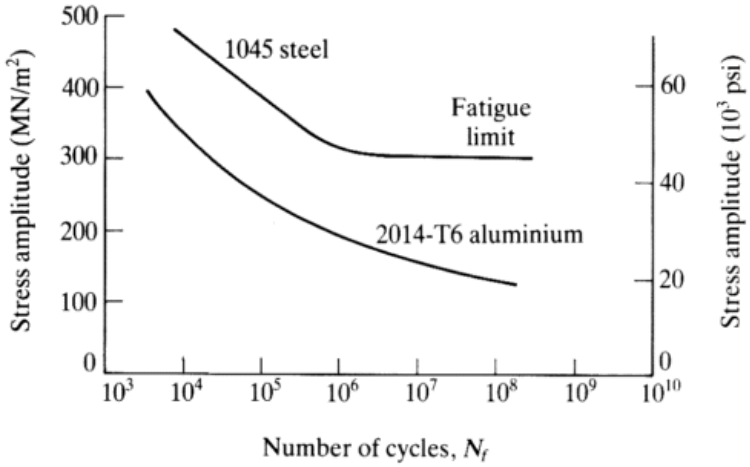


*Figure 3.6. Load cycles before failure (www.efunda.com, High-Cycle loading)*

### 3.5.2. S-N curve fitting and probability of failure

*Regression lines for S-N*

A simple statistical approach to an S-N (also ε–N) analysis is described in ASTM E739–91 (1998). It recommends using the log-normal distribution to fit the data points. Eurocode 3 (2006), which refers to Annex D of EN (1990) for a statistical analysis, also suggests using a log-normal distribution. It is convenient to analyse log ($N$) using models based on the normal distribution because it introduces linearisation which can be easily parameterised and calculated by a linear regression analysis. Therefore, the investigation of fatigue of geomaterials will be also based on the log-normal distribution.

*Normalised S-Curves*

The cyclic results can be presented as a normalised S-N curve defining permissible stress for fatigue-loaded welded joints. The normalised S-N curve is presented as band of a width

$T$=1:($m$+1.28·$s$)/($m$-1.28·$s$). The band describes a probability of survival between $P_u$=90% and $P_u$=10% (see Figure 3.7). The proposed value of the $T_s$ is from 1:1.5 to 1:1.26.

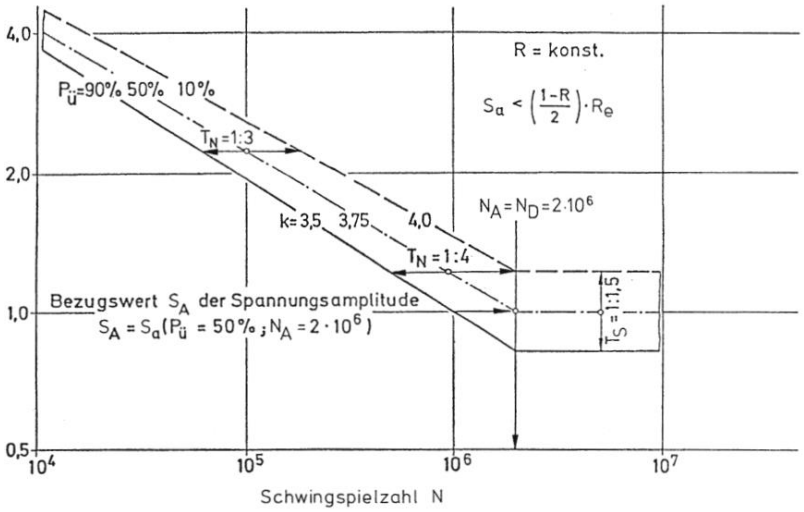


*Figure 3.7. Normalised S-N curves for welded components (Haibach, 1989)*

*Probability of failure for S-N*

According to the ASTM E739–91 (1998) and Eurocode 3 (2006), it is assumed that the scatter in log life is the same for low and high stress levels (Figure 3.8). In most cases the S-N curve is given as the 50% percentile of the survivability line (median curve). Additionally, ASTM E739–91 (1998) and Eurocode 3 (2006) propose 95% confidence band (Figure 3.8); however other probabilities of failures can also be applied. For guideline purposes, the S-N curve data can be described in terms of percentiles other than the 50% of the survivability line. In that case, the percentile is included in the S-N curve description. This way of incorporating probabilistic calculation is sometimes denoted as an S-N-P curve (Figure 3.9). These models usually are based on a Weibull or Gumbel distribution.

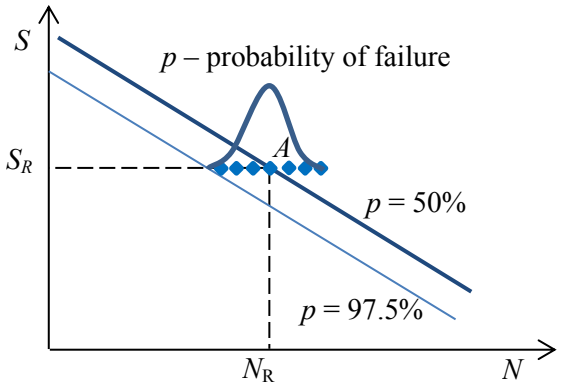


*Figure 3.8. Possibility of survival for a fatigue life at a specified stress level for number of cycles $N_R$*

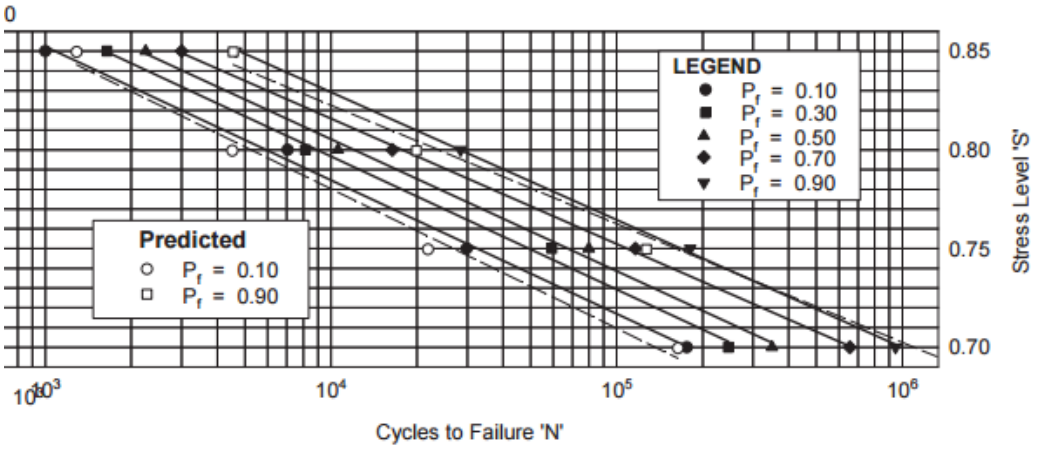


*Figure 3.9. S-N-Pf curves for Hybrid Steel-Polypropylene Fibrous Concrete Beams in Flexure (75% steel fibres + 25% polypropylene fibres) (Singh, 2011).*

In many test results e.g. for concrete (Oh, 1986), the Weibull distribution gives a better correlation than the log-normal one. Whitney's (1981) pooling scheme and the wear out model used by Sendeckyj (1981) for fibre polymers, derive S-N curves by taking into account the probabilistic nature of the fatigue properties of materials. Both the pooling scheme and the wear out models assume that the experimental data follow a Weibull (1949) distribution (in contrast to ASTM and Eurocode standards), which make these models more complicated. Joosse et al. (1994), concluded that the linear regression is more preferable because it is simple and the results are similar for higher number of cycles than the more complicated models.

### 3.5.3. Goodman diagram (constant fatigue life diagram) – effect of a mean stress

Very often a Goodman (1899) equation is presented together with the S-N curves. The Goodman equation (3-10) is a relation used to quantify the interaction of mean stress $\sigma_m$ and cyclic stress amplitude $\sigma_a$ (also denoted as an alternating stresses) on the fatigue life of a material. The Goodman relation can be given as:

$$\frac{\sigma_a}{\sigma_{eff}} + \frac{\sigma_m}{\sigma_u} = 1 \qquad 3\text{-}10$$

Some other empirical curves are given by Soderberg (1930):

$$\frac{\sigma_a}{\sigma_{eff}} + \frac{\sigma_m}{\sigma_y} = 1 \qquad 3\text{-}11$$

by Gerber (1874):

$$\frac{\sigma_a}{\sigma_{eff}} + \left(\frac{\sigma_m}{\sigma_y}\right)^2 = 1 \qquad 3\text{-}12$$

and by Morrow (1968):

$$\frac{\sigma_a}{\sigma_{eff}} + \frac{\sigma_m}{\sigma_f} = 1 \qquad 3\text{-}13$$

where $\sigma_a$ is the cyclic stress amplitude, $\sigma_m$ is the mean stress, $\sigma_{eff}$ effective alternating stress at

failure for a fatigue life of $N$ cycles, $\sigma_y$ is a yield stress, $\sigma_u$ is the ultimate stress and $\sigma_f$ is the true fracture stress.

The Goodman diagram (Figure 3.10 and Figure 3.11) is a graph of mean stress versus cyclic stress amplitude, showing how the fatigue life is changing with changes of mean stress for a given level of alternating stress. In other words, the relation can be plotted to determine the safe cyclic loading of a material. The solid lines represent point with the same estimated fatigue life (number of cycles) and the area below the curve indicates that the material should not fail for a given stress. The area above the curve represents likely failure of the material.

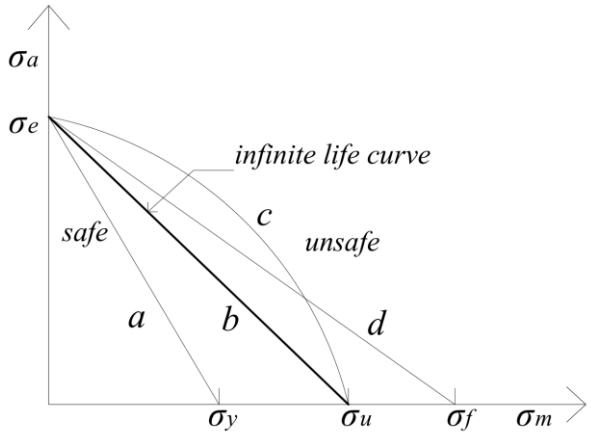


*Figure 3.10. Goodman diagram*

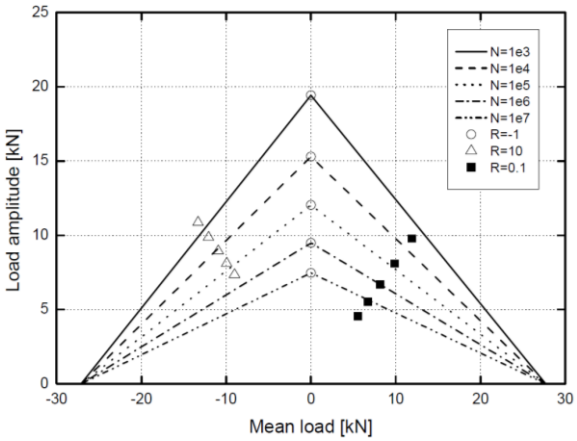


*Figure 3.11. Goodman (constant fatigue life) diagram (Sarfaraz Khabbaz, 2012)*

*Stress ratio R*

The diagram also incorporates the influence of a range of cyclic loading - a ratio of minimum stress $\sigma_{\min}$ to maximum stress $\sigma_{\max}$ in a cycle (Figure 3.1a):

$$\sigma_{max} = \sigma_m + \sigma \qquad 3\text{-}14$$

$$\sigma_{min} = \sigma_m - \sigma \qquad 3\text{-}15$$

This ratio is called (cyclic) stress ratio and is commonly denoted by $R$.

$$R = \frac{\sigma_{min}}{\sigma_{max}} \qquad 3\text{-}16$$

For example, the stress ratio $R$ = -1 represents a test at zero mean stress and $R$ = 0 test in one direction. The most common value of $R$ is 0.1 for a cyclic tests and corresponds to a tension-tension (compression-compression) cycle in which $\sigma_{\min} = 0.1\ \sigma_{\max}$.

### 3.5.4. Cumulative damage approach: Palmgren-Miner rule

The natural load spectrum varies in time and it is important to link fatigue behaviour to damage in the material due to these random loads. The cumulative damage theory states that permanent damages, denoted as a $D_i$, (Equation 3-17) caused by single cyclic loads $i$ or series

of loads, accumulate.

$$\sum_{i=1}^{k} D_i = D_1 + D_2 + D_3 + \cdots + D_i = D \qquad 3\text{-}17$$

It also assumes that the total damage $D$ caused by a number of stress cycles is equal to the summation of damages caused by the individual stress cycle. There a few theories which are based on these suppositions and they are called damage hypothesis.

*The Palmgren-Miner rule*

The Palmgren-Miner rule (Palmgren, 1924), (Miner, 1945) is based on *S-N* curves and this is used in most standards related to fatigue design.

The Palmgren-Miner rule, states that where there are $k$ different stress magnitudes in a spectrum, $S_i$ ($1 \le i \le k$), each contributing $n_i(S_i)$ cycles, then if $N_i(S_i)$ is the number of cycles to failure of a constant stress reversal $S_i$ (see Figure 3.12), so failure occurs when:

$$\sum_{i=1}^{k} \frac{n_1}{N_1} = \frac{n_1}{N_1} + \frac{n_2}{N_2} + \frac{n_3}{N_3} + \cdots + \frac{n_i}{N_i} = D = 1 \qquad 3\text{-}18$$

where $n_i$ is the number of load cycles with a certain amplitude and range; $N_i$ is the corresponding total number of cycles to fatigue failure.

Eurocode 9 (2011) uses for the safe fatigue life design the assumption of a linear damage accumulation (Palmgren-Miner rule); the safe design damage value $D_{L,d}$ for all cycles should fulfil the condition:

$$D_{L,d} \le 1 \qquad 3\text{-}19$$

The Palmgren-Miner rule can be interpreted graphically as a shift of the S-N curve (Figure 3.13). For example, if $n_1$ cycles are applied at stress $S_1$ (where the fatigue life is $N_1$ cycles), the S-N curve is shifted so that goes through a new fatigue life value, $N_{1*}$.

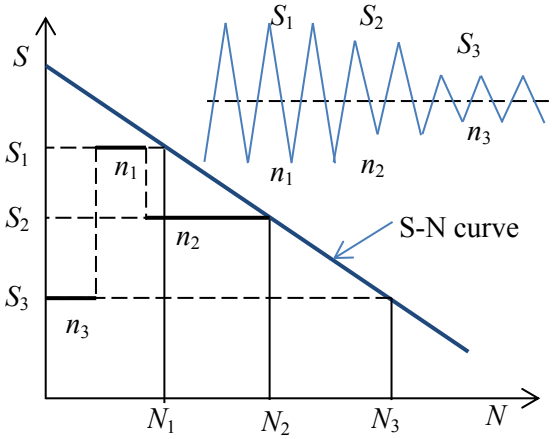


*Figure 3.12. Idealistic Palmgren-Miner rule*

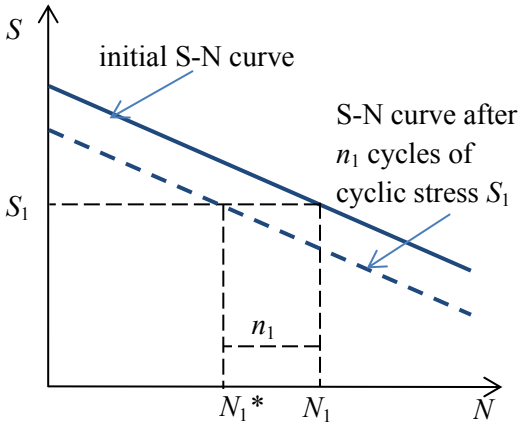


*Figure 3.13. Shift of the S-N curve in Palmgren-Miner rule*

*Advantages and disadvantages of Palmgren–Miner's rule (cumulative damage rule)*

The advantages of Palmgren-Miner rule are:

- It is simple,
- It is widely used as first estimation,
- It is in most cases accurate enough.

The disadvantages of Palmgren-Miner rule:

- It does not well describe the random nature of natural cyclic loading,
- It considers the damage development to be linear,
- The value of the damage parameter only indicates whether or not failure occurred, it does not relate to a physically quantifiable damage,
- It does not well predict the applied load sequences (cycles of low stress followed by high stress cause more damage than in reality but high stress followed by low stress may have less damage),
- It assumes that the small loads have negligible damaging influence,
- The damage accumulation is assumed to be independent of the cyclic stresses.

There is always a risk that this simplistic approach is in a certain situations inaccurate, but it can be useful for basic fatigue life estimation. Nevertheless special care must be taken for implementing this rule in fatigue life estimation procedures and standards. The FKM guideline (2003) proposes value of critical damage sums $D$ for some types of metals e.g. steel, alloy steels, aluminium alloys as 0.3 for non-welded components and 0.5 for welded ones.

*Other cumulative damage models*

Modification of Miner's rule has been a common way of improving the fatigue life prediction retaining the amount of input information. One of the simplest modifications of Miner's rule is multiplying it by a factor $K$, other than 1:

$$D = \sum_{i=1}^{k} \frac{n_i}{N_i} = K \qquad 3\text{-}20$$

High-low fatigue tests are tests where the testing occurs sequentially at two stress levels $S_1 > S_2$. These tests generally show that failure occurs for $K < 1$. This means that the Palmgren-Miner rule is non-conservative for these tests. For low-high tests, $K$ values are typically >1.

Echtermeyer et al. (1996) considers spectrum loading, a $K$ of 0.1 safe for most cases. The value of $K$ is usually determined empirically. Essentially, modifying Miner's rule in this way is identical to shifting the S-N curves towards lower fatigue life (Figure 3.13).

A nonlinear Miner's rule was given by e.g. Goodin et al. (2004) and others. The model parameters in these formulations typically take the quality of fitting parameters, rather than that they are parameters quantifying the physical background of the material degradation. The

basic formulation is given as:

$$D = \sum_{i=1}^{k} \left(\frac{n_i}{N_i}\right)^{\alpha} \qquad 3\text{-}21$$

where $\alpha$ is a parameter describing the nonlinearity.

One of the more complex formulations was proposed by Howe & Owen (1972):

$$D = \sum_{i=1}^{k} \left[A\frac{n_i}{N_i} + B\left(\frac{n_i}{N_i}\right)^{C}\right] \qquad 3\text{-}22$$

This equation was introduced to describe damage in terms of normalised resin cracking (for polymeric material). Introducing additional parameters is not increasing significantly the accuracy, but these nonlinear models lose its biggest advantages – its simplicity.

The safety check expression for the cumulative damage rules can be presented in a very simple way:

$$D \leq \frac{1.0}{FDF} \qquad 3\text{-}23$$

where FDF is a fatigue design factor (the concept of a factor of safety on fatigue life).

Many other cumulative fatigue damage and fatigue life prediction theories were already proposed e.g. Marco & Starkey (1954), Corton & Dolen (1956), etc. A review of these theories was given by e.g. Fatemi & Yang (1998).

### 3.5.5. The impact of static strength on S-N curve

It is still not decided yet, whether the static data should or should not be incorporated into derivation of S-N curves. It seems that neither the incorporation of the static data, nor the exclusion is completely justified (Nijssen, Krause, & Philippidis, 2004). There is a list of arguments pro and contra regarding this discussion:

For the static data inclusion:

- Static data are fatigue specimens which failed in the first load cycle
- Including static data in the linear regression diminishes inconsistencies in low-cycle region
- S-N curves that describe both static and fatigue have the potential of simplifying experimental programmes and fatigue life prediction, since fatigue behaviour can be described by static strength and a slope-parameter

Contra the static data inclusion:

- Static strength is usually not obtained at strain rates corresponding with fatigue strain rates
- Including static data might cause the fatigue life to be poorly represented for higher

number of cycles
- Static and fatigue failure mechanisms are often distinctly different
- Models which include the static strength require more parameters to model the material's behaviour

ASTM and Eurocode do not recommend using the static data in derivation of the S-N curve. A practical argument against the advantages of including static data is the fact that most fatigue calculations, low-cycle fatigue is of little or no interest, given the long design fatigue lives. As presented in Figure 3.14, for different applied cyclic loads (*R*-ratios), different S-N curves are obtained. For a higher cyclic stresses, plasticity plays an important role, and therefore the results for a low cycle fatigue (LCF) are not included in standard S-N curves (Figure 3.15). This is because the use of static strength data could lead to incorrect estimations in high cycle fatigue (HCF). However in geotechnics, in some cases the number of cyclic loads could be small but the loads could be significant and the small number of cycles would be of interest (e.g. during earthquakes or very strong guts or waves).

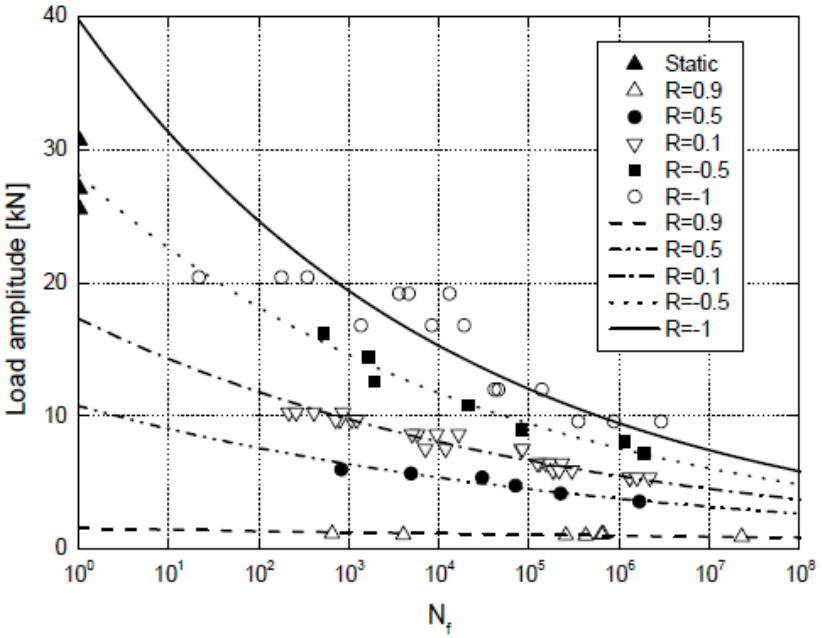


*Figure 3.14. S-N curve for tension and tension-dominant fatigue loading (Sarfaraz Khabbaz (2012)*

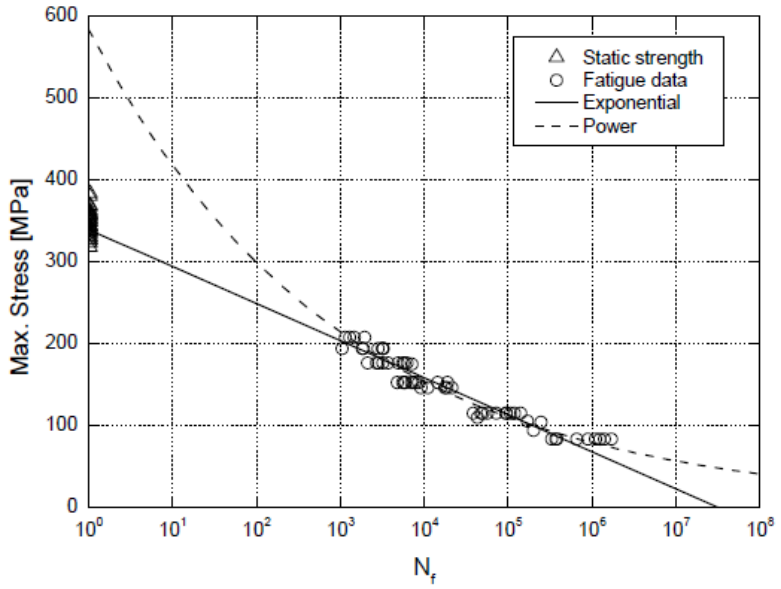


*Figure 3.15. Comparison of exponential and power curves for laminates excluding static data (Sarfaraz Khabbaz, 2012)*

### 3.6. Low cycle fatigue approach

The number of cycles to failure in engineering is considered as $N > 10^4$, however, for some materials (e.g. rocks and concrete) already a low number of cycles in relation with high cyclic stresses could lead to a substantial loss of strength. A material subjected to high cycle fatigue (HCF) loading, is mostly found to be in the elastic range, usually below 2/3 of the yield stress. Very high repeated cyclic loadings due to earthquakes or other catastrophic events may cause failures in less than 100 cycles. These failures are sometimes referred to as low cycle fatigue (LCF).

*Basquin equation*

All general methods for fatigue life estimation under LCF are based on three equations. The first of them has been published for high cyclic stresses by Basquin (1910):

$$\sigma_a = \sigma_f'(2N_f)^b \qquad 3\text{-}24$$

It describes the exponential relationship between the number of cycles to failure $N_f$ and a stress amplitude $\sigma_a$.

*Coffin-Manson equation*

The second equation was given by the Coffin (1954) - Manson (1953):

$$\varepsilon_{ap} = \varepsilon_f'(2N_f)^c \qquad 3\text{-}25$$

where $\varepsilon_{ap}$ is the amplitude of plastic strain and $N_f$ is a corresponding fatigue life. This equation relates empirically the cycles to failure $N_f$ to the plastic strain amplitude $\varepsilon_{ap}$ (similar to Basquin equation). The $\varepsilon_f$ and $c$ are experimentally determined constants.

The third equation describes a total strain as a sum of the elastic and plastic strains:

$$\varepsilon_t = \varepsilon_e + \varepsilon_p = \frac{\sigma}{E} + \left(\frac{\sigma}{K'}\right)^{\frac{1}{n'}} \qquad 3\text{-}26$$

This plotted creates the cyclic stress-strain curve and the curve forms a hysteresis loop in a single fatigue cycle. The area of that loop is the dissipated energy per unit volume during a cycle.

*Morrow equation*

Several of formulae have been proposed for evaluating the parameters in the Coffin-Manson equation for the short fatigue life $N_f$. To the most common belongs the Morrow (1964) notation for universal strain-life, represented by:

$$\frac{\Delta\varepsilon}{2} = \left(\frac{\sigma_r'}{E}\right)(2N_f)^b + \varepsilon_f'(2N_f)^c \qquad 3\text{-}27$$

Here, $\Delta\varepsilon/2$ is the strain amplitude (i.e., half the total strain range), and $2N_f$ is the number of reversals (two reversals for each of the $N_f$ cycles of failure). The terms $\varepsilon_f'$ and $\sigma_f'/E$ are strain intercepts at $2N_f=1$, and $c$ and $b$ are slopes of the plastic and elastic lines, respectively (as in Figure 3.16). The intersection of the two straight lines is known as the "transition point", and its coordinates are designated $\Delta\varepsilon_T/2$ and $2N_T$ respectively.

The universal slope equations were given for the elastic and plastic lines -0.12 and -0.6 respectively for all materials. These slopes were based on 29 materials (metallic) which covered a wide range of strength and ductility. Based on this, Manson-Hirschberg (1964) derived the following equation:

$$\Delta\varepsilon = (3.5S_u/E)N_f^{-0.12} + D^{0.6}N_f^{-0.60} \qquad 3\text{-}28$$

Thus, only the tensile properties $S_u$, $D$ and $E$ are required to determine the relationship between fatigue life and strain range.

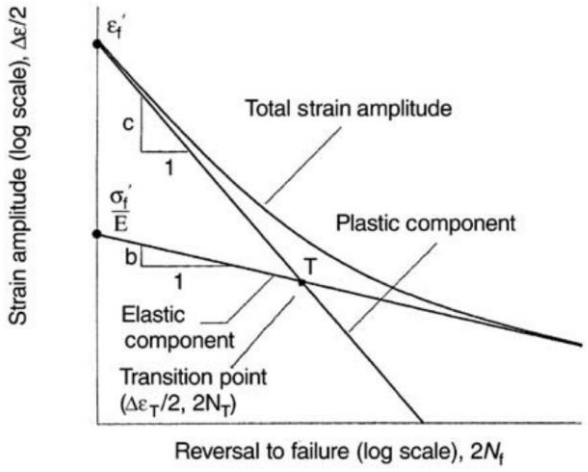


*Figure 3.16. Morrow's notation for use in the Manson-Coffin-Basquin model for fatigue in strain*

*cycling*

The low fatigue cycle is a promising approach to be investigated for a lower number of high cyclic stresses; however, other approaches could be more useful. The LCF could be probably directly incorporated into HCF. This will be further investigated for geomaterials.

### 3.7. Fatigue of geomaterials

To compare behaviour of geomaterials under cyclic loading, the geomaterials are divided into two groups:

- Cohesive
- Cohesionless

*Cohesive geomaterials - rocks*

Burdine (1963) first showed that compressive cycling loading on rock resulted in a weakening of the material. Many other tests on a variety of rock types were presented which clearly demonstrated the progressive weakening of rock due to cyclic loading (Haimson, 1978), (Attewell & Farmer, 1973), (Ishizuka, Abe, & Kodama, 1990), (Mirzaghorbanali, Nemcik, & Aziz, 2013), (Jong & Chan, 1991), (Bagde & Petroš, 2011). Fatigue cyclic tests on artificially cemented soil were conducted by Viana da Fonseca et al. (2013). Only a limited number of cyclic tests have been conducted on rock discontinuities and discontinuous (jointed) rock masses so far; e.g. Canelli et al. (2012) conducted tests cyclic load tests on smooth and rough discontinuities. An S-N curve for limestone was proposed by Lee & Rhee (1992), see Figure 3.17. Liang et al. (1993) also proposed an S-N curve and a simple formula based on cyclic tests on deep coal rock masses:

$$p = B - A \ln N \qquad 3\text{-}29$$

where $A$ and $B$ are the functions: $A = A(\sigma, \dot{p})$, $B = B(\sigma, \dot{p})$ in which p is the cyclic axial pressure amplitude, $\dot{p}$ is the axial loading rate and $\sigma$ is the confining pressure.

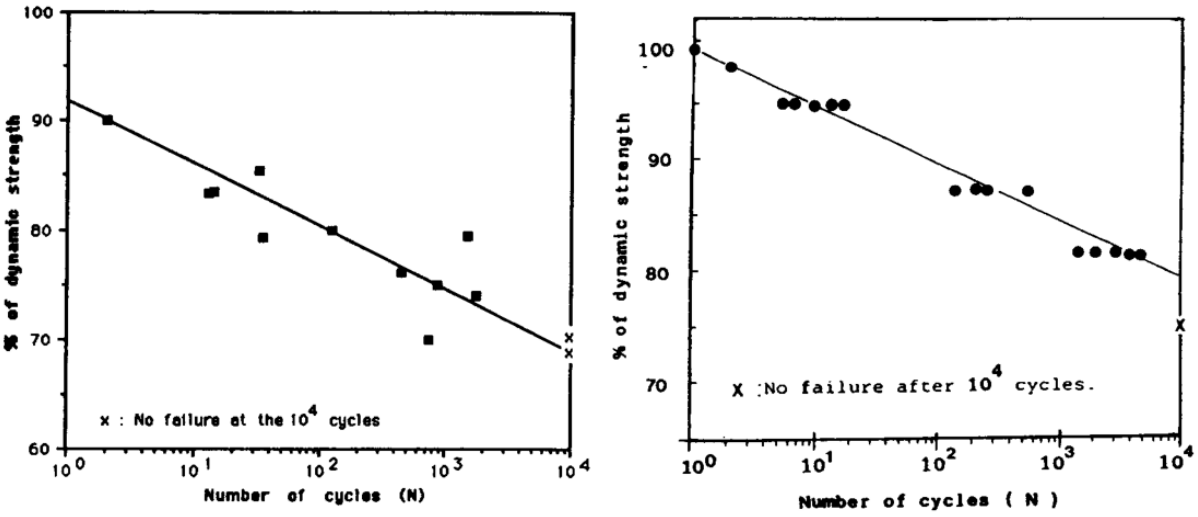


*Figure 3.17. S-N curve for Indiana limestone and Seoung-Ju specimen (Lee & Rhee, 1992)*

Mingming et al. (2015), concluded that the relationship between the fatigue life and loading speed, frequency, and stress amplitude under dynamic cyclic loading for sandstone would be expressed as the S-N curve. They also proposed a formula which best fit is:

$$N = aX^{-b} \qquad 3\text{-}30$$

Ray et al. (1999) studied the impact of cyclic loading on Chunar sandstone. In tests for given number of cycles (similar to remaining strength curve) they found that the UCS decreases in cyclic loading with constant amplitude for higher number of cycles and showed that after certain number of cycles the percentage decreases in uniaxial compressive strength does not increase uniformly. They divided the curve into three zones (see Figure 3.18).

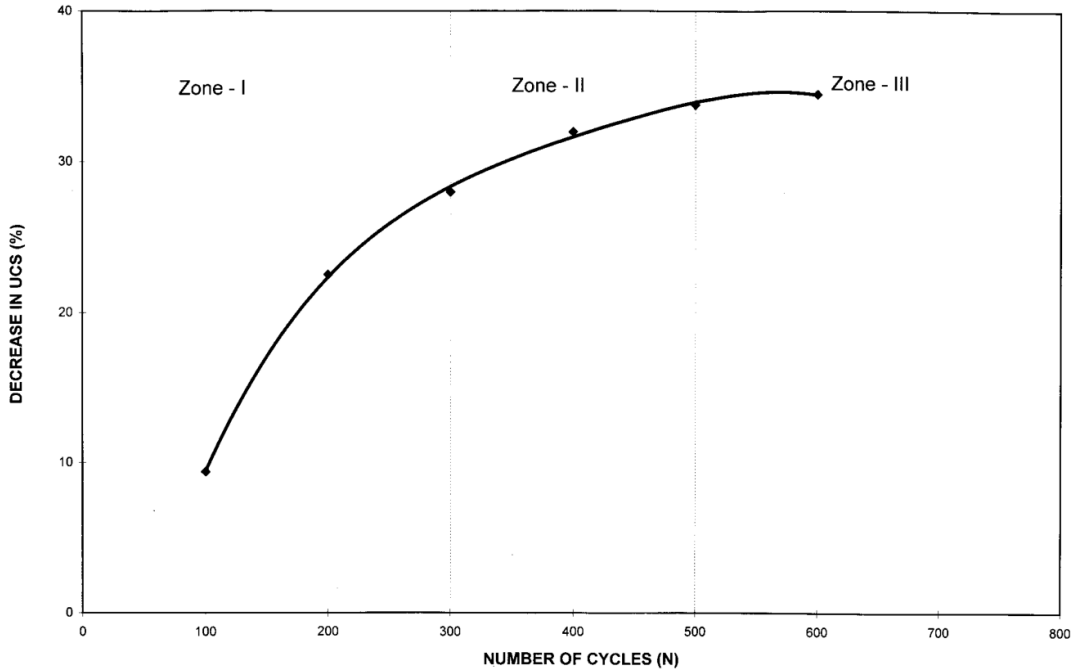


*Figure 3.18. Effect of number of cycles on percentage decrease in UCS (Ray, Sarkar, & Singh, 1999)*

Rocks lose their strength in cyclic loading and the loss of strength is larger than compared with non-geomaterials, which was found by e.g. Bagde & Petroš (2011) and Liu et al. (2014). Cyclic test results for concrete (ACI Committee 215R, 2005), of which one could think it is a similar material to rock, showed that the fatigue strength after 10 million cycles was approximately 55% of the static strength, which is a value often used in design.

*Cohesionless geomaterials - soils*

Soil can be seen as a mixture of rock fragments or mineral grains, sometimes including organic particles. Unfortunately, soil fatigue cannot be treated similarly to that of ductile (metals) or brittle (rocks) materials. Failure does not occur in a typical three-phase order: crack initiation, crack propagation and failure (compare chapter 2.2.4). Cracking, which is the main fatigue mechanism in solid materials, cannot develop in soils, as the soil is already disintegrated. Soil fatigue is only a moderate reduction of the strength which occurs mainly in the vicinities of a foundation that is cyclically loaded, for example shaft skin friction degradation (see chapter 2.1.2).

The nature of strength of a soil is different from solid materials. For soils the friction angle $\phi$ gives the strength, where for many other materials it is mostly, or totally the cohesion $c$. Most soils lack, or only have a very low cohesion, which may be an important factor for the soil fatigue description, and this could be even more challenging for soils than for rock materials.

Cyclic tests on clay show that the shear strength of undrained samples is reduced according to Sangrey et al. (1969), Thiers & Seed (1969), Patiño et al. (2013). Carter et al. (1982) proposed a model for prediction of the mean effective stress reduction in clayey soils under cyclic loading. An improved model was proposed by Sridhanya et al. (2009). However, a series of cyclic tests on pottery clay conducted at the University of Luxembourg (Knaff, 2013) showed no fatigue. On the contrary, the strength of the samples even increased due to cyclic loading. It has to be noticed, however, that the amount of tests and the number of cycles was very limited. The results for cyclically loaded drained soils also showed an increase in shear strength of granular materials (Suiker, 2002). Eurocode 8 (2004), states that "no reduction of the shear strength need to be applied for strongly dilatant cohesionless soils, such as dense sand". In cases of high cyclic loads and high confining pressures, skin shaft friction degradation may occur - see chapter 2.1.2.

### 3.7.1. Factors affecting strength of geomaterials

Basically, factors which are important in fatigue behaviour of materials, like steel and concrete, should also be taken into account of fatigue life of geomaterials. It can be assumed that the most significant effects on fatigue life will be:

- Loading rate (frequency),
- Load history,
- Stress gradients,
- Specimen size,
- Temperature,
- Rest period,
- Varying maximum stresses,
- Shape of the wavelength of loading,
- Confining pressure,
- Material properties,
- Saturation (presence of water),
- Mechanism of fatigue failure,
- Impact of environment (humidity, salinity, corrosive agents, etc.).

Some of the factors are very similar to concrete fatigue factors (Appendix A.C). All of these effects, however, have to be taken into account for the preparation of laboratory tests and the description of the fatigue of geomaterials.

*Frequency of load*

One of the important parameters of cyclic loading is the frequency. It is well known, for example Zhao (2000), Li et al. (1999), and Lockner (1998) that the dynamic strength of rock depends on the loading rate. Ishizuka et al. (1990), Bagde & Petros, (2011), Haimson & Kim (1972), Liu et al. (2012) reported that the fatigue life increases with increasing frequency.

For wind turbines, the frequency of wind turbulence lies below $f = 0.1$ Hz. The rotational speed is typically in the range of 10-20 revolutions per minute, corresponding to a full revolution, in the range $f = 0.17$ - 0.33 Hz. For traffic, machine, wave and earthquake loading frequencies tend to be in range $f = 0.1 – 20$ Hz (see Table 3-2). The dominating force in offshore wind turbine foundations is the wave load, which has a much longer period, around 10 ~ 20 seconds (large waves can reach even 200 s) that means a frequency of $f = 0.1–0.05$ Hz.

Even though the span of the loading frequency, which is important for geotechnical structures, is wide (Figure 3.19), it is still in the range of the cyclic loading (see Table 3-2).

*Table 3-2. Approximate classification of repeated loading of soils [Peralta, 2010]*

| Repeated Loading of Soils | Cyclic | Cyclic-Dynamic | Dynamic |
|---|---|---|---|
| Frequency $f$ | 0 to 1 Hz | 1-10 Hz | >10 Hz |
| Inertia | No (negligible) | Yes (relevant) | Yes (relevant) |
| Strain accumulation | Predominantly plastic | Plastic and elastic | Predominantly elastic |

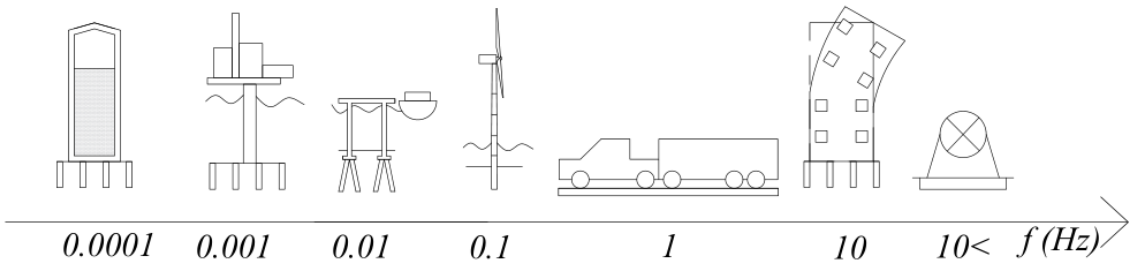


*Figure 3.19. Frequency of cyclic loading range in geotechnics*

*Number of cycles*

The number of cyclic loads, especially in offshore structures, can be quite significant. Wind turbine rotor blades can be subjected to the number of load cycles up to $10^8$ or $10^9$ according to Mandell et al., (1992) and Van Delft et al., (1997). The number of load cycles, that a standard wing turbine might be subjected to over its 20-year life time given by Janssen et al., (2012), is 100 million to 1 billion. For other geotechnical structures the number of loads may be much smaller, e.g. for sluices, underground gas storage facilities, or during mining operations and earthquakes. The range of applied number of cycles has a significant impact on the fatigue of materials. There is a lack of tests in the literature, which investigated the behaviour of geomaterials under a large number of cycles.

Usually two different ranges of load cycles are investigated:

- High cycle fatigue (HCF): in case material requires more than $N > 10^3 – 10^4$ cycles to

failure.
- Low cycle fatigue (LCF): in case material requires less than $N < 10^3 – 10^4$ cycles to failure.

*Static fatigue*

Brantut et al. (2013) gave a summary of a brittle creep - a process which leads to *static fatigue*. Static fatigue is a delayed failure of rock material when loaded to a stress lower than the short-term failure stress (Kranz, 1980), (Lockner, 1998). The time to failure was found empirically to be related to a stress, through an exponential or power law (Kranz, 1980). Static fatigue was found to be one of the main mechanisms responsible for weakening over time of iron ore pillars in underground mines in Lorraine (Grgic & Giraud, 2014). Static fatigue of geomaterials should also be considered in order to describe cyclic fatigue.

*Stress amplitude*

Attewell & Farmer (1973) found that for higher cyclic stress amplitude the fatigue life decreased. The same result was given by Zhenyu & Haihong (1990), Bagde & Petros (2005) and Kranz (1980), Xiao et al. (2009) and others.

*Influence of confining pressure $\sigma_3$ on a static and cyclic strength of geomaterials*

The yield criteria for metals; Tresca and Von Mises, are one parameter criteria, which are not taking into account the confining (lateral) pressure. However, most non-metallic materials, and some high-strength steel and alloys, have their static strength dependent on the lateral pressure. Some studies (Crossland, 1954), (Hu, 1959) show that the effect of the lateral stress on the plastic behaviour of metals can be significant. Still, in metal engineering, the influence of the lateral pressure $\sigma_3$ on the static strength $S_0$ is neglected.

A number of experiments conducted by Bridgman (1923) show that the confining pressure is unimportant for metal fatigue. Hudson (1973) summarised fatigue tests on metal alloys and found that lower air confining pressure produces longer fatigue lifes. Different results were found earlier by Libertiny (1967). He observed that a large hydrostatic pressure produces an increase in the short fatigue life of the metal. Wadsworth & Hutchings (1958) tested strip polycrystalline copper, aluminium and gold in both air and a vacuum. The ratio of fatigue life-in-air to fatigue life-in-vacuum was about 1:20 for copper, 1:5 for aluminium, and 1:1 for gold. The impact of the confining pressure on metal fatigue life is still subject of research.

For rock, concrete and soil, an increase in static strength for higher lateral (confining) pressure is well known (Kwasniewski & Takahashi, 2006), and is incorporated in the Mohr-Coulomb failure theory since Coulomb's first publication in 1773.

Even though the experimental and theoretical studies on cyclic loading on rocks primarily focus on the influence of the stress amplitude and loading rate, only a small concern is given to the influence of the confining pressure. The increase in number of cycles, with an increase

in confining pressure, was confirmed by Burdine (1963), Kranz (1980) and Zafar & Rao (2010) and Haimson (1978).

*Intermediate stress $\sigma_2$ effect on fatigue*

The Mohr-Coulomb theory, because of its big advantage of simplicity, has unfortunately a limitation, because it does not include the intermediate principal stress $\sigma_2$. The results of many experiments show that with increase in the intermediate principal stress $\sigma_2$, higher strengths are obtained (Figure 3.20 and Figure 3.21).

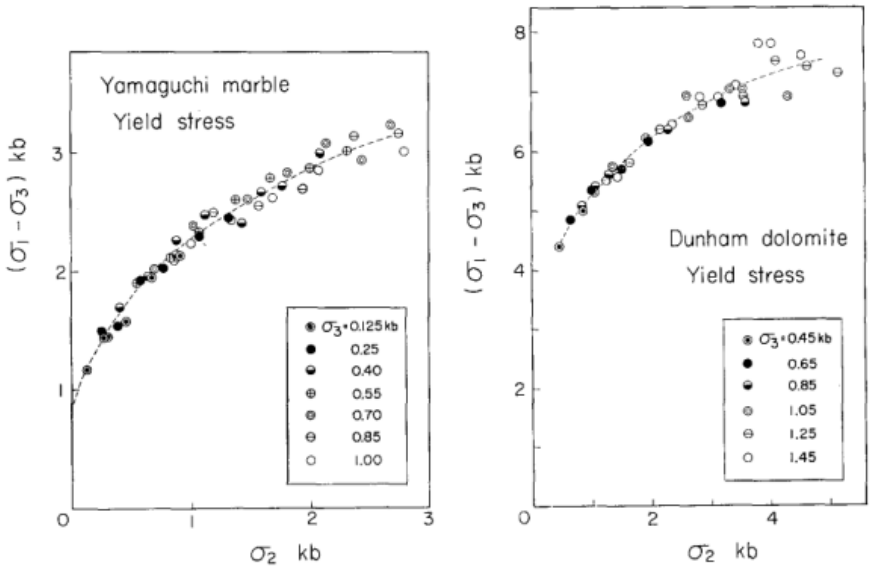


*Figure 3.20. Relation between strength and intermediate principal stress $\sigma_2$ (Mogi, 1972)*

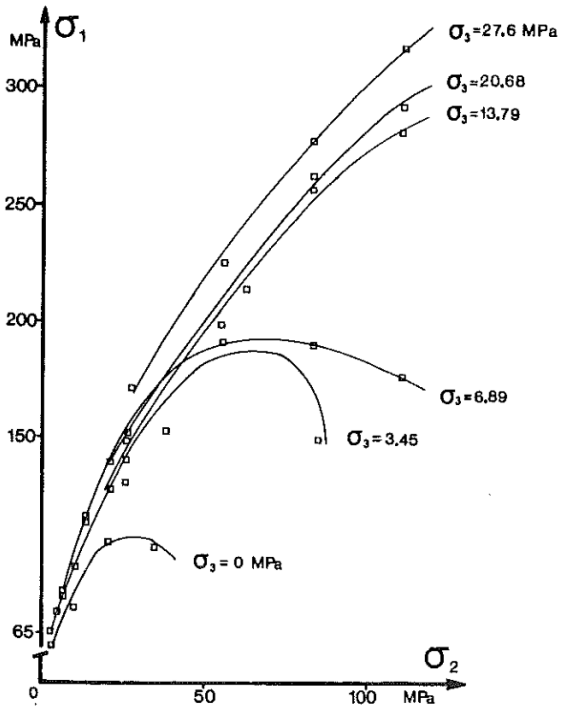


*Figure 3.21. Effect of intermediate principal stress $\sigma_2$ on Naxos Marble (Michelis, 1985)*

Mogi (1972) was the first one, who studied the effect of the confining pressure, intermediate principal stress and minimum principal stress on a differential stress-axial strain characteristic of rocks. The results of true triaxial compression tests (Kwasniewski & Takahashi, 2007), show that the effect of intermediate principal stress $\sigma_2$ on the ultimate strength of the limestone is weaker than the effect of confining pressure $\sigma_3$. El-Gammel (1984) investigated the effect of the intermediate principal stress and he observed significant changes in the stress-strain behaviour of samples. Xu & Geng (1985) pointed out that, varying $\sigma_2$ while keeping the other principal stresses $\sigma_1$ and $\sigma_3$ unchanged could lead to a rock failure, and this fact could also be attributed to the inducement of earthquakes.

So far, no cyclic fatigue tests were conducted to investigate the impact of $\sigma_2$ on the remaining strength because those tests would be extremely difficult to conduct and these results alone could be insufficient to make any conclusions.

*Type of failure*

For uniaxial compression test of rocks, there is a range of different failure mechanisms possible of which the two most common are illustrated in Figure 3.22. One failure mechanism involves axial splitting, which is dominated by tensile stresses induced by plate friction and other end effects. The other failure mechanism is shearing. A uniaxial compressive strength tests should produce an inclined shear plane, or planes, through the test sample, if is to represent compressive stress conditions (Johnston, 1991).

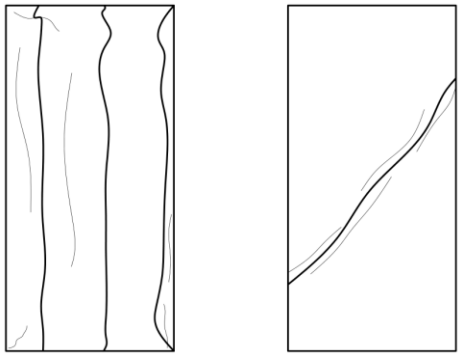

*Figure 3.22. Failure mechanism in the uniaxial compression tests: a) axial splitting and b) shearing*

The type of fracture also depends on the confining pressures as is presented in Figure 3.23 and in Figure 3.24. The type of fracture has a significant impact on the plastic strain (and the critical energy accumulation) and strongly depends on the confining pressure (Karman, 1911). Liu & He (2012) found that the confining pressure had a significant influence on the cyclic deformation and fatigue damage of the sandstone samples, because the axial strain at failure increased with increasing confining pressure. Therefore it is clearly visible that for geomaterials the strain and critical energy models would lead to difficulties to properly describe the cyclic plastic strains and critical energy accumulation. Johnston (1991) stated that the yield point which exists between brittle ductile behaviour could be the same for rocks (brittle ductile transition pressure) and soils (maximum overburden pressure). It can be summarised that a very limited scientific effort was done to investigate the type of failure on

the fatigue behaviour on geomaterials.

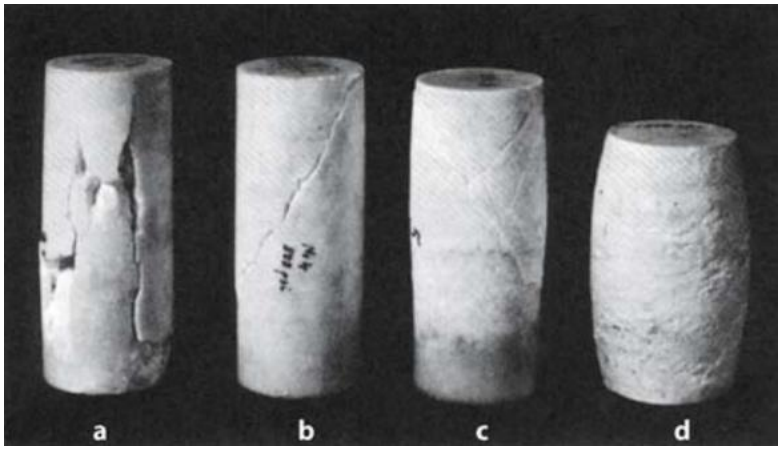


*Figure 3.23. Types of fractures or flow in Wombeyan marble at various confining pressures. a) axial splitting failure at atmospheric pressure; b) single shear failure at 3.5 MPa; c) conjugate shears at 35 MPa; d ductile behaviour at 100 MPa (Paterson, 1958)*

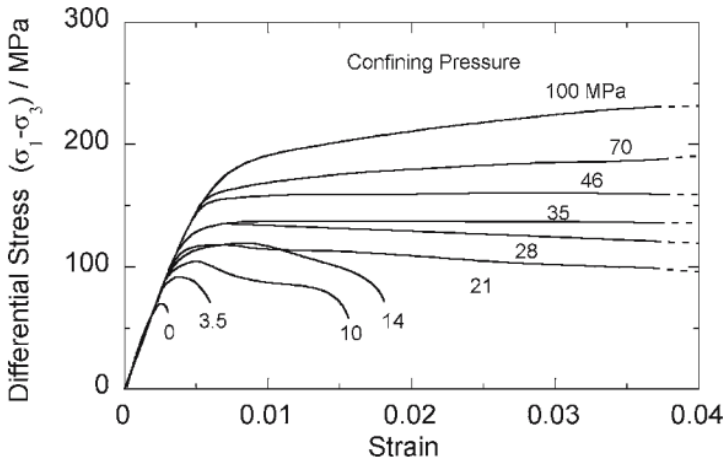


*Figure 3.24. Progression in the natures of the stress-strain curve in triaxial compression of Wombeyan marble as confining pressure is increased as shown (Paterson, 1958)*

### 3.8. Conclusions

Fatigue of geomaterials in terms of shear strength (shear strength parameters $c$ and $\phi$) has not been deeply investigated. The existence of fatigue of geomaterials was already confirmed, but unfortunately not many research was done in order to investigate the relationship involving the shear strength parameters reduction, cyclic loading, confining pressure, type of cyclic loading and etc. The main concern of researchers in the past was related to dynamic strength of rock and shaft skin friction degradation of soil. No comprehensive description of cohesion or friction angle reduction in cyclic loading was found.

# 4. REMAINING SHEAR STRENGTH CURVE FOR GEOMATERIALS

## 4.1. Introduction

The microvoids and cracks, created during geological life of rocks, expand due to the cyclic loading because of a concentration of high stresses. Compared to other materials, especially to metals (microcraks in quenched and tempered steel are around 130 μm length, Barsom, 2009), the initial microcracks in rocks are larger (1-3 mm in Stanstead granite Nasseri, et al. 2007) and the internal structure is much more inhomogeneous. This makes the rock fatigue life prediction very complex. To evaluate fatigue in metals, the measurement of the maximum stress and the fatigue life is sufficient, where for rocks this may be not enough.

Many non-geomaterials lose their strength in cyclic loading (chapter 3) and in contrast to geomaterials, their fatigue life has already been described. For geomaterials, which are also affected by cyclic loading (see chapter 2.2), no remaining strength model exists yet. Due to this lack of available models, used for describing the remaining strength, a simple remaining shear strength model for geomaterials will be proposed in this thesis. Based on this model, laboratory tests on geomaterials will be conducted and the fatigue life prediction, as well as the impact of the confining pressure and the different cyclic stresses will be studied.

First, the static strength of geomaterials has to be described, second, the S-N curve for shear strength will be updated and finally the remaining shear strength curve will be proposed. Additionally, based on the assumption of a constant friction angle in cyclic loading on geomaterials, a curve for the remaining cohesion will be given. At the end of this chapter, similarities and differences between the S-N curve and remaining shear strength curve will be presented.

## 4.2. Static shear strength - Mohr-Coulomb failure criterion

Strength characteristics of soils and rocks, even though they are quite different materials, are still similar (Johnston, 1991). The static strength of geomaterials is usually given as a shear strength and for both materials the shear strength can be described by a Mohr-Coulomb

failure criterion. The most important property of the Mohr-Coulomb theory is that the shear strength increases with an increase in the confining pressure. The Mohr-Coulomb failure theory is a linear failure criterion which gives two parameters: the cohesion and the friction angle.

There are few methods which can be used to describe the stress state in soil mechanics. One way is to give four components (in a plane state of stress) with a fixed coordinate system ($\sigma_{xx}$, $\sigma_{yy}$, $\tau_{xy}$, $\sigma_{zz}$). Another way is to specify the stress state using the principal stresses ($\sigma_1$, $\sigma_2$, $\sigma_3$). The function defining the Mohr-Coulomb failure criterion is usually presented in terms of the maximum $\sigma_1$ and minimum principal stresses $\sigma_3$ as:

$$\left(\frac{\sigma_1 + \sigma_3}{2}\right) sin\,\phi - \left(\frac{\sigma_1 - \sigma_3}{2}\right) + c \cdot cos\,\phi = 0 \qquad 4\text{-}1$$

where $c$ is the cohesion, and $\phi$ is the friction angle. The two parameters $c$ and $\phi$ can be obtained from laboratory tests (e.g. triaxial or direct shear tests) or field investigation (e.g. vane shear test). Stresses at failure in triaxial tests are normally presented on a 2D failure surface considering only the minor and major principal stresses $\sigma_1$ and $\sigma_3$ (Figure 4.1a).

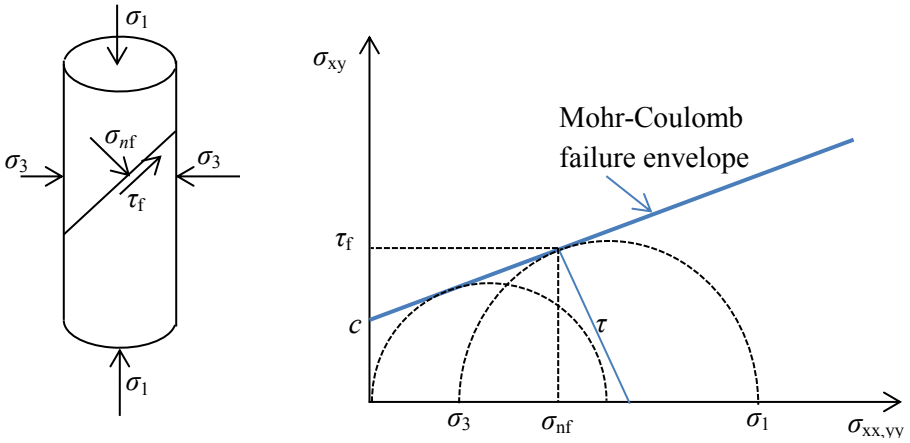


*Figure 4.1. Failure in triaxial compression test (a) the stress-state, (b) the Mohr-Coulomb failure envelope*

The Mohr-Coulomb failure criterion can also be given as:

$$\tau = \sigma\, tan\,\phi + c \qquad 4\text{-}2$$

where $\tau$ is the shear strength, $\sigma$ is the normal stress, $c$ is the cohesion (intercept of the failure envelope with the $\tau$ axis) and $\phi$ is the slope of the failure envelope (Figure 4.1b).

Other failure criterions, like Drucker-Prager and Hoek-Brown, will not be taken into consideration due to two main limitations: they are more complicated and less used in geotechnical engineering.

*Shear strength at failure to the predicted shear strength*

The measured shear strength at failure can be compared to the predicted shear strength according to the equation:

$$\frac{\tau}{\tau_0} \stackrel{\text{def}}{=} \frac{\tau_{measured}(N \gg 1)}{\tau_{predicted}(N = 1)} \qquad 4\text{-}3$$

where $\tau_{\text{measured}}$ is the measured in triaxial test shear strength (of single or cyclic test for $N$ number of cycles), $\tau_{\text{predicted}}$ or $\tau_0$ is the predicted shear strength based on Mohr-Coulomb shear strength parameters (cohesion $c$ and friction angle $\phi$ obtained in series of static triaxial tests). The $\tau_{\text{predicted}}$ is calculated for the same confining pressure $\sigma_3$, as was applied for the $\tau_{\text{measured}}$. This is presented in Figure 4.2:

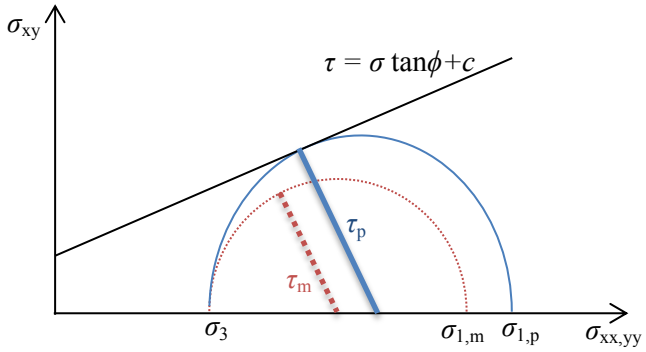


*Figure 4.2. Measured shear strength to the predicted shear strength (where subscripts $_m$ and $_p$ denotes measured and predicted value correspondingly).*

The shear strength is given as:

$$\tau = \frac{\sigma_1 - \sigma_3}{2} \qquad 4\text{-}4$$

where $\sigma_1$ and $\sigma_3$ are the maximum and minimum principal stresses

The relation from Equation 4-3 can be also written in terms of principal stresses:

$$\frac{\tau}{\tau_0} = \frac{\frac{\sigma_{1,m} - \sigma_3}{2}}{\frac{\sigma_{1,p} - \sigma_3}{2}} \qquad 4\text{-}5$$

where $\sigma_{1,\text{m}}$ is the measured maximum principal stress and $\sigma_{1,\text{p}}$ is the predicted maximum principal stress. Based on an equation for deviatoric stress:

$$\sigma_d = \sigma_1 - \sigma_3 \qquad 4\text{-}6$$

the relationship of the measured to the predicted shear strength can be also calculated as:

$$\frac{\tau}{\tau_0} = \frac{\sigma_{d,m}}{\sigma_{d,p}} \qquad 4\text{-}7$$

where, $\sigma_{\text{d,m}}$ is the measured deviatoric stress and $\sigma_{\text{d,p}}$ is the predicted deviatoric stress. The deviatoric stress is calculated simply as:

$$\sigma_d = \frac{F}{A} \qquad 4\text{-}8$$

where $F$ is an applied force in triaxial apparatus and $A$ is a cross-sectional area of a sample.

### 4.3. S-N curve for geomaterials

In the case of the S-N curve for non-geomaterials, the $S$ corresponds to the cyclic stress $\sigma_{cyc}$. For geomaterials though, the hypothesis is that the fatigue depends in the same way as the static strength on the confining stress. This will be investigated in this thesis.

*S-N shear strength curve*

To be able to describe for geomaterials the shear strength reduction by S-N curves, instead of the cyclic stress $\sigma_{cyc}$, the ordinate axis has to be described by a $\sigma_{cyc}/S_0$ ratio, which is the ratio of the applied cyclic stress $\sigma_{cyc}$ to the static strength $S_0$.

For the shear strength reduction in cyclic loading, the $S_0$ is replaced by the static shear strength (shear stress based on the linear regression for static tests):

$$S_0 = \tau_0 \qquad 4\text{-}9$$

The applied cyclic stress $\sigma_{cyc}$ is also proposed as a cyclic shear stress:

$$\sigma_{cyc} = \tau_{cyc} \qquad 4\text{-}10$$

For the non-dimensional S-N curve, the cyclic stress ratio can be proposed as a ratio of the applied cyclic shear stress to the maximum (static) shear strength:

$$\frac{\tau_{cyc}}{\tau_0} = i \qquad 4\text{-}11$$

Because for geomaterials the static shear strength $\tau_0$ depends on the confining pressure $\sigma_3$, the cyclic stress $\tau_{cyc}$ should also be adjusted to that confining pressure. That means the fatigue strength is normalised to its static strength and should not be influenced by parameters such as strength, type of aggregate, age, and the confining pressure etc. This is already taken into account by dividing the $\tau_{cyc}$ by the $\tau_0$. In other words:

$$\frac{\tau_{cyc}(\sigma_3)}{\tau_0(\sigma_3)} = i \qquad 4\text{-}12$$

For further description and calculations it is assumed that the static and cyclic stresses correspond to a given confining pressure, therefore the symbol ($\sigma_3$) will be omitted in the equations. It can be noticed that, the tests with a confining pressure equal to 0 kPa are similar to unconfined compression tests (UCS) which are normally used for concrete (ACI Committee 215R, 2005) and steel (ASTM E739-91, 1998).

The S-N curve for the shear strength reduction can be based on the formulas described in chapter 3.5, and proposed by Eurocode 3 (2006) and ASTM E739-91 (1998):

$$\frac{\tau_{cyc}}{\tau_0} = \frac{A}{\tau_0} - \frac{B}{\tau_0} log_{10} N \qquad 4\text{-}13$$

where $A$ and $B$ are coefficients obtained in a linear regression analysis for a log-normal distribution.

The final step is to prepare a plot (Figure 4.3) with regression line and a 95% confidence

band and 95% prediction band (Figure 4.3). The 95% confidence band encloses area between 2.5% and 97.5% of probability that the band contains the true curve with reliability level 50%. It gives a visual sense of how well data define the best-fit curve. The confidence band is calculated, according to ASTM E739-91 (1998), as:

$$\hat{A} + \hat{B}X \pm \sqrt{2F_p}\sigma \left[\frac{1}{k} + \frac{(X-\bar{X})^2}{\sum_{i=1}^{k}(X_i-\bar{X})^2}\right]^{0.5} \qquad 4\text{-}14$$

where $F_p$ is value of $F$ distribution.

The 95% prediction band (tolerance limits or confidence interval, according to (ASTM E739-91, 1998) encloses an area between 2.5% and 97.5% of probability that the band contains 95% of the data points. The prediction band, according to ASTM E739-91 (1998), is given as:

$$\hat{A} + \hat{B}X \pm t_p\hat{\sigma} \left[1 + \frac{1}{k} + \frac{(X-\bar{X})^2}{(k-1)s_x^2}\right]^{0.5} \qquad 4\text{-}15$$

where $t_p$ is value of Student's t distribution, and $\hat{\sigma}$ is the standard error of the prediction.

Other types of curve fitting can be investigated (power, exponential etc.), whether they describe the S-N curve more accurately or not.

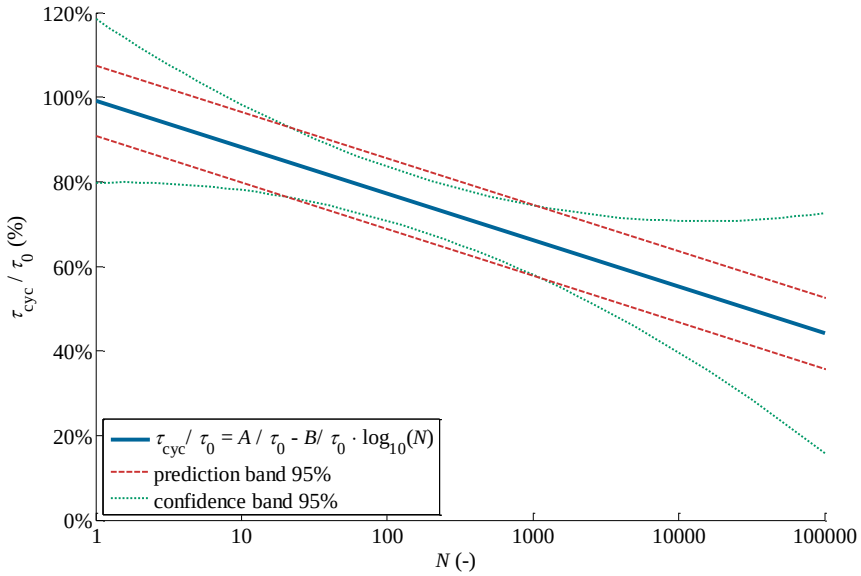


*Figure 4.3. S-N curve for geomaterials with confidence and prediction band*

### 4.4. Remaining strength curve for geomaterials

In this thesis a remaining shear strength curve for geomaterials is proposed. This remaining strength curve describes the amount or percentage of the remaining strength after a number of cycles has been applied. The advantage of using the remaining strength instead of the S-N curve is that the information of the remaining strength is, in some cases, more important than the remaining life. Because the strength decreases after each cycle, it is important to know if the strength after a certain fraction of the fatigue life still has the capacity to carry its loads.

For the remaining shear strength curve, the constant fatigue life diagram (Goodman diagram, see chapter 3.5.3) and the cumulative damage rule (Palmgren-Miner rule, see chapter 3.5.4) can be directly incorporated into the remaining strength curve.

### 4.4.1. Analytical description of the remaining strength curve

The remaining strength curve assumes that the initial static strength $S_0$ after a number of cyclic loads $n$ is reduced. This phenomenon is called strength reduction or remaining strength curve after fatigue. The goal is to describe the remaining strength $S_{rem}$ as a function of the cyclic stress $\sigma_{cyc}$, the number of applied cycles $n$ and the initial static strength $S_0$:

$$S_{rem} = f(\sigma_{cyc}, n, S_0) \qquad 4\text{-}16$$

Since $N$ is the fatigue life or the number of cycles until failure in the S-N curve, for the remaining strength curve the letter $n$ will be used to describe the number of applied cycles. The number of applied cycles $n$ is always smaller than the fatigue life $N$ which means $n \leq N$. The predetermined number of load cycles $n$ is given before testing. Powers of 10 are used to present conveniently the results on a semi – logarithmic plot (linearised on log-normal plot) with a base of 10. The maximum possible number of applied cycles $n_{max}$ should be more or less the same as the fatigue life $N$ obtained in the S-N testing for the same cyclic stress $\sigma_{cyc}$. This would also correspond to the same loss of strength for both the S-N and the remaining strength curves ($S_{rem} = \sigma_{cyc}$) in the case the same cyclic loading has been applied. In case where $n = 1$, the remaining strength $S_{rem}$ equals the static strength $S_{rem} = S_0$.

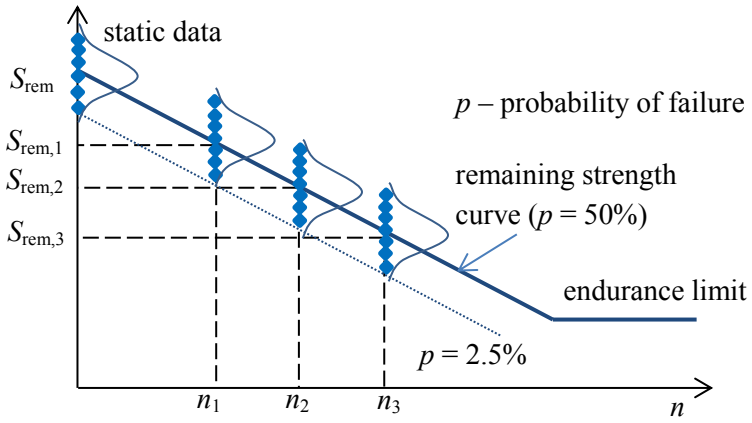


*Figure 4.4. Remaining strength curve*

The remaining strength is a straight line for each ($j_{th}$) cyclic stress $\sigma_{cyc}$ (Figure 4.5):

$$S_{rem,j}(n) = C_j(\sigma_{cyc}) - D_j(\sigma_{cyc})\, log_{10}\, n \qquad 4\text{-}17$$

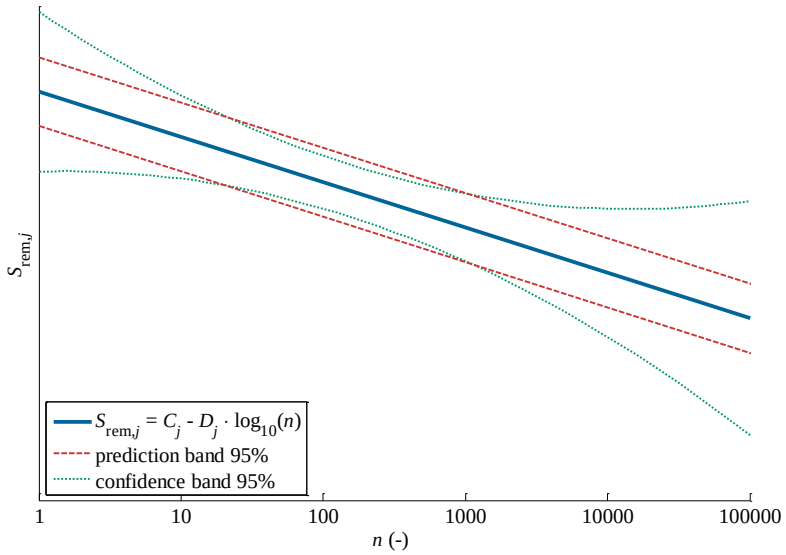


*Figure 4.5. Remaining strength curve*

The parameters $C$ and $D$ depend on the cyclic stress $\sigma_{cyc}$ and will be obtained by a linear regression analysis. For each cyclic stress $\sigma_{cyc}$, a single linear curve can be plotted (Figure 4.6).

A simplified version of Equation 4-17 will be used from here on in the thesis:

$$S_{rem,j} = C_j - D_j \, log_{10} \, n \qquad 4\text{-}18$$

The final plot for the remaining strength curve is presented in Figure 4.6. The plot denotes the loss of strength in number of cycles $n$ for a given cyclic stresses $\sigma_{cyc}$.

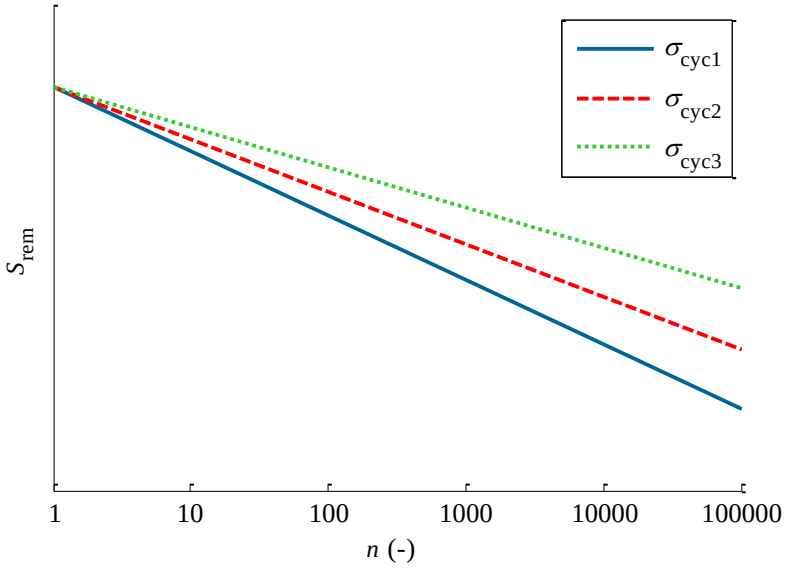


*Figure 4.6. Remaining strength for different cyclic stresses $\sigma_{cyc}$*

Remaining strength curve for metals and polymers (degraded strength models) are based usually on the Tresca or Von Mises yield criterions e.g. Broutman & Sahu (1972), Whitney (1981), Reifsnider & Stinchcomb (1986) and Sarfaraz Khabbaz (2012) etc. These curves

(models) unfortunately may not necessarily be suitable for geomaterials.

### 4.4.2. Remaining shear strength curve

The remaining shear strength equation for geomaterials can be given in the same way as the simple remaining strength equation (Equation 4-18). According to the Mohr-Coulomb failure theory, the shear strength $\tau$ depends on the confining pressure $\sigma_3$. Thus the equation for single remaining shear strength curve is given as:

$$S_{rem} = \tau_{rem}(\sigma_3) = C(\sigma_{cyc}) - D(\sigma_{cyc}) \log_{10} n \qquad 4\text{-}19$$

where $\tau_{rem}$ denotes the remaining shear strength under confining pressure $\sigma_3$ and $C$ and $D$ are again regression coefficients. The same cyclic load acting on a material under different confining pressures $\sigma_3$ will lead to a different reduction of strength, however.

To remove the dependency on the confining pressure $\sigma_3$, the formula is normalised by dividing the whole equation by the static strength $\tau_0$. The remaining shear strength is given as a ratio of the initial strength $\tau_0$ to the remaining strength $\tau_{rem}$. This is similar to the S-N curve for the remaining shear strength:

$$\frac{\tau_{rem}(\sigma_3)}{\tau_0(\sigma_3)} = \frac{C}{\tau_0(\sigma_3)} - \frac{D}{\tau_0(\sigma_3)} \log_{10} n \qquad 4\text{-}20$$

The coefficients $C/\tau_0$ and $D/\tau_0$ are replaced by the parameters $\alpha$ and $\beta$.

$$\frac{\tau_{rem}}{\tau_0} = \alpha - \beta \log_{10} n \qquad 4\text{-}21$$

The cyclic stress $i$ is defined in the same way as for the S-N curve for geomaterials, as a ratio of the applied cyclic shear stress to the maximum (static) shear strength:

$$i = \frac{\tau_{cyc}}{\tau_0} \qquad 4\text{-}22$$

For a number of sets $j$ of cyclic stress ratios $i$, the Equation 4-25 becomes:

$$\frac{\tau_{rem,j}}{\tau_0} = \alpha_j - \beta_j \log_{10} n \qquad 4\text{-}23$$

The parameters $\alpha_j$ and $\beta_j$ depend on the cyclic stresses $\tau_{cyc}$. For different cyclic stresses the $\beta_j$ value should be different. It is expected that the higher the cyclic stress $\tau_{cyc}$ the higher the declination of the $\beta_j$ and also, the faster the strength reduction occurs. After conducting laboratory tests, the parameter $\beta$ can be presented as a function of cyclic stress $\tau_{cyc}$, material properties etc.:

$$\beta = \beta_j(\tau_{cyc}, material\ properties, etc) \qquad 4\text{-}24$$

Because for $n = 1$, the remaining shear strength equals to the static strength $\tau_{rem} = \tau_0$ for all cyclic stress ratios $i$, the intercept $\alpha_j$ equals 1.0 and Equation 4-18 can be transformed to:

$$\frac{\tau_{rem}}{\tau_0} = 1.0 - \beta \log_{10} n \qquad 4\text{-}25$$

### 4.4.3. Prematurely failed samples in remaining strength curve

Because the strength of a material is randomly distributed, it may happen that for some samples the expected strength has a greater value than the real strength of the sample. For those particular samples the cyclic loading will lead to a faster strength reduction and therefore, the sample will not survive the planned number of applied cycles. In that case, the sample is called a prematurely failed sample and is not taken into consideration to obtain the remaining strength curve (Figure 4.7).

The removal of a part of the tests samples which are the weakest brings up a question about the reliability of the remaining strength curve. One of the proposed solutions is to use lower probabilities of failure. This, however, will not necessarily increase the accuracy of the material fatigue life prediction. Another solution is to include these prematurely failed samples in the calculation of the remaining strength parameters. This is, however, uncommon in remaining strength testing and could lead to erroneous calculation of the fatigue life. To avoid the problems with prematurely failed samples Yao & Himmel (1999) proposed a two parameter Weibull distribution of remaining strength. This problem, however, is still not properly solved yet.

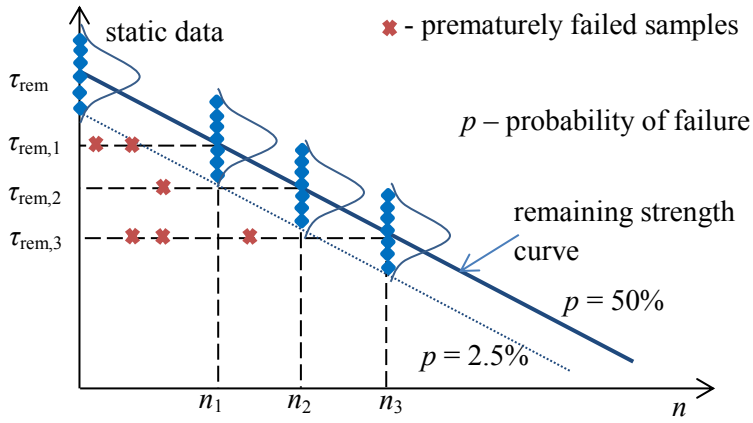


*Figure 4.7. The remaining strength curve with prematurely failed samples*

### 4.4.4. Fatigue life span for the remaining strength curve - the maximum number of cycles

For the remaining shear strength curve, the fatigue life $N$ can be calculated directly from the equation of the remaining strength (Equation 4-21), without introducing any degradation parameter.

For a given cyclic stress $\tau_{cyc}$, after transformation, one can obtain the fatigue life until failure as:

$$log_{10} n = \frac{\alpha_j - \tau_{rem}}{\beta_j} \qquad 4\text{-}26$$

and finally:

$$N = n = 10^{\frac{\alpha_j - \tau_{rem}}{\beta_j}} \qquad 4\text{-}27$$

where $\alpha_j$, $\beta_j$ are linear regression coefficients for a $j_{th}$ cyclic stress ratio $i$. If the material was not previously cyclically loaded, the remaining shear strength equals to the static strength $\tau_{rem} = \tau_0$ and the intercept $\alpha_j$ equals 1.0

One of the expressions for an equivalent number of cycles $n_{eq}$ was given by Schaff & Davidson (1997a) and Schaff & Davidson (1997b). These proposals are, however, more complicated and will not be used for the investigation in the fatigue of geomaterials.

### 4.4.5. Cumulative damage rule for the remaining shear strength

*Remaining shear strength*

The remaining shear strength after a series of loads can found by a subtraction of individual strength losses for each of the cyclic loading sets. This can be presented mathematically as:

$$\tau_{rem} = \tau_0 - \sum_{j=1}^{k} d_j = \tau_0 - d \qquad 4\text{-}28$$

where the $d_j$ is the strength reduction in a one load sequence, for $j_{th}$ sequence. This formula can replace the Palmgren-Miner rule and the $\tau_{rem}$ parameter replaces the damage parameter $D$ from Equation 3-17 (compare with Palmgren-Miner rule described in chapter 3.5.4). By incorporating Equation 4-18 into Equation 4-28, the remaining strength can also be presented as:

$$\tau_{rem} = \tau_0 - \sum_{j=1}^{k} (\alpha_j - \beta_j \log_{10} n_j) \qquad 4\text{-}29$$

where $\alpha_j$, $\beta_j$ are parameters obtained from the regression line of a given cyclic stress ratio $i$, and a given number of cycles $n_j$ in $j_{th}$ sequence, $k$ is the number of cyclic loading sequences. For one loading sequence the cyclic stress ratio $i$ is constant.

*Remaining life*

Based on Equation 4-27 one can also calculate the remaining number of cycles (fatigue life) for different loading sequences:

$$N_{rem} = N - (n_1 + n_2 + \cdots + n_i) = N - \sum_{j=1}^{k} n_j \qquad 4\text{-}30$$

This can be written as:

$$N_{rem} = 10^{\frac{\alpha_j - \tau_{rem}}{\tau_j}} - \sum_{j=1}^{k} n_j \qquad 4\text{-}31$$

In which the $N_{rem}$ is the remaining life for cyclic stress ratio $i$ given for a certain remaining shear strength ($\tau_{rem}$). The single sequence of fatigue life reduction can be given by:

$$n_j = 10^{\frac{\alpha_j-(\tau_{aj}-\tau_{bj})}{\beta_j}} \qquad 4\text{-}32$$

where $n_j$ is the number of cycles consumed under an $j_{th}$ cyclic stress ratio $i$, leading to a reduction of the strength from $\tau_0$ to a strength level denoted as $\tau_{bj}$. In the case, when the remaining strength was already reduced (due to e.g. a past cyclic loading, or previous cyclic load set) the consumed fatigue life has to start from a lower strength equal to $\tau_{aj}$. This idea is presented in Figure 4.8. Also here, the $\alpha_j$, $\beta_j$ parameters are obtained from a regression line for a cyclic stress ratio $i_j$.

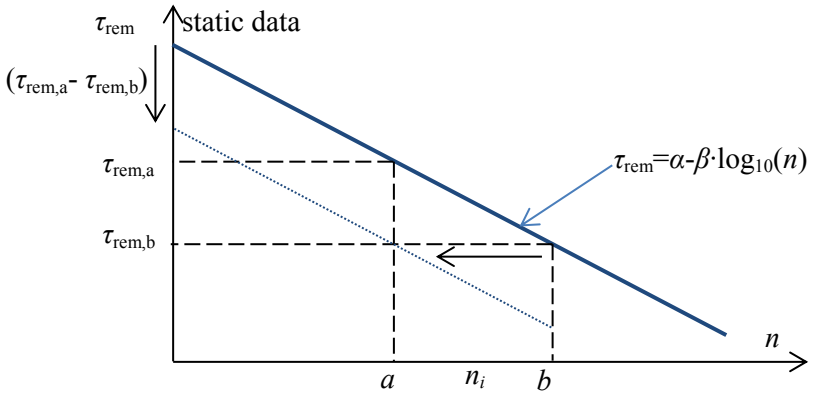


*Figure 4.8. Consumed part of the fatigue life in one sequence*

This gives final formulation for the remaining life:

$$N_{rem} = 10^{\frac{1.0-\tau_{rem}}{\beta} - \frac{\alpha_j-(\tau_{aj}-\tau_{bj})}{\beta_j}} \qquad 4\text{-}33$$

Care must be taken, however, that the lack of the sequence order effect has not been proven yet, and some tests on e.g. concrete show that the statement, that the fatigue damage is accumulated linearly, does not hold (Murdock, 1965). The proposed cumulative damage rule ignores the effects of loading sequence (similar to Palmgren-Miner rule). To overcome these shortcomings non-linear damage theories have been proposed e.g. Anderson (1991).

### 4.4.6. Effect of the mean stress and *R* ratio on the remaining strength of geomaterials

Additionally, the effects of the different mean and amplitude stresses on the remaining strength should also be investigated (chapter 3.5.3). These effects are included in the regression variable $\beta_j$. It is expected that the effects of the amplitude and mean loading on the remaining strength should be similar to the one described for the S-N curve (described in chapter 3.5). It means that the constant fatigue life diagram or Goodman diagram (see chapter 3.5.3) can be skipped for the remaining strength curve and the effects of different mean and amplitude stresses can be included directly into the $\beta_j$ parameter.

## 4.5. Constant friction angle in soil mechanics

In order to investigate more precisely the cyclic behaviour of geomaterials, the research into reduction of the shear strength $\tau$, given by the parameters $c$ and $\phi$, should be further extended.

It was assumed that the friction angle $\phi$ has a constant value. This corresponds to a statement of Van Baars (1996) who, based on discrete element modelling, notified that: "The strength of a cohesive material depends on the contact strength and the normal force distribution. The friction angle is constant and does not even depend on the contact force. The cohesion depends only on the strength of a single contact and on the number of contacts per micro volume."

The assumption of the constant friction angle $\phi$ was also confirmed by laboratory tests. Vyalov (1978) observed that for rocks, the decrease of strength over time is a result of a decrease in cohesion $c$ while the friction angle $\phi$ remains constant. Brantut et al. (2013), gave a summary of his tests, proving that brittle creep (permanent deformations under the influence of mechanical stresses) reduces the cohesion of rocks, but does not directly affect their internal friction. A cohesion reduction in weak rocks, based on similarities with creep and microcracks growth, was described by Larson (1998). Zhao (2000) found that rock material strength under dynamic loads can be approximately described by the Mohr-Coulomb criterion when the confining pressure was low and that the variation of cohesion with loading rate mainly led to a change in strength. From this all it must be concluded that only the cohesion is reduced by cyclic loading, while the friction angle $\phi$ remains constant.

### 4.6. Remaining cohesion curve

Based on the hypothesis of constant friction angle, one can propose a similar to remaining shear strength curve (see Figure 4.5), a curve for a remaining cohesion (see Figure 4.9). The remaining shear strength ratio $\tau_{rem}/\tau_0$ (or cyclic stress ratio $\tau_{cyc}/\tau_0$ for S-N curve) can be replaced by the remaining cohesion ratio $c_{rem}/c_0$.

$$\frac{c_{rem,j}}{c_0} = 1.0 - Y_j \log n \qquad 4\text{-}34$$

where $Y_j$ is a regression parameter, $c_{rem,i}$ is the remaining cohesion after an applied number of cycles $n$ at a given cyclic stress $\tau_{cyc,j}$ and $c_0$ is cohesion based on the linear regression for static tests. The intercept point of the regression line will be equal 1.0 (or 100%).

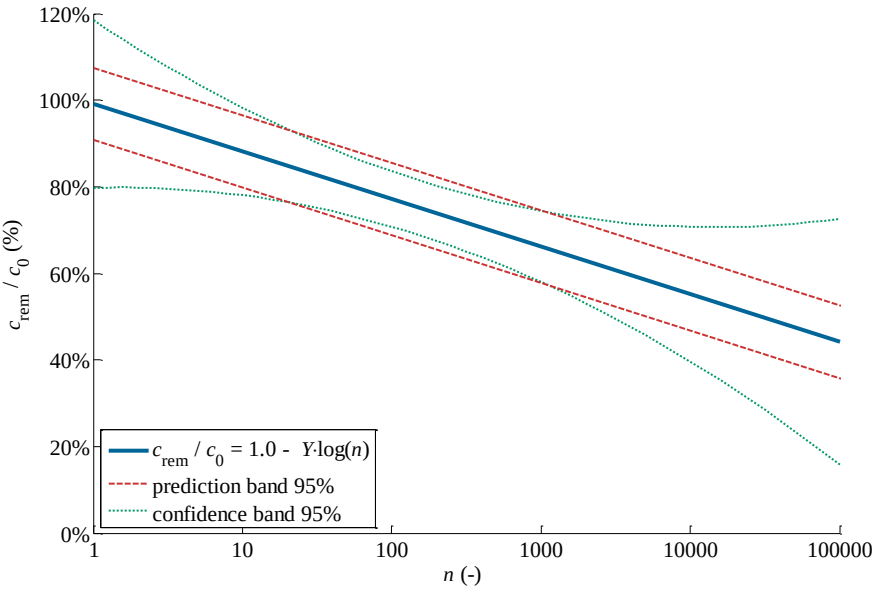


*Figure 4.9. Theoretical plot of the remaining cohesion curve*

*Remaining cohesion for the remaining shear strength curve*

For each test at the end of the cyclic loading, the remaining cohesion $c_{rem}$ is obtained simply, first by loading until failure and secondly by recalculating the cohesion from the remaining strength by using the Mohr-Coulomb equation. In Equation 4-1, the principal stresses correspond to the principal stresses in this loading until failure ($\sigma_{1,rem}$ and $\sigma_{3,rem}$). The friction angle $\phi$ is assumed to be equal to the friction angle calculated from the static tests. Based on this, the remaining cohesion for each test can be calculated from the following formula:

$$c_{rem,j} = \left(\frac{\sigma_{1,rem,j} - \sigma_{3,rem,j}}{2}\right)\frac{1}{cos\,\phi} - \left(\frac{\sigma_{1,rem,j} + \sigma_{3,rem,j}}{2}\right)tan\,\phi \qquad 4\text{-}35$$

where $\sigma_{1,rem,j}$ and $\sigma_{3,rem,j}$ are the principal stresses at failure after number of cycles $n$ (or $N$) for $j_{th}$ sample.

*Remaining cohesion for the S-N curve*

In the S-N curve the remaining cohesion can be obtained simply by replacing in Equation 4-1 the principal stresses by the cyclic stress parameters $\sigma_{1,cyc}$ and $\sigma_{3,cyc}$:

$$c_{rem,j} = \left(\frac{\sigma_{1,cyc,j} - \sigma_{3,cyc,j}}{2}\right)\frac{1}{cos\,\phi} - \left(\frac{\sigma_{1cyc,j} + \sigma_{3,cyc,j}}{2}\right)tan\,\phi \qquad 4\text{-}36$$

where $\sigma_{1,cyc,j}$ and $\sigma_{3,cyc,j}$ are the principal cyclic stresses at failure for $j_{th}$ sample.

### 4.6.1. Endurance limit for geomaterials – minimum level of a damaging cyclic loading

The existence of an endurance limit $\sigma_e$ of geomaterials is confirmed when a small cyclic stress ratio $\tau_{cyc}$ / $\tau_0$ does not cause a cohesion reduction and a large ratio does. One can propose three hypotheses for the description of this minimum level of the applied cyclic stress.

According to a first hypothesis of this endurance limit, the endurance limit $\sigma_e$ is higher than the cohesion $\sigma_e > c_0$ (Figure 4.10). It also means that the frictional part of the total strength is first cyclically loaded and the cohesion is loaded only at high cyclic stresses.

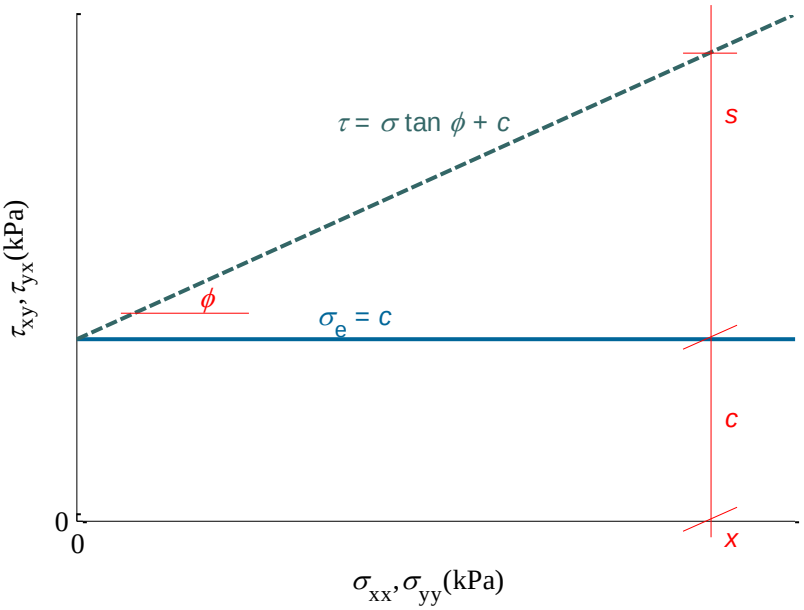


*Figure 4.10. Cohesion and frictional part of the strength - case 1*

According to a second hypothesis, the endurance limit $\sigma_e$ is higher than the frictional part of the strength (Figure 4.11) for a given confining pressure $\sigma_3$.

$$\sigma_e > \sigma \tan \phi \qquad 4\text{-}37$$

This also means that that the endurance limit increases when higher confining pressures are applied, and both, the frictional and cohesive part of total strength, are cyclically loaded proportionally. The cohesion reduction does not much depend on the cyclic stress ratio, but more on the frictional part of the total strength $\sigma \tan \phi$.

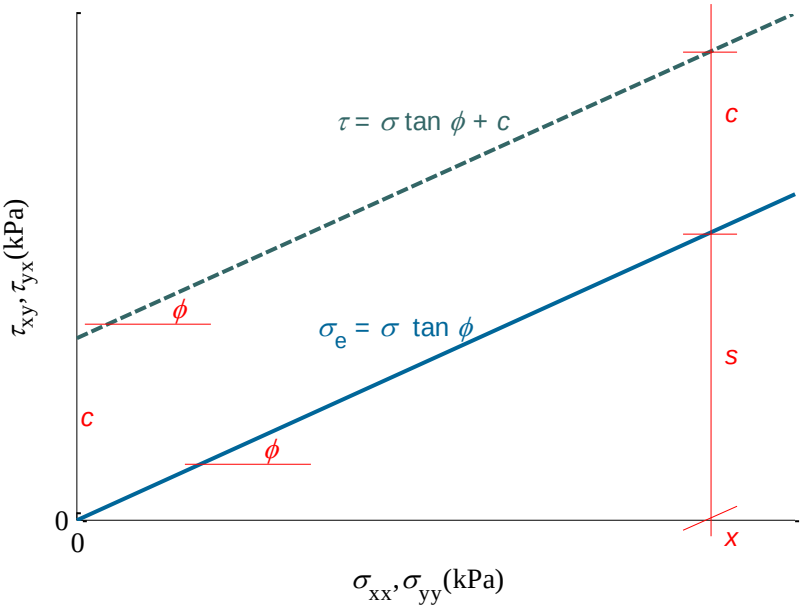


*Figure 4.11. Cohesion and frictional part of the strength - case 2*

According to a third hypothesis (Figure 4.12), the cohesion will always be reduced. The cyclic stress ratio is unimportant, so the endurance limit is $\sigma_e = 0$. It means that, as a first the cohesive part of total strength is cyclically loaded.

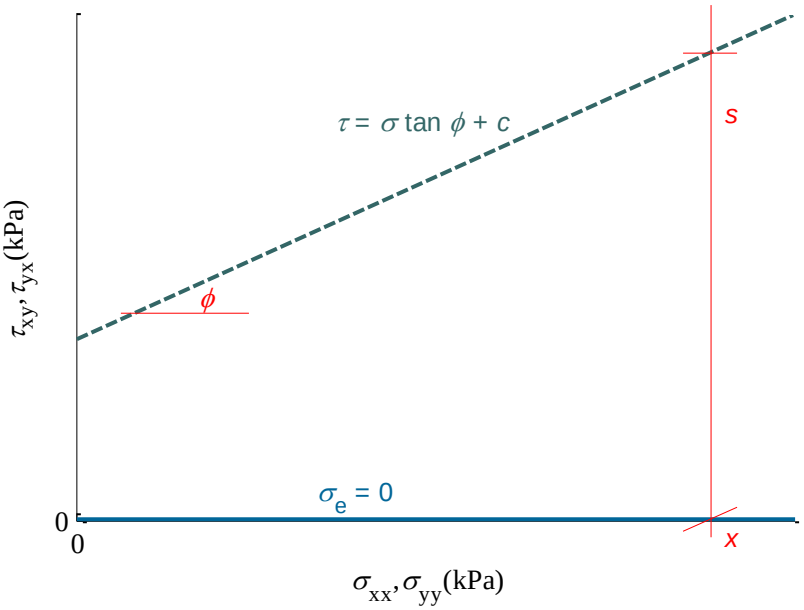


*Figure 4.12. Cohesion and frictional part of the strength - case 3*

The hypothesis of the existence of the endurance limit $\sigma_e$ for geomaterials can only be proven in laboratory tests. The first hypothesis is confirmed, when there is a threshold for the cyclic loading, higher than the cohesion, for which no cohesion reduction occurs. For the second hypothesis, the cohesion reduction becomes lower for higher confining pressures. The third hypothesis will be confirmed when the cohesion reduction always occurs, and the size of the cyclic loading and the confining pressure does not have any impact on the remaining shear strength.

### 4.6.2. Impact of confining pressure on cohesion in cyclic loading

The cohesion is only a part of the total shear strength of a geomaterial and it varies with the confining pressure according to the Mohr-Coulomb failure envelope. From the Mohr-Coulomb theory it follows that, for normal stress $\sigma = 0$ the whole strength comes from the cohesion (because $\tau = 0 \cdot \tan\phi + c$). It means that the cyclic load is fully applied on the cohesive part of the strength.

For an increasing normal stress $\sigma > 0$ (related to increase in confining stress $\sigma_3$), the part of the strength which comes from the cohesion $c$, decreases and the part of the strength coming from the friction increases (Mohr–Coulomb failure envelope).

*Cyclic loading on cohesion*

If one assumes that the second hypothesis from previous chapter (4.6.1) for geomaterials is valid (the endurance limit is dependent on the confining pressure), the cyclic loading acting on a material is loading only partially the cohesion of the material. Part of the cyclic loading

is "taken" by cohesion $c$ and part by the frictional part of the strength given as $\sigma \tan \phi$. The remaining cohesion depends thus not only on the cyclic stress ratio but also on the confining pressure $\sigma_3$. For higher confining pressures, the cyclic loading has thus probably lower impact on the shear strength reduction than for lower confining pressures (Burdine, 1963).

The cohesion $c$ can be calculated from:

$$c = \left(\frac{\sigma_1 - \sigma_3}{2}\right)\frac{1}{\cos\phi} - \left[\left(\frac{\sigma_1 - \sigma_3}{2}\right) + \frac{2\sigma_3}{2}\right]\tan\phi \qquad 4\text{-}38$$

where $\sigma_1$, $\sigma_3$ are the minor and major principal stresses.

Including into the Mohr-Coulomb equation the cyclic shear stress ratio $i$, the cyclically "loaded" cohesion $c_{\text{"loaded"}}$ can be calculated as:

$$c_{"loaded"} = \left(\frac{\sigma_1 - \sigma_3}{2}\right)\frac{i}{\cos\phi} - \left[\left(\frac{\sigma_1 - \sigma_3}{2}\right)\cdot i + \frac{2\sigma_3}{2}\right]\tan\phi \qquad 4\text{-}39$$

where $i$ is the cyclic stress ratio $\tau_{cyc}/\tau_0$. For $i$ =1.0, the cyclic load corresponds to the static strength and the equation is the same as for the Mohr-Coulomb failure envelope. It also means that the whole part of cohesion is in that case "loaded", which leads to failure of a material. For smaller values of $i$, the part of the cohesion, which is "loaded", decreases, because the $c_{\text{"loaded"}}$ is dependent on the confining pressure $\sigma_3$. The cyclic stress ratio $\tau_{cyc}/\tau_0$ = 50% is loading exactly 50% of the cohesion only for confining pressure $\sigma_3 = 0$. A plot of cyclically "loaded" cohesion as a part of the total cohesion under cyclic stresses for different confining pressures is given in Figure 4.13.

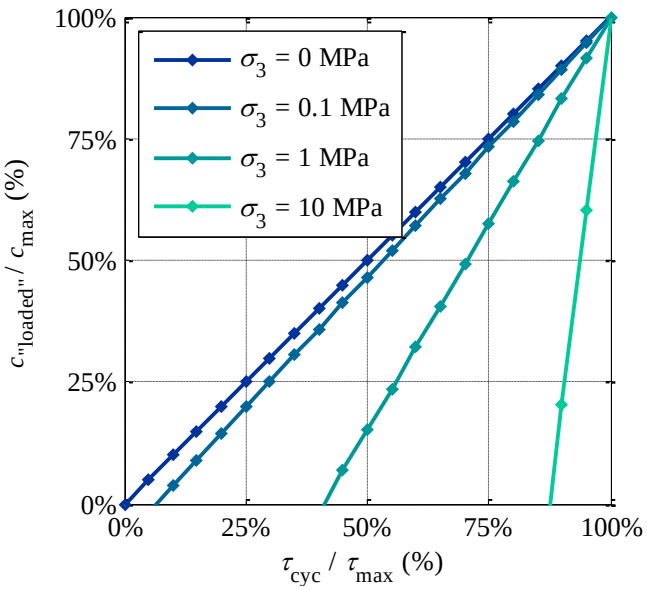


*Figure 4.13. Cyclically "loaded" cohesion as a part of the total cohesion under cyclic stresses for different confining pressures*

If a different cohesion reduction for the same cyclic stress but varied confining pressure is expected, one can consider what cyclic stress ratio $i$ should be applied to obtain the same cohesion reduction as under confining pressure of 0 MPa. If the cohesion should be loaded

e.g. 50% of the maximum cohesion $c$ under confining pressure e.g. $\sigma_3 = 0.5$ MPa, the cyclic stress ratio should be raised up to $i = 58\%$ according to the Equation 4-39 and Figure 4.13.

The consideration presented here can only be confirmed or rejected by cyclic triaxial tests. Some already conducted tests: e.g.: Kranz (1980) show that the life to fracture increased with increasing pressure, even when the stress differences were normalised to account for the increase in strength with pressure.

## 4.7. Unsolved issues for fatigue of geomaterials

There are many questions about the behaviour of geomaterials under repeated loading that need be answered. The most significant are:

- What is the main mechanism of soil and rock failure under cyclic loading?
- Which curve is the most suitable for describing the fatigue of geomaterials?
- Is a model with low number of variables adequate to describe the remaining shear strength of geomaterials under cyclic loading?
- What is the relation of the applied cyclic loading to the loss of shear strength?
- What is the fatigue limit or endurance limit (if applicable) for geomaterials?
- How can variable-amplitude loading be incorporated into the remaining shear strength curve?
- Is the linear cumulative damage rule (e.g. Palmgren-Miner) adequate for geomaterials?
- Is the order of various cyclic loadings important for the loss of strength of geomaterials?
- How can multiaxial fatigue problems and different cyclic loading stress directions ($\sigma_3$ as a cyclic loading, when $\sigma_1 - \sigma_3$ stays constant) be incorporated into the model?
- What is the impact of the environment on the strength results (temperature, water content, grain size, humidity etc.)?
- Is the behaviour of geomaterials the same for low confining pressures as for higher pressures?
- Can both, the low cycle fatigue and high cycle fatigue, be incorporated into one remaining shear strength formulation?

## 4.8. Conclusions

In this chapter a simple remaining shear strength curve was proposed. The curve has some advantages and can be competitive to the standard S-N curve. Laboratory tests are required to confirm of neglect the usefulness of the remaining shear strength curve. Additionally, based on the assumption of a constant friction angle in soil mechanics, the remaining shear strength curve was extended to the remaining cohesion curve. Thus, the fatigue of geomaterials can be described as a fatigue of the cohesion, which can be easily incorporated into the geotechnical standards. The proposed remaining cohesion curve was given for both, the S-N and the remaining shear strength curves. It can be noticed that both formulations are very simple and similar (see Equations 4-13 and 4-23), which is a big advantage for an application of this

formula in standards.

# 5. LABORATORY TESTS

## 5.1. Introduction

The remaining shear strength curve, proposed in chapter 4, should be tested and proved in laboratory tests before being adopted into guidelines. The number of laboratory fatigue tests for geomaterials described in literature is very small (see chapter 3.7), and therefore insufficient to validate the remaining shear strength curve. For this validation triaxial laboratory tests were chosen. The advantage of the triaxial machine is that the machine can be electronically controlled which makes it possible to conduct cyclic tests and register all important data.

Prior to the triaxial tests, several points have been considered. First, the planning and the test preparation had to be done. Second, a specially designed controlling program has been written, based on the required models and parameters for the cyclic triaxial testing procedure. Third, the right type of material has to be properly chosen; since the material should be as homogeneous and isotropic as possible, so that the results will be most accurate and useful for describing and calibrating the remaining shear strength curve.

## 5.2. Triaxial laboratory tests

The triaxial test is one of the most common and widely performed geotechnical laboratory tests for determination of the shear strength and stiffness parameters. The strength parameters obtained from the test, the friction angle $\phi$ and cohesion $c$, will be investigated on its reduction during cyclic loading.

### 5.2.1. Laboratory test equipment

The main components of the triaxial cell and servo-hydraulic loading system for the deviatoric and confining stress are presented in Figure 5.1 and Figure 5.2.

The laboratory equipment at the University of Luxembourg consists of 3 sets of:

- Triaxial machine 28-WF4005 Tritech 50 kN (Figure 5.1) built on a triaxial loading frame (Figure 5.3),
- Plexiglas chamber (Figure 5.5 and Figure 5.2),
- Displacement gauges,
- Pressure and force transducers,

- Hydraulic cell and back pressure controllers (Figure 5.4),
- PC connected with National Instruments data logging system with installed LabVIEW software.

*Figure 5.1. Triaxial apparatus*

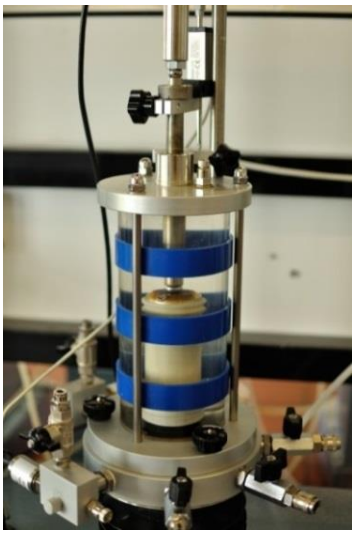

*Figure 5.2. Plexiglas chamber*

*Measurement precision*

The axial transducer stress measurement precision is ±0.001 kN. Both, the loads (forces) and the axial strains, are measured. The strains are monitored by potentiometric displacement transducer. Measurement precision of the axial displacement is ±0.002 mm. The confining pressure was held constant up to ±10 kPa during each experiment. The precision of the measured confining pressure is about ±1 kPa. The pressure, axial stress and displacement were sampled every half a second. The measurement instruments were calibrated by the manufacturer, who provided corresponding certificates. Additionally, the calibration check was done in the lab by comparing the readings with the model set up.

*Figure 5.3. Triaxial load frame*

*Figure 5.4. Cell and back pressure controllers*

*Influence of friction on sample ends*

The triaxial tests can be influenced not only by the machine setup but also the sample placement in the triaxial machine. One of the causes of the internal non-uniformity is the contact between the sample and caps at the top and bottom end platens. Because the sample ends are restricted, some additional shear stress has to be applied to cause a failure and the true shear strength is unknown. Some techniques are sometimes used to reduce the friction at sample ends e.g. bearings.

However, elimination of friction has little effect on samples of standard height. Goto and Tatsuoka (1988) showed that the value of friction angle in dense sand can be larger of about 1° for regular end that with lubricated ends, which is not a high value. The ball-seated platens can also induce shear stresses at the sample ends which are likely to vary as the test proceeds.

The enlarged end platens were not used because the radial expansion of the specimen is small (low shear strains) and e.g. the bulging of the specimens was not happening.

### 5.2.2. Test set-up

In the triaxial machine set-up presented in this thesis, (Figure 5.5and Figure 5.1) a cylindrical soil specimen is surrounded with a confining medium (water) and the vertical stress is applied by a piston (Figure 5.5), along the axis of the cylindrical sample. The vertical stress is different from the stresses applied in the horizontal directions (the confining pressure).

The confining pressure is transmitted through the water surrounding the test specimen in a plexiglas chamber (Figure 5.5 and Figure 5.2), where the pressure is applied by a constant pressure hydraulic pump. To remain dry, each specimen is sealed on the top and bottom by platen and a latex membrane in the sides. The confining pressure is equal for all horizontal directions and only in a true triaxial test the stresses can be different for all three directions. The pressure is monitored by a pressure transducer connected to the triaxial cell. The pore pressure changes were not measured because all tests were conducted on dry (unsaturated) samples. The diameter of each sample is 38mm.

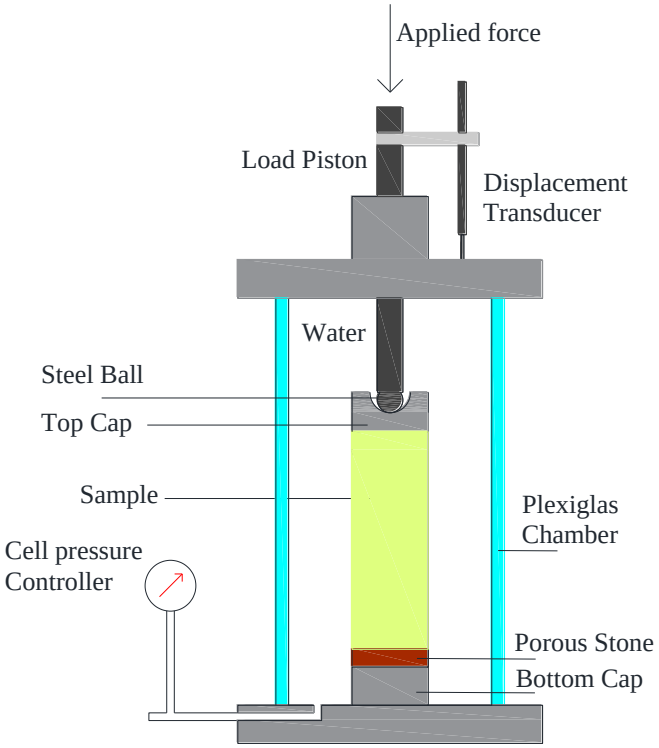


*Figure 5.5. Load cell scheme*

The deviatoric loading is applied through a piston that enters the top cell through a bushing, and pushes against the top cap of the specimen. The movement of the piston is controlled by an electro-mechanical actuator and measured by a 5 kN load cell. A ball-bearing fitted between the coned end of the piston and a similar recess in the cap. This allows correcting a small misalignment while loading is gradually applied, but it may give however, an uncertain start to the stress-strain curve. The displacement is measured outside the cell and the force transducer is attached after the piston.

The piston was loosely fitted (BS 1377:1990 specifies that friction between the piston or seal and its bushing shall be small enough to allow the piston to slide freely under its own weight when the cell is empty). Because the friction was small no correction for friction on loading piston with load cell was applied.

To simulate cyclic loading on geomaterials, the triaxial machine was programed to apply constant cyclic loading up to certain threshold. The cyclic load stress ratio was set to $\tau_{cyc}/\tau_0$ = 40%, 60%, 80%, of the maximum strength respectively, for each confining pressure $\sigma_3$ (100, 300, and 500 kPa). For the remaining shear strength curve, a series of $n$ = 10, 100, 1000, 10 000 and 100 000 cycles were investigated. 20% of the cyclic stress was applied for the highest number of cycles $n$ = 100 000, to assure that no failure will occur before reaching this number of cycles. In the case of the S-N curve, the tests were run until failure (until the moment where the sample could not be loaded up to certain cyclic load threshold). More details of the cyclic triaxial tests is presented in the subsequent chapters.

### 5.2.3. Organisation of the laboratory triaxial tests

The triaxial laboratory tests are divided into two series:

1. Static triaxial tests
2. Cyclic triaxial tests

### 5.2.4. Series I - static tests

A series of static load tests are conducted in order to determine the shear strength parameters of the Mohr-Coulomb failure criterion. These parameters (cohesion and friction angle) will be calculated from the regression line (described in chapter 5.5). The static triaxial tests were conducted according to the norms e.g. BS 1377: Part 8 (1990) and testing manuals e.g. Day (2001).

### 5.2.5. Series II - cyclic triaxial tests

The aim of the cyclic tests is to investigate the remaining shear strength of geomaterials after cyclic loading has been applied. This will be done by comparing the shear strength parameters $c$ and $\phi$ obtained from the static tests with the results from cyclic tests. The cyclic tests are based on multiple loadings and unloadings under constant confining pressure: $\sigma_2 = \sigma_3$.

Two different types of cyclic tests have been performed based on the testing method:

I – S-N curve
II – Remaining shear strength curve

Modifications of the two main curves can also be considered:

III – Cyclic confining pressure
IV – Various mean and amplitude cyclic loadings

The first two test types (I and II) are used for investigating the fatigue of geomaterials. The last two test types (III and IV) provide a better insight into the material behaviour, however, due to time and equipment limitations, they have not been performed. All types of test are explained below.

*I – S-N curve*

The methodology to obtain the S-N curve is to count the number of cycles until failure $N$ for a given cyclic loading $\tau_{cyc}$ (Figure 5.6). Each test is conducted under constant confining pressure $\sigma_3$. Based on tests of several cyclic stress ratios, the S-N curves for soils and rocks can be developed. This type of test is a typical fatigue test in mechanical engineering (described in chapter 3.5.2). Unfortunately it is difficult to predict the time required for fatigue description, which is a problem, because triaxial tests require more time. Insight into the required time is given by e.g. ASTM E739–91 (1998), which recommends a minimum number of specimens needed to prepare an S-N curve as 6 to 12 for preliminary and exploratory and 12 to 24 for design allowable data and reliability data (for steel).

*II – Remaining shear strength curve*

In the remaining shear strength tests the samples are first subjected to cyclic loading $\tau_{cyc}$ for a given number of cycles $n$. In the last cycle, the samples are loaded until failure following the same procedure as the static strength tests (Figure 5.7). These tests will provide information about the remaining shear strength of the material after a number of applied cycles. Since the time of one cycle is known from static tests, all tests can be scheduled easily. The prematurely failed samples are not taken into account in the calculations.

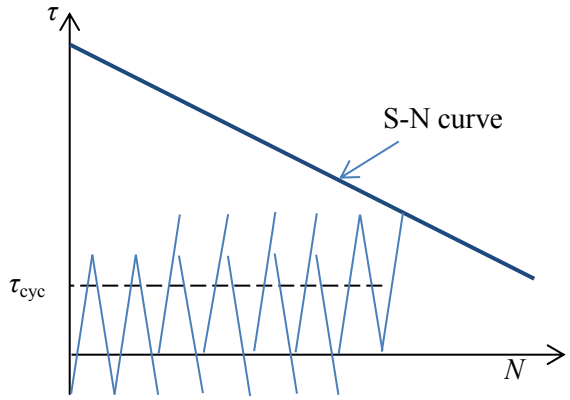


*Figure 5.6. S-N curve*

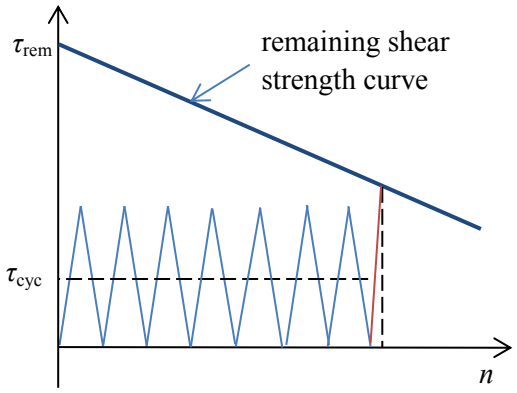


*Figure 5.7. Remaining shear strength curve*

*III – Cyclic confining pressure*

This type of test is similar to the previous two types (the S-N and the remaining shear strength curve), but in this case the minimum principal stress $\sigma_3$ is cyclically changed instead of $\sigma_1$. These tests give the information about the influence of the smallest principal stress changes $\sigma_3$ on the strength parameters reduction and increase the accuracy of the prediction of fatigue of geomaterials. The biggest disadvantage of this type of test is that the pressure $\sigma_3$ is difficult to be controlled accurately in a reasonable time. That means that this type of test is challenging to carry out in a laboratory and it can take more time.

*IV – Various mean and amplitude cyclic loadings*

In this type of test, different cyclic stresses are applied in which the minimum stress does not return to "zero". Using different cyclic stresses (with different mean and amplitude stresses) make it possible to predict more accurately the total strength reduction due to various types of cyclic loading and also to make a more accurate prediction of the fatigue life for the material. This however requires a lot of laboratory testing.

The overview of the laboratory tests is presented in the Table 5-1. The detailed description of each test is presented in appendix in the referenced tables (from Table A-1 to Table A-24).

*Table 5-1. Overview of the laboratory tests*

| Type of triaxial test | Type of geomaterial | Table | No of conducted tests |
|---|---|---|---|
| Static tests | Artificial gypsum | Table A-1 | 37 |
| | Mortar (beach sand, 1week, cement/sand = 0.5) | Table A-2 | 11 |
| | Mortar (coarse sand, 1week, cement/sand = 1.5) | Table A-3 | 5 |
| | Mortar (coarse sand, 1week, cement/sand = 1.0) | Table A-4 | 6 |
| | Mortar (coarse sand, 1month, cement/sand = 1.0) | Table A-5 | 7 |
| | Limestone (vertical samples) | Table A-6 | 4 |
| | Limestone (horizontal samples) | Table A-7 | 6 |
| | Crumbled limestone | Table A-8 | 6 |
| | Norm sand | Table A-9 | 4 |
| | Beach sand | Table A-10 | 3 |
| | Coarse sand | Table A-11 | 3 |
| Cyclic tests (S-N curve) | Artificial gypsum | Table A-12 | 47 |
| | Mortar (beach sand, 1 week, cement/sand = 0.5) | Table A-13 | 9 |
| | Mortar (beach sand, 1 week, cement/sand = 1.0) | Table A-14 | 4 |
| | Mortar (coarse sand, 1 month, cement/sand = 1.0) | Table A-15 | 3 |
| Cyclic tests (Remaining curve) | Artificial gypsum | Table A-16 | 44 |
| | Mortar (beach sand, 1week, cement/sand = 0.5) | Table A-17 | 19 |
| | Mortar (beach sand, 1week, cement/sand = 1.0) | Table A-18 | 16 |
| | Mortar (beach sand, 1month, cement/sand = 1.0) | Table A-19 | 10 |
| | Limestone | Table A-20 | 10 |
| | Crumbled limestone | Table A-21 | 7 |
| | Norm sand | Table A-22 | 7 |
| | Beach sand | Table A-23 | 6 |
| | Coarse sand | Table A-24 | 2 |
| | | Total | 276 |

## 5.3. Cyclic test parameters

In cyclic tests the several parameters affect the test results to a greater or lesser extent (chapter 3.7.1). Among these, the following can be identified as being important in fatigue testing:

- Loading pattern,
- Cyclic stress and cyclic stress ratio,
- Stress ratio $R$,
- Control mode,
- Frequency,
- Waveform,
- Type of triaxial tests.

This will be further explained below.

*Loading pattern*

To be able to conduct cyclic tests, the most important parameter is the type of cyclic loading. The loading can be divided in terms of the sign of the acting loading:

- From zero $\sigma_{min}$ to max $\sigma_{max}$ and back (load is applied to a maximum value and later the load is completely removed),
- From positive $\sigma_{min}$ to max $\sigma_{max}$ and back (the acting load is not completely removed),
- From negative (minimum) $\sigma_{min}$ to positive (maximum) $\sigma_{max}$ and back (fully-reversing loads, typical compression-tension tests).

For the tests presented in this thesis, a constant amplitude with zero minimum stress level $\sigma_{min} = 0$ was chosen, because it is the basic type of cyclic loading and it is easy to be controlled by the program. Probably the total removal of stress is causing smaller sample disturbance than the disturbance which could be caused by applying some minimum load different from zero. This could be supported by the fact, that the total removal of load did not produce disturbances in the stress–strain plot. Importantly, the lower range of cyclic loading is probably also less important on the strength reduction than the $\sigma_{max}$.

The pattern of the cyclic loading is presented in Figure 5.8.

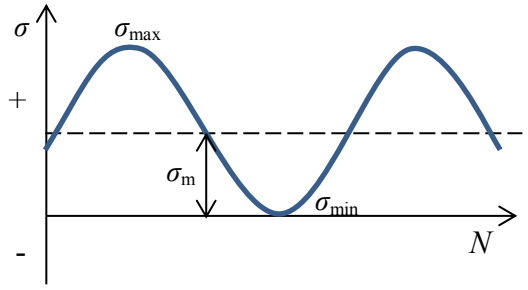


*Figure 5.8. Cyclic loading pattern*

*Cyclic stress*

The cyclic stress ratio is given as a ratio of applied cyclic shear stress $\tau_{cyc}$ to the shear stress $\tau_0$ based on the linear regression for static tests:

$$i = \frac{\tau_{cyc}}{\tau_0} = \frac{\frac{(\sigma_{1,max} - \sigma_{1,min}) - \sigma_3}{2}}{\frac{\sigma_1 - \sigma_3}{2}} \qquad 5\text{-}1$$

where $\sigma_{1,max}$ is the maximum and $\sigma_{1,min}$ is the minimum principal cyclic stress. Finally, the cyclic shear stress ratio can also be given as a ratio of the deviatoric cyclic stress $\sigma_{d,cyc}$ to the static deviatoric stress $\sigma_{d,0}$:

$$i = \frac{\sigma_{d,cyc}}{\sigma_{d,0}} \qquad 5\text{-}2$$

Three different cyclic stress ratios were applied $i = \tau_{cyc}/\tau_0 = 40\%$, 60%, and 80%. Only for the tests with the highest number of cycles this ratio was lowered to 20%. These applied values assure that the range of applied cyclic loads is widely covering most of the spectrum of

possible cyclic loads, when the extreme values are avoided.

In all tests the minimum cyclic loading $\sigma_{1,\min}$ was equal to 0 Pa (complete unloading) and thus the mean stress $\sigma_m$ is therefore simply a half of the deviatoric cyclic stress $\sigma_{d,cyc}$:

$$\sigma_m = \frac{\sigma_{d,cyc}}{2} \qquad 5\text{-}3$$

*Stress ratio R*

The type of the applied load, whether tensile or compressive or even a combination of both, can be easily determined by the stress ratio *R*, i.e. the ratio of the minimum to the maximum applied cyclic stress (here as a cyclic deviatoric stresses). The geomaterials usually have a very low tensile strength, and the most important strength parameter is the shear strength, therefore, the $R \geq 0$. In the laboratory tests presented here, all tests were conducted for $R = 0$, because:

$$R = \frac{\sigma_{min}}{\sigma_{max}} = \frac{0}{\sigma_{max}} = 0 \qquad 5\text{-}4$$

*Control mode*

In general, a fatigue test can be performed under load (stress) or under displacement (strain) control. Even though the triaxial machine is originally displacement controlled machine, a special program written in LabVIEW allowed the triaxial machine being stress controlled (by setting up the maximum and minimum axial stresses). The precise stress level obtained by constant slow displacement application decrees the measurement and loads uncertainties and also allows registering the post-peak behaviour of materials. The maximum and minimum stresses have to be controlled because usually the stress is the parameter which is directly measured (e.g. the loading of a track on the bridge) and the purpose of this research is to investigate shear strength reduction, not cyclic strain behaviour, which was already studied in literature (chapter 2.2.1).

*Frequency*

In contrast to metals, the fatigue life of geomaterials is probably affected by the frequency of loading (see chapter 3.7.1). Another important factor which has to be considered is the triaxial machine and laboratory data logger sensitivity: the higher the strain rate, the less accurate reading from data loggers is. To provide a typical low speed cyclic loading condition for geomaterials (see chapter 3.7.1) and accurate data readings of the force, the applied speed of the cyclic loading was set to $v = 0.5$ mm/min. This corresponds to a frequency of the loading equal $f = 0.01$ Hz (e.g. a wave load) and would reduce the data error readings, especially for higher frequencies. Therefore, the cyclic-dynamic and dynamic loading can be omitted and only the cyclic loading will be considered in this paper.

*Waveform*

The shape of the applied load can affect the fatigue test results. The sinusoidal waveform Figure 5.9) is the most commonly used in fatigue testing. Other types of loading are: the

triangular, step, square, and saw-tooth waveforms. In the thesis presented here the shape is not exactly sinusoidal, because the unloading speed was higher in order to save the time.

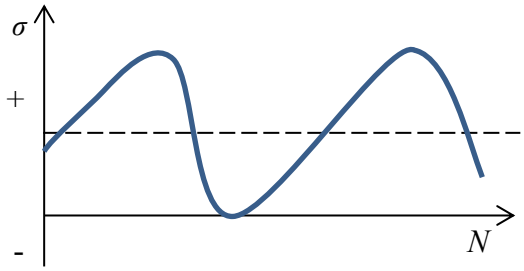


*Figure 5.9. Wave form of the applied cyclic loading*

*Type of triaxial tests and saturation*

All performed laboratory tests are drained with natural moisture conditions. Introducing pore pressure would significantly complicate the description of shear strength reduction in cyclic loading. Therefore the changes in pore pressure due to cyclic loading were omitted, and e.g. the liquefaction mechanism (chapter 2.2.2) did not have to be investigated.

All used materials had a natural degree of saturation. The limestone blocks were kept covered in dark and cool place, in order to preserve the natural water content of that rock. The gypsum material and mortar samples (after curing time) were also kept in dark place in constant room temperature. During the tests, all samples were sealed in a rubber membrane, and no saturation was provided.

## 5.4. Triaxial machine setup

The triaxial machine is connected through a RS 232 port with a computer. A program was written in LabVIEW (Figure 5.11) for applying cyclic loading on the sample in the triaxial machine and to log data from sensor readings (Figure 5.12). The program allows to control the speed of applied cyclic loading, to adjust the applied cyclic stress (minimum and maximum cyclic stress) and to run a desired number cycles (in case of S-N test, the number of cycles is set very high, so that the material will fail before). The program can be easily modified for other types of cyclic tests (different loading pattern or control mode). The schematic LabVIEW program loop is presented in Figure 5.10.

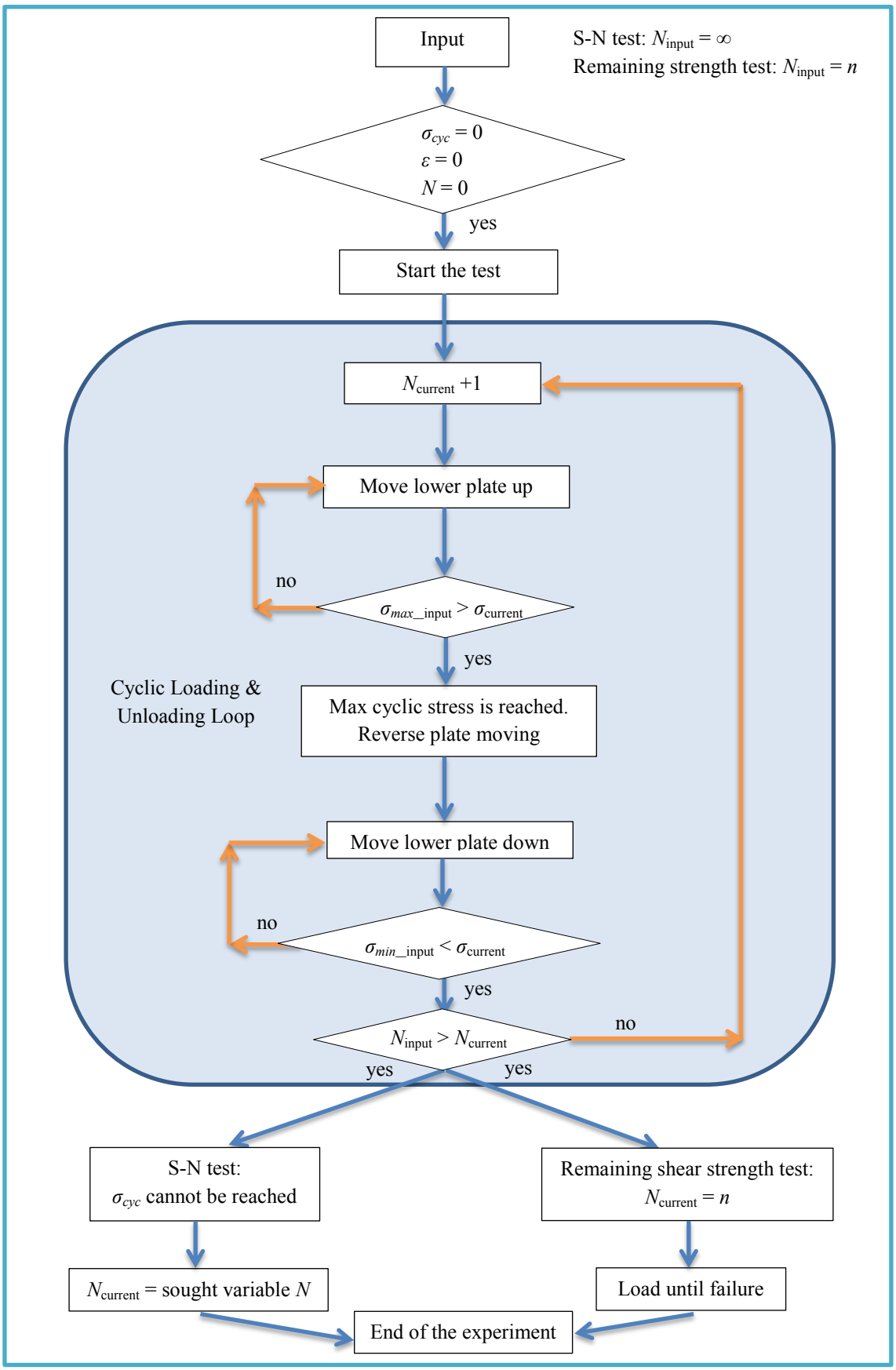


*Figure 5.10. LabVIEW cyclic loading program – scheme*

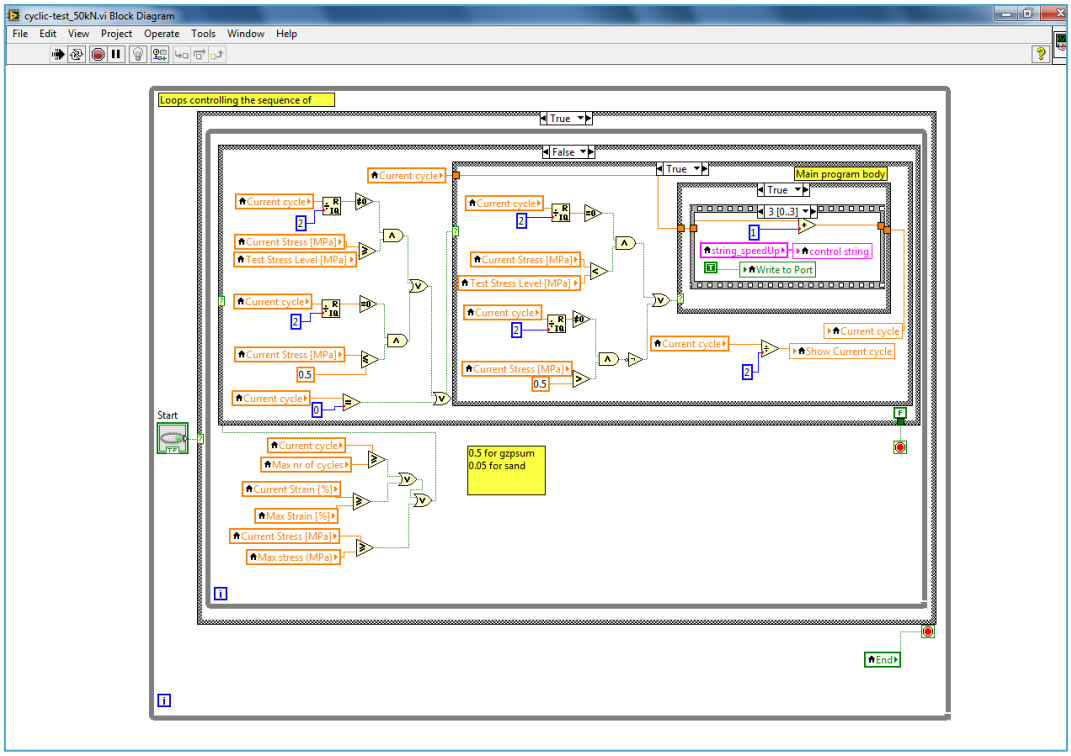


*Figure 5.11. LabVIEW program - graphical block diagram (the LabVIEW-source code)*

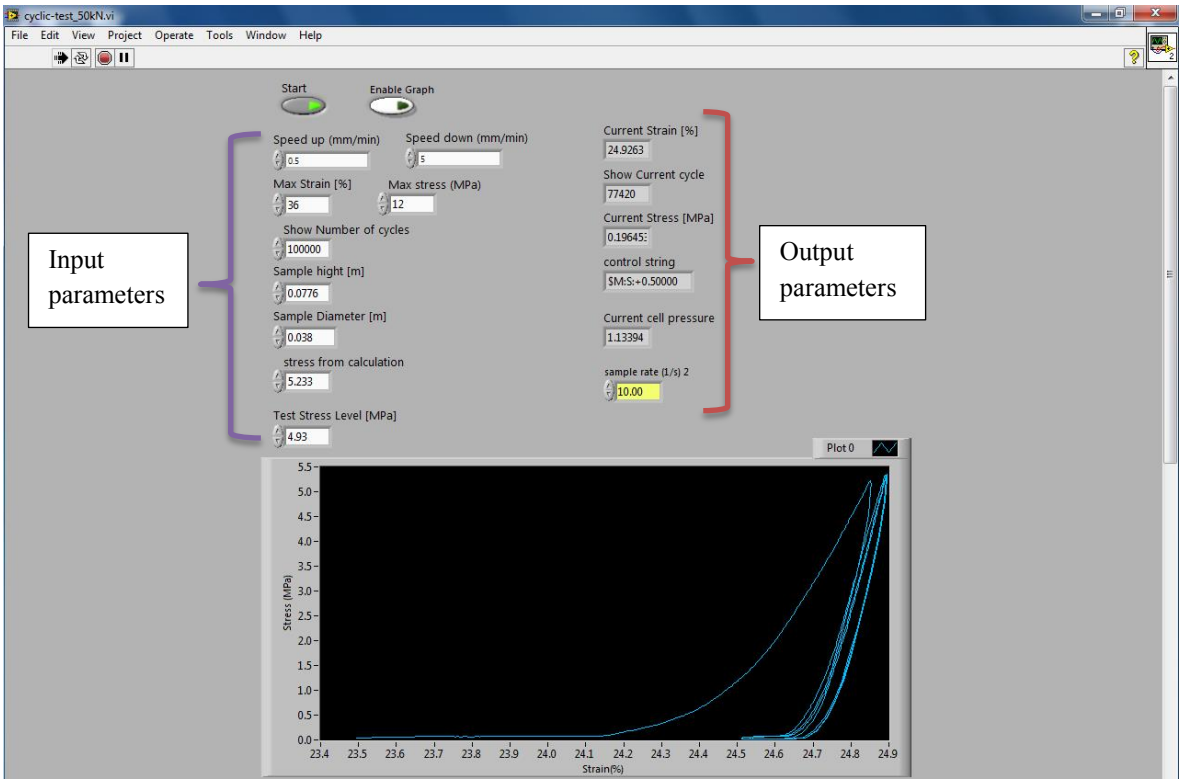


*Figure 5.12. LabVIEW program main window*

*Input parameters and equipment limitations*

- Sample diameter $d = 38$ mm
- Sample height $h = 78$ mm

- Max load of triaxial load frame $F_{max}$ = 50 kN
- Speed of the applied displacements $v$ = 0.25 mm/min
- Max possible speed of the app. displacement $v_{max}$ = 9.9 mm/min,
- Max possible confining pressure $\sigma_{3,max}$ = 1.7 MPa

*Measured parameters in static test*

- Deviatoric stress $\sigma_d$
- Strains $\varepsilon$
- Confining pressure $\sigma_3$

*Input parameters for cyclic test*

- Speed of the displacement up 0.25 mm/min
- Speed of the displacement down 5 mm/min
- Time of fatigue test for 1000 cycles 1 day
- Cyclic stress ratio $\tau_{cyc}/\tau_0$ (40%, 60% and 80%)
- Applied number of cycles $n$ (for remaining shear strength curve)

*Measured parameters in cyclic test*

- Number of cycles $N$ (for S-N curve)
- Cyclic stresses $\sigma_{cyc}$
- Plastic strain accumulation $\varepsilon_p$

### 5.5. Data presentation convention

Three common ways are applied in geoengineering to present in a graphical form the laboratory data of the stress state:

- Mohr's circles,
- Stress path,
- $\sigma_3$ - $\sigma_1$ space plot.

Mohr's circle provides a graphical representation of the stresses in any direction acting at a point. The stress paths method is a convenient technique in which the stresses in a point are represented by two characteristic parameters $\delta$ – is the slope and $b$ – interception with the $y$ axis. The $\sigma_3$ - $\sigma_1$ space is commonly used in rock engineering because it can provide quick and simple estimation of the increase in strength $\sigma_1$ with an increase in the confining stress $\sigma_3$.

*Mohr circles*

Usually the failure envelope (Figure 5.13) is presented in the form of the Mohr-Coulomb equation (compare with Equation 4-1):

$$\tau = c + \sigma \tan\phi \qquad 5\text{-}5$$

where

$$\tau = \frac{\sigma_1 - \sigma_3}{2}, \sigma = \frac{\sigma_1 + \sigma_3}{2} \qquad 5\text{-}6$$

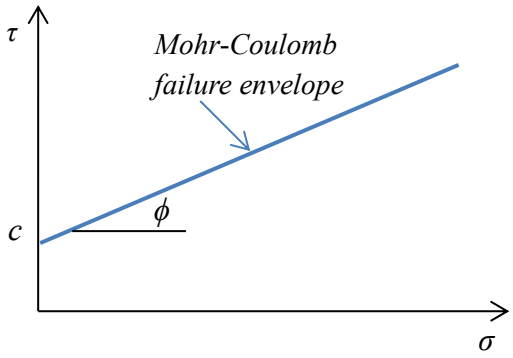


*Figure 5.13. Mohr-Coulomb failure envelope*

*p-q space*

In $p - q$ space (sometimes also denoted as a $\tau - \sigma$ space) each point can be characterised by the average of the minor and major principal stresses and the difference of the major and minor principal stresses. The introduction of the factor 0.5 in the two definitions of $q$ and $p$ make them the location of the centre, and the radius of the circle in Mohr's diagram.

There are two common methods of presenting the stress path:

- The MIT convention described by Lambe & Whitman (1969), which is more accurate in describing the strength in stress plots,
- The critical state convention – Oxford convention given by Schofield & Wroth (1968) which is often used in constitutive model, like Cam Clay, which describes better the stiffness of the soil.

The MIT stress path convention is given as

$$p = \frac{\sigma_1 + \sigma_3}{2}$$
$$q = \frac{\sigma_1 - \sigma_3}{2} \qquad 5\text{-}7$$

The Oxford convention is:

$$p = \frac{\sigma_1 + \sigma_2 + \sigma_3}{2}$$
$$q = \sigma_1 - \sigma_3 \qquad 5\text{-}8$$

In this thesis the MIT notation is used, because this notation gives more accurate results than the Oxford one for the strength description of geomaterials (Coulomb).

The possible stress states are limited by the Mohr-Coulomb failure criterion expressed as:

$$q = p \sin\phi + c \cos\phi \qquad 5\text{-}9$$

This describes a straight line in the $p$ - $q$ diagram. This straight line has been showed in Figure 5.14. The slope of this line $\delta$ is equal to sin $\phi$, which is slightly less steep than the

envelope in the diagram of Mohr circles (in this case tan $\phi$). The intersection with the vertical axis is:

$$b = c \cos \phi \qquad 5\text{-}10$$

For $\sigma_2 = \sigma_3$ the shear strength of the material is probably at its lowest point, because $\sigma_3$ is the minimal principal stress and for $\sigma_2$ the Mohr-Circles in 3D gives the minimum radius and strength (in case $\sigma_2$ has any influence on the strength).

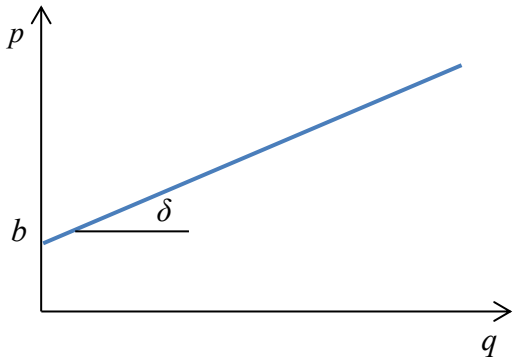


*Figure 5.14. Stress paths*

The cohesion - $c$, the friction angle - $\phi$, and uniaxial tensile strength - UTS can be calculated from the formulas given below:

$$\phi = arc \sin \delta \qquad 5\text{-}11$$

$$c = b / \cos \phi \qquad 5\text{-}12$$

$$UTS = c \frac{c \cos \phi}{1 + \sin \phi} \qquad 5\text{-}13$$

where, $\delta$ is the tangent angle of failure line, and $b$ is the ordinate for $\sigma = 0$ in a $p$ - $q$ diagram from the Equation 4.4.

*$\sigma_3$ - $\sigma_1$ space*

The Mohr-Coulomb failure parameters can be calculated from the plot in $\sigma_1$-$\sigma_3$ space as

$$\phi = asin\left(\frac{tan\,\theta - 1}{tan\,\theta + 1}\right) \qquad 5\text{-}14$$

$$c = \sigma_c \left(\frac{1 - \sin \phi}{2 \cos \phi}\right) \qquad 5\text{-}15$$

where $\theta$ is slope and $\sigma_c$ - intercept in $\sigma_3$ - $\sigma_1$ space – see Figure 5.15.

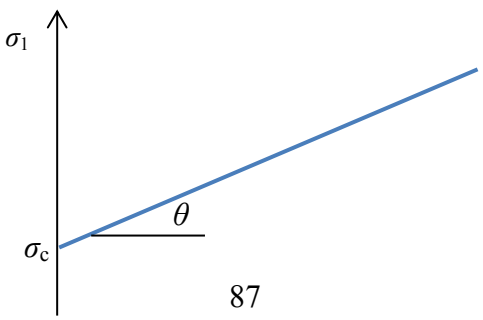

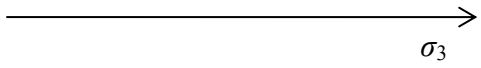


*Figure 5.15. $\sigma_3$ - $\sigma_1$ space*

*The chosen method used in this thesis*

It was found (see Appendix A.a) that the most accurate prediction of the friction angle $\phi$ and cohesion $c$ can be obtained from the p-q plot. Also for the p-q method the derivation of the Mohr-Coulomb failure envelope parameters is the easiest. Therefore, the p-q convention has been chosen to calculate the shear strength parameters for both the static and the cyclic tests.

## 5.6. Characteristic of used materials

Four different kinds of geomaterials were chosen for the investigation of the cyclic behaviour and fatigue of geomaterials. These four materials are divided into 2 groups:

a) Cohesive
- artificial gypsum,
- mortar (cemented sand),

b) Cohesionless (low-cohesive or non-cohesive)
- limestone,
- crumbled limestone and various sands.

Several standards for rock and soil sampling were taken into account for the preparation of the samples for triaxial tests e.g. ASTM D4543-01 (2001), ISRM (1979, 1983 and 1999). Based on these standards, the samples were prepared in order to assure flatness of the surfaces, which were parallel to each other and perpendicular to the sample vertical axis. All samples had the same diameter to length ratio equal 1:2 (diameter $d$ = 38 mm and height $h$ = 78 mm). In the following chapters (5.6.1 and 5.6.2) a more detailed description of the materials is given.

### 5.6.1. Cohesive materials

First experiments have been carried out on an artificial gypsum (construction block), because it was assumed that this artificial gypsum can provide more accurate and consistent results than natural materials and can be used as an example of a weak unjointed brittle rock.

Later, artificially prepared mortar samples, made from a mixture of sand, water and cement were used to simulate weak rocks. It was expected that samples prepared in a controlled way in the lab, would have very accurate and coherent strength properties.

*Artificial gypsum*

The artificial gypsum is a typical material (Figure 5.16 and Figure 5.17) used in a construction of a non-load bearing partition wall and is usually composed of gypsum plaster and water.

*Figure 5.16. Standard gypsum construction block*

*Figure 5.17. Samples drilled from the standard gypsum block*

Gypsum blocks are manufactured according to the European norm EN 12859 (EN 12859, 2012). The dimensions of European standard gypsum blocks are: length: 666 mm, height: 500 mm. Three blocks thus make area an $A$ =1 m².

The investigated gypsum block has a thickness equal to a 100 mm. This allowed trimming of the samples after the drilling phase. The drilling was done by a core drilling machine. Water cooling was not necessary because the material was soft (Figure 5.17). The average density of the used gypsum blocks is $\rho$ = 1.0 g/cm$^3$.

*Mortar – cemented sand*

Mortar can be used to simulate rock and cemented soil material. The mortar samples were prepared from a mixture of clean durable sand, cement and water with constant proportions (Figure 5.18). Typical construction sand (coarse sand), meeting grading requirements for fine aggregates, was mixed with a high amount of quick cement to ensure high strength. Great care was made in preparing identical, high-quality samples to improve reproducibility of the tests results.

The proportion which would give the best result (high cohesion with small data point spread) had to be investigated first. After testing of a several proportions (see chapter: 6.2.2), the best ratio was found to be 3:3:1 (sand to cement to water). The water-cement (*w*/*c)* ratio was set to 0.33 to provide easy flow and placement of the mixture into a metal mould.

*Figure 5.18. Setup for mortar samples preparation*

*Figure 5.19. Preparation of mortar samples*

The mixture after blending all components, was quickly put in metal forms (Figure 5.19) and kept in the form for a time of a one day (Figure 5.20-a). After removal from the form (Figure 5.20-b), the samples were cured for a period of a one month in a dark and dry place, following the norm EN 12390-2:2000 (2000). At one time 6 samples were prepared simultaneously. The average density after 28 days was found to be $\rho_d$ = 1.87 g/cm$^3$ (c/s = 1.0, for coarse sand).

The static strength was determined at 28$^{th}$ day, according to norm Eurocode 2: EN 1992-1-1:2004 (2004) and ASTM C192 / C192M-15 (2015). The age of the specimens at the time of initiation the cyclic loading, ranged from 28 to max 36 days. The samples which were not tested within than time interval were excluded from testing.

*Figure 5.20. Mortar samples during curing process*

### 5.6.2. Cohesionless (low-cohesive) materials

According to the proposed remaining shear strength curve, only the cohesion is reduced.

Even though many soils and rocks have zero or very small cohesion, the acting cyclic loading can also cause their shear strength reduction. Therefore, cohesionless (low-cohesive) materials are investigated in order to fully describe the behaviour of geomaterials under cyclic loading for all type of geomaterials. Two types of cohesionless (or very low cohesion) materials were investigated: weak rock (limestone) and typical sands (crumbled limestone, coarse sand, rounded beach sand).

*Limestone*

The sedimentary rock limestone (carbonate sandstone, also known as Marl or "Mergel") came from the site of the highway tunnel pit Geusselt A2 in Maastricht (see Figure 5.21-Figure 5.24). To obtain samples for the triaxial testing, a visitation and sampling was organised on site on 5 of September 2013. A team from the University of Luxembourg with the assistance of the company Avenue2 (Strukton and Ballast Nedam) dug rock samples from the site presented in Figure 5.21.

The Maastricht Formation (Dutch: Formatie van Maastricht; abbreviation: MMa), for which this limestone belongs, is a geological formation in the Dutch Limburg, Belgian Limburg and adjacent areas in Germany. The rock belonging to Maastricht Formation, locally called "mergel", is an extremely weak, porous rock, consisting of soft, sandy shallow marine weathered carboniferous limestone, which is in fact chalk and calcareous arenite. These lithologies locally alternate with thin bands of marl or clay.

The laboratory tests were conducted on a very young and shallow layer of that rock (Figure 5.21), so the material is not much compacted and cemented (Pytlik & Van Baars, 2015). It was expected that the strength parameters will be low. The samples were prepared according to the Eurocode 7: part 2 (2007) (Figure 5.26). The bulk density of the limestone (in this case dry density) was found to be $\rho_d = 1.16$ g/cm$^3$ based on the linear measurement method described in the norm CEN ISO/TS 17892-2 (2004).

*Crumbled limestone and various sands*

Intact limestone crumbles very easily when being brought to the surface. This disintegrated crumbled limestone looks like a fine dry sand, and consists of small particles of carbonates (see Figure 5.27 and Figure 5.28). The density of the crumbled limestone was calculated for a loose packing: $\rho_{min} = 1.06$ g/cm$^3$ and for a dense packing: $\rho_{max} = 1.26$ g/cm$^3$. Comparing this results with the intact limestone ($\rho_{max} = 1.16$ g/cm$^3$) it was found that the intact limestone packing lays somewhere between the loose and dense packing of the already disintegrated rock (sand). The loose packing (minimum density) was calculated according to ASTM D 4254 (2016) (the A method), by pouring slowly in air the sand through a funnel to a standard cylindrical mold. The dense packing (max density) was obtained by shaking multiple times a cylinder with sand and constantly refilling the mold up to maximum possible volume.

The density of the particles (particle density or true density) was found to be $\rho_p = 2.5$ g/cm$^3$.

The particle density was calculated based on the water displacement method. This value of the density of particles is lower than that of the typical Maastricht calcarenite (typical value of Maastricht stone is usually around 2.7 g/cm$^3$, given by e.g. Hall & Hamilton, 2016). The porosity of the intact limestone was then calculated as $n$ = 54%, which is a high value for a limestone.

The crumbled limestone samples were prepared by filling the membrane with sand through a funnel directly into a 38 mm diameter split form. In order to obtain a density more or less similar to that of the natural state of the crumbled limestone, a compaction was done by a hand tamping with a steel rod.

Three other sands: the norm sand DIN EN 196-1 (2005) presented in Figure 5.29, rounded sand from the beach (Figure 5.30) near the city the Hague and coarse sand (construction sand) were also tested in order to compare the different types of sands with the crumbled limestone. The crumbled limestone and other sands were completely dry during testing and prepared in the same way as the crumbled limestone samples.

*Figure 5.21. Limestone excavation site*

*Figure 5.22. Mechanical cutting of the rock*

The grain size details for crumbled limestone are given in Figure 5.31. Table 5-2 presents the parameters, average grain size $D_{50}$, uniformity coefficient $C_u$, coefficient of curvature $C_C$, void ratio $e$, and porosity $n$. Norm sand, beach and the coarse sand are also included here. Following the ASTM D2487 (2011) norm, all these geomaterials are classified as poorly graded.

*Figure 5.23. View of the freshly unveiled rock*

*Figure 5.24. Rock samples ready for transportation*

*Table 5-2. Sand parameters*

| | Crumbled limestone | Norm sand | Coarse sand | Beach sand |
|---|---|---|---|---|
| $D_{50}$ (mm) | 0.2 | 0.73 | 0.45 | 0.28 |
| $C_u$ (-) | 2.24 | 6.14 | 2.34 | 2.27 |
| $C_c$ (-) | 0.82 | 1.80 | 0.85 | 1.12 |
| $e$ (-) | 1.15 | 0.49 | 0.66 | 0.28 |
| $n$ (-) | 0.53 | 0.33 | 0.39 | 0.22 |

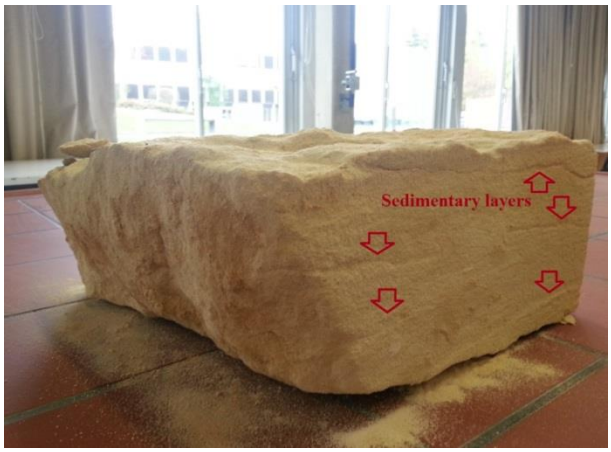


*Figure 5.25. Limestone sample on the laboratory table (visible stratification)*

*Figure 5.26. Limestone sample preparation*

*Figure 5.27. Partially crumbled Limestone*

*Figure 5.28. Completely crumbled Limestone*

*Figure 5.29. Norm Sand*

*Figure 5.30. Beach sand*

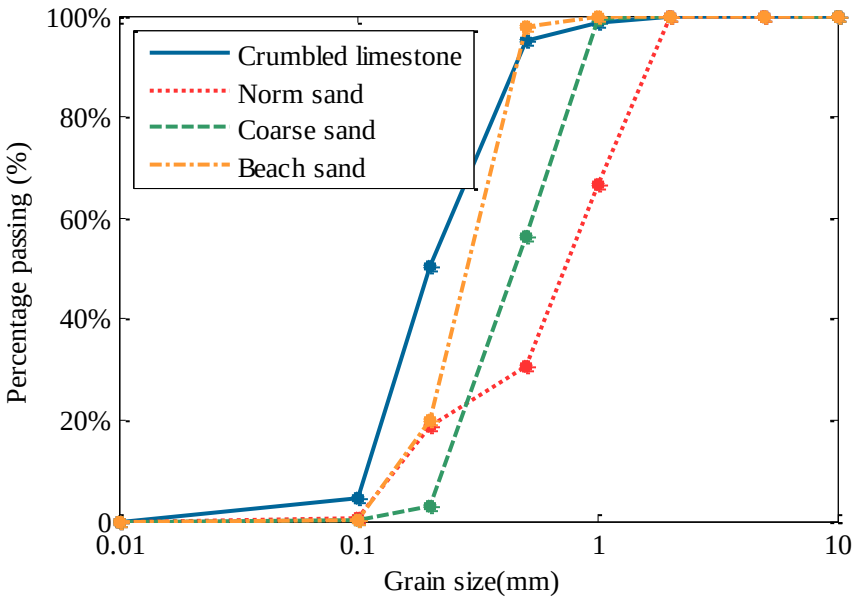


*Figure 5.31. The grain size distribution curve of the crumbled limestone, norm sand, beach sand and coarse sand*

# 6. STATIC TEST RESULTS

## 6.1. Introduction

In this chapter triaxial static test results are presented. The triaxial static tests are conducted in order to find the maximum deviatoric stress. The maximum deviatoric stress in triaxial apparatus is indicated by a decrease in stress state for increasing strains when sample is loaded until failure. The maximum deviatoric stress for a set of samples with different confining pressures allowed finding the shear strength parameters for cohesive and cohesionless materials. The cohesive materials used in the tests are respectively: artificial gypsum and mortar; and the cohesionless are: intact limestone, crumbled limestone and various sands (described in chapter 5.6).

The Mohr-Coulomb envelope strength parameters $\phi$ and $c$ will be obtained from the stress points plots (chapter 5.5). The best fit line will be presented together with the 95% confidence band and 95% prediction band.

It has to be mentioned that not many tests were carried out for the confining pressure $\sigma_3 = 0$ MPa because the main aim of the static tests was to calculate most accurately the Mohr-Coulomb shear strength parameters. More tests for different confining pressures increase the accuracy of the linear regression of the MC failure envelope. Therefore, usually only one typical UCS test ($\sigma_3 = 0$) was carried out for each material. The spread of the static test results for tests without applied confining pressure (UCS tests) was also not investigated.

## 6.2. Cohesive materials

A total number of 37 samples were tested to obtain the shear strength parameters $c$ and $\phi$ in static triaxial tests of artificial gypsum.

For mortar, the number of investigated samples was also significant. For different proportions of sand and cement, as well as different types of sand, the total number of samples was 17. For one set at least 5 samples were tested to be able to create the p-q plot and to obtain the shear strength parameters.

### 6.2.1. Artificial gypsum

The linear least-square regression parameters from the p-q plot for artificial gypsum are presented in Table 6-1. The values of cohesion $c$ and the friction angle $\phi$ resulting from the p-

q plots are given in Figure 6.3 and Table 6-2. It can be noticed that the internal friction angle $\phi$ and cohesion $c$ are quite high - similar to weak rocks e.g. sandstone or a weak concrete (Verruijt, 2001, 2006).

The results presented in Table 6-1 indicate, that the standard error of estimate (i.e. standard error of the predicted $y$-value for each $x$ in the regression) is $s_{est}$ = 76 kPa. This value is smaller than the standard deviation of all points without regression $s_{all}$ = 174 kPa. The coefficient of determination is $r^2$ = 0.82, therefore the assumption of linearity seems valid.

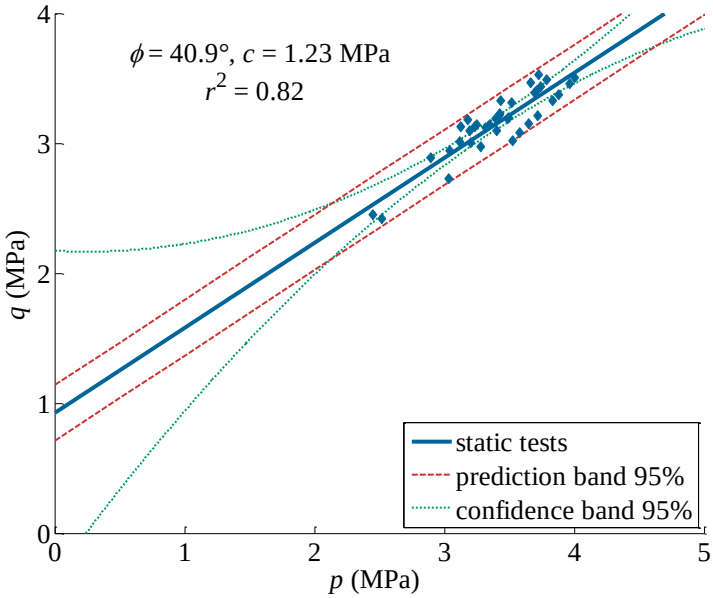


*Figure 6.1. Stress points for 37 static tests in the stress points plot for artificial gypsum*

*Table 6-1. Linear regression coefficients and standard errors*

| Slope $\delta$ (-) | Intercept $b$ (MPa) | Standard deviation of slope $\delta$ (-) | Standard deviation of intercept $b$ (MPa) | Standard error of estimate (MPa) | Coefficient of determination $r^2$ (-) |
|---|---|---|---|---|---|
| 0.65 | 0.94 | 0.05 | 0.17 | 0.11 | 0.82 |

*Table 6-2. Mohr-Coulomb envelope parameters for static tests for artificial gypsum*

| Total number of samples | $\phi$ (°) | $c$ (MPa) | UCS (MPa) |
|---|---|---|---|
| 37 | 40.7 | 1.24 | 6.02 |

Additionally, the 0.975 quantile of the Student' $t$-distribution with 35 degrees of freedom ($t_{35}$ = 2.069 for 37 samples) was obtained, and the 95% confidence intervals for slope $\delta$, and intercept $b$ were calculated. The results are presented in Table 6-3.

*Table 6-3. The 0.975 quantile of the Student's t-distribution with 35 degrees of freedom*

| 0.975 quantile | | min | max |
|---|---|---|---|
| Slope $\delta$ | (-) | 0.55 | 0.76 |
| Intercept $b$ | (MPa) | 0.58 | 1.29 |

*Pressure dependence*

It was observed that for higher confining pressures ($\sigma_3$ > 0.5 MPa) the artificial gypsum samples had smaller strength than would result from the linear Mohr–Coulomb failure theory. The reason can be that the shear strength for this artificial gypsum is nonlinear for higher confining pressures, which is the case for rocks e.g. (Barton, 1976). Another explanation is that the set of the tested samples for higher confining pressures has on average smaller strength than the ones used for lower confining pressures.

*Spread of data points*

It may be of interest to note that during the static tests on artificial gypsum, the data points were very close to each other (this can be seen also on Figure 6.1). The reason is that, due to the limitation of the level of applied confining pressure $\sigma_3$, (at 1 MPa water starts to leak from the chamber, even though the maximum possible pressure is 1.7 MPa), higher shear strengths could not be reached. The estimation of the friction angle $\phi$ and cohesion $c$ is less accurate for a small range of data points. The uncertainty of the shear strength parameters is significant ($r^2$ value is 0.82), which is clearly visible by the wide range of the confidence and prediction bands.

### 6.2.2. Mortar – (cemented sand)

Before the static and cyclic testes on mortar can be started, a correct amount of sand, cement and water had to be determined in order to prepare samples giving the best range of strength with the highest accuracy. The best range of strength means that the strength reduction in cyclic loading depends on the lab equipment, which has to be able to carry the necessary loads to cause a failure of a sample in a reasonable time.

The values of cohesion $c$ and the friction angle $\phi$ were obtained (Table 6-4) from the plot of stress points (Figure 6.2 - Figure 6.3). First, shear strength tests have been performed for a cement/sand ratio = 0.5. The cohesion had a small value ($c$ = 0.39 MPa). Because of that, the cement/sand ratio was increased up to 1.5, which is a very high value. As a result, the cohesion was much larger ($c$ = 2.73 MPa) than that for the previous smaller amount of cement. Unfortunately, adding more cement increased significantly the strength and stiffness of the mortar samples. This caused a new problem. For these samples, the stiffness of the laboratory triaxial frame was not high enough, so the tests for higher confining pressures could not be conducted. Therefore the cement/sand ratio was lowered to a ratio of 1. This ensured a high cohesion (1.4 MPa), small spread of data points and allowed that the laboratory machine easily handled the applied stresses.

*Table 6-4. Mohr-Coulomb envelope parameters for static load tests for mortar*

| | No of samples | *cement/sand* | *water/cement* | $\phi$ (°) | $c$ (MPa) | UCS (MPa) |
|---|---|---|---|---|---|---|
| Attempt I | 7 | 0.5 | 0.5 | 41.3 | 0.39 | 1.72 |
| Attempt II | 5 | 1 | 0.5 | 51.4 | 1.40 | 8.01 |
| Attempt III | 5 | 1.5 | 0.5 | 49.4 | 2.73 | 14.79 |

The static tests on mortar show that the shear strength parameters are close to weak rocks, just as in the case of the previously investigated artificial gypsum. The advantage of using mortar samples is that by changing the cement/sand ratio one can control the cohesion, while the friction angle does not change much and lies between 41.3° and 51.4°.

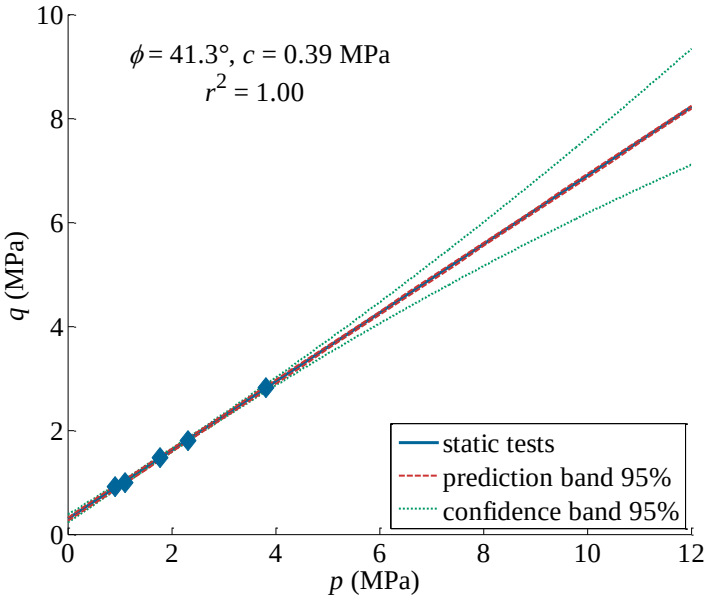


*Figure 6.2. Stress points for mortar for c/s= 0.5*

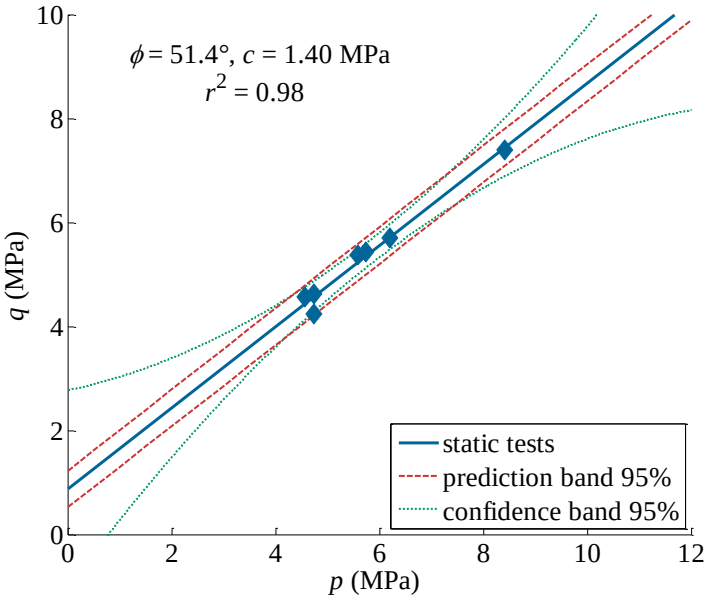


*Figure 6.3. Stress points for mortar for c/s =1*

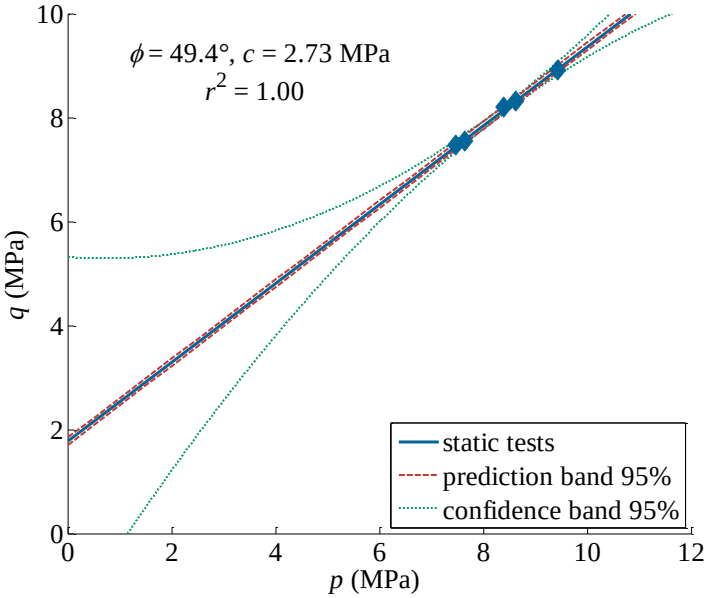


*Figure 6.4. Stress points for mortar for c/s=1.5*

The estimates of the regression coefficients and their standard errors are presented in Table 6-5. The coefficient of determination $r^2$ for all three attempts is very high (0.98-1.0), therefore the assumption of linearity seems valid and the samples are homogeneous and prepared in a proper way. However, care must be taken, because the high $r^2$ value can be caused by a small number of test results.

Additionally, the 0.975 quantile of Student's *t*-distribution with *n* degrees of freedom was obtained, and thus the 95% confidence intervals for slope $\delta$ and intercept *b* were calculated. The results again are showing a very low spread of data points.

*Table 6-5. Linear regression coefficients and their standard errors*

| | Slope $\delta$ (-) | Intercept *b* (MPa) | Standard deviation $\delta$ (slope) (-) | Standard deviation *b* (intercept) (MPa) | Standard error of estimate (MPa) | Coefficient of determination $r^2$ |
|---|---|---|---|---|---|---|
| Attempt I | 0.66 | 0.29 | 0.007 | 0.016 | 0.017 | 0.99 |
| Attempt II | 0.78 | 0.87 | 0.055 | 0.32 | 0.18 | 0.98 |
| Attempt III | 0.76 | 1.78 | 0.023 | 0.19 | 0.036 | 0.99 |

*Table 6-6. The 0.975 quantile of the Student's t-distribution for mortar*

| | *cement/sand* | *δ (-)* | | *b* (MPa) | |
|---|---|---|---|---|---|
| | | *min* | *max* | *min* | *max* |
| Attempt I | 0.5 | 0.57 | 0.60 | 2.49 | 3.35 |
| Attempt II | 1 | 0.58 | 0.74 | 1.12 | 1.63 |
| Attempt III | 1.5 | 0.61 | 0.69 | 1.29 | 2.26 |

*Influence of the cement / sand ratio on the strength results*

It was investigated, how the cement/sand ratio affects the cohesion (Figure 6.5) and the friction angle (Figure 6.6). The cohesion increases according to a power law:

$$c = 1.35 \cdot x^{1.78} \qquad 6\text{-}1$$

where $x$ is the cement/sand ratio. This power law gives the highest value of $r^2 = 1$. This means that the correlation between the amount of cement and cohesion is very strong (see Figure 6.5). By using a power regression, the value of the cohesion for 0 amount of cement is also automatically equal 0. Care must be taken with extrapolation of this curve, because the cohesion cannot increase infinitely according to a power law for higher cement/sand ratios.

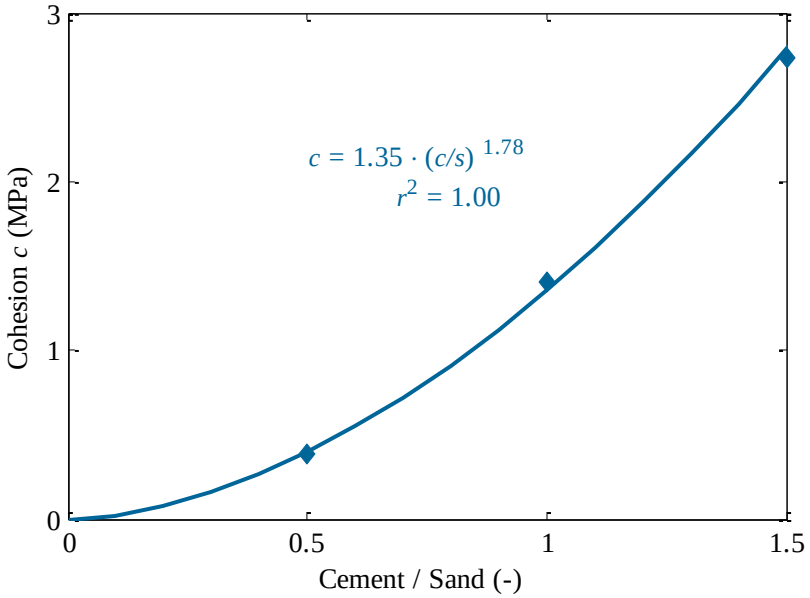


*Figure 6.5. Influence of cement/sand ratio on the cohesion*

The friction angle $\phi$ dependency on the cement/sand ratio was checked and this correlation is very weak (Figure 6.6). The value of $r^2$ is not very high and no strong relationship could be found. The friction angle varies but stays more or less constant (compare with the friction angle of the sand which was used to prepare the samples – at point cement/sand = 0, in Figure 6.6). This agrees with the prediction of a constant friction angle given by Van Baars (1996). It can be noticed that the friction angle reaches a maximum value for a cement/sand ratio, which is here around 1.

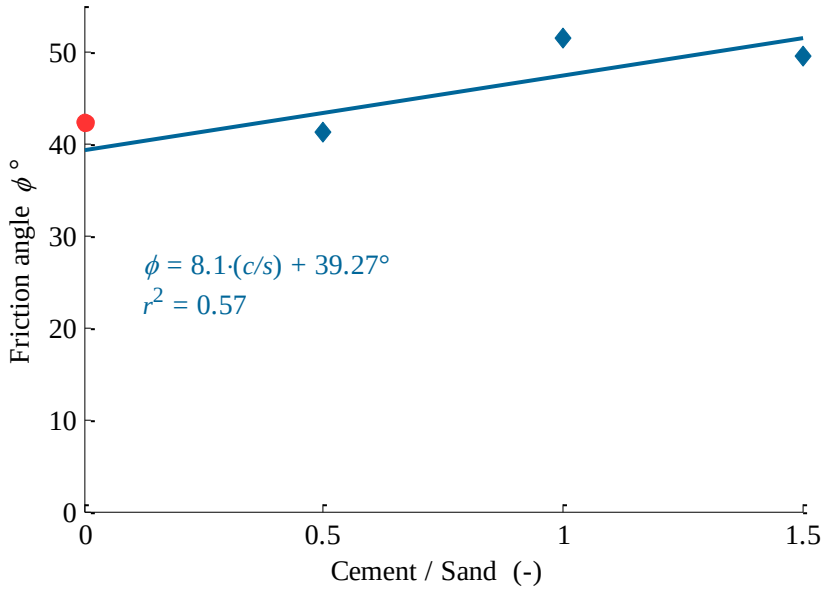


*Figure 6.6. Influence of cement/sand ratio on the internal friction angle*

## 6.3. Cohesionless materials

To make the description of the static loading on geomaterials complete, a series of tests on weak cohesive and cohesionless materials were conducted. In the following subchapters, results for a very weak rock and several types of sands are presented.

First, 10 static (4 for vertical and 6 for horizontal direction) triaxial tests were performed on intact limestone from the Maastricht tunnel construction site (more details in chapter 5.6.2). Later, triaxial tests were carried out on a crumbled limestone (7 samples) and several types of sands (for each sand 3 samples were tested).

### 6.3.1. Intact limestone

The triaxial tests on limestone were conducted with a confining pressure $\sigma_3$, which varied from 0 kPa to 300 kPa. The results (Table 6-7 and Figure 6.7) for different directions (in terms of rock stratification) show that for vertical samples the cohesion $c$ = 89.9 kPa is more than twice as big as for horizontal ones $c$ = 37.4 kPa.

As a result, the uniaxial compression strength (UCS) is also almost twice as big as for the vertical samples. This is a typical anisotropic behaviour. In contrast, the calculated friction angle is almost equal for both directions: $\phi$ = 40.2° for horizontal and $\phi$ = 38.9° for vertical samples. The other regression coefficients are presented in Table 6-8.

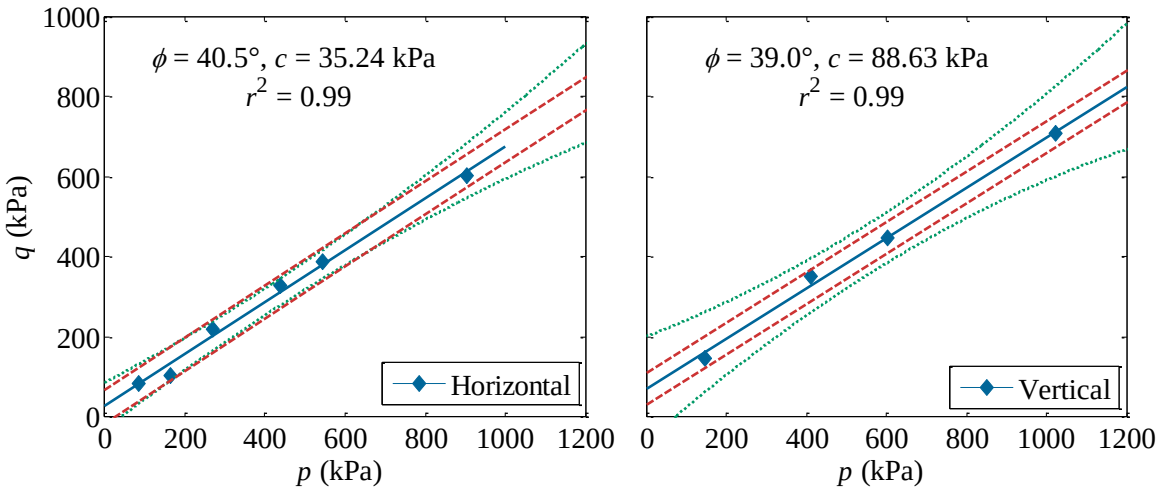


*Figure 6.7. Stress points for limestone (horizontal & vertical samples)*

*Table 6-7. Limestone strength parameters obtained from triaxial tests.*

| | | Horizontal samples | Vertical samples |
|---|---|---|---|
| $\phi$ | (°) | 40.2 | 38.9 |
| $c$ | (kPa) | 37.4 | 89.9 |
| UCS | (kPa) | 167.0 | 292.0 |
| tensile strength | (kPa) | 32.5 | 84.5 |

*Table 6-8. Linear regression coefficients and their standard errors for limestone*

| Slope $\delta$ (-) | Intercept $b$ (kPa) | Standard deviation $\delta$ (slope) (-) | Standard deviation $b$ (intercept) (kPa) | Standard error of estimate (kPa) | Coefficient of determination $r^2$ |
|---|---|---|---|---|---|
| 0.65 | 26.78 | 0.032 | 15.44 | 21.31 | 0.99 |

Due to a low cohesion and a high friction angle, the tensile strength is very low, which was noticed during the excavation stage. The excavated rock cracked and crumbled very easily, especially at the sedimentary layers (Figure 5.25). But, as long as the limestone remains unexcavated, it seems as if the confining pressure binds the material, and the rock contains its strength. This is the reason why after a visual inspection it was first believed that the rock is stronger.

The process of preparing samples was time consuming (chapter 5.6.2), because this limestone was very brittle and fragile and was constantly cracking (Figure 5.25). The coefficient of determination was very high for both the horizontal and the vertical direction ($r^2 > 0.99$), even though it was very difficult to obtain good samples for the triaxial tests. The biggest problem occurred at obtaining samples for the vertical direction, because these samples were constantly breaking along the sedimentary layers.

It is important to notice that only the undamaged samples were used in the triaxial tests and the strength of the weaker parts of the rock was not taken into account. For this reason, the

shear strength obtained from the triaxial tests it expected to be higher than in situ. Therefore, the question arises, whether the shear strength in triaxial tests is not overestimated.

### 6.3.2. Crumbled limestone

The stress points at failure of the crumbled limestone are plotted in a p–q coordinate system (see Figure 6.8, Figure 6.9 and Table 6-9). The triaxial tests on crumbled limestone resulted in the values $\phi = 43°$ and $c = 26$ kPa (Table 6-9). This is a very surprising result, because these parameters are very close to the intact limestone (Figure 6.9) and the crumbled limestone seems to have some cohesion. Since sand is a cohesionless material it should not have any cohesion. Using the same laboratory data for the Mohr-Coulomb failure envelope and assuming that $c = 0$ kPa, the friction angle was recalculated and found to be equal $\phi = 45.5°$ (Pytlik & Van Baars, 2015). This is even a higher value than for the intact limestone.

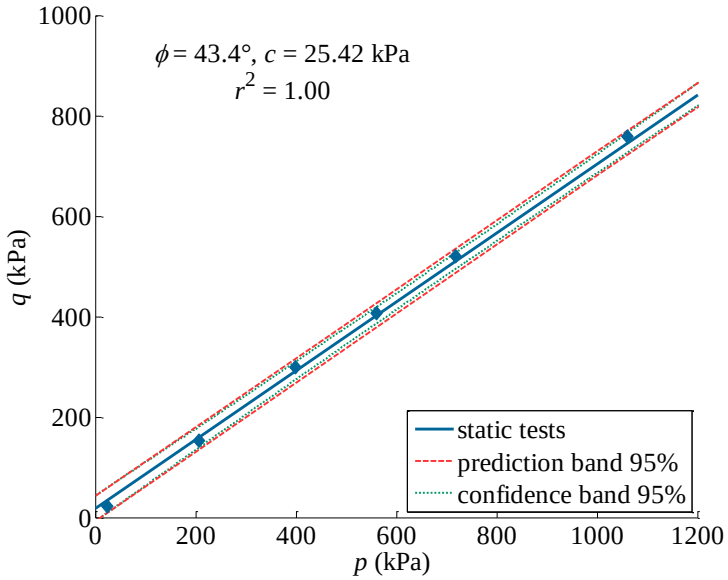


*Figure 6.8. Stress points for crumbled limestone*

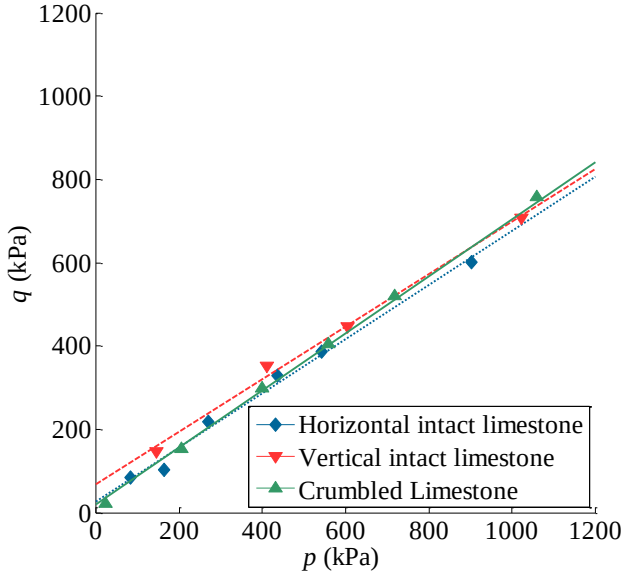


*Figure 6.9. A p-q plot at failure in triaxial tests for crumbled and intact limestone*

*Table 6-9. Crumbled limestone strength parameters*

| | | Crumbled limestone (recalculated) | Horizontal intact limestone | Vertical intact limestone |
|---|---|---|---|---|
| $\phi$ | (°) | 43.3 (45.5) | 40.2 | 38.9 |
| $c$ | (kPa) | 25.9 (0) | 37.4 | 89.9 |
| tensile strength | (kPa) | 20.9 (0) | 32.5 | 84.5 |
| UCS | (kPa) | - | 161 | 376 |

The linear regression correlation of the data points is very high for the crumbled limestone ($r^2 > 0.99$). More details of the linear regression are presented in Table 6-10.

*Table 6-10. Linear regression coefficients and their standard errors for crumbled limestone*

| Slope $\delta$ (-) | Intercept $b$ (kPa) | Standard deviation $\delta$ (slope) (-) | Standard deviation $b$ (intercept) (kPa) | Standard error of estimate (kPa) | Coefficient of determination $r^2$ |
|---|---|---|---|---|---|
| 0.68 | 18.78 | 0.01 | 7.66 | 12.2 | 0.99 |

*Stress-strain comparison between intact and crumbled limestone*

Since the strength parameters are so similar for intact and crumbled limestone, also a comparison between the intact limestone stress-strain behaviour and the crumbled one is presented in Figure 6.10. For both materials the confining pressure was 50 kPa. It can be noticed that the stiffness of the intact limestone is much higher; however, its strength is not reaching the maximum value of the crumbled material. The intact limestone demonstrates typical brittle failure behaviour, where the crumbled one exhibits a ductile one (strain softening behaviour). Despite the fact that the densities and the material building both geomaterials are the similar, the post peak behaviour for the intact and crumbled limestone is completely different. It can be easily observed that the cemented materials are characterised by the brittle failure behaviour with significant drop in strength in post peak curve.

This comparison also shows, that the Mohr-Coulomb failure envelope is not particularly well describing the strength of weak rock, as it cannot model the non-linearity of the failure envelope e.g. Johnston (1991), Hoek (2000).

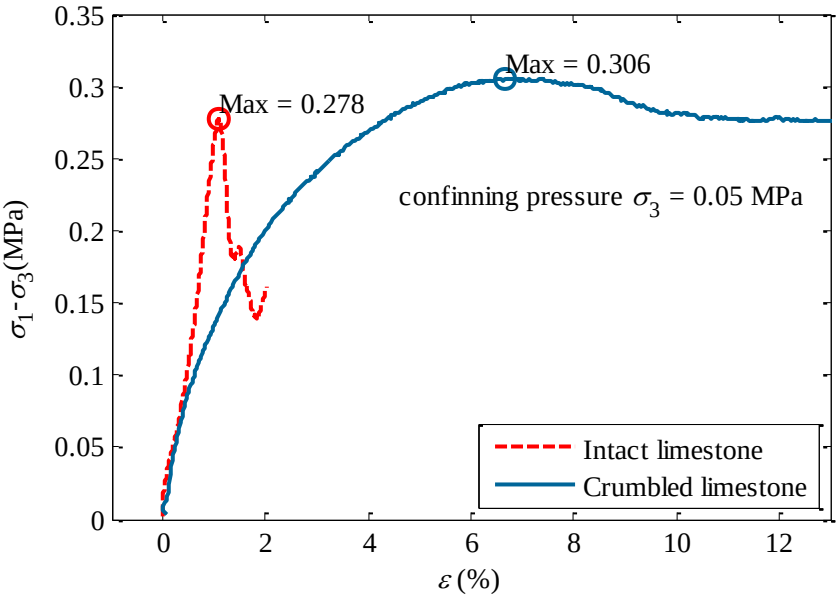


*Figure 6.10. Stress-strain plot for intact and crumbled limestone*

### 6.3.3. Other sands

Results for other sands are presented in Figure 6.11 and Table 6-12.

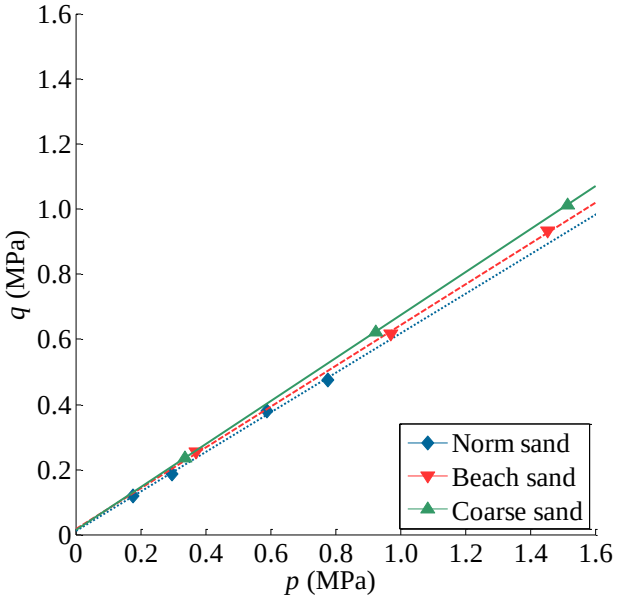


*Figure 6.11. Stress-strain plot for Norm, Beach and Coarse sand*

The linear regression correlation of the data points for all sands is very high ($r^2 > 0.99$). More details of the linear regression are presented in Table 6-11.

*Table 6-11. Linear regression coefficients and their standard errors for various sands*

| Sand | Slope $\delta$ (-) | Intercept $b$ (kPa) | Standard deviation $\delta$ (slope) (-) | Standard deviation $b$ (intercept) (kPa) | Standard error of estimate (kPa) | Coefficient of determination $r^2$ |
|---|---|---|---|---|---|---|
| Norm sand | 0.61 | 12.1 | 0.022 | 11.55 | 10.6 | 0.99 |
| Beach sand | 0.63 | 17.6 | 0.014 | 14.84 | 11.1 | 0.99 |
| Coarse sand | 0.66 | 13.1 | 0.0001 | 0.152 | 0.12 | 1.00 |

It can be noticed that all sands have a small cohesion (Table 6-11, column *Intercept*), which of course is not true. For further calculation the cohesion for the sands is taken as 0 and the friction angles are recalculated for this value (see Table 6-12, last column titled: $\phi$ (°) *recalculated*). For most sands, the friction angle increases when the coefficient of uniformity $c_u$ decreases. The sand which contains more fine particles, has larger gradation and will have higher friction angle $\phi$. Any strong correlation, however, has not been found. Similar results were given by Kim & Ha (2014). They also noted that other researches were not conclusive.

*Table 6-12. Strength parameters of various sands*

| | $d_{50}$ | $c_u$ | $\phi$ (°) | $c$ (kPa) | $\phi$ (°) (recalculated) |
|---|---|---|---|---|---|
| Norm sand | 0.73 | 6.14 | 37.5 | 15 | 39.1 |
| Beach sand | 0.28 | 2.27 | 38.8 | 22 | 39.9 |
| Coarse sand | 0.45 | 2.34 | 41.4 | 17 | 42.3 |
| Crumbled limestone | 0.20 | 2.24 | 43.3 | 25 | 45.5 |

## 6.4. Conclusions

The static test results were presented in this chapter for various materials. For artificial gypsum, the Mohr-Coulomb failure envelope does not match exactly the strength results. This means that the strength of the artificial gypsum behaves nonlinearly. Also the spread of the test results for artificial gypsum is significant.

The mortar samples, which were prepared in laboratories in a strict way, gave very accurate results and their strength parameters could by easily adjusted to the requirements of the tests conditions. The cohesion can be controlled by changing the cement/sand ratio, while the friction angle has more or less a constant value. The friction angle of mortar samples depends strongly on the friction angle of the sand, which is used to prepare these samples.

In Figure 6.12 and Figure 6.13 typical shear band for both, the artificial gypsum and mortar samples, is well visible and this band looks like the shear band of weak rocks. The static tests on artificial gypsum and mortar proved that the manmade samples can give similar strength parameters and can model quite well the strength behaviour of weak rocks.

The tested limestone is a very weak rock, because during the sample preparation, many samples easily cracked. The cracked samples were not taken into account; therefore, the strength results for this material are slightly overestimated. The limestone presented also a typical anisotropic behaviour, which can also affect the cyclic test results.

*Figure 6.12. Gypsum sample after triaxial test*

*Figure 6.13. Mortar sample after triaxial test*

Triaxial tests on other sands (i.e. coarse, norm, and beach sand) showed that the coefficient of determination $r^2$ is very high for all sands, therefore, only a small number of tests was needed to achieve high accuracy. For the crumbled limestone, obtained from the intact limestone, the strength parameters have very similar value to the intact limestone, which is a very surprising result.

During testing the following points were discovered.

- Material inhomogeneity (imperfections etc.) had a significant impact on scatter of the results (especially for artificial gypsum),
- Due to a low stiffness of the triaxial frame (the frame buckle), higher loads could not be applied, which means that the stronger rock material could not be tested,
- Higher confining pressure than 0.5 MPa could not be applied for a longer time due to slow fluid leakage of that system.

The artificial gypsum, mortar and natural limestone exhibit mostly brittle behaviour, where the crumbled limestone and other sand typical ductile one. All the sands as well as the crumbled limestone were slightly densified before testing; therefore, they can be treated as dense sands. The UCS for the crumbled limestone is 0.17 MPa and standard error of estimate $\sigma_{est}$ = 0.021 MPa, where for mortar UCS = 9.11 MPa with $\sigma_{est}$ = 0.18 MPa and for gypsum UCS = 6.02 MPa with standard deviation = 0.53.

# 7. CYCLIC TEST RESULTS

## 7.1. Introduction

The results of the cyclic loading tests on geomaterials are presented in this chapter. S-N curves are created for geomaterials and compared with the remaining shear strength curves. To create those curves, for artificial gypsum a total number of 94 samples were tested (50 samples for the S-N and 44 samples for the remaining shear strength curve). For mortar, the number of samples was 16 for the S-N and 45 for the remaining shear strength curve. The 45 mortar samples tested for the remaining shear strength curve were divided into 3 sets with different cement/sand ratio and curing time.

In the case of cohesionless materials, no tests were conducted for S-N curve. For limestone, the number of available samples was only 10, so all samples were used for obtaining the remaining shear strength curve. Additionally, 14 samples were tested for crumbled limestone, 13 for norm sand, 13 for beach sand and 4 for coarse sand.

The cyclic load stress ratio, for both the S-N curves and the remaining shear strength curves, was set to $\tau_{cyc}/\tau_0$ = 40%, 60%, 80%, of the maximum strength respectively, for each confining pressure $\sigma_3$ (100, 300, and 500 kPa). For the remaining shear strength curve, a series of $n$ = 10, 100, 1000, 10 000 and 100 000 cycles were investigated. 20% of the cyclic stress was applied for the highest number of cycles $n$ = 100 000, to assure that no failure will occur before reaching this number of cycles.

Also other damage parameters (e.g. stiffness, plastic strain accumulation and rate of plastic strain) were measured and their changes in cyclic loading investigated in order to see if these damage parameters can lead to a better, or even earlier determination of the fatigue life of geomaterials.

## 7.2. The S-N curve

The S-N curves were prepared according to the procedure described in chapter 4.3 and 5.2.5. Instead of the strength (denoted as an $S$) on the ordinate axis, the cyclic load stress ratio is given ($\tau_{cyc}/\tau_0$). It has to be mentioned, that most of the data for the S-N curves came from samples tested for the remaining shear strength curves but failed before reaching the desired number of cycles $n$. Although, this is not the typical S-N curve obtaining procedure; this data was still used for a comparison, due to a lack of data (and testing time). This, of course can

lead to problems, such as overestimating the fatigue life and decreasing probabilities of failure.

The low number of tested mortar samples, was caused by a much higher strength of these samples which leads to a higher number of applied cycles, in case if no higher cyclic stress is applied.

### 7.2.1. The S-N curve for a cohesive material

*The S-N curve for artificial gypsum*

A number of different types of fatigue models (S-N curves) have been presented in the literature, which take into account parameters affecting the fatigue behaviour such as the stress ratio, frequency, etc. (see chapter 3.5.1). The most simple and also the most common are the logarithmic (linearised), power (Basquin, 1910), and the exponential regression. These models are parametrised for artificial gypsum, and the results are presented in Figure 7.1, Figure 7.2 and Figure 7.3.

The logarithmic regression (Figure 7.1) gave the best fit result (highest $r^2$) and is also the easiest to obtain the regression parameters (except, of course, for the linear regression).

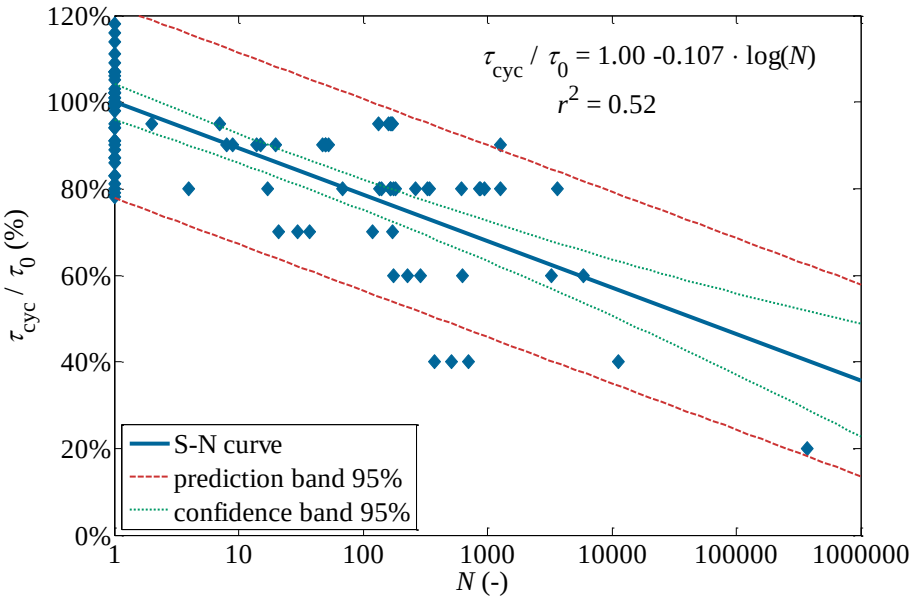


*Figure 7.1. Logarithmic regression of the Stress – Life (S-N) plot for artificial gypsum*

In Figure 7.2 the best fit line for the power regression (Eq. 3-2) is presented and it also gives a very good fit, similar to the logarithmic regression.

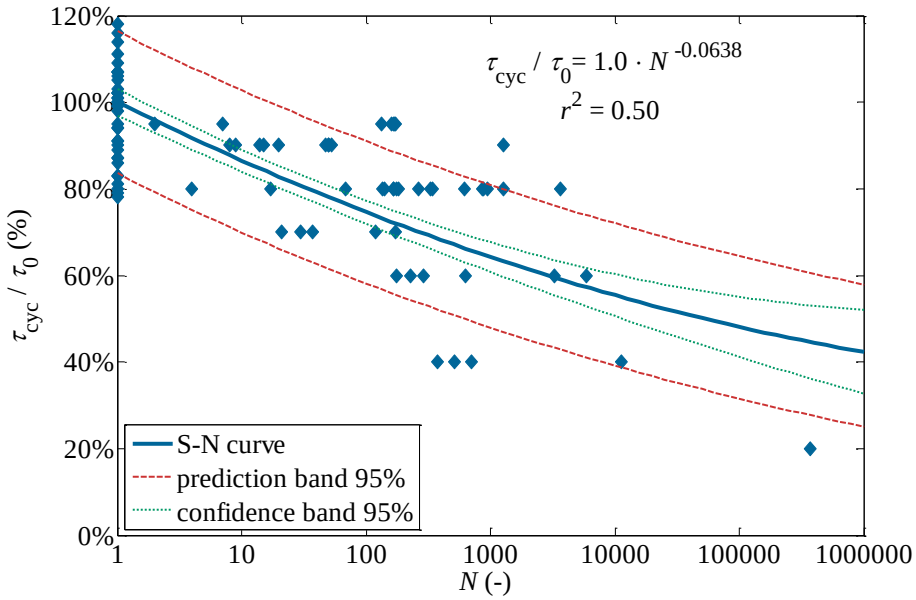


*Figure 7.2. Power (Basquin) regression of the Stress – Life (S-N) plot for artificial gypsum*

The exponential regression was also investigated, but it represented the worst performance among all types of regressions (Figure 7.3). A sudden loss of strength is observed on the right side of the last data point; this was not caused by a real material behaviour, but by a lack of data points for higher cycle numbers.

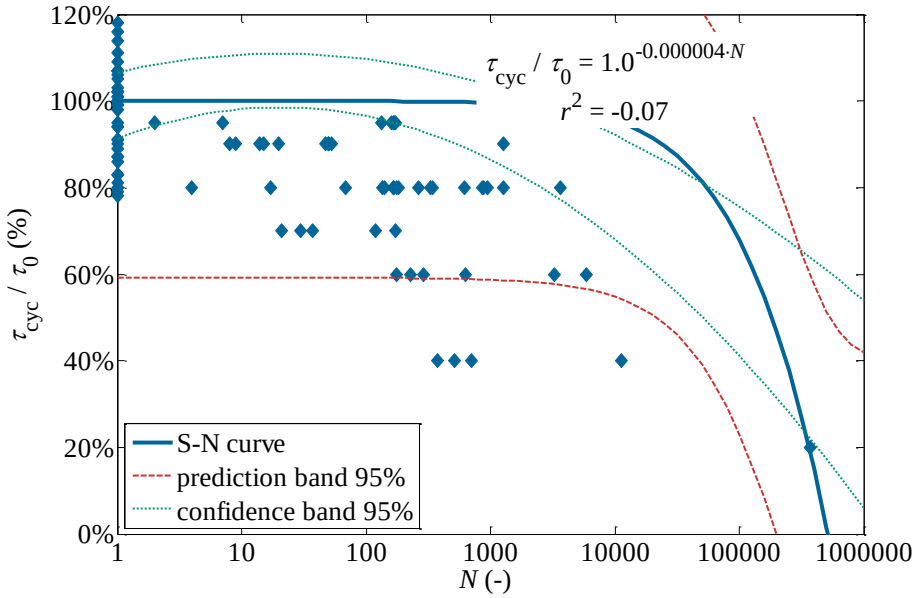


*Figure 7.3. Exponential regression of the Stress – Life (S-N) plot for artificial gypsum*

In Table 7-1 four different regressions mentioned before are presented. The logarithmic model will be used in further calculations because it provides the easiest way of obtaining the regression coefficients, has very high accuracy, same as of the other models (the estimate of $r^2$ was very low for the exponential regression) and it is described in most standards e.g. ASTM E739-91 (1998). The biggest difference between the regressions is in the fitting of the data points for higher number of cycles (Table 7-1). Of course, the more points on the right

side of the S-N curve, the more accurate the prediction of fatigue life is.

*Table 7-1. S-N curve parameters for different regressions*

| Regression | Basic regression | Parametrised regression | $r^2$ |
|---|---|---|---|
| Linear | $\tau_{cyc}/\tau_0 = \alpha - \beta \cdot N$ | $\tau_{cyc}/\tau_0 = 1.0 - 0.000002 \cdot N$ | -0.44 |
| Logarithmic | $\tau_{cyc}/\tau_0 = \alpha - \beta \cdot \log N$ | $\tau_{cyc}/\tau_0 = 1.0 - 0.107 \cdot \log N$ | 0.52 |
| Power | $\tau_{cyc}/\tau_0 = \alpha \cdot N^{\beta}$ | $\tau_{cyc}/\tau_0 = 1.0 \cdot N^{-0.064}$ | 0.50 |
| Exponential | $\tau_{cyc}/\tau_0 = \alpha \cdot e^{\beta \cdot N}$ | $\tau_{cyc}/\tau_0 = 1.0 \cdot e^{-0.000004 \cdot N}$ | -0.07 |

*S-N curve for mortar*

The S-N curve for 3 different sorts of mortar samples is presented in Figure 7.4, Figure 7.5 and Figure 7.6. The low number of test results is caused by a longer fatigue life of this material, which also means that more cycles are necessary to cause failure. The fatigue is clearly visible for all sorts of mortar samples (cement/sand ratio = 0.5, 1.0 and 1.5) when the static tests are included (1.0 intercept point). It must be mentioned, however, that the tests for lower cyclic stress ratio $\tau_{cyc}/\tau_0$ were not performed due to time limitation. It is also worth to notice that the spread of data is comparable with artificial gypsum and is therefore quite large.

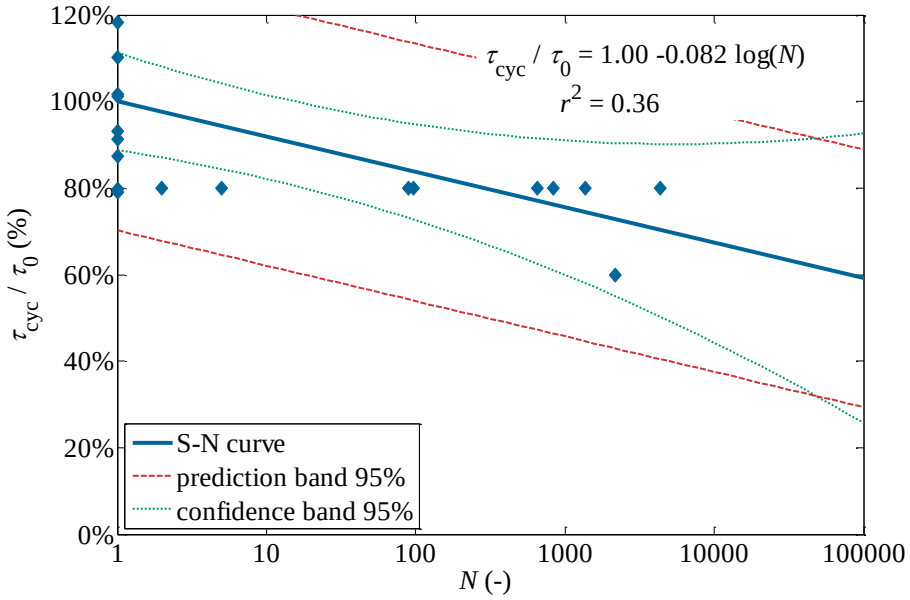


*Figure 7.4. S-N curve for mortar (1 week, cement/sand ratio = 0.5) /beach sand*

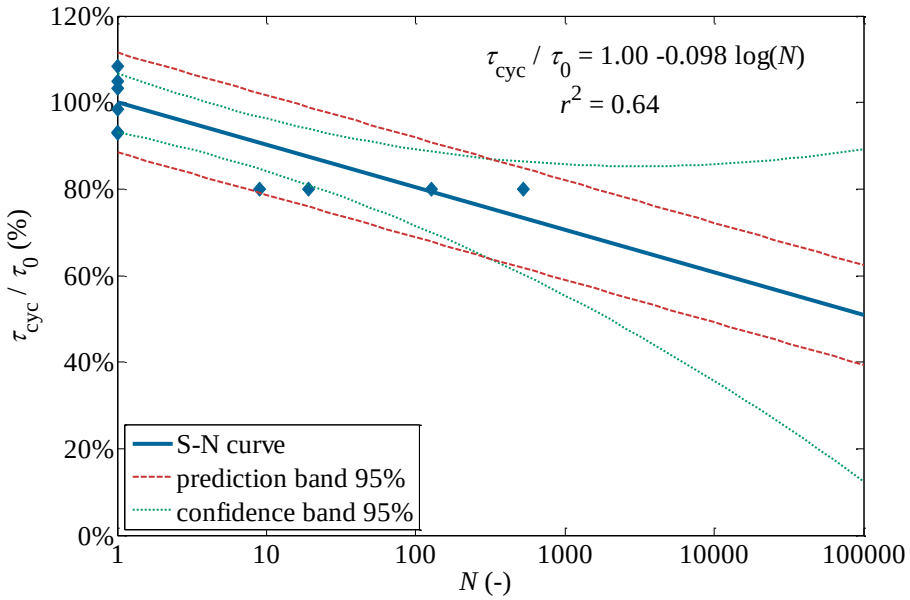


*Figure 7.5. The S-N curve for mortar (1 week, cement/sand ratio = 1.0)/beach sand*

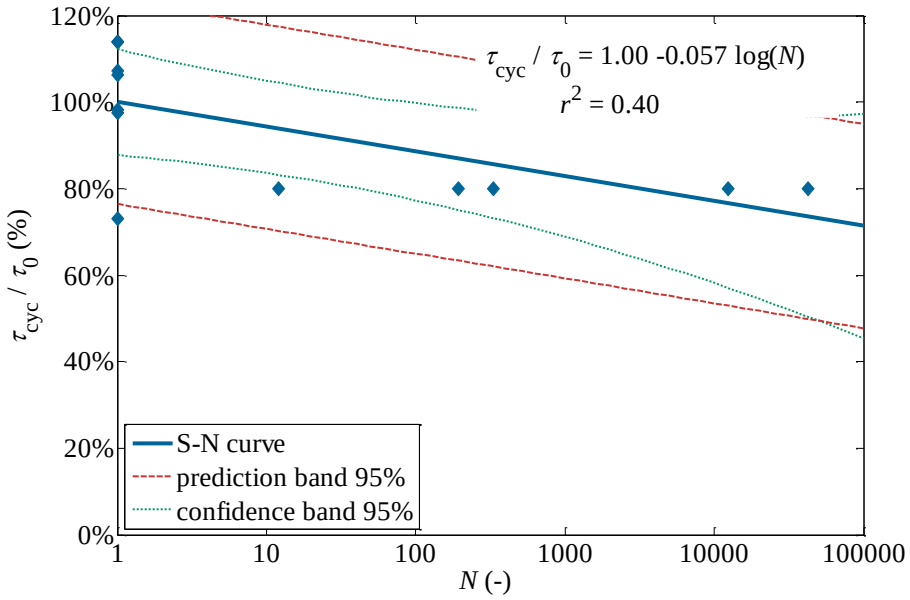


*Figure 7.6. The S-N curve for mortar (1 month, cement/sand ratio = 1.0) /coarse sand*

### 7.2.2. The S-N curve for a cohesionless material

The number of tests carried out on intact limestone was very small due to lack of good (unbroken) samples and therefore only tests were performed for preparing a remaining shear strength curve. It was found that for this weak rock, up to 1000 cycles it was impossible to cause a fatigue failure. Therefore, no data is available for making an S-N curve. Because the maximum number of cycles applied on an intact limestone was small (1000), the chance of existence of fatigue failure for a higher number of cycles cannot be neglected.

Also for crumbled limestone and other sands, a typical fatigue failure (loss of shear strength)

was not observed up to 100 000 cycles (for norm sand).

### 7.2.3. Conclusions from the S-N curves

Cohesive geomaterials lose their strength in cyclic loading and the loss of strength is much larger than compared with non-geomaterials. For artificial gypsum and mortar the fatigue strength was found to be lower than 50% of the static strength for a number of cycles of less than 100 000.

The spread of the data results, for both artificial gypsum and mortar is very large. The confidence and prediction bands, with 95% of probability, are much wider than those for metals and composite materials. The strength reduction for a number of cycles equal $10^5$ is within the range of 0.85-0.35 of the static strength. Similar results were also found by Ishizuka et al. (1990), who reported, that the reduction of the rock strength due to repeated loading differs greatly.

The highest $r^2$ coefficient was obtained for a logarithmic regression but the value of the coefficient of determination is very low ($r^2 = 0.26$ for artificial gypsum). The power regression also performed quite well, while the exponential and linear one had a very poor fit.

No endurance limit is found, even at a cyclic stress ratio $i = 20\%$. Similar results were recently presented in literature e.g. Liu et al. (2014). Ohnaka & Mogi (1982) and Brown & Hudson, (1974) confirm that cracks may appear even for low applied deviatoric stresses, in small parts of the rock, where a stress concentration exceeds the local strength. This could confirm the observation that even small cyclic loads will cause damage in geomaterials.

## 7.3. The remaining shear strength curve

*Introduction:*

The purpose of the remaining shear strength curve is to describe the loss of shear strength for several cyclic stress ratios by a simple logarithmic equation. The methodology is described in chapter 4.4 and the testing procedure in chapter 5.2.5.

Normally, in case that the fatigue tests are carried and for more than $10^4$ cycles and for lower ranges of applied cycles, a low static fatigue approach is used (see chapter 3.7.1). Perhaps, a single description could be given for all ranges of cyclic loading. The remaining shear strength curve will be investigated if it can incorporate the whole range of cyclic loads.

### 7.3.1. The remaining shear strength curve for cohesive materials

*The remaining shear strength for artificial gypsum*

The linear regression lines for artificial gypsum are presented in Figure 7.7, for three cyclic stress ratios and excluding static results. These lines can also be forced to be as close as possible to intercept the ordinate at 100% (Figure 7.8 and in Table 7-2). It can be noticed that

all three lines have in this case almost the same slope (Pytlik & Van Baars, 2014). That suggests the cyclic stress ratio does not have any effect on the loss of strength. This is a very surprising result. One would expect that different cyclic stresses will cause different strength reductions (see chapter 3.5). This lack of correlation between the cyclic stresses $\tau_{cyc}$ and the remaining shear strength $\tau_{rem}$ should be further investigated because it can be caused by the high scatter of the data results. One of the explanations could be that, due to the scatter of the results, the influence of the cyclic stress ratio is obscured by that scatter. The slope of the curve for different cyclic loading ratio is more sensitive to the initial strength of the sample (and the scatter of the results) than the loss of strength in cyclic loading.

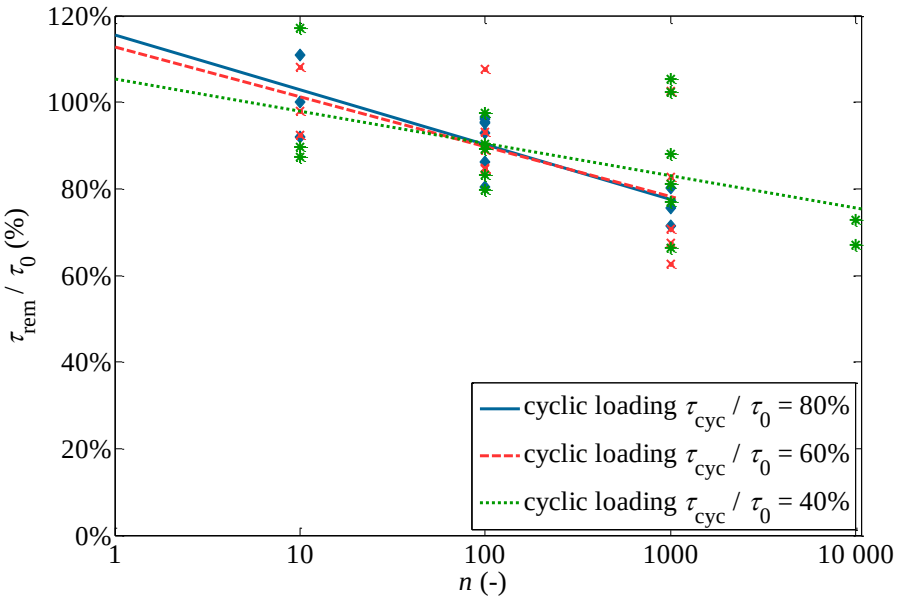


*Figure 7.7. The remaining shear strength curves for artificial gypsum (excluding static tests)*

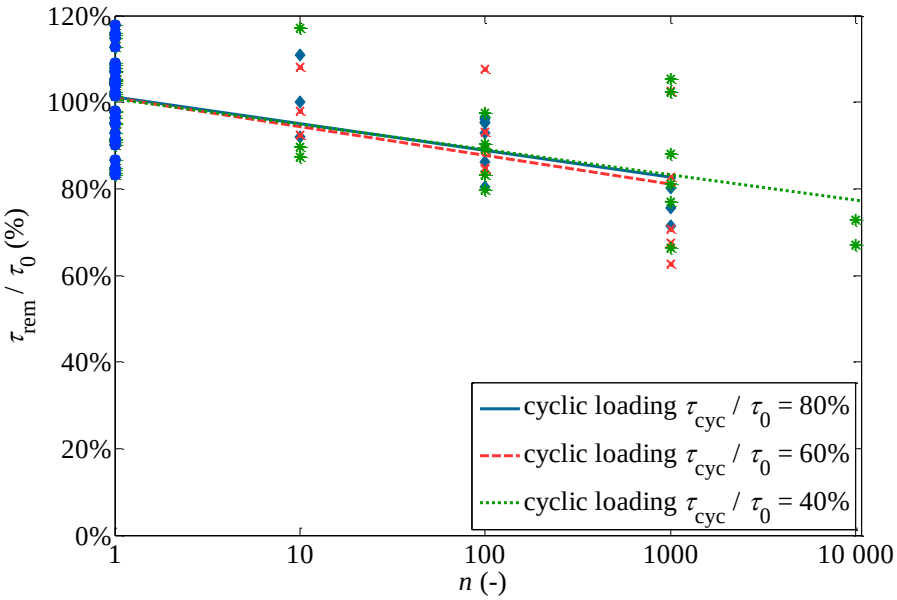


*Figure 7.8. The remaining shear strength curve for artificial gypsum (including static tests)*

If an assumption is made that the strength of material does not depend much on the cyclic

loading, a single log-normal curve can be given for all cyclic tests (Figure 7.9). This curve takes for the regression fit all tested samples into account, and thus omits the information of the cyclic stress ratio $\tau_{cyc}/\tau_0$. This implies that the remaining shear strength curve is losing one of its advantages – the estimation of a fatigue life for different cyclic stress ratios.

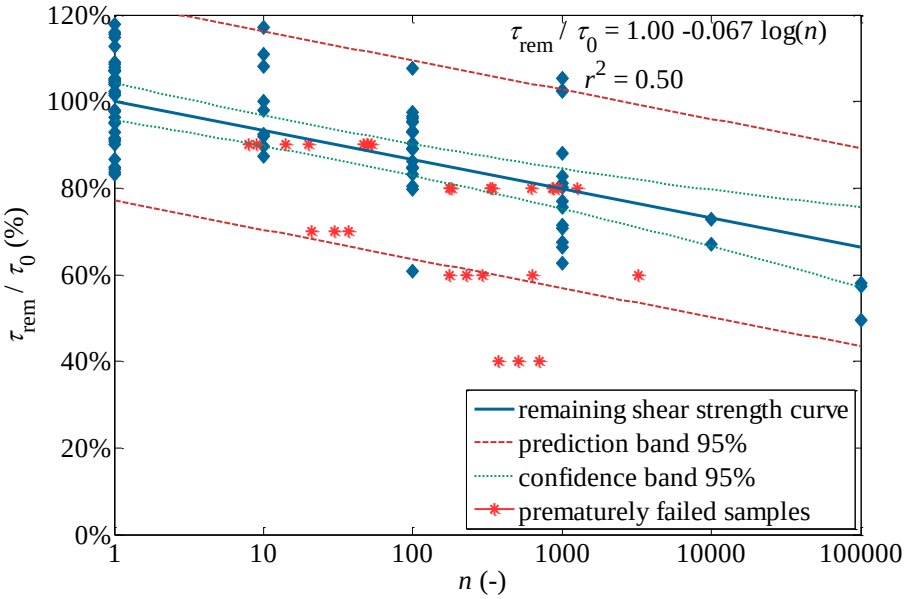


*Figure 7.9. The remaining shear strength curve for artificial gypsum excluding the cyclic stress ratio*

In Figure 7.9 it can also be noticed that especially for cyclic tests, the prediction band and data spread are very high. For the static test results (chapter 6.2.1), the coefficient of determination in p-q plot is equal $r^2 = 0.82$, while the $r^2$ for cyclic tests (Table 7-2) is very low. This means, that the cyclic test results are much more influenced by the material discontinuity properties than the static test results, even if static tests show that the material has very uniform strength properties.

*Table 7-2. The remaining shear strength curve parameters for different cyclic stress ratios (including static data)*

| $\tau_{cyc}/\tau_0$ | $r^2$ | *slope* | *intercept* |
|---|---|---|---|
| 40% | 0.32 | 0.068 | 1.00 |
| 60% | 0.34 | 0.086 | 1.00 |
| 80% | 0.28 | 0.072 | 1.00 |

*The remaining shear strength curve for mortar*

In Figure 7.10, Figure 7.11 and Figure 7.12, the remaining shear strength curves for mortar are presented. When the number of cycles increases, the shear strength of mortar increases, for some tests (Figure 7.11, Figure 7.12); while for some other decreases (Figure 7.10). This is different from the results for the S-N curve of mortar (compare with chapter 7.2.1). The increase in strength and lack of fatigue can be caused by the higher cement/sand ratio (higher cohesion) for the samples, for which the cement/sand ratio was the highest. A lack of fatigue for low cycles can indicate that the stronger the material the longer the fatigue life is.

A longer curing time can also play a role and therefore, the increase in strength of samples for times longer than one month has to be further investigated. For the number of cycles 10 000 the tests can last up to 1 week, in which the strength of mortar samples can further increase due to still continuing hardening process. Unfortunately, the impact of time hardening on the strength has not been investigated, and no corrections which take the curing period could be included. Due to this, the time of curing of a one week has to be extended to a one month.

It is worth to mention that, the best fit of the static test results for mortar was very high ($r^2$ = 1.0) and it was therefore expected that cyclic tests on this material would also give more accurate results than artificial gypsum. Nevertheless as it can be noticed for the cyclic tests, the spread of data points is large, even though high homogeneous and isotropic samples were used.

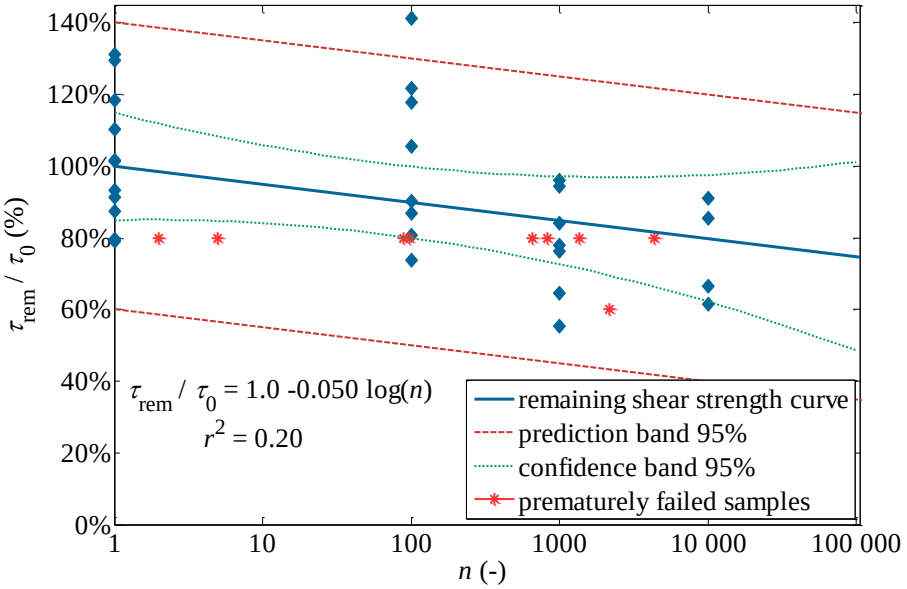


*Figure 7.10. The remaining shear strength curve for mortar (1 week, cement/sand ratio = 0.5)*

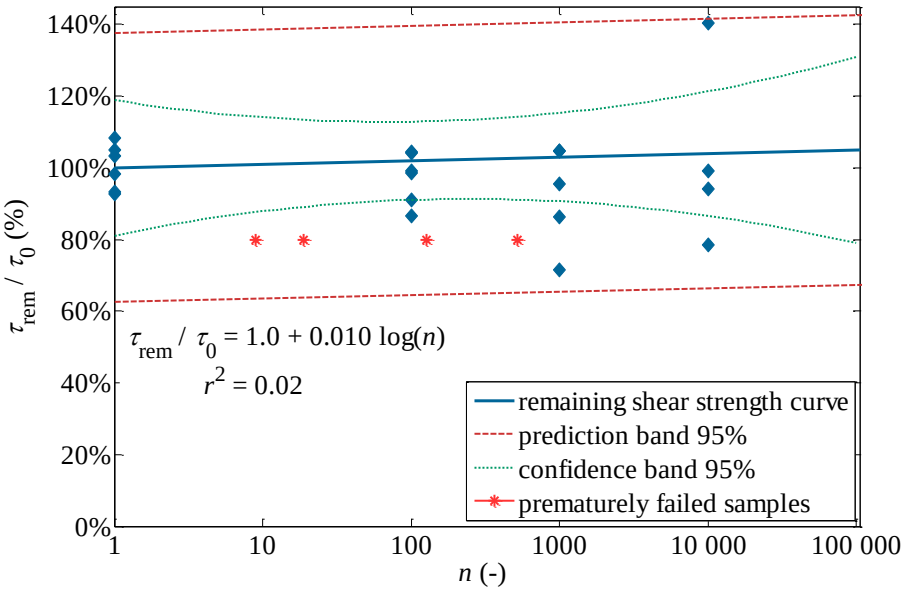


*Figure 7.11. The remaining shear strength curve for mortar (1 week, cement/sand ratio = 1.0)/ beach sand*

For the remaining shear strength curve from Figure 7.11 and Figure 7.12 (for a cement/sand ratio of 1) there is even a negative fatigue. This is probably caused by the fact that the mortar was still hardening during the tests.

In the presented Figure 7.11 and Figure 7.12, the coefficient of determination is very low (close to 0). It means that the model does not explain any variation. The line is constant and no correlation between the number of cycles and strength reduction exists. By looking at the data points it can be found, however that neither strength reduction increase, nor decrease is found.

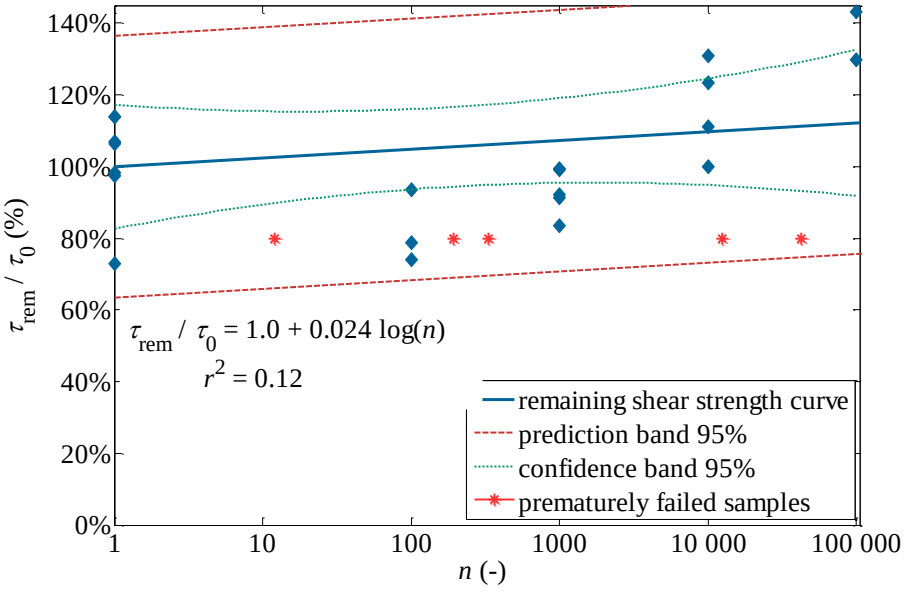


*Figure 7.12. The remaining shear strength curve for mortar (1 month, cement/sand ratio = 1.0) /coarse sand*

### 7.3.2. The remaining shear strength curve for cohesionless materials

*Intact limestone*

In case of limestone material, only horizontally drilled samples were tested in triaxial cyclic tests. Series of 10, 100 and 1000 applied cycles were carried out. Due to a low number of available samples, only one cyclic stress ratio was applied - $\tau_{cyc}/\tau_0 = 80\%$. By comparing the static test results (Figure 6.7) with the cyclic ones, it was found that the shear strength slightly increased (Figure 7.13 and Table 7-3). This means there is negative fatigue in limestone, which is remarkable. From the p-q plot in Figure 7.14, it can be noticed that the friction angle is almost unaffected by cyclic loading.

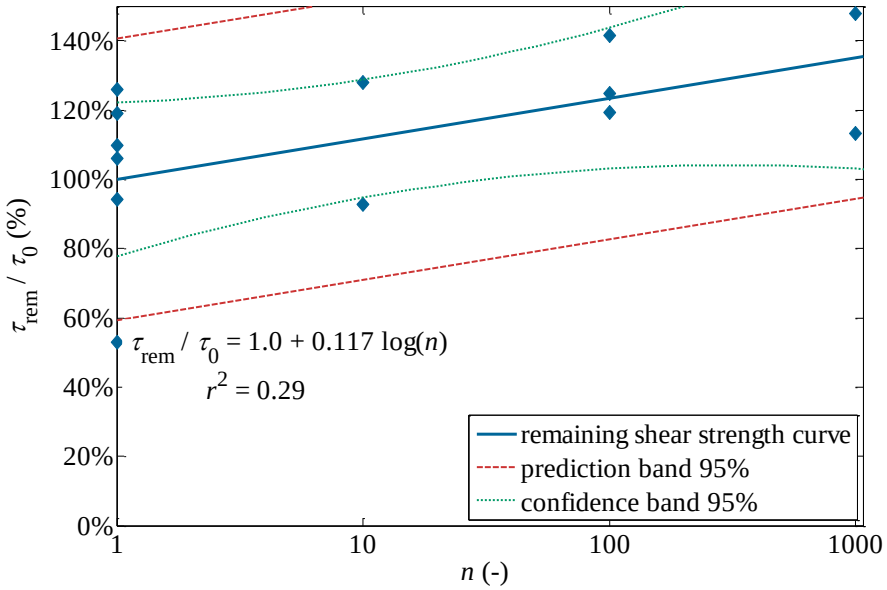


*Figure 7.13. The remaining shear strength curve for limestone ($\tau_{cyc}$ = 80%)*

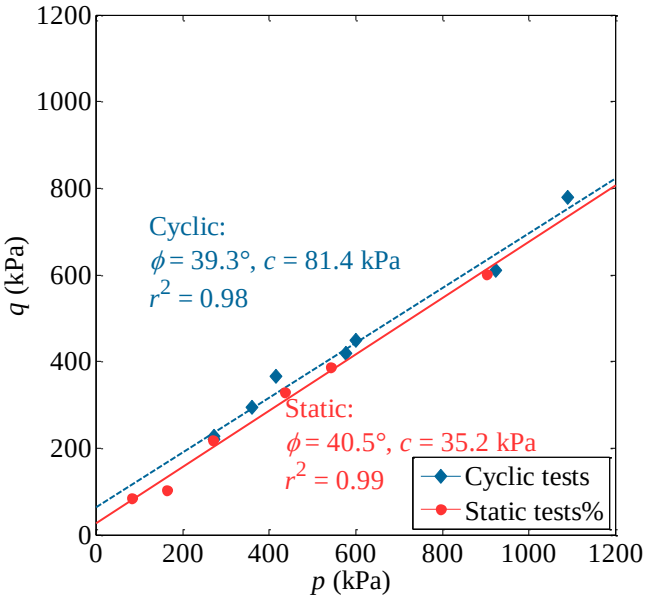


*Figure 7.14. Effect of cyclic loading on limestone for 100 cycles and $\tau_{cyc}/\tau_0$ = 80%*

*Table 7-3. Limestone strength parameters from triaxial tests in cyclic loading*

| Parameter | | Static | 100 cycles tests, $\tau_{cyc}/\tau_0 = 80\%$ |
|---|---|---|---|
| $\phi$ | (°) | 40.5 | 42.5 |
| $c$ | (kPa) | 35.2 | 58.6 |

*Crumbled limestone & other sands*

Cyclic triaxial tests have also been carried out on crumbled limestone. The results can be found in Figure 7.15 and Table 7-4.

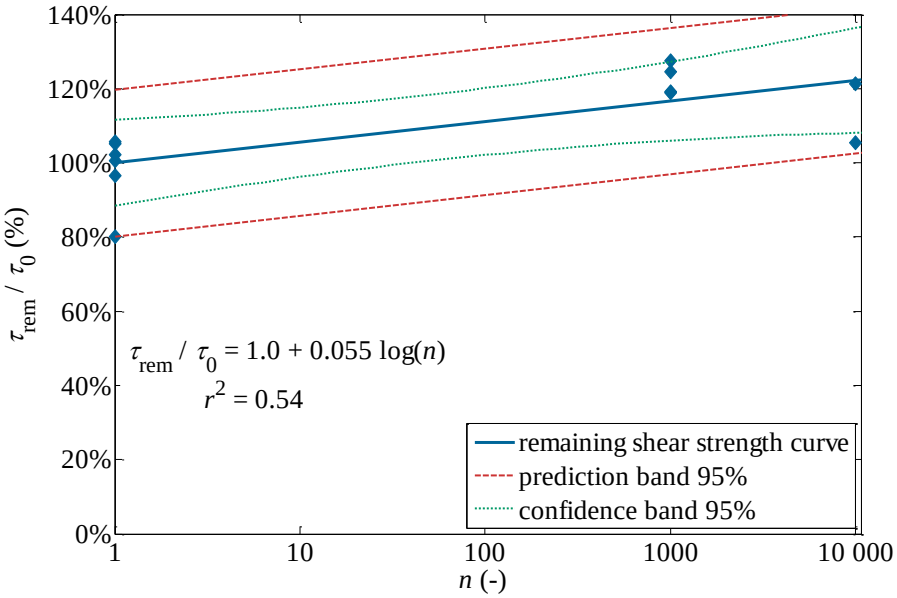


*Figure 7.15. The remaining shear strength curve for crumbled limestone*

*Table 7-4. Friction angle of crumbled limestone for cyclic and static triaxial tests*

| | $\tau_{cyc}/\tau_0 = 40\%$ | $\tau_{cyc}/\tau_0 = 80\%$ |
|---|---|---|
| $\phi$ (°) for 1 cycle | 44.8 | 44.8 |
| $\phi$ (°) for 1000 cycles | 47.9 | 49.3 |
| $\phi$ (°) for 10000 cycles | 46.5 | 51.9 |

Since the strength of crumbled limestone increased during cyclic loading, similar to intact limestone, no fatigue was found. This behaviour agrees with laboratory tests on coarse gravel conducted by e.g. Suiker (2002). He stated that granular materials influenced by cyclic loading can obtain a higher strength than for static loading.

Other types of sands (i.e. beach sand, coarse sand and norm sand) present the same behaviour as the crumbled limestone. The increase in shear strength was found for all sands (Figure 7.16). The shear strength increase is significant and the maximum increase is as high as 15% for a cyclic loading $\tau_{cyc}/\tau_0 = 80\%$ and $n = 10\,000$ cycles in the case of crumbled limestone. This value is similar for all tested sands. The higher strength is probably obtained by higher compaction (densification) caused by the high cyclic loading. This agrees with the shakedown theory (Yu, 2006). The changes of density were, however, not measured.

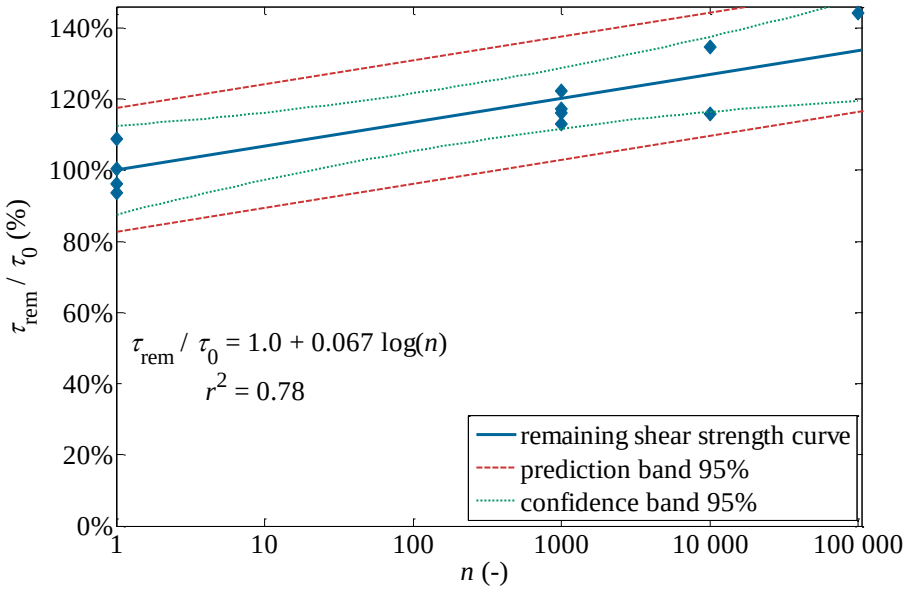


*Figure 7.16. Remaining shear strength curve for norm sand (cyclic stress ratio $\tau_{cyc}/\tau_0$ = 80%)*

*Friction angle in cyclic loading for cohesionless materials*

For cohesionless granular materials the only strength parameter is the friction angle $\phi$. Therefore, the ratio of the remaining shear strength to the static shear strength $S_{rem}/\tau_0$ can be replaced by the ratio of the remaining friction angle $\phi_{rem}$ to the static $\phi_0$ (static) friction angle. In a similar way as for the remaining shear strength curve, a plot can be generated (Figure 7.17). It can be easily noticed that the friction angle increases with the increase in number of cycles $n$.

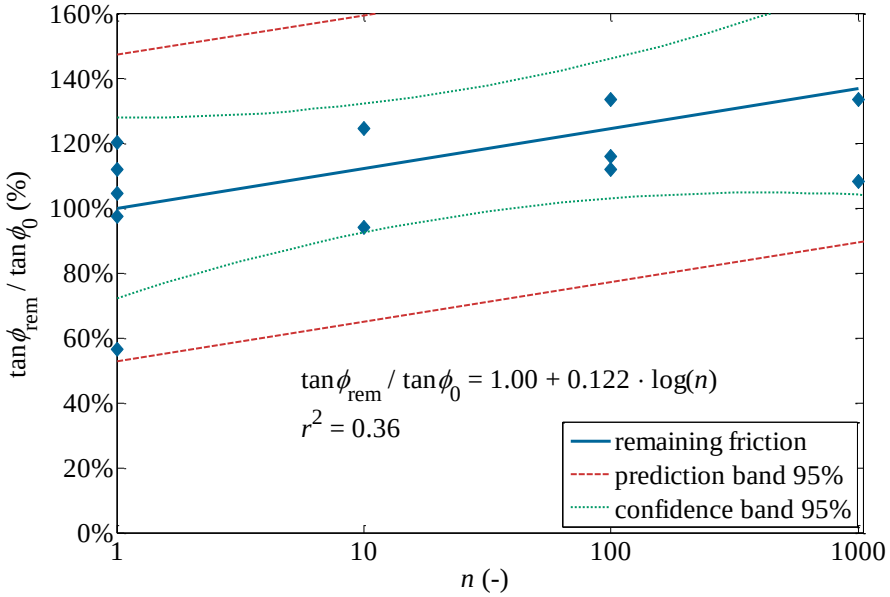


*Figure 7.17. Remaining friction angle versus the initial friction angle after a given number of cycles for intact limestone ($\tau_{cyc}$ /$\tau_0$ = 80%)*

The friction angle of the static tests is compared with the friction angle of the cyclic tests (Table 7-5, Table 7-6 and Table 7-7). In all cases the friction angle increased.

*Table 7-5. Friction angle of norm sand for static triaxial and cyclic triaxial tests*

| | $\tau_{cyc}/\tau_0 = 80\%$ | $\tau_{cyc}/\tau_0 = 40\%$ |
|---|---|---|
| $\phi$ (°) for 1 cycle | 39.1 | 39.1 |
| $\phi$ (°) for 1000 cycles | 41.4 | 40.0 |
| $\phi$ (°) for 10 000 cycles | 41.7 | 41.8 |
| $\phi$ (°) for 100 000 cycles | 46.8 | - |

*Table 7-6. Friction angle of beach sand for static triaxial and cyclic triaxial tests*

| | $\tau_{cyc}/\tau_0 = 80\%$ | $\tau_{cyc}/\tau_0 = 40\%$ |
|---|---|---|
| $\phi$ (°) for 1 cycle | 39.9 | 39.9 |
| $\phi$ (°) for 1000 cycles | 43.1 | 42.2 |
| $\phi$ (°) for 10 000 cycles | 45.0 | 43.6 |

*Table 7-7. Friction angle of coarse sand for static triaxial and cyclic triaxial tests*

| | $\tau_{cyc}/\tau_0 = 80\%$ | $\tau_{cyc}/\tau_0 = 40\%$ |
|---|---|---|
| $\phi$ (°) for 1 cycle | 42.3 | 42.3 |
| $\phi$ (°) for 1000 cycles | 42.8 | 42.2 |
| $\phi$ (°) for 10 000 cycles | 44.8 | 42.4 |

### 7.3.3. Conclusions from the remaining shear strength curves

The remaining shear strength curves confirm a reduction of the shear strength due to the cyclic loading on cohesive materials (artificial gypsum and some mortar tests). An impact of cyclic stress ratio was not found, which is very surprising. It means that for the remaining shear strength curve, the number of cycles *n* is more crucial than the cyclic loading.

Fatigue was not observed for cohesionless materials. Limestone does not lose its strength in cyclic loading, which is remarkable. Additionally, the friction angle is almost unaffected in cyclic loading. Even more, the friction angle slightly increases. The fatigue of geomaterials is governed primarily by a loss of the cohesion, while the friction angle remains constant. Other cohesionless granular materials show the same pattern as intact limestone. Cyclic loading leads in cohesionless (very weak cohesive) materials to an increase in the friction angle $\phi$, which is caused by densification (see chapter 2.2.6).

## 7.4. Stiffness changes in cyclic loading

*Stiffness changes for geomaterials*

The stiffness reduction in cyclic loading may be an interesting parameter to investigate as it requires less laboratory testing than strength tests and can be additionally assessed by non-destructive techniques. The stiffness reduction progress can be used as a rough estimation of the actual fatigue life and a strength reduction process. The changes in stiffness could improve the assessment of fatigue life, but unfortunately, only several tests were conducted on stiffness reduction for geomaterials, and thus there is not enough data and no good

prediction model is available. One of the very few examples gave Bagde & Petros (2011), who found that stiffness modulus degrades for sandstone in compressional cyclic tests.

For other materials (composite materials), remaining stiffness fatigue prediction models have already been proposed. Hwang & Han (1986) stated however, that the estimation of the stiffness reduction is not errorless and does not provide very accurate results. Post et al. (2006), showed that for composite materials, there was no correlation between the stiffness and the remaining strength or the fatigue life.

*Stiffness calculation*

Usually the stiffness is calculated as a proportion of the stress difference at a certain level to a strain difference corresponding to this stress (see Figure 7.18, left). For instance, the measure of static Young's modulus varies depending on the loading/unloading path and the level of confining pressure (Plona & Cook, 1995). Eurocode 7 (2007), suggests that the Young's modulus may be characterised by a complete curve, or by conventional values:

1) at a fixed percentage of ultimate strength (i.e. 50 %) – $E_{tan}$; (see Figure 7.18, left).
2) the mean value $E_{av}$ at the linear section of the axial stress-strain curve; (see Figure 7.18, right).
3) the secant modulus $E_{sec}$, measured from zero stress to a certain fixed percentage of the ultimate strength(see Figure 7.18, left).

For the purpose of this investigation, the Young's modulus is measured at a fixed percentage $E_{av}$ - 80% of the maximum strength and 10% as the minimum strength (see Figure 7.18, right). This assures that the range of stresses is linearly proportional to the strain. Taking the minimum 10% of the maximum strength allowed avoiding problems with the equipment readings, because for lower stresses the readings of the stiffness from the laboratory equipment are not very accurate.

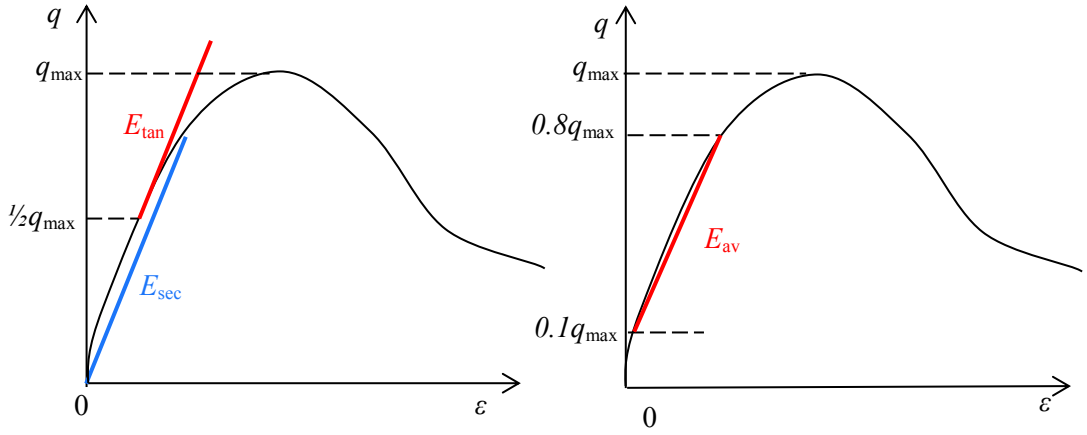


*Figure 7.18. Stiffness measurement for geomaterials*

*Stiffness – Strength correlation in static tests*

It was found that no strong correlation between the static strength (normalised to static

strength at given confining pressure $\sigma_3$) and static stiffness exists for artificial gypsum (Figure 7.19) and limestone (Figure 7.20). Weak correlation was found for mortar (Figure 7.21). The lack of a strong correlation is for all materials evident.

Some correlations between stiffness and strength for rocks are proposed in literature e.g. Horsrud (2001). The derivation of the strength from the stiffness was investigated by Chang et al. (2006). They found that some of the empirical relations work fairly well for some rocks; however most of the relations do not fit the measured data.

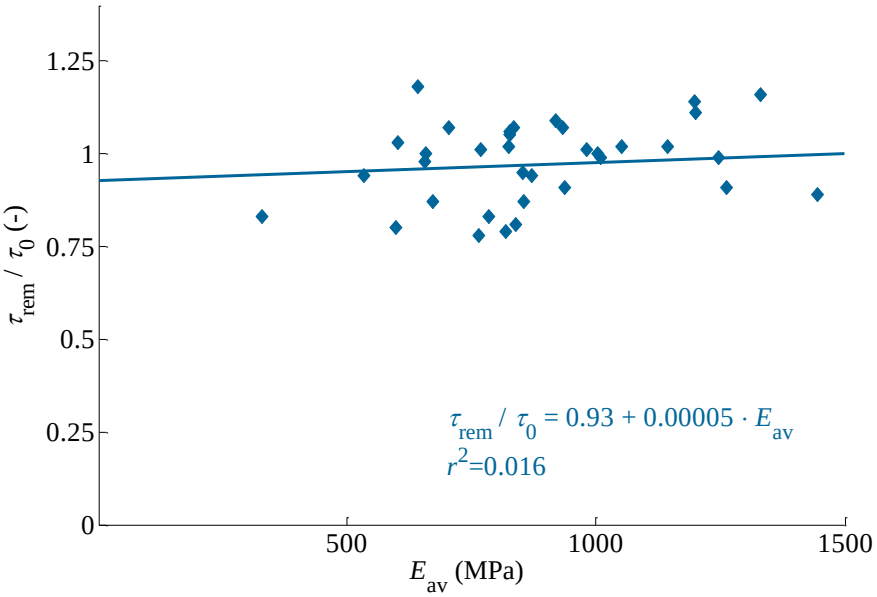


*Figure 7.19. Correlation between static stiffness and static strength for artificial gypsum*

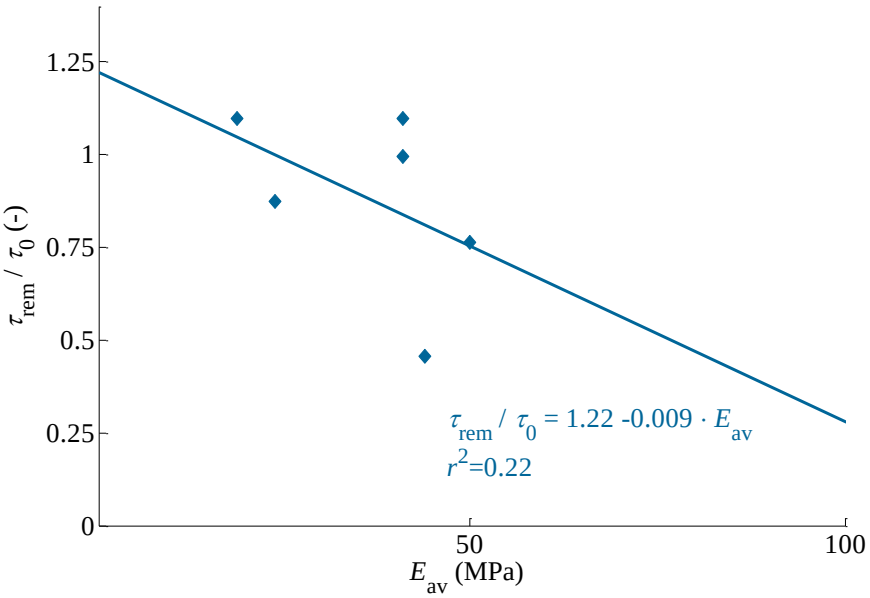


*Figure 7.20. Correlation between static stiffness and static strength for limestone*

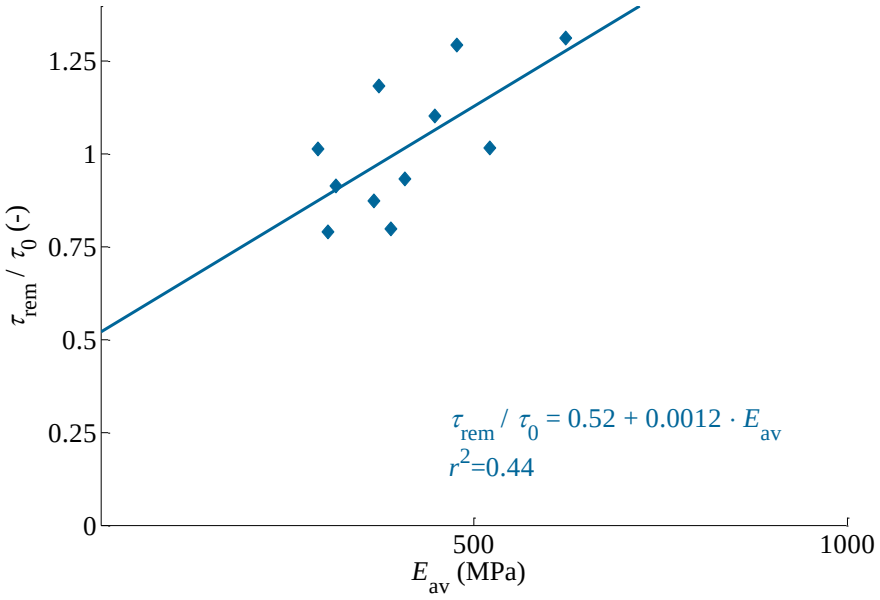


*Figure 7.21. Correlation between static stiffness and static strength for mortar*

*Stiffness reduction for cohesive materials*

In cyclic tests on artificial gypsum, as well as for mortar and limestone, the first cycle has a much smaller stiffness (slope) than the next several dozen cycles (see Figure 7.22). The increase in stiffness after the first cycle is much larger than in subsequent cycles, which leads to an increase in stiffness.

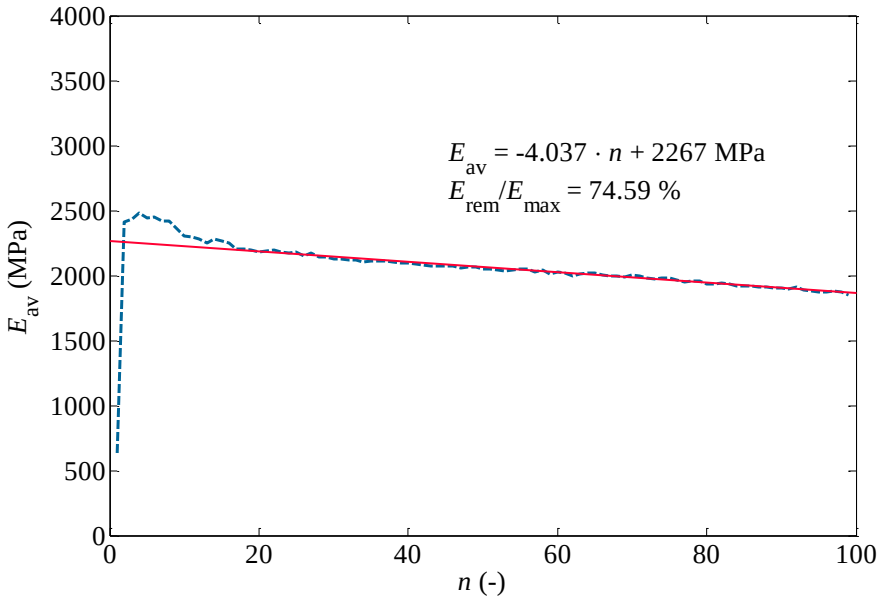


*Figure 7.22. Stiffness reduction in 100 cycles of one sample for artificial gypsum*

In order to describe the changes in stiffness under cyclic loading, the ratio $E_{rem}/E_{max}$ is introduced as a ratio of the stiffness in the last cycle $E_{rem}$ to the maximum stiffness $E_{max}$ during the whole cyclic loading test. The reason why the whole cyclic test run was considered is that, for the first several cycles, the stiffness can vary significantly (see Figure 7.22) and the maximum stiffness $E_{max}$ is usually somewhere at the beginning of cyclic loading, but not

for the first cycle.

The data used to create the stiffness reduction curve was obtained from the same tests used to create the remaining shear strength curve (Figure 7.23 and Figure 7.24) and S-N curve (Figure 7.25 and Figure 7.26). This was possible, because the strains were also measured during the cyclic shear strength tests. For all the plots, the curve was force to intercept the y-axis at 100%. During cyclic loading, the cohesive materials lose their stiffness with increase in number of cycles as can be noticed from Figure 7.22. The stiffness reduction is for all samples in Figure 7.23 very similar to the corresponding remaining shear strength curve for artificial gypsum (compare Figure 7.9 with Figure 7.23). Similar results are found for mortar.

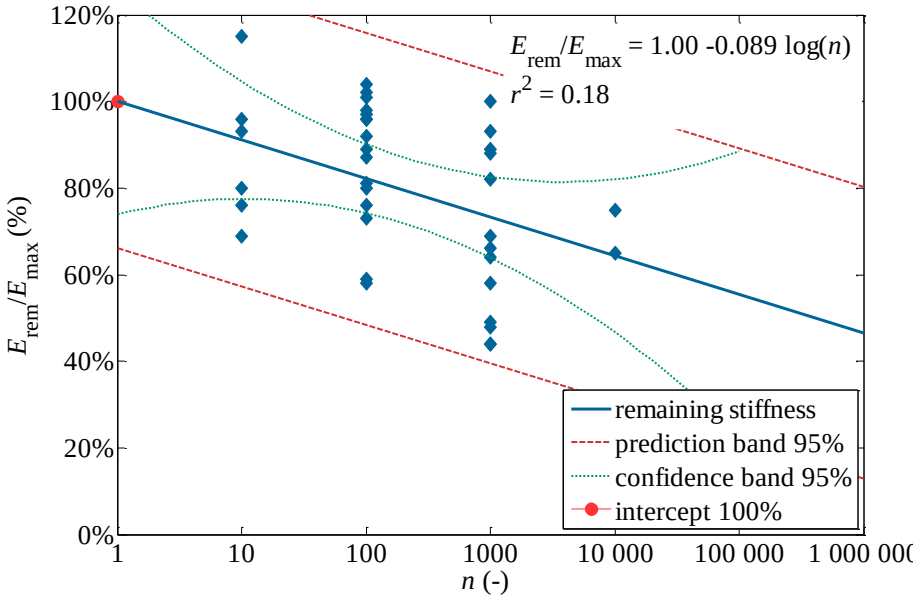


*Figure 7.23. Remaining stiffness curve for artificial gypsum (based on remaining shear strength curve data)*

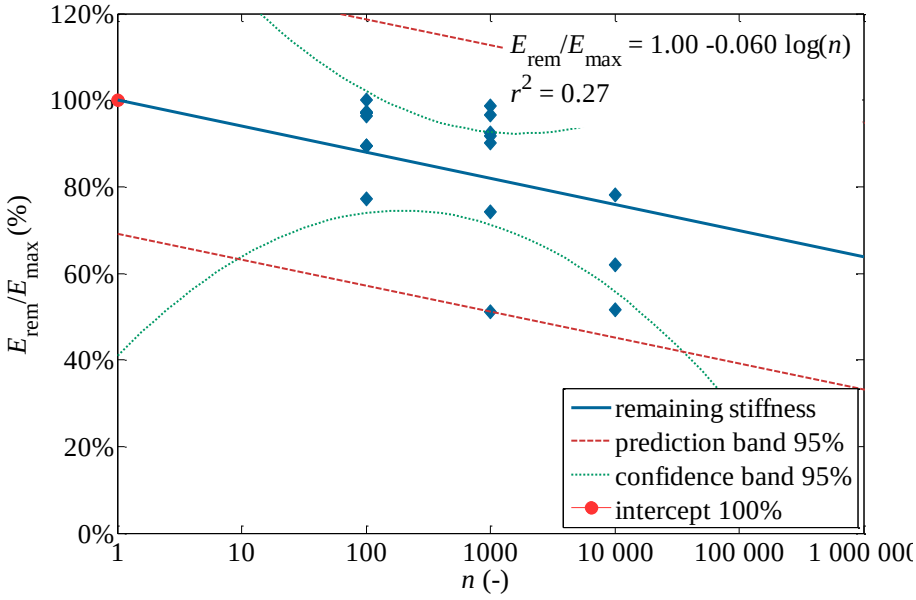


*Figure 7.24. Remaining stiffness curve for mortar (1 week, cement/sand ratio=0.5) (based on*

*remaining shear strength curve data)*

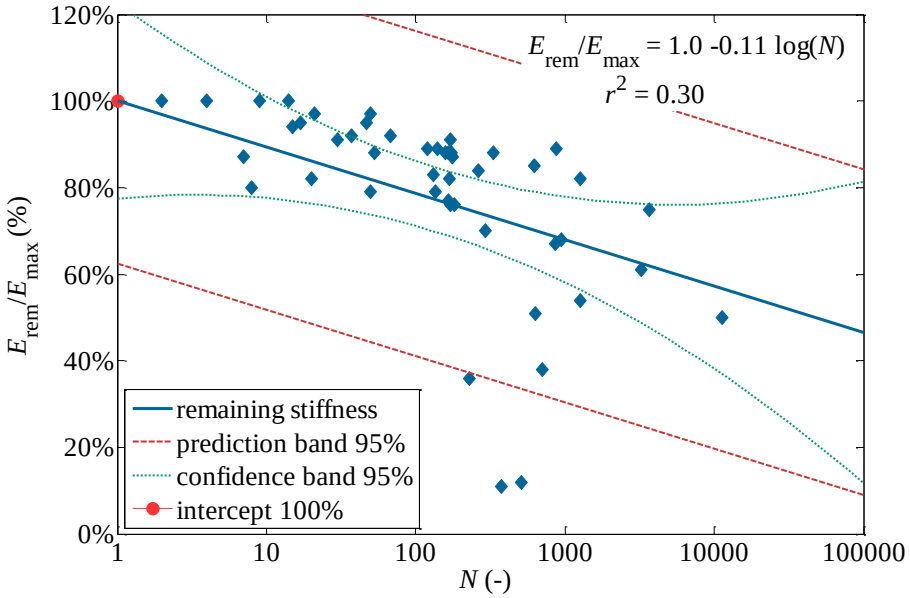


*Figure 7.25. Remaining stiffness curve for artificial gypsum (based on S-N curve data)*

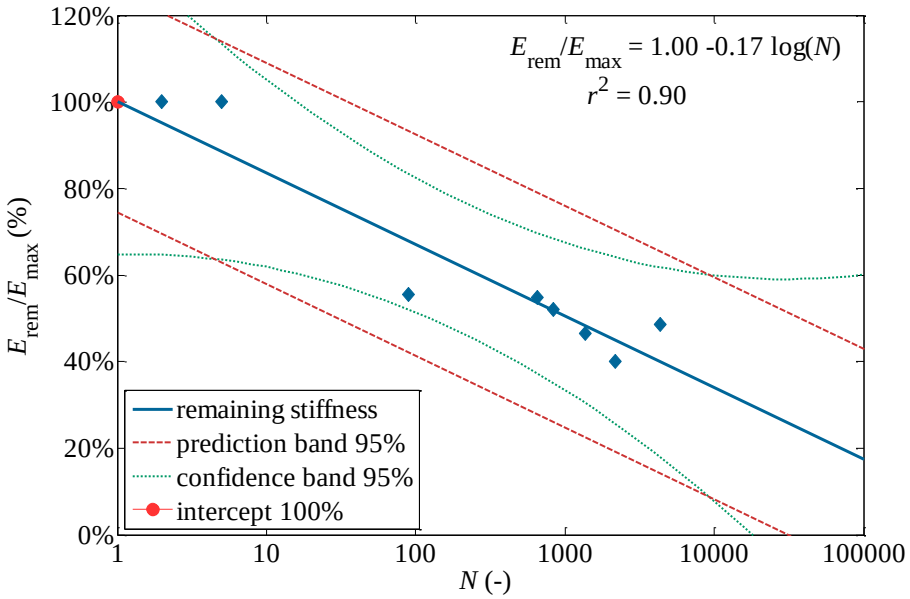


*Figure 7.26. Remaining stiffness curve for mortar (1 week, cement/sand ratio=0.5) (based on S-N curve data)*

In the Figure 7.27 a plot which combines the cyclic strength and cyclic stiffness is presented. As it can be noticed no strong correlation could be found, which is similar to the static strength and stiffness lack of correlation. Similar results (lack of correlations, where also found for other materials and different mortar mixtures).

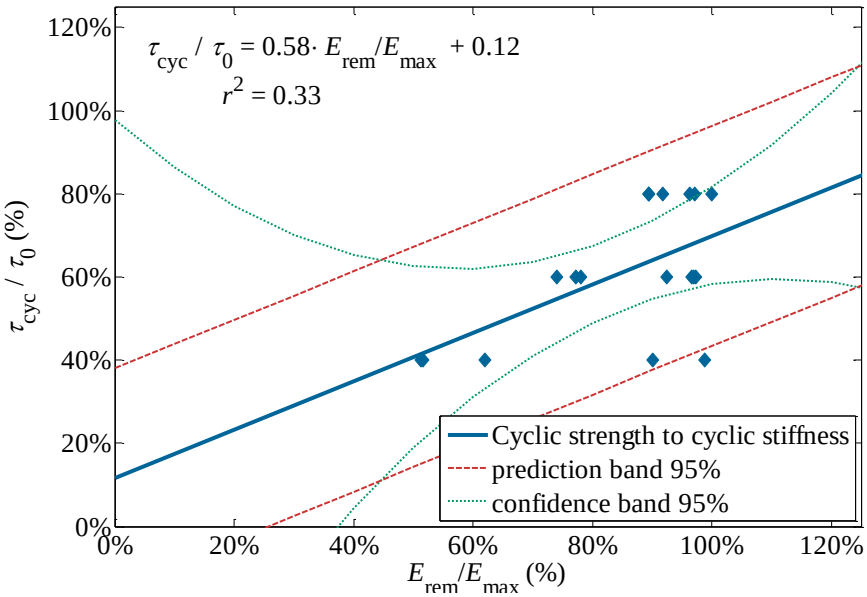


*Figure 7.27. Cyclic strength to cyclic stiffness correlation for mortar samples (1 week, cement/sand ratio=0.5) (based on remaining shear strength curve data)*

*Stiffness increase for cohesionless materials*

For cohesionless materials the cyclic loading induces an increase in stiffness as it can be seen in Figure 7.28 for limestone. This also corresponds to the results for the remaining shear strength tests on cohesionless materials (compare Figure 7.13 with Figure 7.28), where the increase in stress is caused by sample densification. For other sands the same stiffness increase was found.

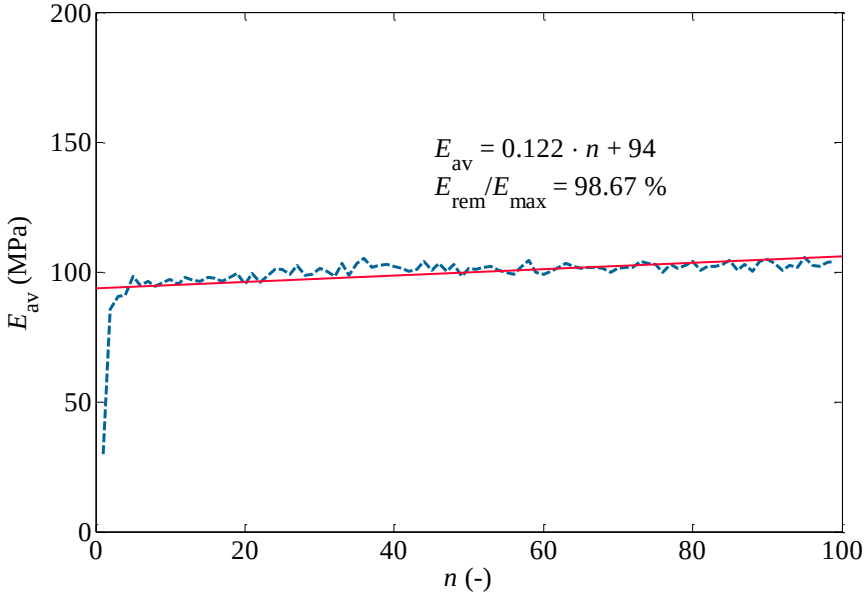


*Figure 7.28. Stiffness change of limestone in one test (100 cycles)*

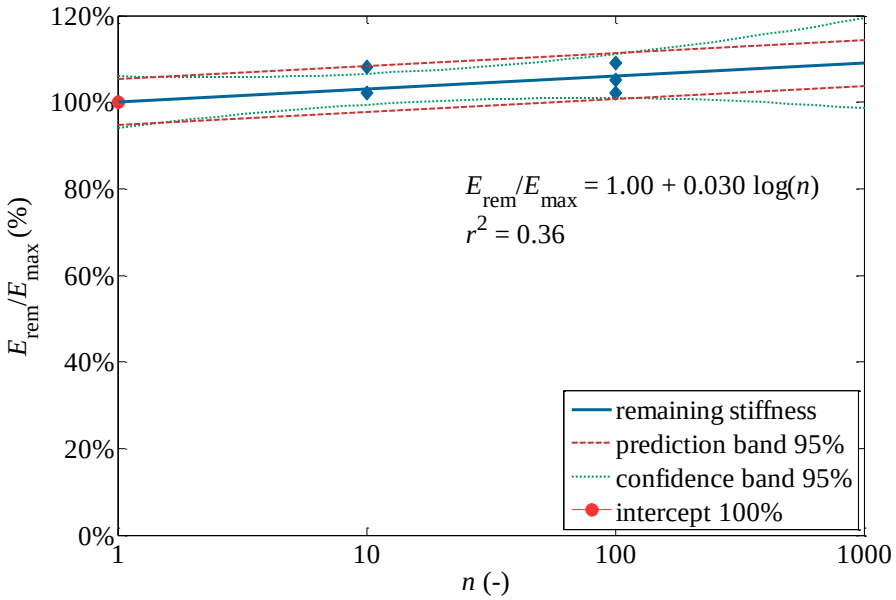


*Figure 7.29. Stiffness "reduction" curve for limestone*

## 7.5. Cyclic strain accumulation

*Strains of geomaterials in static tests*

In Figure 7.30 and Figure 7.31 the typical stress-strain behaviour for artificial gypsum is plotted (for other material the stress-strain behaviour is very similar). It is interesting to note that prior to failure, the stiffness decreases while the strains increase nonlinearly. For a low confining pressure $\sigma_3$ = 0 MPa (Figure 7.30) after the maximum load is reached, a typical brittle behaviour is observed. For a confining pressure $\sigma_3$ > 0.5 MPa (Figure 7.31) the stiffness decreases and an increase in plastic deformations is clearly visible. The strain-stress relationship becomes ductile and the plastic strains increase nonlinearly prior to failure, which indicates that the same cyclic stress ratio cause larger plastic deformations for higher confining pressure than for the lower one.

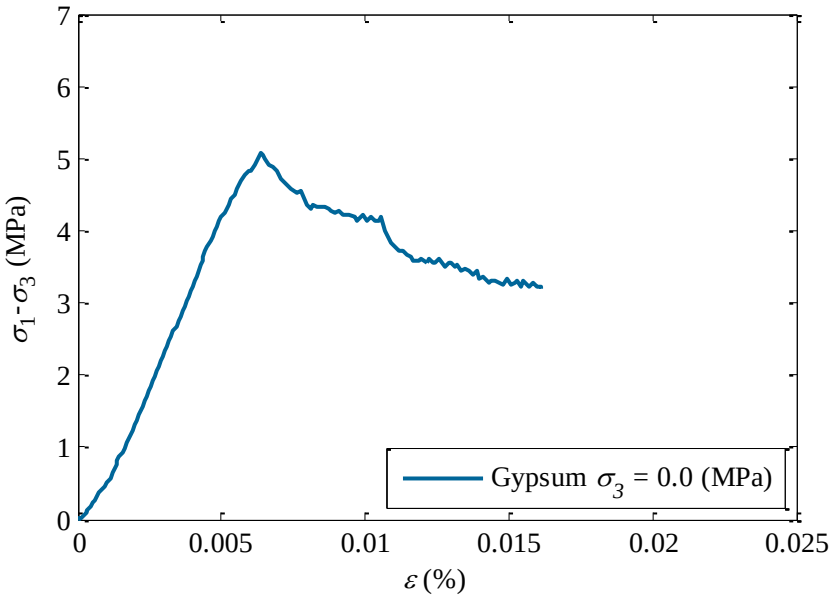


*Figure 7.30. A typical triaxial compression test plot of artificial gypsum for $\sigma_3$=0 MPa*

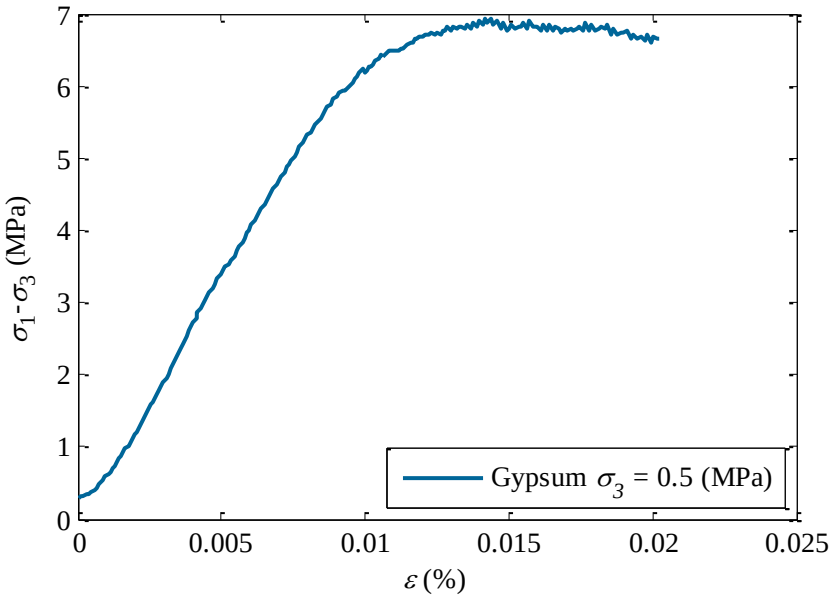


*Figure 7.31. A typical triaxial compression test plot of artificial gypsum for $\sigma_3$=0.5 MPa*

After failure of the material, the stresses are decreasing much slower in the case of a ductile material (strain softening), and remain at higher levels than for a brittle material. The same pattern can be found for concrete e.g. Malcot et al (2010), Poinard et al. (2010).

This difference in stress-strain plot for static tests may indicate that the cyclic behaviour is also different for lower and higher confining pressures. This can lead to difficulties in developing of a single cyclic strain accumulation model for all geomaterials. The development of a fatigue model based on strain and plastic strain energy accumulation would require a lot of laboratory testing and the results could be insufficient. For this reason, the accumulation of plastic strain is shortly discussed in this thesis.

*Accumulation of strains for geomaterials in cyclic tests*

One of the effects of cyclic loading on geomaterials is plastic strain accumulation (chapter 2.2.1). A typical strain accumulation is presented for drained conditions in Figure 7.32 and for undrained in Figure 7.33.

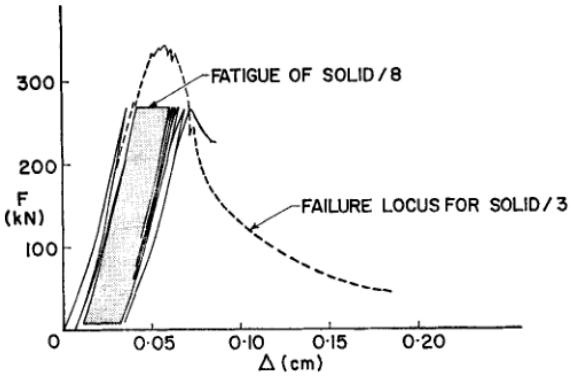


*Figure 7.32. Residual strength locus (Brown & Hudson, 1974)*

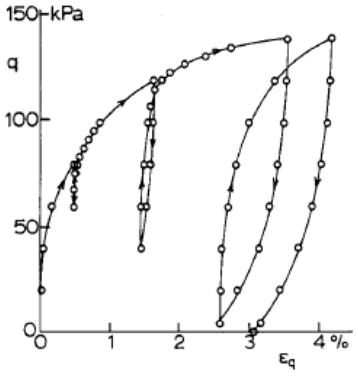


*Figure 7.33. Spestone kaolin: cycles of undrained loading (Roscoe & Burland, 1968)*

The strain in single cycle can be divided into two parts: recoverable (elastic – $\varepsilon^e$) and unrecoverable (plastic – $\varepsilon^p$) strain. The total incremental strain in one cycle $\Delta\varepsilon$ is a sum of the elastic strain component $\Delta\varepsilon^e$ and the plastic strain component $\Delta\varepsilon^p$:

$$\Delta\varepsilon = \Delta\varepsilon^e + \Delta\varepsilon^p \qquad 7\text{-}1$$

In cyclic loading, the amplitude of the recoverable elastic strain $\Delta\varepsilon^e$ is almost constant for each cycle and completely reversible (but only for small amplitudes).

In contrast to the elastic strains, the plastic strain $\Delta\varepsilon^p$ may decreases or increase with a progressive number of cycles. For cohesive geomaterials the rate of the plastic strain accumulation is increasing prior to failure. In case of cohesionless materials, both a decrease and an increase in the strain rate may occur. The different cyclic behaviour of strains for cohesionless material can be described by the characteristic state and shakedown theory, which will be further briefly investigated (see chapter 7.5.2).

### 7.5.1. Strain accumulation and strain rate of cohesive materials in cyclic loading

During cyclic loading on cohesive geomaterials, after a first several cycles (marked as stage *A* in Figure 7.34), the plastic strain in each cycle seems to reach a stable intermediate cycle state $\Delta\varepsilon^p$ = const. (stage *B*). With an increasing number of cyclic loads, the strains accumulate for each cycle and this is a clear evidence of a permanent strain build-up during cyclic loading.

The last several cycles before failure (stage *C*) show that the plastic strain increases much faster than that for the intermediate cycle stage (stage *B*).

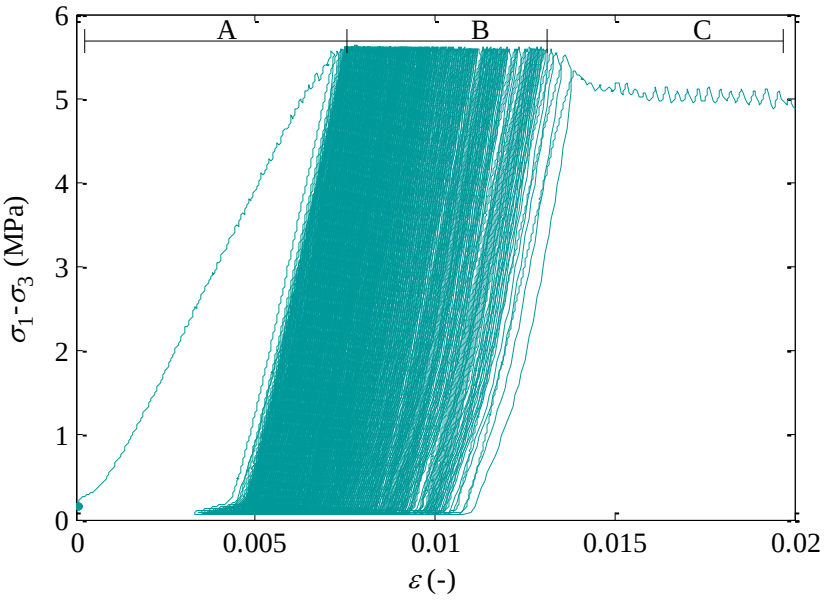


*Figure 7.34. A typical stress-strain plot for artificial gypsum under cyclic loading until failure*

The increase (or decrease) of the plastic strains can be described by the plastic strain rate:

$$\Delta\dot{\varepsilon}^p = \frac{d\varepsilon^p}{dN} = \frac{d}{dN}\left(\frac{l^p(N) - l_0}{l_0}\right) \qquad 7\text{-}2$$

here, $\Delta\dot{\varepsilon}^p$ is the plastic strain ratio in one cycle, $\varepsilon^p$ is the plastic strain, $N$ is the number of cycle, $l$ is length of a sample after cyclic loading, $l_0$ is the initial length of the sample.

The increase in plastic strain rate indicates that the damage of the sample is progressing very fast and this leads to an inevitable failure. The strain rate can be an indicator of an upcoming failure. This is probably related to an increase in number of microcracks and damages in the sample. At a certain level of damage, when the number of cracks is high enough, the sample deteriorates fast enough to fail.

The incremental build-up of plastic strains is sometimes called cyclic creep because it is similar to the creep behaviour of brittle materials described by e.g.: Haimson & Kim (1972), Brown & Hudson (1974), Haimson (1978) and Yamashita et al. (1999). This typical creep behaviour is also divided into three zones, similar to the ones in Figure 7.34. It should be mentioned, however, that creep and fatigue are different phenomena.

*Limitations*

During the laboratory triaxial cyclic tests, it was found that the plastic strain rate for some artificial gypsum and mortar tests did not follow the typical ABC pattern presented in Figure 7.34. For example, in Figure 7.35, another common pattern of plastic strain accumulation can be found. Around the middle of the cyclic loading a several cycles with much higher plastic strains occurred. The increasing strain rate is thus not necessarily implying an upcoming failure of the material. The cyclic loading still proceeds after this high accumulation of strains.

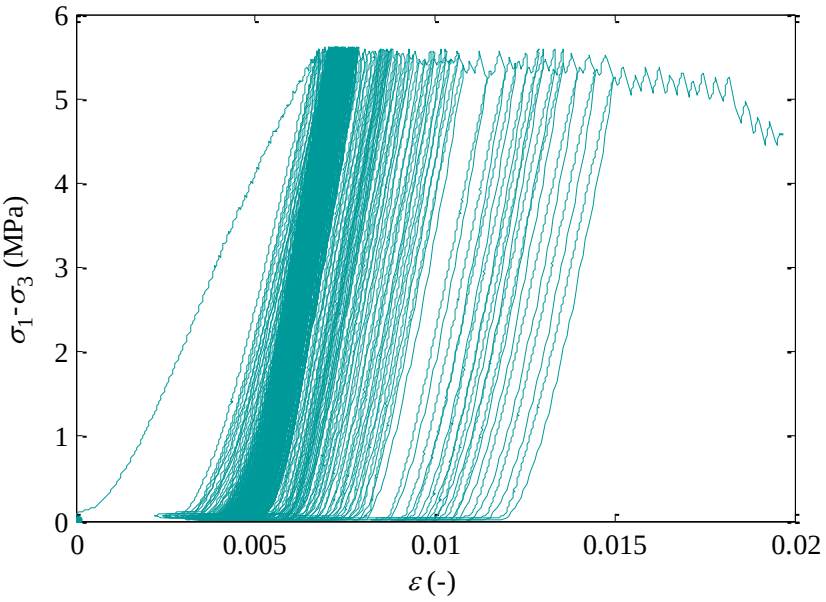


*Figure 7.35. Stress-strain plot for another common type of plastic strain accumulation*

*Artificial gypsum*

A plot based on all artificial gypsum tests is presented in Figure 7.36 (tests for the S-N curve) and in Figure 7.37 (tests for remaining shear strength curve). It can be seen that the total plastic strain accumulation until failure increases with an increasing number of cycles (the more cycles the higher the total plastic strain accumulation). The coefficient of determination $r^2$ = 0.17-0.18 has a very low value, so the data points are highly spread. Therefore, predictions based on strain accumulation do not give proper results for the fatigue life of artificial gypsum. Hilsdorf & Kesler (1966) also noted that the strain at failure was independent of the fatigue life.

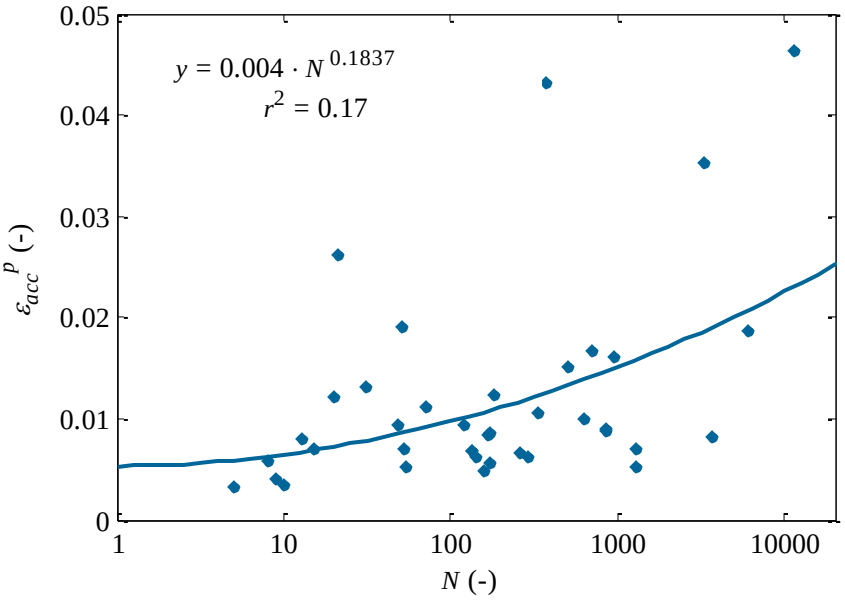


*Figure 7.36. Plastic strain accumulation until failure (all artificial gypsum samples for the S-N curve)*

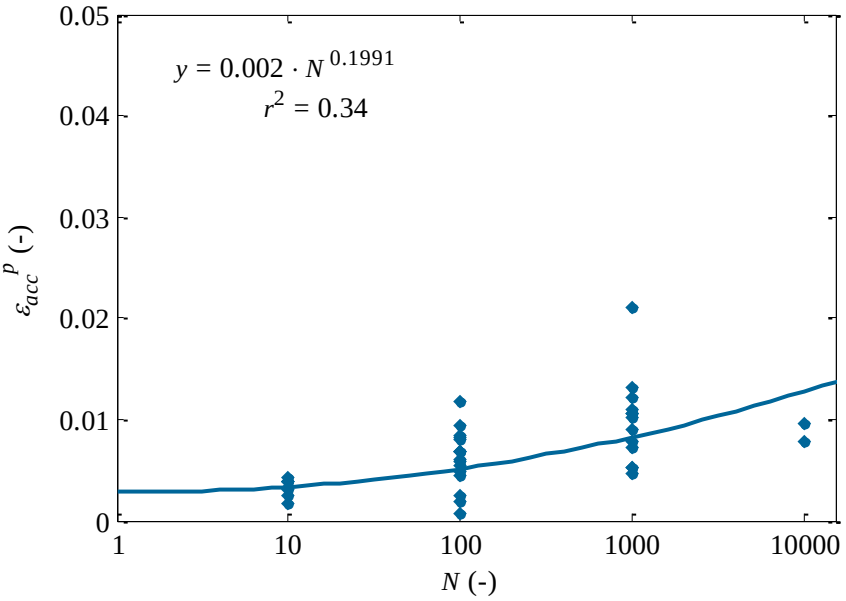


*Figure 7.37. Plastic strain accumulation until failure (all artificial gypsum samples for the remaining shear strength curve)*

*Mortar:*

For mortar the same results as for artificial gypsum is found. Based on the data from the remaining shear strength tests, no strong correlation between the plastic strain accumulation and number of cycles exists (Figure 7.38). A complete different behaviour is found, when the strains are calculated from tests for the S-N curve (Figure 7.39). Some correlation exists for which there is no clear explanation yet.

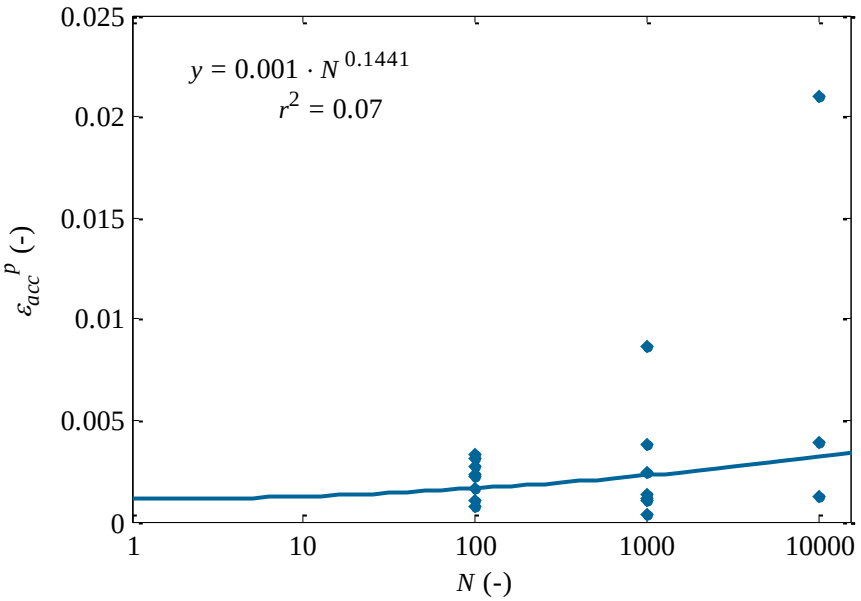


*Figure 7.38. Plastic strain accumulation until failure (1 week, c/s =0.5 mortar test for the remaining shear strength curve)*

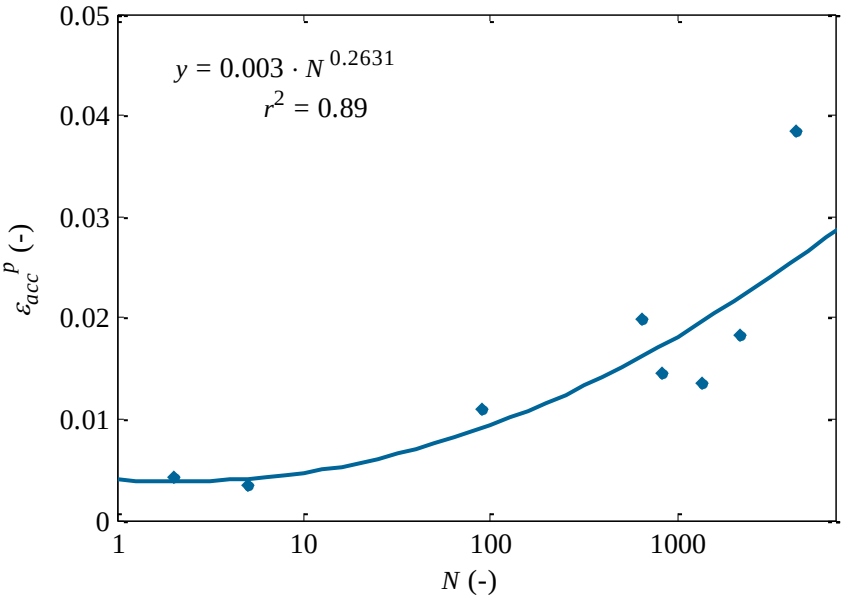


*Figure 7.39. Plastic strain accumulation until failure (1 week, c/s =0.5 mortar samples tested for S-N curve)*

*Remarks for the plastic strain accumulation of cohesive materials*

From a micromechanical point of view, the energy which is stored in a sample is much higher for a high confining pressure $\sigma_3$ than for a lower one. The cyclically loaded sample for with a higher confining pressure $\sigma_3$ can store more energy, accumulate more plastic strains $\varepsilon^p$, and thus have longer fatigue life (for remaining shear strength curve for the same applied number of cycles, the remaining shear strength is higher for higher confining pressure). According to energetic models, the more plastic strain energy the sample can store, the longer its fatigue life is. In other words, a higher confining pressure should decrease susceptibility to cyclic fatigue. This agrees with Brown & Hudson (1974), who stated that increasing ductility can result in post-peak curve flattening. This limits fatigue when brittle rocks are subjected to a high confining pressure.

The results of the strain accumulation in cyclic loading for cohesive samples, could not however, give conclusive remarks to that hypothesis.

### 7.5.2. Strain accumulation of cohesionless materials in cyclic loading

More detailed description of the effect of cyclic loading on cohesionless soils can be given by the characteristic state theory (Luong, 1980) and shakedown theory.

*Characteristic state*

The characteristic state line (Figure 7.40) describes the transition from compressive to dilative behaviour of cohesionless drained geomaterial (phase transformation line for undrained tests). When the cyclic stress is higher than the characteristic state it can lead to dilation. For dilative sands, a significant amount of strain due to cyclic loading can develop.

For stresses smaller than the maximum stress of previous loading, sand behaves much stiffer, compacted and gains strength. With an increasing number of cycles, the strain in each cycle decreases, reaching a stable state after a certain number of cycles. This is called cyclic shakedown (Yu, Khong, & Wang, 2007). Sand with a higher relative density dilates more and gains therefore higher ultimate shear strength. However, for very loose sands and for sands under a very high confining pressure, the characteristic line coincides with the failure envelope.

*Shakedown theory*

The basic assumption of the shakedown theory is that below a certain load the ultimate response will be purely elastic (reversible) and therefore, there is no more accumulation of plastic strain. If the applied load is higher than the shakedown load, uncontrolled permanent deformations will develop and therefore unstable conditions will progress (Figure 7.41).

The European Standard Committee has included in the actual standard for granular materials under cyclic loads (CEN, 2004) three classification ranges according to the work of Werkmeister (2003),

- range A–plastic shakedown–stable deformation behaviour;
- range B–plastic creep–failure at a high number of load cycles;
- range C–incremental collapse–failure at low number of load cycles.

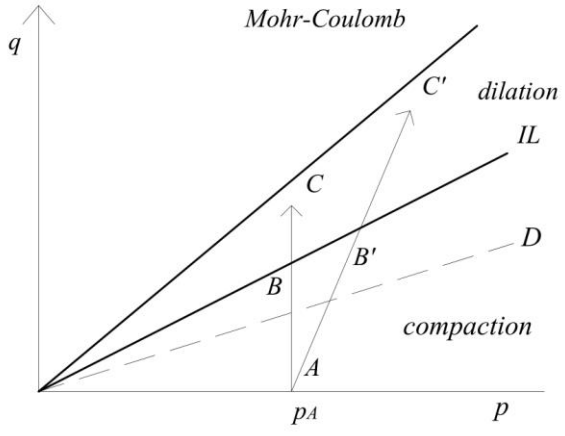


*Figure 7.40. A characteristic state (IL-instability line and compaction/dilation zones)*

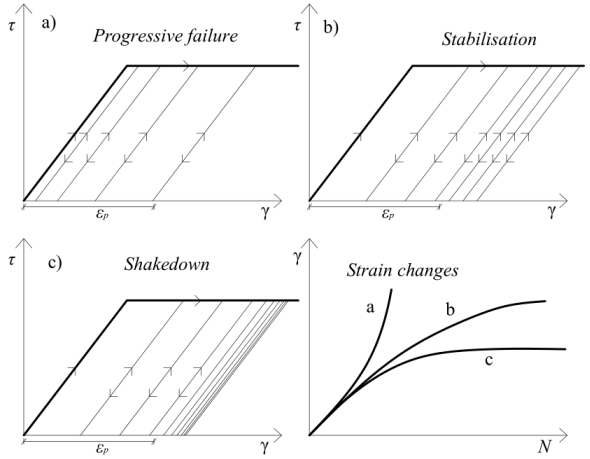


*Figure 7.41. Shakedown theory*

*Accumulation of plastic strains for cohesionless materials in cyclic loading*

The accumulation of plastic strains in cyclic loading can be easily noticed for intact limestone in Figure 7.42 and Figure 7.43. Similar results for cohesionless geomaterials were found by e.g. Galjaard et al. (1996). For both, the intact and the crumbled limestone, the accumulation of strains corresponds to a decreasing strain rate $\mathrm{d}\dot{\varepsilon}^{p}$, because the plastic strain rate reaches a stable state after a certain number of cycles (Figure 7.43). The decreasing strain rate $\mathrm{d}\dot{\varepsilon}^{p}$ indicates that the strain response of the material after certain number of cycles is purely elastic (shakedown). For all cohesionless materials the patter of strain accumulation () is the

same. It also means that probably all sands were already slightly densified before applying cyclic loading, leading to a shakedown (decrease in plastic strains with increasing number of cycles), see Figure 7.42.

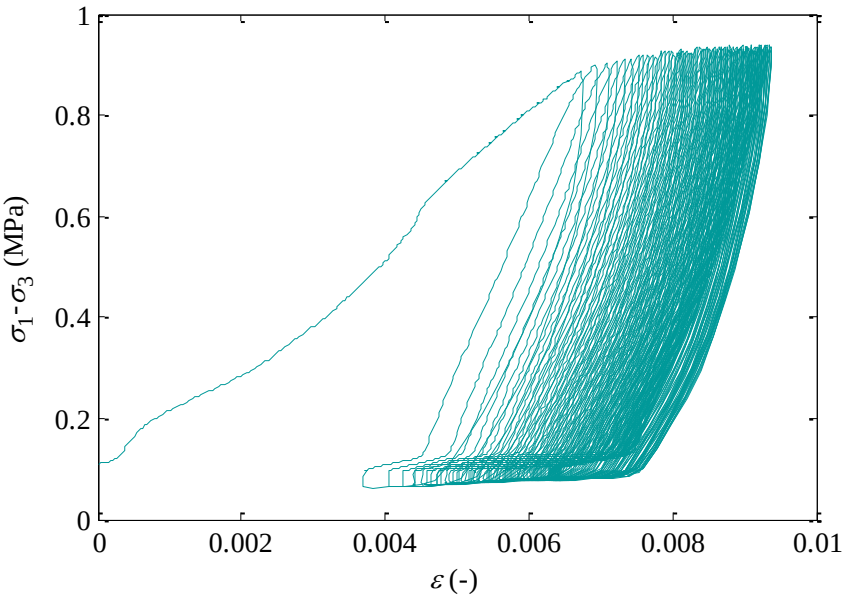


*Figure 7.42. Stress – Strain plot of intact limestone for 100 cycles*

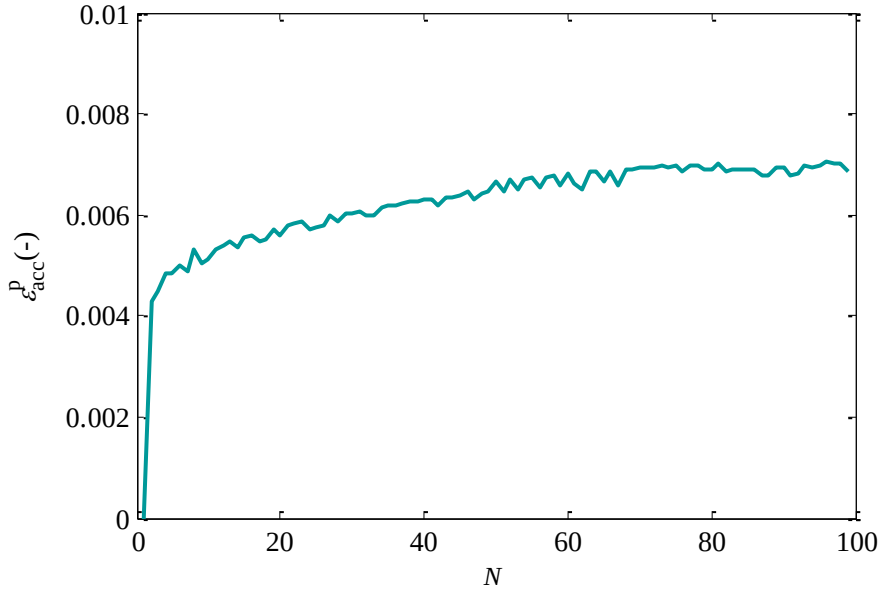


*Figure 7.43. Plastic strain accumulation in number of cycles for intact limestone*

## 7.6. Conclusions

All triaxial tests were conducted on dry samples in their natural state, without presence of water (no pore pressure). The range of the confining pressure was between 0 MPa and 0.5 MPa. The carried out cyclic tests were typical multiple loading tests with constant displacement ratio up to a certain stress level. The frequency was kept low to allow for precise application of cyclic loads and accurate data readings. What is more, the frequency of

the cyclic loading corresponds to the natural loading of waves and winds. The number of applied cycles ranged between few cycles and up to few hundred thousand cycles (max number of applied cycles was 370 000).

It must be noticed that, since the upper piston in the triaxial machine was pushed up through the water pressure in the cell, the force did not reduce to zero. Therefore, the minimum cyclic stress $\sigma_{min}$ is equal 0 only when the confining pressure $\sigma_3$ is also equal to 0.

The main constraint in the cyclic triaxial laboratory tests is the speed of the data logging system. Due to a slow response time, a quick application of constant and accurate cyclic loading was not possible and it could even lead to overloading of samples. The frequency had to be kept low in order to avoid misreading and overloading the samples, thus limiting the number of available tests.

Cyclic laboratory tests prove that the cohesive geomaterials lose strength in cyclic loading. The loss of strength can be described by an S-N curve or by a remaining shear strength curve. Laboratory tests on cohesionless materials prove that the friction angle remains constant during cyclic loading. For sand, due to densification caused by the cyclic loading the shear strength increases slightly.

A good quality of data is of utmost importance for the description of fatigue of geomaterials. The strength results of the cyclic laboratory tests have a significant spread. This spread has many causes, from differences in test setup, sample preparation and imperfections, to testing conditions (temperature, humidity, etc.). Unfortunately, all these factors cannot be incorporated into a fatigue description due to insufficient data.

The impact of the size of cycling loading on the strength reduction for the remaining shear strength curve is negligible. Therefore there is no parameter which describes the cyclic stress ratio in the remaining shear strength curve. The strength reduction is strongly dependent only on the applied number of cycles.

In cyclic loading, the stiffness change of geomaterial follows the shear strength change. For cohesive materials the stiffness decreases and for cohesionless increases in increasing number of cycles. The main limitation of using the stiffness reduction in cyclic loading for describing the fatigue is that the derivation of static strength from static stiffness was not successful. This was because no correlation between the static strength and static stiffness was found and the stiffness is independent on the strength of the material. The usefulness of the stiffness reduction in order to predict strength reduction in cyclic loading, therefore, is questionable.

Application of the accumulation of strain to describe the fatigue of geomaterials does not seem to be promising. Sometimes the measured strains do not follow the typical stress-strain path because plastic deformations can be significant even before failure. Describing the fatigue life by the accumulation of strains is not possible, because there is no correlation

between accumulated strains and sample fatigue life. Also the plastic strain rate thus cannot be applied to predict the progress of strength loss.

Because the strain and stiffness changes cannot be used as a standard method for estimating geomaterial damages in terms of cyclic loading, the empirical (S-N or remaining shear strength curves) approach seems more appropriate.

In some cases, the accumulation of plastic strains can reach the maximum allowable value (chapter 7.5). For that reason the strain accumulation has to be checked separately (see chapter 2.2.1). Crack opening, and liquefaction were not investigated in this thesis, however in some cases, during the design stage, they must be checked separately for cyclic loading (e.g. saturated undrained conditions, large expected displacements, non-homogeneous material etc.).

The fatigue of geomaterials under realistic loading conditions - variable amplitude loading as well as multiaxial loading and cyclic confining pressure $\sigma_3$ has not been investigated in this dissertation due that time limitation.

The spread of static points for the remaining shear strength curve and the S-N curve is different than that for the static tests, because of different methods (coordinate system) of presenting the same tests results. For the remaining shear strength curve and S-N curve, the test results are normalised to the predicted shear strength at a given confining pressure $\tau_{rem}/\tau_0$ (see the methodology in chapter 4.2). For the typical static p-q plot (e.g. Figure 6.1) the results are not normalised and by presenting the test results in the p-q coordinate system, the information how the tests results are spread for the same confining pressure is not clearly visible. Therefore, the p-q (and similarly $\tau$-$\sigma$ plot) hide the real spread of data results.

# 8. S-N CURVE VS REMAINING SHEAR STRENGTH CURVE

## 8.1. Introduction

In this chapter, the S-N curve and the proposed remaining shear strength curve are compared by presenting the similarities and differences between these two curves. The comparison is based on the laboratory cyclic triaxial tests. The impact of the static data, confining pressure and cyclic stress ratio is investigated in this chapter. The cumulative damage rule for the remaining shear strength is compared with the cumulative damage rule for the S-N curve. At the end of the chapter, the remaining shear strength curve will be converted into a remaining cohesion curve, which was proposed in chapter 4.6.

## 8.2. The remaining shear strength curve as a S-N curve

The remaining shear strength curve is independent of the cyclic stress ratio $\tau_{cyc}/\tau_0$ according to the triaxial test results (chapter 7.3.1). When $\tau_{cyc} < \tau_{rem}$, the size of cyclic stress $\tau_{cyc}$ is unimportant until the cyclic stress is not touching the remaining shear strength curve. The remaining shear strength $\tau_{rem}$ depends on the number of cycles (Figure 8.1) only. As long as the applied number of cycles $n$ is not higher than the number of maximum cycles $N$ for a certain remaining shear strength, the cyclic loading can progress. While cyclic loading progresses, the $\tau_{rem}$ is decreasing, and at some point the cyclic shear stress touches the remaining shear strength $\tau_{cyc} = \tau_{rem}$ and the material fails.

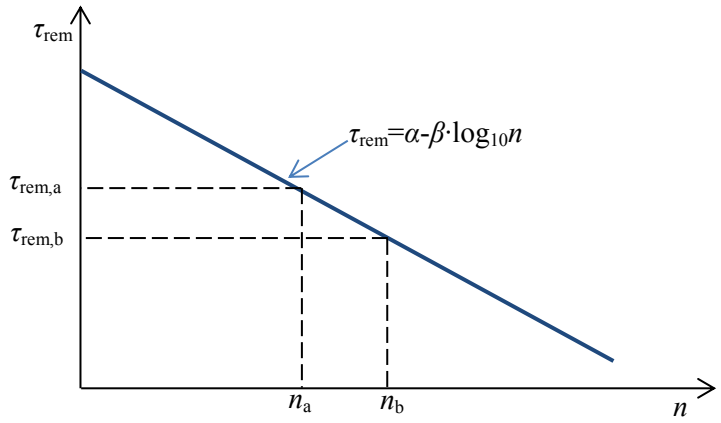


*Figure 8.1. The remaining shear strength curve*

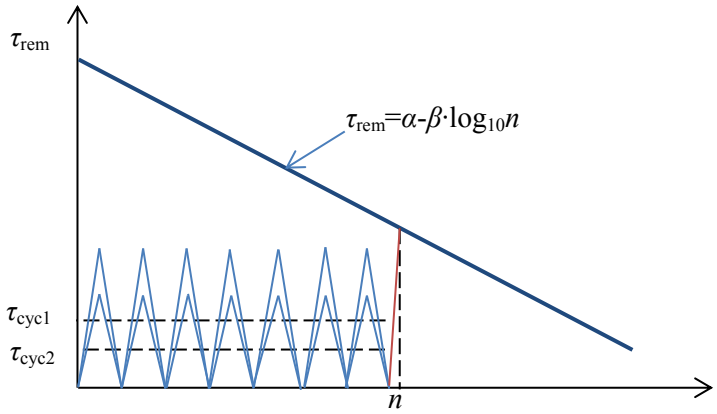


*Figure 8.2. The remaining shear strength curve for different cyclic stresses*

Because $\tau_{rem}$ is only related to $N$, it does not matter how the material is cyclically loaded (Figure 8.2). This has a big impact on the cumulative damage rule, because the accumulation of damage should also be independent of the cyclic stress $\tau_{cyc}$. This can be easily investigated in laboratory tests (see chapter 8.7).

Even though the static stress-strain behaviour (see chapter 7.5) is different under different confining pressures, the fatigue life seems unaffected by the confining pressure. The impact of a higher confining pressure (up to 0.5 MPa) is not found and the hypothesis of different strength reductions for different confining pressure $\sigma_3$, as described in chapter 4.6.2, is not confirmed. It was expected that the higher the confining pressure, the longer the fatigue life (remaining strength), but any cyclic stress ratio for any confining pressure is a causing similar shear strength loss.

Similarly, the strain accumulation in cyclic loading described in chapter 7.5.1 could not give conclusive remarks to the hypothesis of different strain accumulation for different confining pressures. The strain accumulation does not depend on the confining pressure, similarly to the decrease of strength. The lack of effect of different cyclic loading ratios on the remaining shear strength curve is a very important material property and this can be related to the stage *B* of an elastic strain in cyclic loading, as described in chapter 7.5.1. The strain starts to increase mainly prior to failure and the last cycles are the most important, because the cyclic stress $\tau_{cyc}$ quickly approaches $\tau_{rem}$.

If the plastic strain accumulation is unimportant for fatigue life of geomaterials, one can assume that the energy stored in the sample has also no impact on the fatigue life. The lack of correlation between energy and life, could lead to the conclusion that the cyclic stress ratio is not very important for the strength reduction, which could confirmed the statement that the fatigue of geomaterials primarily depends on the maximum number of cycles $N$ for a certain remaining shear strength.

The remaining shear strength can be then recalculated from the S-N curve, based on the fact

that the shear strength is reduced to $\tau_{cyc}$ one cycle prior to failure:

$$\tau_{rem} = A - B\, log_{10}(N-1) \qquad 8\text{-}1$$

where $A$ and $B$ are S-N curve fit parameters. The S-N curve can be treated therefore as a remaining shear strength curve one cycle before the failure in tests for S-N curve. This means that the remaining shear strength curve is similar to as the S-N curve, and the impact of $\sigma_a$ and $\sigma_{mean}$ can be omitted. The remaining shear strength gives then simple formula for obtaining the remaining shear strength without any transformations and vice-versa. Other differences and similarities will be investigated in subsequent chapters.

## 8.3. Comparison between the S-N curve and the remaining shear strength curve

*Artificial gypsum*

The slope and the intercept of both the S-N curve (Figure 8.3) and the remaining shear strength curve (Figure 8.4) are presented in Table 8-1. The S-N curve gives a steeper slope than the remaining shear strength curve. This implies that the S-N curve give shorter life and faster reduction in comparison to the remaining shear strength curve. This is not a very surprising result, because the prematurely failed samples are not included in the calculations and in this case, a significant number of the S-N samples are the prematurely failed samples from the remaining shear strength tests. This means an exact comparison is not possible.

*Table 8-1. The S-N and remaining shear strength curve parameters for artificial gypsum*

| | *slope* | *intercept* |
|---|---|---|
| S-N curve | 0.107 log(*N*) | 1.0 |
| Remaining shear strength curve | 0.067 log(*n*) | 1.0 |

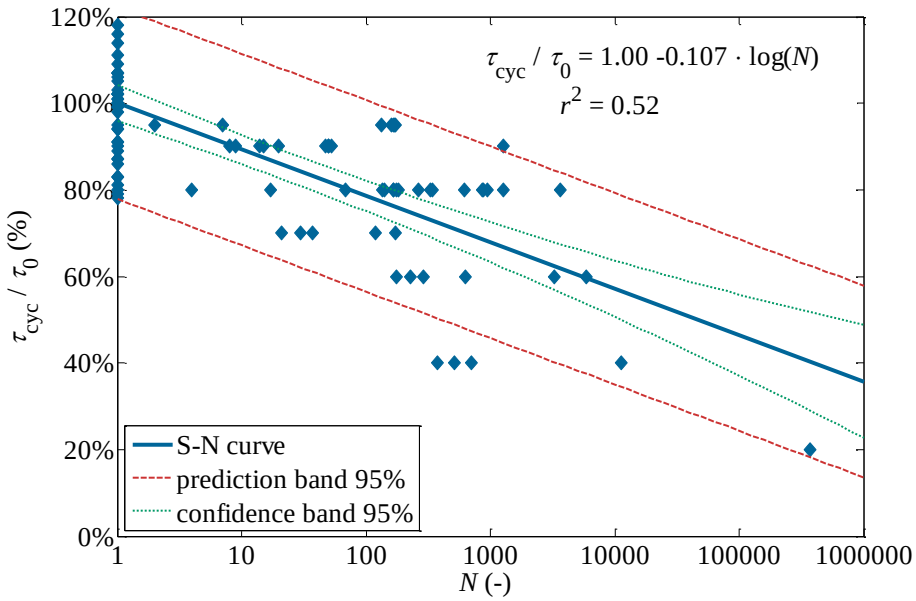


*Figure 8.3. The S-N curve for artificial gypsum*

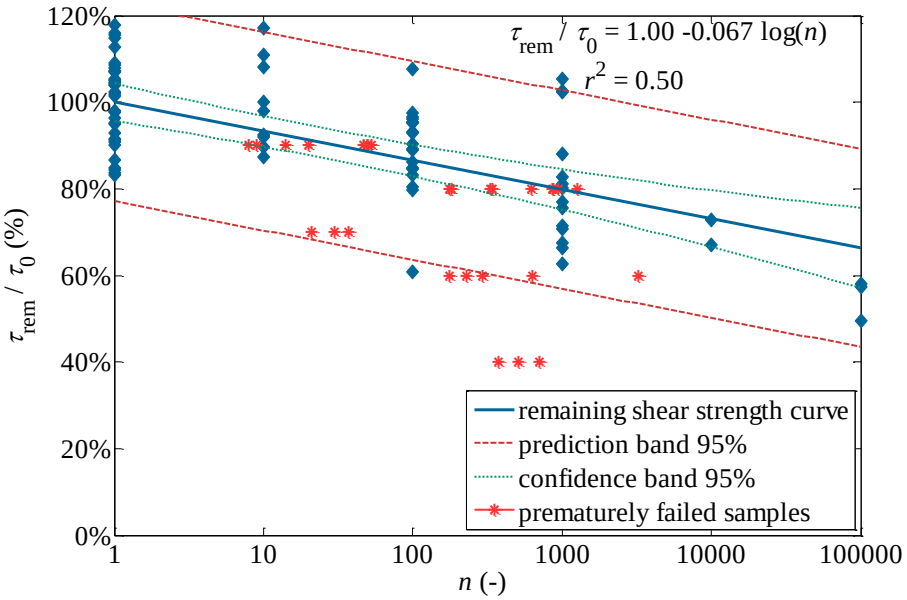


*Figure 8.4. The remaining shear strength curve for artificial gypsum*

*Mortar*

The comparison between the S-N (Figure 8.5) and the remaining shear strength curve (Figure 8.6) for mortar shows different slopes, so the S-N curve indicates a higher strength loss in cyclic loading than the remaining shear strength curve (Table 8-2). This is the same result as for the artificial gypsum, which also presented higher loss of strength for the S-N curve.

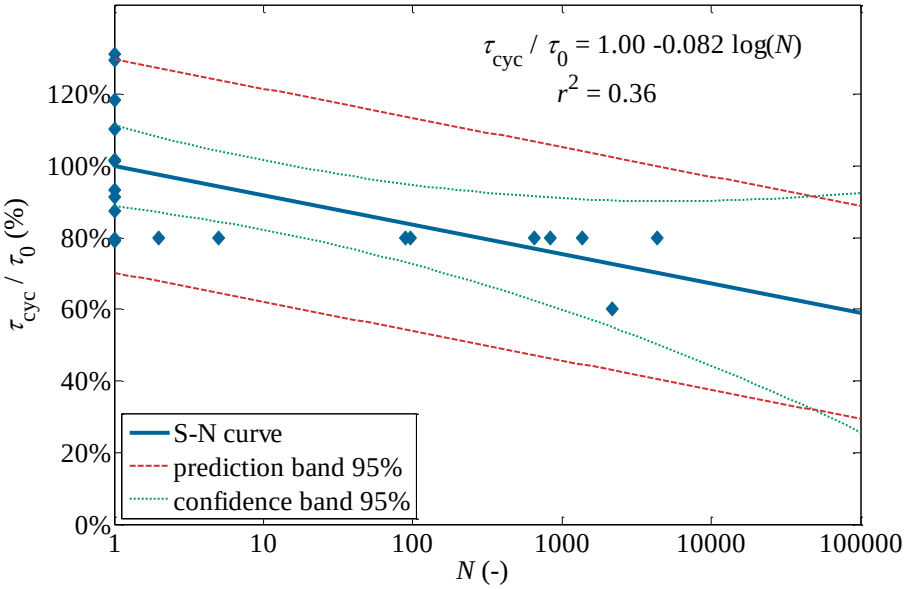


*Figure 8.5. The S-N curve for mortar (1 week, cement/sand ratio =0.5)*

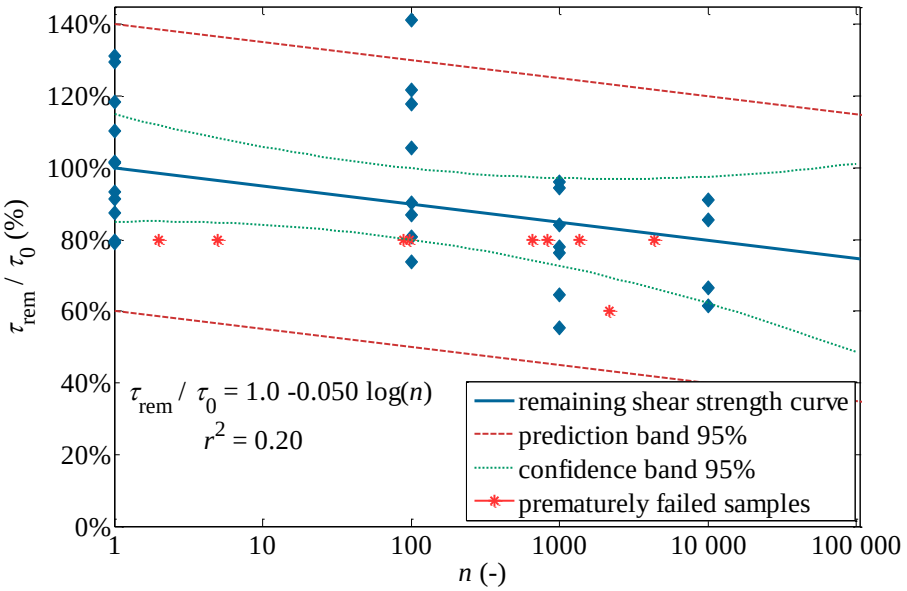


*Figure 8.6. The remaining shear strength curve for mortar (1 week, cement/sand ratio = 0.5)*

*Table 8-2. The S-N and the remaining shear strength curve parameters for mortar (1 week, cement/sand ratio = 0.5)*

| | *slope* | *intercept* |
|---|---|---|
| S-N curve | 0.082 log(*N*) | 1.0 |
| Remaining shear strength curve | 0.050 log(*n*) | 1.0 |

### 8.3.1. Palmgren-Miner rule & the remaining shear strength curve

In the Figure 8.7, the sum of damages (cyclic and final static) calculated according the Palmgren-Miner rule (see chapter 3.5.4) is presented.

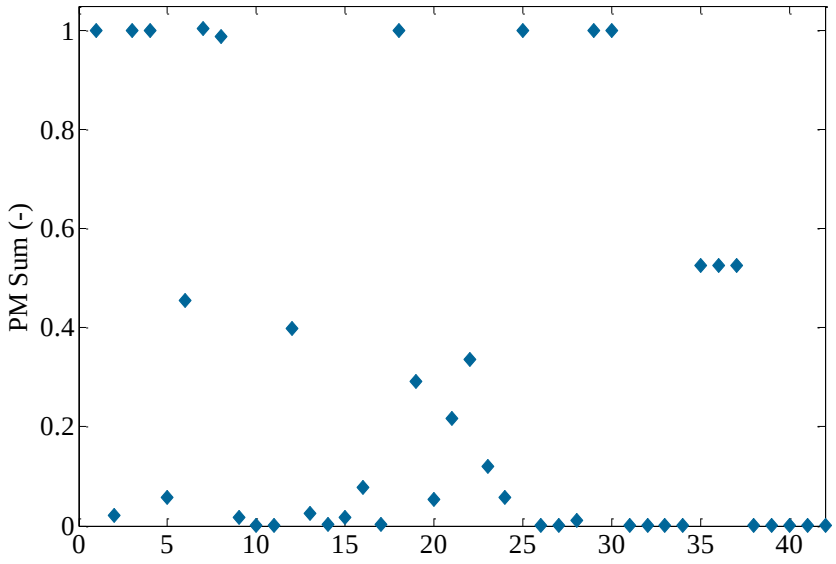


*Figure 8.7. Palmgren-Miner sum for 42 samples from remaining shear strength tests (artificial gypsum)*

It can be noticed that the sum for most samples is much lower than 1. All values of the sum higher than 1, are plot as 1. The conclusion can be given that the Palmgren-Miner rule does not well predict the life in the case of the remaining curve for artificial gypsum. For mortar samples the sum is similar to the pattern exhibited by artificial gypsum.

### 8.3.2. Advantages and disadvantages of the standard S-N and the remaining shear strength curve

The S-N curve and the remaining shear strength curve methodology have both their advantages and disadvantages. The biggest disadvantages of both curves are that they are not taking into account all available data. The S-N curve does not take into account "run outs" (samples for which no failure occurred) and the remaining shear strength curve does not take into account prematurely failed samples (samples which do not reach the required number of cycles).

*The remaining shear strength curve*

The biggest advantage of the remaining shear strength curve compared to the S-N curves is that this curve does not only predict failure, but it also predicts the remaining shear strength. The remaining shear strength is measured directly and in a simple way. Besides, the empirical damage parameter used in describing the cumulative damage by Palmgren-Miner rule, can be replaced by the remaining shear strength.

Another advantage of the remaining shear strength curve is that it can predict more accurately the fatigue life for a low number of cycles and for a high cyclic stress. The S-N curve is valid and used mainly for a higher number of cycles and a low cyclic stress. For low number cycles before failure, the low cycle fatigue approach is commonly used (chapter 3.6). Moreover, the tests for the remaining shear strength curve can be easily scheduled.

The biggest disadvantage of the remaining shear strength curve is that it accounts only for the samples which survived the number of applied cycles. This leads to the conclusion that the remaining shear strength curve overestimates the strength. The S-N curve gives then "safer" results than compared to the remaining shear strength curve (see Table 8-2 and Figure 8.3 and Figure 8.4). Same results can be seen in Figure 8.8 (Philippidis & Passipoularidis, 2006) indicating a lower fatigue life (strength) prediction for the S-N curve in case of composite materials.

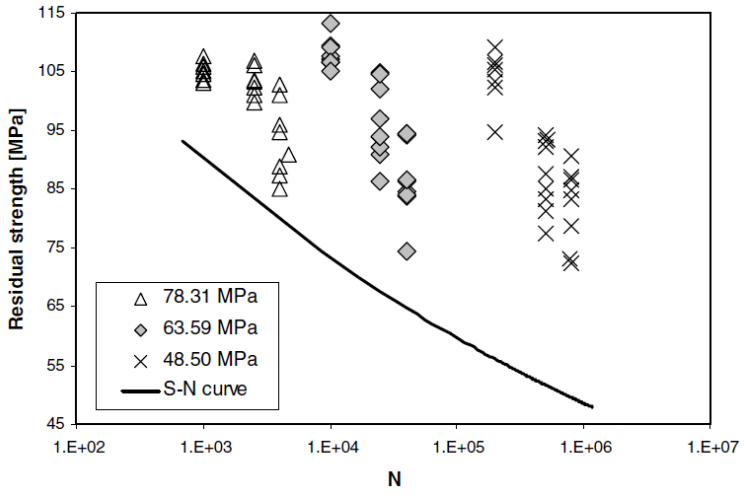


*Figure 8.8. Remaining strength and S-N curves (Philippidis et al., 2006)*

In the laboratory triaxial tests it was found that the cyclic stress ratio is unimportant, so only one remaining shear strength curve is necessary to be obtained, which makes the effort similar to prepare the S-N curve.

*S-N curve*

To the main advantages of the S-N curve belongs: it is easily applicable (cyclic tests for compression, tension or both combined); it is fairly accurate; and it is well described and widely used (in material science).

The S-N curve has few disadvantages. The S-N curve does not give directly the remaining strength, which is the parameter needed in design. The static tests usually are not taken into account in the calculations (in this thesis, the static tests were, however, included). The presence of censored data – "run outs" can lead to erroneous fatigue life estimation.

## 8.4. Spread of test results & probability of failure in cyclic loading

*Spread of test results*

For both, the artificial gypsum and mortar, the spread of the static results is lower than the spread of the cyclic results (Figure 8.9 and Figure 8.10). To compare the static tests with the cyclic, all artificial gypsum samples loaded for 1000 cycles are taken, disregarding their cyclic stress ratio $\tau_{cyc}/\tau_0$. In the case of mortar, all samples loaded with 10000 cycles are considered. For tests series with different number of applied cycles, the spread of the cyclic results is also higher than the spread of the static tests.

The wider spread of cyclic test results has to be taken into account for calculating the design values of the strength. For all tested materials, the spread of static tests was significant, so the design static strength has to also be significantly reduced. For cyclic tests the spread is even bigger, which results in an even bigger reduction of the design strength. To describe the design strength in cyclic loading one has to not only reduce the strength because of the

material degradation caused by cyclic loading but also has to consider higher spread of the tests results. The higher spread can also suggest that to estimate what part of material strength has been consumed in cyclic loading is difficult, based on e.g. core tests from sites to evaluate the remaining strength.

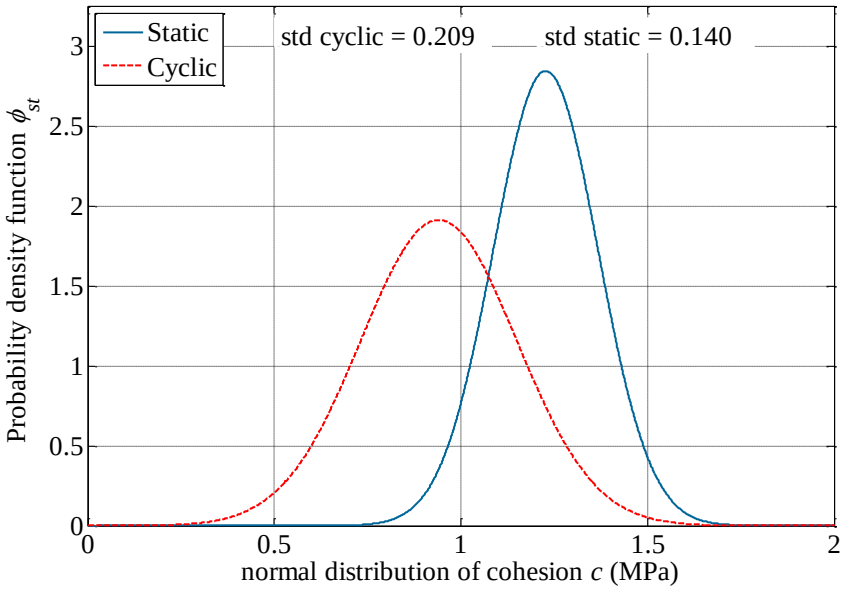


*Figure 8.9. Normal distribution curve of cohesion for static and cyclic tests (1000 cycles) for artificial gypsum*

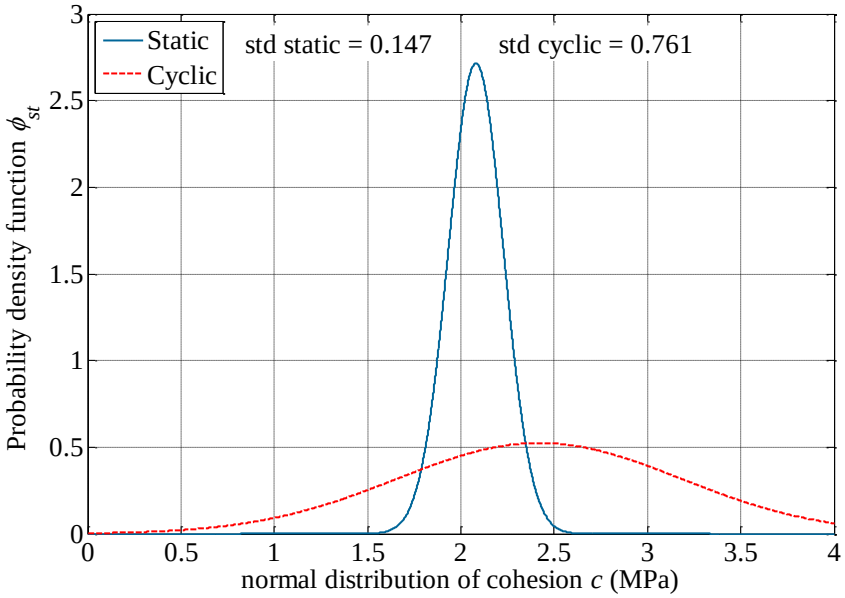


*Figure 8.10. Normal distribution curve of cohesion for static and cyclic tests for mortar samples (1 week, cement/sand ratio =1 and for 10000 cycles)*

### *Probability of failure*

The probability of failure is described by the prediction band. The prediction band of the S-N curve depends on the distribution of samples at the cyclic stress level; see Figure 3.8, ASTM E739-91, (1998) and Eurocode 3, (2006). In contrast, the prediction band of the remaining

shear strength curve depends on the distribution of the tests for a certain number of cycles (see Figure 4.4). The distribution of the cyclic tests for the remaining shear strength curve for a given number of cycles is similar to the static tests (see previous chapter - 8.3). The spread of the data shows no significant difference between the S-N curve and the remaining shear strength curve (see Figure 8.11, Figure 8.12 and Table 8-3).

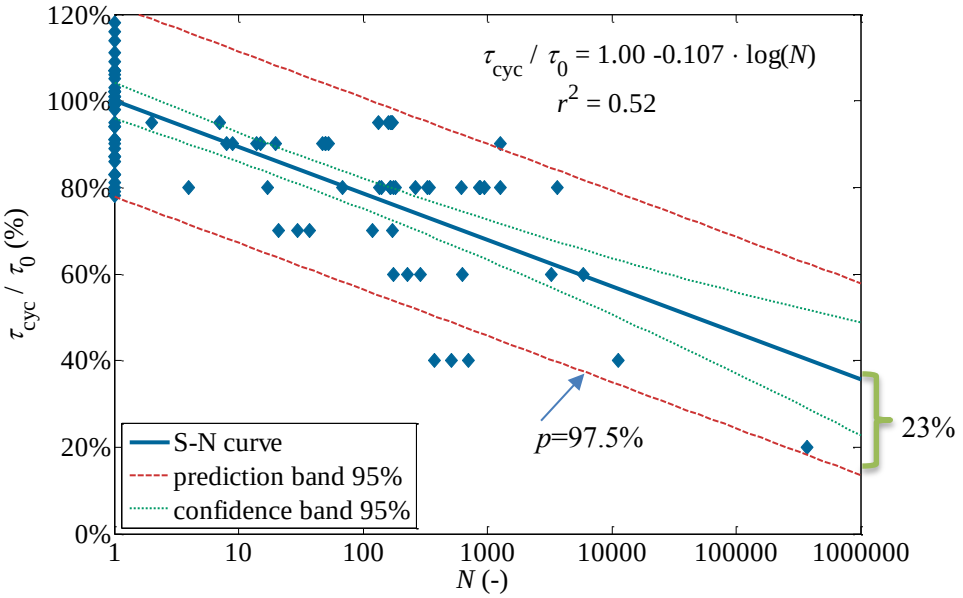


*Figure 8.11. The S-N curve data spread for artificial gypsum*

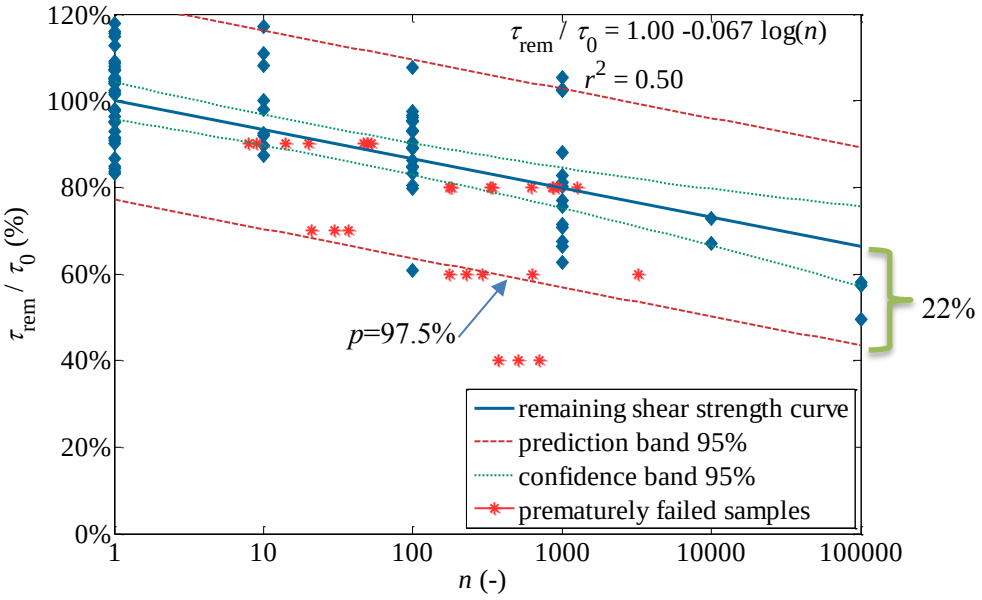


*Figure 8.12. The remaining shear strength curve data spread for artificial gypsum*

*Table 8-3. Probability of failure p < 2.5% (lower prediction line 2.5%)*

| | Distance from the curve (1.96·sandard error of estimate %) |
|---|---|
| S-N curve | 23% |
| Remaining shear strength curve | 22% |

## 8.5. Impact of the static test results on the S-N curve and remaining shear strength curve

*The impact of the static test results on S-N curve*

The S-N curve including static data (Figure 8.14) presents only a slight increase in the accuracy in comparison to the curve which excludes the static data (Figure 8.13). Improvement in the fatigue life estimation in the LFC region is found. Because the number of applied cycles is small ($N$ > 100 000 cycles), a conclusive remark cannot be made whether the static results should be included in the calculations or not. The slops of the curves are only slightly smaller (Table 8-4) and the use of the static data for the derivation of the S-N curves is, therefore, not conclusive.

*Table 8-4. Comparison between parameters including and excluding static test results*

| Regression | Forced intercept 1.0 | Excluding static tests |
|---|---|---|
| Logarithmic | $\tau_{cyc}/\tau_0 = 1.0 - 0.107 \cdot \log(N)$ | $\tau_{cyc}/\tau_0 = 1.02-0.114 \cdot \log(N)$ |

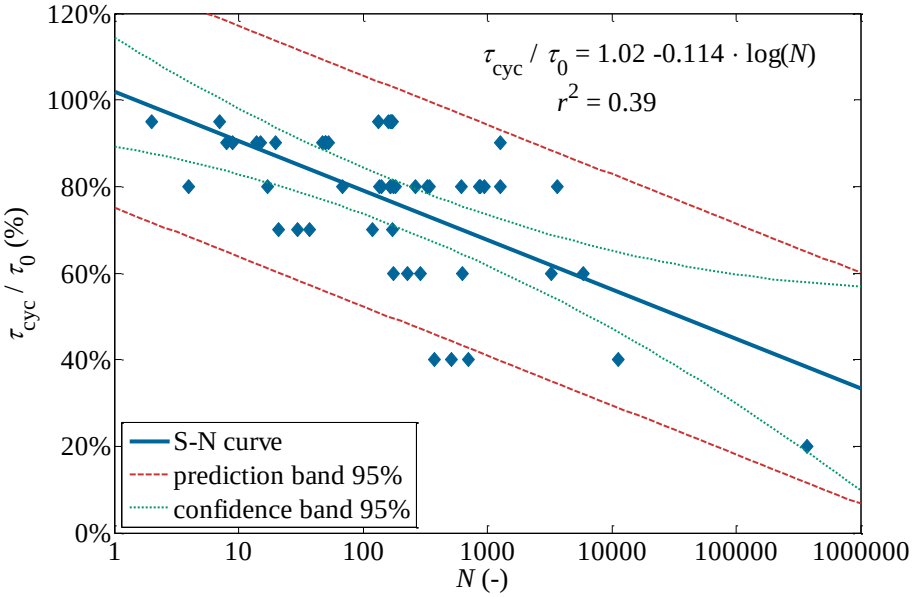


*Figure 8.13. The S-N curve excluding static test results for artificial gypsum*

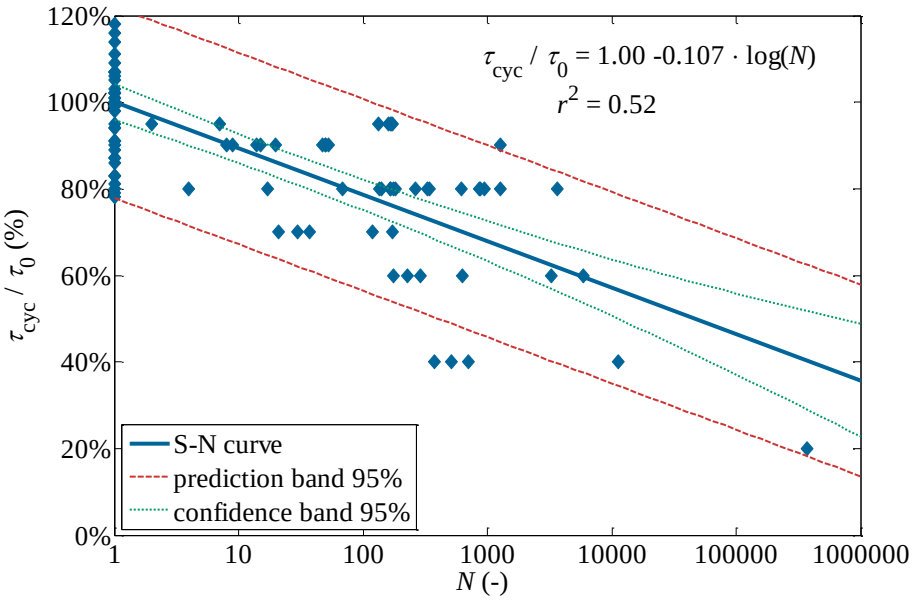


*Figure 8.14. The S-N curve including static test results for artificial gypsum*

*The impact of static test results on the remaining shear strength curve*

The static test results are usually included in the description of remaining shear strength curves (see chapter 4.4). The static tests can be treated as a cyclic tests for $n = 1$.

The remaining shear strength curves, where each curve corresponds to different cyclic stress ratios $\tau_{cyc}/\tau_0$, are presented including (Figure 8.16) and excluding (Figure 8.15) static test results. Significant increase in the accuracy of the remaining shear strength curve was found (Table 8-5 and Table 8-6). The same increase in accuracy was observed for the single remaining shear strength curve for all cyclic stress ratios $\tau_{cyc}/\tau_0$ (Table 8-7, Figure 8.18 and Figure 8.17).

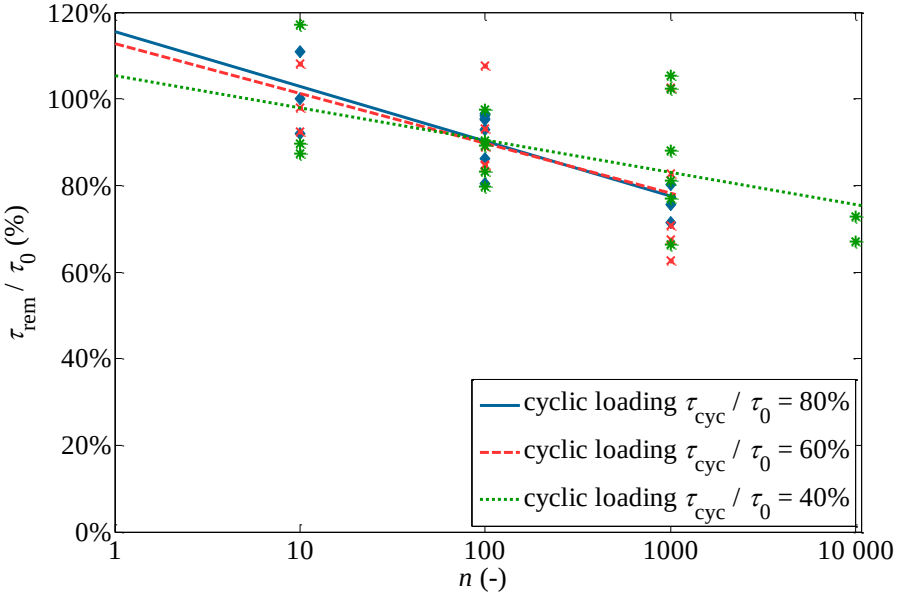


*Figure 8.15. The remaining shear strength curve excluding static test results for artificial gypsum*

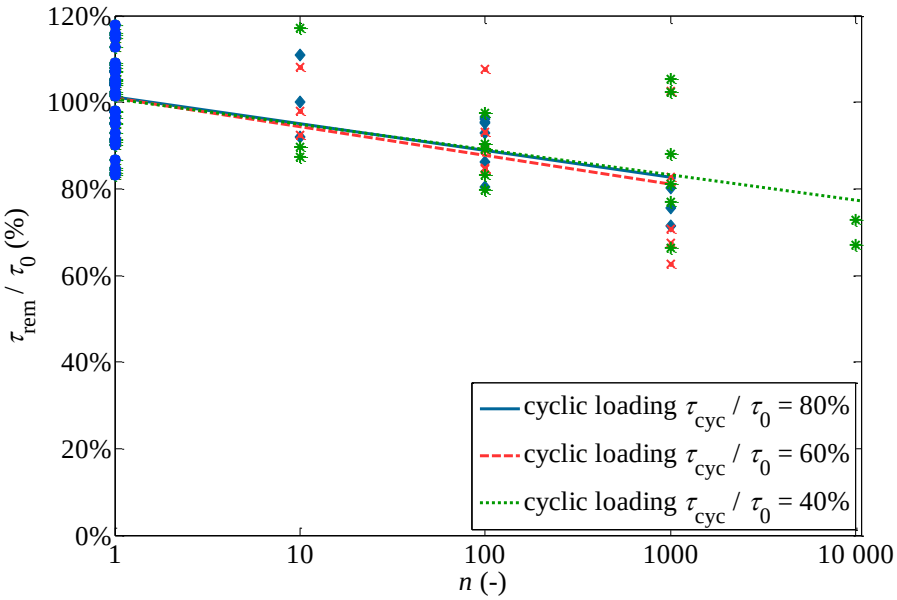


*Figure 8.16. The remaining shear strength curve including static test results for artificial gypsum*

*Table 8-5. The remaining shear strength curve parameters for different cyclic stress ratios (excluding static tests) for artificial gypsum*

| $\tau_{cyc}/\tau_0$ | $r^2$ | *slope* | *intercept* |
|---|---|---|---|
| 40% | 0.27 | 0.07 | 1.05 |
| 60% | 0.39 | 0.11 | 1.13 |
| 80% | 0.66 | 0.13 | 1.15 |

*Table 8-6. The remaining shear strength curve parameters for different cyclic stress ratios (including static data) for artificial gypsum*

| $\tau_{cyc}/\tau_0$ | $r^2$ | *slope* | *intercept* |
|---|---|---|---|
| 40% | 0.33 | 0.055 | 1.0 |
| 60% | 0.31 | 0.062 | 1.0 |
| 80% | 0.28 | 0.056 | 1.0 |

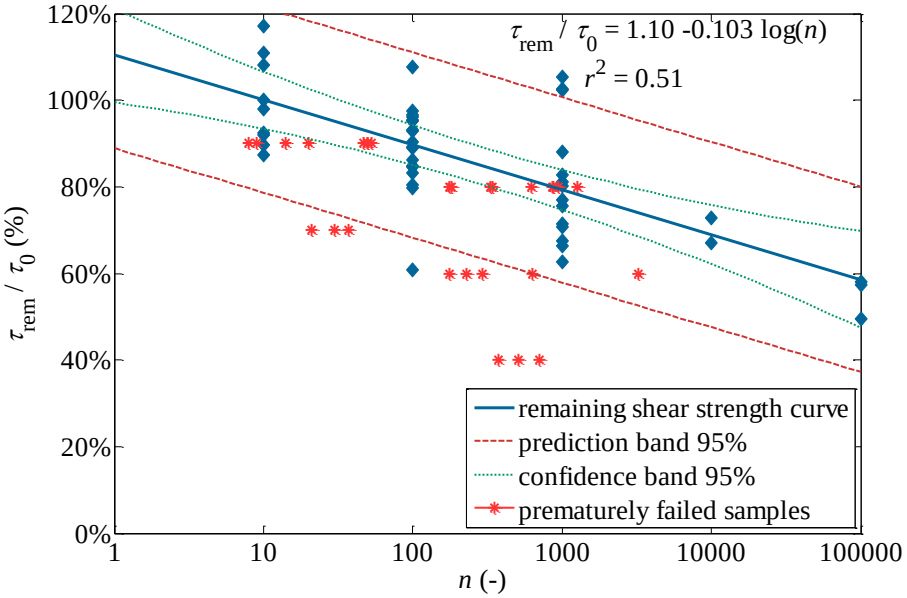


*Figure 8.17. A single remaining shear strength curve excluding static test results for artificial gypsum*

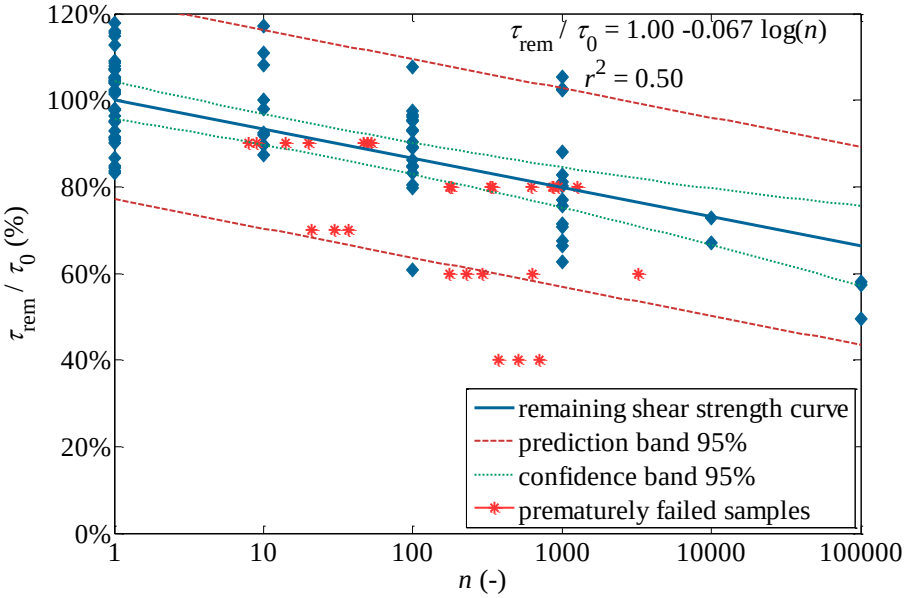


*Figure 8.18. A single remaining shear strength curve including static test results for artificial gypsum*

*Table 8-7. Regression coefficients including and excluding static test results for artificial gypsum*

| Regression | Including static tests | Excluding static tests |
|---|---|---|
| Logarithmic | $\tau_{rem}/\tau_0 = 1.0 - 0.067 \cdot \log(n)$ | $\tau_{rem}/\tau_0 = 1.10 - 0.104 \cdot \log(n)$ |

## 8.6. Impact of the confining pressure on fatigue of geomaterials

Impact of a confining pressure $\sigma_3$ on the remaining shear strength was checked for artificial gypsum (for mortar there was an insufficient number of samples to make a comparison).

*The S-N curve*

For the S-N curve no strong correlation between the remaining shear strength and confining

pressure $\sigma_3$ is found (Table 8-8). Only a very small increase in strength is observed (steeper slope) for confining pressure $\sigma_3$ = 0.5 MPa.

*Table 8-8. The remaining shear strength curve parameters for different confining pressures for artificial gypsum*

| Confining pressure $\sigma_3$ (MPa) | *slope* | *intercept* |
|---|---|---|
| 0.1 | 0.093 | 1.0 |
| 0.3 | 0.099 | 1.0 |
| 0.5 | 0.165 | 1.0 |

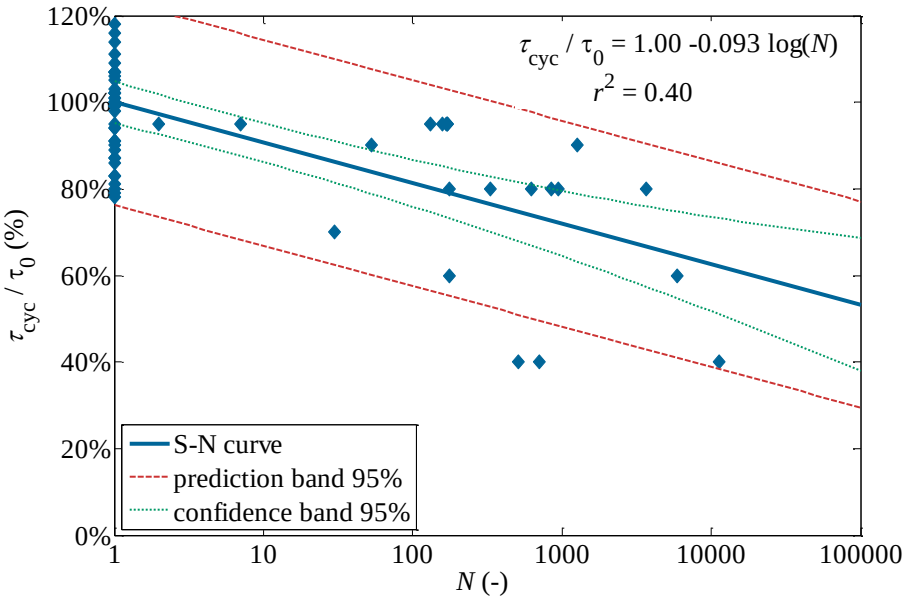


*Figure 8.19. The S-N curve for $\sigma_3$= 0.1 MPa for artificial gypsum*

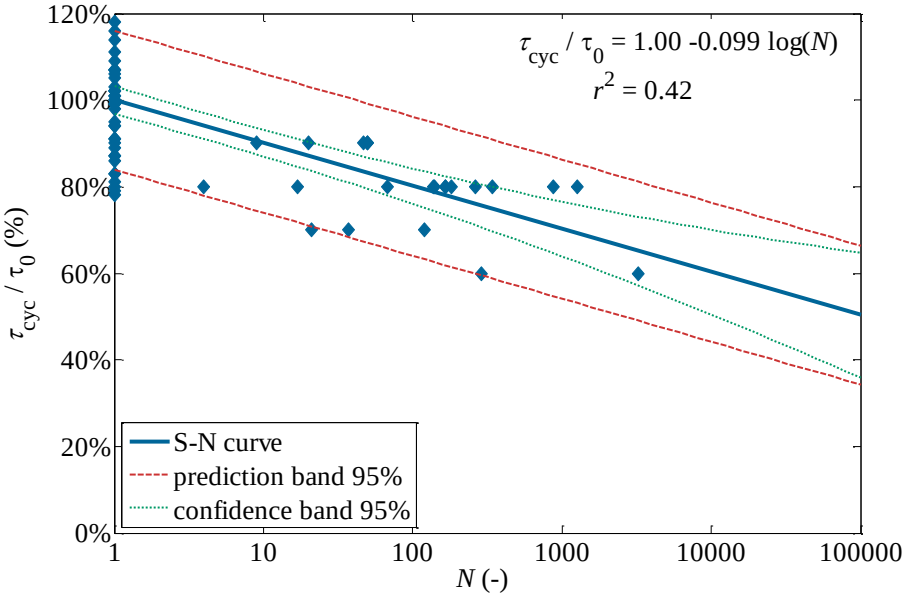


*Figure 8.20. The S-N curve for $\sigma_3$= 0.3 MPa for artificial gypsum*

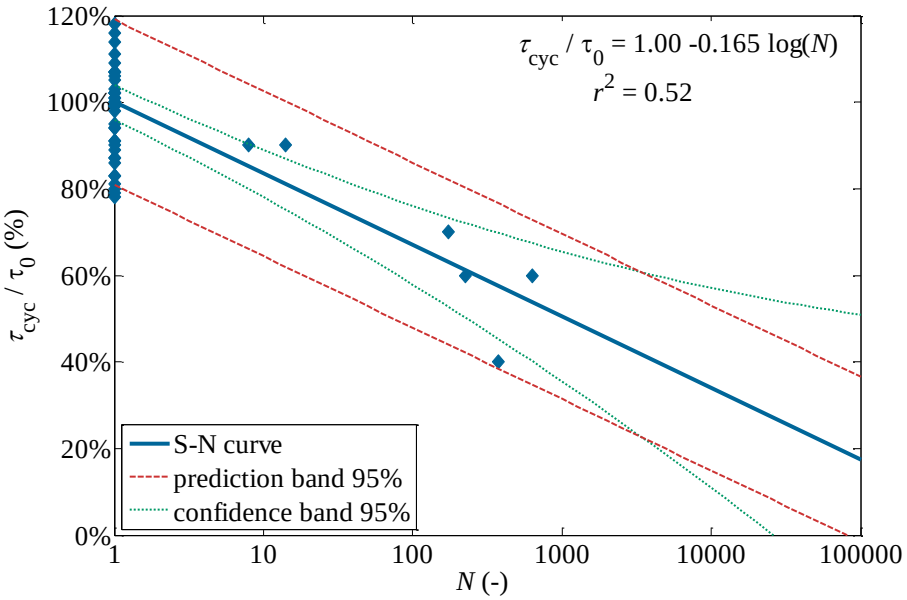


*Figure 8.21. The S-N curve for $\sigma_3$= 0.5 MPa for artificial gypsum*

*The remaining shear strength curve*

For the remaining shear strength curve similar results are found as obtained for the S-N curve. There is no strong correlation between the remaining shear strength and the confining pressure for artificial gypsum (Table 8-9).

*Table 8-9. The remaining shear strength curve parameters under different confining pressures for artificial gypsum*

| Confining pressure $\sigma_3$ (MPa) | *slope* | *intercept* |
|---|---|---|
| 0.1 | 0.041 | 1.0 |
| 0.3 | 0.082 | 1.0 |
| 0.5 | 0.083 | 1.0 |

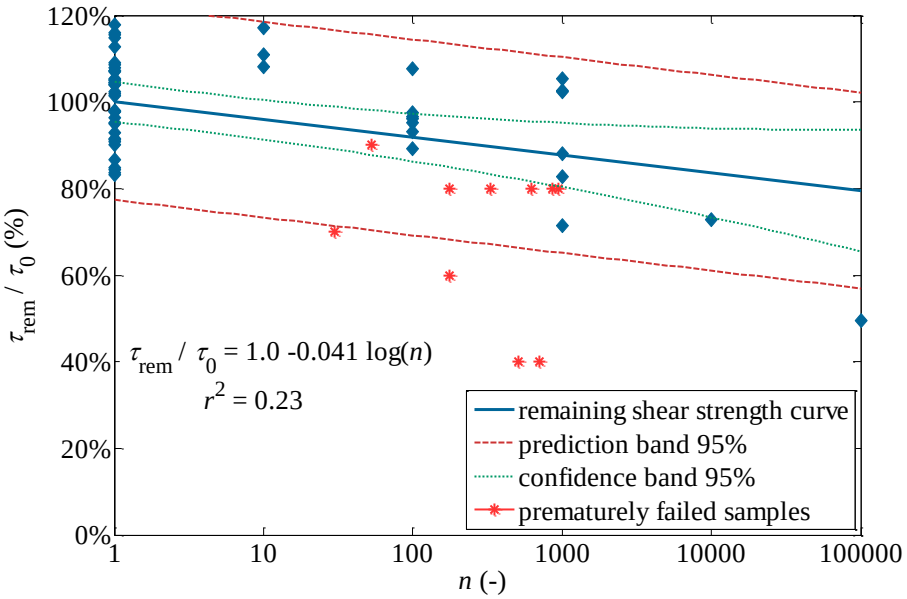


*Figure 8.22. The remaining shear strength curve for $\sigma_3$= 0.1 MPa for artificial gypsum*

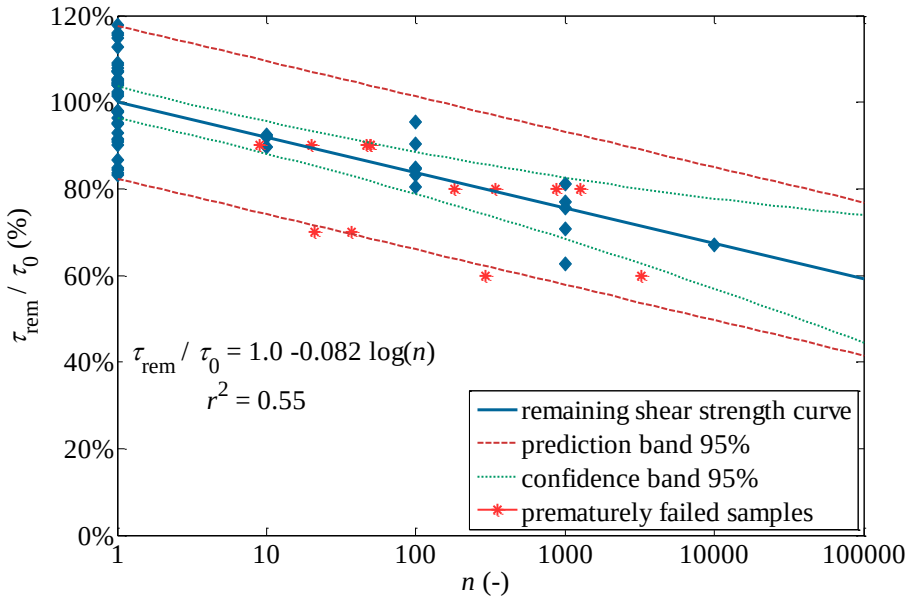


*Figure 8.23. The remaining shear strength curve for $\sigma_3$= 0.3 MPa for artificial gypsum*

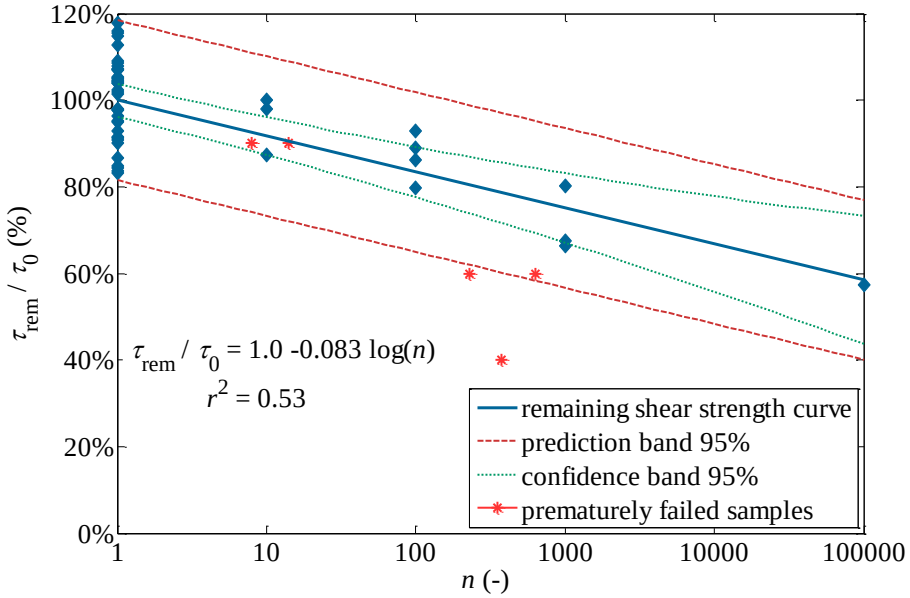


*Figure 8.24. The remaining shear strength curve for $\sigma_3$= 0.5 MPa for artificial gypsum*

For both, the S-N curve and the remaining shear strength curve, the loss of strength in number of cycles was slightly higher for the highest confining pressure. The differences in the stress reduction for higher confining pressure are, however, insignificant.

## 8.7. Cumulative damage rule for geomaterials

The fatigue life of a geomaterial (number of cycles $N$ until failure) can be predicted when the parameters of the remaining shear strength curve (Table 7-2) are known.

*Cumulative damage rule for remaining shear strength curve*

For the remaining shear strength curve the consequence of excluding the information of the

cyclic stress ratio (see chapter 7.3.1) implies that the fatigue life is independent on the cyclic stress ratio and depends only on the number of cycles. The fatigue life of a geomaterial is simply just the fatigue life minus the sum of the consumed lives of previous cyclic loads. This assumption is presented in Equation 8-2 and Figure 8.25.

$$n = n_1 + n_2 + n_3 + \cdots + n_i \qquad 8\text{-}2$$

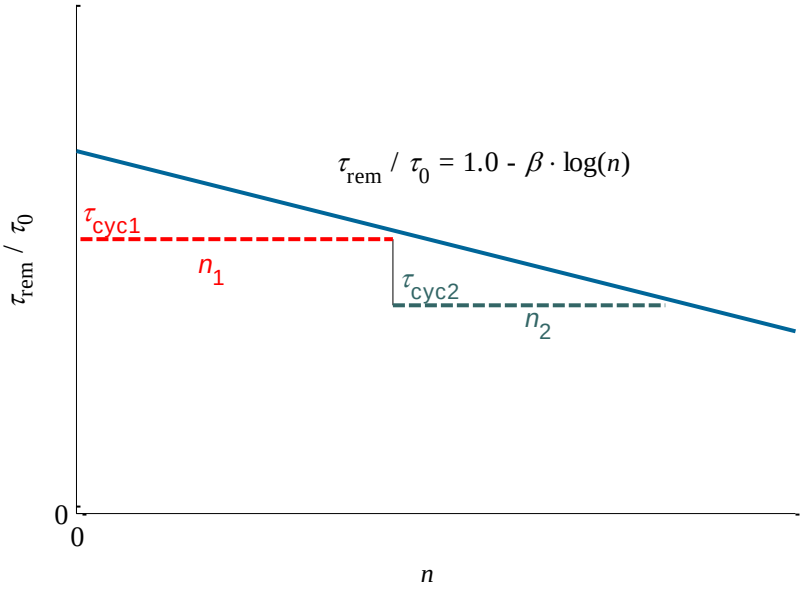


*Figure 8.25. Predicting the fatigue life based on a remaining shear strength curve*

The fatigue life *N* for the remaining shear strength curve is calculated from the Equation 4-27:

$$N = n = 10^{\frac{\alpha - \tau_{rem}}{\beta}} \qquad 8\text{-}3$$

where, $\tau_{rem}$ is the remaining shear strength, $\beta$ is the slope and $\alpha$ is the intercept of the remaining shear strength curve. The above equation is parameterised for the artificial gypsum. It yields with equation:

$$\tau_{rem} = 1.0 - 0.067 \cdot log_{10}\, n \qquad 8\text{-}4$$

To be able to compare the remaining shear strength cumulative damage rule with the Palmgren Miner rule for S-N, the $\tau_{rem}$ in Equation 8-3 will be replaced by $\tau_{cyc.}$

The remaining life for two sets of cyclic loads can be calculated according to the remaining shear strength curve as:

$$n_2 = N - n_1 \qquad 8\text{-}5$$

*Cumulative damage rule for S-N (Palmgren-Miner rule)*

According to the Palmgren-Miner rule for the S-N curve, the remaining life is:

$$n = \frac{1}{\frac{z_1}{N_1} + \frac{z_2}{N_2} + \frac{z_3}{N_3} + \cdots + \frac{z_k}{N_k}} \qquad 8\text{-}6$$

where $n$ is the number of cycles before failure, $z_i$ is the part of life spent at cyclic stress ratio $i$, and $N_i$ is the life for that cyclic stress ratio.

The remaining life for two sets of cyclic loads according the Palmgren-Miner cumulative damage rule for the S-N curve can be calculated as:

$$n = \frac{1}{\frac{z_1}{N_1} + \frac{1 - z_2}{N_2}} \qquad 8\text{-}7$$

*Cumulative damage – laboratory tests*

Some basic assumptions of the cumulative damage rules, for both the remaining shear strength curve and the S-N curve, can be proven in cyclic triaxial laboratory tests. The comparison between cumulative damage rules for the remaining shear strength and S-N will allow checking if the remaining shear strength curve indeed is independent on the cyclic stress ratio $i$ and if the predicted life from the remaining shear strength curve is correct and similar to that given by the S-N curve.

In the proposed here laboratory tests, each sample is loaded with two sets of loads. For the first set the cyclic stress ratio is $\tau_{cyc}/\tau_0 = 80\%$ and the applied number of cycles is $n_1 = 400$ cycles. The number of 400 cycles is less than the calculated fatigue life for that cyclic loading, $N_{80\%} = 966$) and is based on the equation for the remaining shear strength curve (Equation 8-4). Next, a lower cyclic stress ratio $\tau_{cyc}/\tau_0 = 70\%$ (60%, 40%, etc.) will be applied and the number of cycles until failure $n_2$ will be counted.

The searched number of cycles until failure $n_2$ for $\tau_{cyc}/\tau_0 = 70\%$ is (the fatigue life is 30 000 cycles for that cyclic stress ratio):

- According to remaining shear strength cumulative damage rule:
  $n_2 = 30\,000 - 966 = 20\,044$
- According to the Palmgren-Mine rule for the S-N curve:

$$n_2 = \frac{1}{\frac{\frac{400}{966}}{966} + \frac{1 - \frac{400}{966}}{30\,000}} = 2231$$

It can be noticed, that the Palmgren-Miner rule gives much smaller number of cycles $n_2$ which can be applied in comparison to the simpler cumulative damage rule for the remaining shear strength curve. The difference is very big (9 times more) and it should be easy to prove which one is correct by conducting tests.

*Results*

The result is the number of counted cycles until failure $n_2$ for the second cyclic stress ratios ratio $\tau_{cyc}/\tau_0 = 70\%$. Two tests were conducted and the number of cycles is:

test 1: $n_{2,I} = 7307$ cycles

test 2: $n_{2,II} = 5435$ cycles

More tests were carried out, but all of them ended before reaching the 400 cycles for 1st set of cyclic loading (sample failed in 151 cycles). Additionally, a lower first cyclic set was applied with cyclic stress ratio $\tau_{cyc}/\tau_0 = 60\%$. Unfortunately also in that case the samples failed during the first cyclic loading set at a number of cycles $n_1 = 877$, and 116.

*Conclusions*

The real value of applied cycles lies between the number given by the strength reduction cumulative damage rule and the Palmgren-Miner rule. No conclusive results were obtained. It also means that that the remaining shear strength cumulative damage rule is not validated and it is still not proven whether the fatigue of geomaterials is independent on the cyclic stress ratio according the remaining shear strength curve or not. The Palmgren-Miner rule gives safer results than the simple additive rule for remaining shear strength curve.

### 8.8. The remaining shear strength – the remaining cohesion

*Constant friction angle*

To extend the shear strength reduction in cyclic loading, the cohesion reduction in cyclic loading is proposed (chapter 4.4.6). The shear strength in cyclic loading is independent on the friction angle based on the comparison between the static and cyclic test results for artificial gypsum for different confining pressures (chapter 8.6, and Figure 8.26), and as well as the cyclic testes on cohesionless materials (chapter 7.3.2).

The Figure 8.26 shows a spread of the data points for distance of the remaining shear strength points in cyclic loading (normalised to the static strength $\tau_0$) for different confining pressures $\sigma_3$. The plot shows that there is no correlation between the spread of the data points and the confining pressure $\sigma_3$.

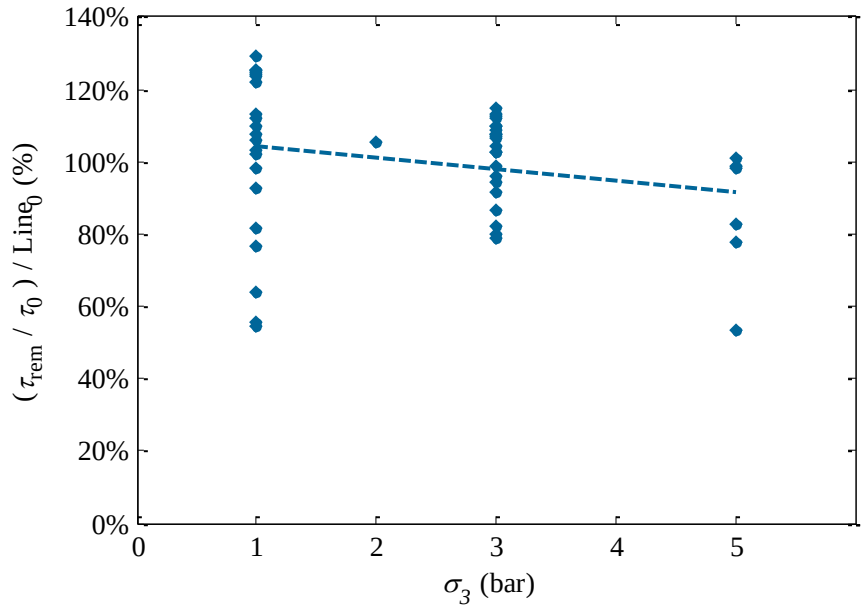


*Figure 8.26. Strength reduction in correlation to $\sigma_3$ for artificial gypsum*

The cyclic test results on cohesive and cohesionless materials pointing out that the shear strength reduction in cyclic loading is not related to a decrease in friction angle $\phi$, but with a decrease in cohesion $c$.

*The remaining cohesion*

Applying constant friction angle into the fatigue description of geomaterials, similar curves as for the remaining shear strength curve – Figure 7.9, can be created for the remaining cohesion (described in chapter 4.6). The remaining shear strength ratio $\tau_{rem}/\tau_0$ can be replaced by the remaining cohesion ratio $c_{rem}/c_0$ as presented in Figure 8.27.

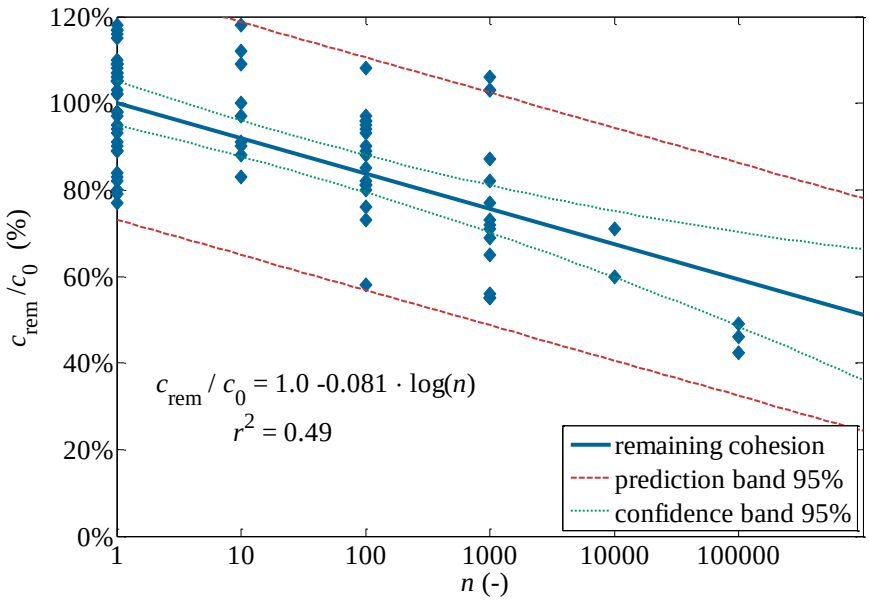


*Figure 8.27. The remaining cohesion (% of the initial cohesion) after given number of cycles n for all cyclic samples including the static results*

The interpolated formula for all samples can be written:

$$c_{rem} = c_0 \cdot [\alpha - \beta \cdot log(n)] \qquad 8\text{-}8$$

where $\alpha$ and $\beta$ are parameters obtained from the regression lines, and are specific to the tested material. In case the material is intact, the parameter $\alpha$ can be taken as a 1.0 (100% of the initial strength).

*The Mohr-Coulomb failure criterion for cyclically loaded material*

For cohesionless materials (e.g. sand) no cohesion is present ($c$ = 0 kPa) thus, a shear strength reduction can be neglected for such a material. Therefore, a clear distinction has to be made between the cohesive and the cohesionless materials under cyclic stresses.

The updated shear strength $\tau$ according to the above considerations can be given as:

$$\tau = \sigma \, tan \, \phi + c_{rem} \qquad 8\text{-}9$$

where the remaining cohesion $c_{\text{rem}}$ replaces the best fit "static" cohesion $c_0$. This can also be written as:

$$\tau = \sigma \, tan \, \phi + c_0 \cdot [\alpha - \beta \cdot log \, n] \qquad 8\text{-}10$$

Based on this an updated Mohr-Coulomb failure criterion described by principal stresses is proposed:

$$\left(\frac{\sigma_1 - \sigma_3}{2}\right) - \left(\frac{\sigma_1 + \sigma_3}{2}\right) sin\phi - c_{rem} \cdot cos \, \phi = 0 \qquad 8\text{-}11$$

or:

$$\left(\frac{\sigma_1 - \sigma_3}{2}\right) - \left(\frac{\sigma_1 + \sigma_3}{2}\right) sin\phi - c_0 \cdot [\alpha - \beta \cdot log \, n] \cdot cos \, \phi = 0 \qquad 8\text{-}12$$

The fatigue life is then related to a complete loss of cohesion during cyclic loading.

*Fatigue life of geomaterials at a certain cyclic stress ratio for remaining shear strength curve*

In order to describe fully the fatigue of geomaterials for the remaining shear strength curve, the fatigue life of a material has to be known. The number of cycles before fatigue life for the remaining shear strength curve $n_{\text{max}} = N$ can be found from a simple transformation of Equation 8-8:

$$log_{10} \, n_{max} = \frac{c_0 \cdot \alpha - c_{rem}}{c_0 \cdot \beta} \qquad 8\text{-}13$$

Which gives:

$$n_{max} = N = 10^{\frac{c_0 \cdot \alpha - c_{rem}}{c_0 \cdot \beta}} \qquad 8\text{-}14$$

*Proposed procedure for reduction of bearing capacity of foundations*

The basic methodology for a designer, who is using the remaining shear strength curve, is to apply a simple equation which predicts the remaining shear strength. This simple equation must be a result of laboratory analysis of cyclic loading acting on a specified geomaterial. A percentage of the remaining shear strength (or cohesion) is obtained by dividing the

remaining shear strength by the static shear strength. To evaluate the strength reduction of geomaterials, a natural spectrum of cyclic loading (see chapter 3.2) has to be simplified by using a method to count the cycles (rainflow method, described in chapter 3.3) and by a cumulative damage rule (chapter 8.7) which has to be used for a set of cycles with different cyclic stress ratios. For predicting the fatigue life of geomaterials, a nomenclature from steel fatigue can be incorporated e.g. Eurocode 3 (2006).

As described in chapter 2.1.1, to calculate the bearing capacity of a shallow foundation the following equation can be used:

$$p = cN_c + qN_q + \frac{1}{2}\gamma BN_\gamma \qquad 8\text{-}15$$

For cyclically loaded foundations a modification of this formula can be proposed:

$$p = c_{rem}N_c + qN_q + \frac{1}{2}\gamma BN_\gamma \qquad 8\text{-}16$$

The $c_{\text{rem}}$ is the remaining cohesion after cyclic loading, calculated by:

$$c_{rem} = c_0 \cdot [\alpha - \beta \cdot log\, n] \qquad 8\text{-}17$$

The same procedure can be applied for pile foundations (see chapter 2.1.2, Equation 2-6):

$$R_b = \left(c_{rem}N_c + q_0N_q + \frac{1}{2}\gamma dN_\gamma\right)A_b \qquad 8\text{-}18$$

## 8.9. Conclusions

The strength of geomaterials is low in comparison to the strength of other materials (e.g. metals) and the spread of test points for geomaterials varies significantly. This makes, therefore, the description of fatigue life very conservative and in order to assure safety, a high strength reduction factors has to be applied.

For the comparison purpose for both types of curves (S-N and remaining shear strength) the static tests are incorporated in the strength reduction description. The static test results do not significantly improve the accuracy of the S-N curve and the remaining shear strength curve.

The shear strength reduction of geomaterials was not affected by different levels of the confining pressure up to 0.5 MPa. The loss of strength, therefore, is independent of the confining pressure. The proposed hypothesis for lower strength reduction under higher confining pressures (described in chapter 4.6.1 and 4.6.2) does not seem valid.

An unexpected result of the cyclic tests is that, in tests for remaining shear strength curve, no impact of the cyclic stress ratio on the fatigue life was found. This makes the remaining shear strength curve similar to the S-N curve.

To describe fatigue of geomaterials many tests have to be conducted. The effects of the initial sample damage, loading frequency etc. are not yet investigated. Future research should

involve higher number of cycles and lower cyclic loadings, as well as combinations of various cyclic loads (different minimum cyclic loading, amplitude loading). Future research should also confirm or reject the cumulative damage rule for geomaterials, because the cumulative damage rule was here only briefly checked. More laboratory tests have to be conducted. An attempt should also be made to investigate cycling loading, where $\tau$ remains constant and $\sigma_3$ is cyclically changing.

# 9. CONCLUSIONS & RECOMMENDATIONS

## 9.1. Conclusions

Cyclic loading on geomaterials can cause different types of effects (Figure 9.1). The results of the large number of laboratory tests presented in this thesis, confirm that the shear strength of cohesionless materials increases during cyclic loading, while the shear strength of cohesive materials decreases. The conducted triaxial tests are showing the following results. The loss of strength can lead to fatigue (Table 9-1 and the red path in Figure 9.1) and the fatigue of geomaterials is proposed as a reduction of cohesion, while the friction angle remains constant. The existence of a constant friction angle has been validated in laboratory tests. It still has to be verified whether all natural cohesive geomaterials present a similar behaviour or not.

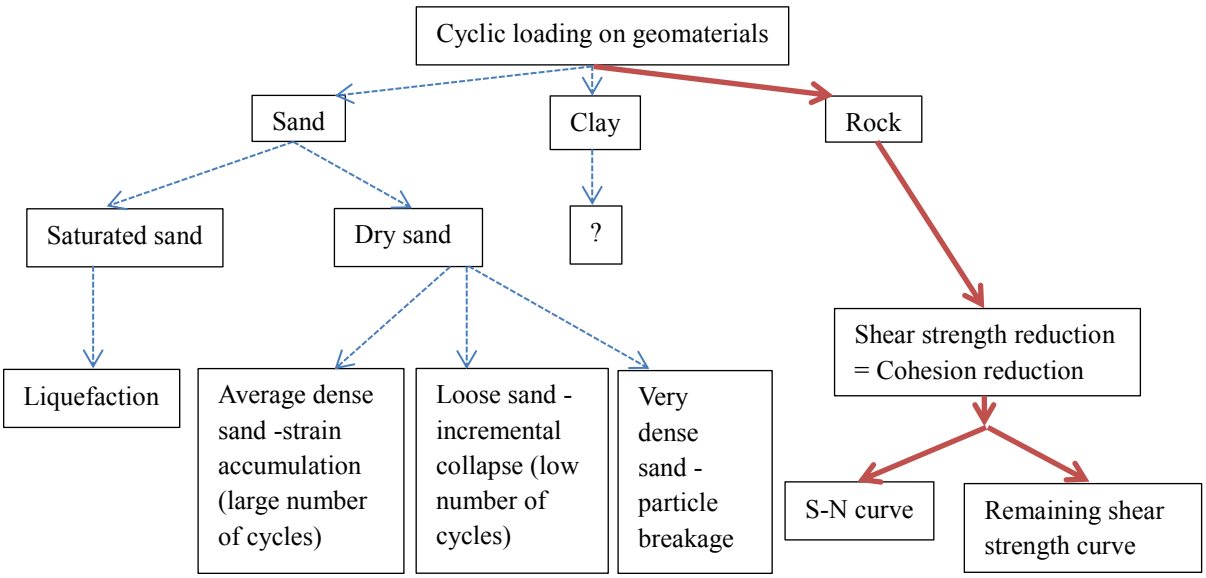


*Figure 9.1. Effects of cyclic loading on geomaterials*

*Table 9-1. Effects of cyclic loading on sand and rock*

| Material property | Sand | Rock |
|---|---|---|
| Shear strength | Not found | Significant reduction |
| Strains | Large | Small |
| Water pore pressure | Increase – it can lead to liquefaction | None or negligible |
| Stiffness | Increase or decrease | Significant reduction |
| Cracks and microcracks | Material is already crushed, eventually crushing of the grains | Growth of cracks and microcraks |

A small variation of the material properties, which cannot be avoided, leads to a high spread of the static shear strength results and a wide range of the prediction band (probability of failure). The imperfections of artificial gypsum and mortar were found to have a significant impact especially on the cyclic shear strength results. This is also the reason why a high number of samples prematurely failed (for remaining shear strength curve) and why the fatigue life for S-N curve has a very high spread.

The remaining shear strength curve slightly overestimates the prediction of the fatigue life because it neglects the prematurely failed samples excluded from the calculations. It means that the standard S-N curve offers a safer life prediction.

From the remaining shear strength tests it was found that, the strength reduction does not depend on the size of the cyclic stress ratio. This is an unexpected result, because it was believed that this significant laboratory testing effort will bring more detailed data about fatigue of geomaterials than the S-N curves. The remaining shear strength curve resembles therefore the S-N curve.

The impact of different types of cyclic stresses (varying the minimum cyclic stress, amplitude stress etc.) as well as the frequency of the cyclic loading was not investigated due to time limitation. The cumulative damage rule, for various set of cycles and cyclic stress ratios, has not been extensively investigated in cyclic loading of geomaterials. Additionally, an endurance (fatigue limit) has not been found.

Strength reduction due to cyclic loading is sometimes described as a stiffness reduction or a plastic strain accumulation. The accumulation of strains for cohesive materials cannot be used as a damage parameter, because the strain accumulation cannot be described in a simple way and it varies greatly between samples.

For the investigated materials, the stiffness reduction curve follows the shear strength reduction curve. For cohesive materials the stiffness decreases and for cohesionless materials the stiffness increases with an increasing number of cycles. The main limitation of the stiffness reduction during cyclic loading is that no correlation between the static strength and static stiffness is found and therefore a derivation of the strength from the stiffness is not successful.

The change of the stiffness and strains during cyclic loading cannot be used to describe the fatigue of geomaterials and the empirical (S-N curve or remaining shear strength curve) approaches seem more appropriate to predict the loss of strength in cyclic loading.

To be able to incorporate the fatigue description of geomaterials into geotechnical guidelines, the static cohesion can be replaced by a remaining cohesion. Methods which are used and well developed in standard fatigue life (like methods of counting the numbers of cycles, or statistical methods, etc.) can be directly applied into the S-N or remaining shear strength

curve. Statistical analysis can also provide a reliable estimation of the safety factors for the cyclic strength of geomaterials. The full description of the design value of the strength depends then on two important aspects:

- the strength reduction in cyclic loading,
- the increased spread of data in cyclic loading (see chapter 8.4).

Both this aspects has to be taken into account to properly describe the loss of strength of geomaterials in cyclic loading.

## 9.2. Recommendations

The following recommendations for further investigations are proposed:

1. It is recommended to conduct more various tests on geomaterials in order to increase the accuracy of the fatigue life estimation (e.g. various minimum cyclic stresses ratio, different “zero” stress level and its combinations etc.).
2. The influence of the water content, humidity and other environmental parameters as well as the loading frequency on the strength reduction is recommended to be investigated.
3. The effect of the cyclic stress, when the cyclic stress is the minor principal stress on the sample fatigue life, is recommended to be checked.
4. The possibility of using prematurely failed samples in the calculation of the remaining shear strength curve should be considered.
5. The impact of higher confining pressures on geomaterials fatigue should be further checked.

# REFERENCES


Abu-Lebdeh , T., & Voyiadjis, G. (1993, July). Plasticity-Damage model for Concrete Under Cyclic Multiaxial Loading. *Journal of Engineering mechanics, 119*(7), 1465-1484.

Achmus, M., Kuo, Y., & Abdel-Rahman, K. (2008). Zur Bemessung von Monopiles zyklische Lasten. *Bauingenieur, 83*(7-8), 303-311.

ACI Committee 215R. (2005). *Considerations for Design of Concrete Structures Subjected to Fatigue Loading.* ACI Committee 215R-74 (1996). Farmington Hills: American Concrete Institute.

Aglan, H., & Bayomy, F. (1998). Innovative approach to fatigue crack propagation in concrete pavements. *Transportation Research Record, 1568*, 17-23.

Ahmad, S., & Shah, S. (1982). Complete Triaxial Stress-Strain Curves for Concrete. *Journal of the Structural Division, 108*(ST4), 728-742.

Airey, D., Al-Douri, R., & Poulos, H. (1992). Estimation of pile friction degradation from shear box tests. *ASTM Geotech. Test, 15*(4), 388-392.

Al-Douri, R., & Poulos, H. (1991). Static and Cyclic Direct Shear Tests on Carbonate Sands. *Geotech. Test. J., 15*(2), 138-157.

Allotey, N., & El Naggar, M. (2008). A consistent soil fatigue framework based on the number of equivalent cycles. *Journal of Geotechnical and Geological Engineering*(26(1)), 65-77.

Al-Tabbaa, A., & Wood, D. (1989). An experimentally based 'bubble' model for clay. (S. Pietruszczak, & G. Pande, Eds.) *Numerical models in Geomechanics NUMOG III*, 91-99.

Andersen, K. (2009). Bearing capacity under cyclic loading – offshore, along the coast, and on land, The 21st Bjerrum Lecture presented in Oslo, 23 November 2007. *Canadian Geotechnical Journal*(46(5)), 513-535.

Andersen, K., & Lauritzsen, R. (1988). Bearing Capacity for Foundations with Cyclic Loads. *J. Geotech. Eng., 114*(5), 540-555.

Andersen, K., Puech, A., & Jardine, R. (2013). Cyclic resistant geotechnical design and parameter selection for offshore engineering and other applications. *Proceedings of TC 209 Workshop – Design for cyclic loading: piles and other foundations*, *18 ICSMGE.* Paris.

Anderson, T. (1991). Fracture Mechanics: Fundamentals and Applications. *CRC Press*, 793.

Ansell, P., & Brown, S. (1978). A cyclic simple shear apparatus for dry granular materials. *Geotechnical Testing Journal, 1*(2), 82-92.

API RP2A-WSD. (2007). *Recommended Practice for Planning, Designing, and Constructing Fixed Offshore Platforms, Twentieth ed, Supplement 3.* Washington, DC: American Petroleum Institute.

ASTM C192 / C192M-15. (2015). *Standard Practice for Making and Curing Concrete Tests Specimens in the Laboratory.* West Conshohocken: ASTM International.

ASTM D2487-11. (2011). *Standard Practice for Classification of Soils for Engineering*

*Purposes (Unified Soil Classification System).* West Conshohocken, PA: ASTM International.

ASTM D4543-01. (2001). *Standard Practices for Preparing Rock Core Specimens and Determining Dimensional and Shape Tolerances.* West Conshohocken, PA: ASTM International.

ASTM D6066-11. (2011). *Standard Practice for Determining the Normalized Penetration Resistance of Sands for Evaluation of Liquefaction Potential.* West Conshohocken: ASTM International.

ASTM E 1049-85 (Reapproved 2005). (2005). *Standard practices for cycle counting in fatigue analysis.* Philadelphia: ASTM International.

ASTM E739-91. (1998). *Standard Practice for Statistical Analysis of Linear or Linearized Stress-Life (S-N) and Strain-Life (e-N) Fatigue Data.* West Conshohocken: ASTM International.

Attewell, P., & Farmer, I. (1973). Fatigue behaviour of rock. *International Journal of Rock Mechanics and Mining Sciences, 10*, 1-9.

AWS D1.1:2000. (2000). *Structural Welding Code - Steel.* Miami, FL: American Welding Society (AWS).

Bagde, M., & Petroš, V. (2005). Fatigue properties of intact sandstone samples subjected to dynamic uniaxial cyclical loading. *International Journal of Rock Mechanics and Mining Sciences, 42*, 237–250.

Bagde, M., & Petroš, V. (2009). Fatigue and dynamic energy behaviour of rock subjected to cyclical loading. *International Journal of Rock Mechanics & Mining Sciences 46*, 200– 209.

Bagde, M., & Petroš, V. (2011). The Effect of Micro-Structure on Fatigue Behaviour of Intact Sandstone. *International Journal of Geoscience*(2), 240-247.

Bahn, B., & Hsu, C. (1998). Stress-strain behaviour of concrete under cyclic loading. *ACI materials journal*(95(2)), 178-193.

Bardet, J. (1986). A Bounding Surface Plasticity Model for Sands. *Journal of Engineering Mechanics, 112*(11), 1198 -1217.

Barsom, J. (2009). A Study of Micro-cracks in Overheated Forgings of Ultra-Low Sulfur Steels for Aircraft Engine Crankshafts. *Materials Science & Technology 2009 Conference and Exhibition (MS&T Partner Societies)*, 1192-1203.

Barton, N. (1976). The shear strength of rock and rock joints. *International Journal of Rock Mechanics and Mining Sciences and Geomechanics Abstracts, 13*(9), 255–279.

Basquin, O. (1910). *The exponential law of endurance tests.* Philadelphia: ASTM.

Bastenaire, F. (1972). *New method for the statistical evaluation of constant stress amplitude fatigue-test results.* Philadelphia: ASTM.

Bazant, Z., & Oh, B. (1983). Crack Band Theory for Fracture of Concrete. *Material Construction (RILEM)*, 155-177.

Bazant, Z., & Xu, K. (1991). Size effect in fatigue fracture of concrete. *ACI Mat. J., 88*(4), 390-399.

Bea, R., Audibert, J., & Dover, A. (1980). Dynamic Response of Laterally and Axially Loaded Piles. *Proc. 12th OTC Conf.*, (pp. 129-139). Houston.

Begemann, H. (1969). *The Dutch static penetration test with the adhesion jacket cone. Chapter III Tension Piles.* Delft: LGM Mededelingen.

Bjerrum, L. (1973). Problems of Soil Mechanics and Construction on Soft Clays and Structurally Unstable Soils. *8th Int. Conf. S.M. & F.E.*, *3*, pp. 111-159. Moscow.

Boulon, M., Desrues, J., Foray, P., & Forgue, M. (1980). Numerical model for foundation under cyclic loading, application to piles. In Pande, & Zienkiewicz (Ed.), *In Proceedings of the International Symposium on Soils under Cyclic and Transient Loading* (pp. 681–694). Rotterdam: A.A. Balkema.

Brantut, N., Baud, P., Heap, M., & Meredith, P. (2013). Time-dependent cracking and brittle creep in crustal rocks: A review. *Journal of Structural Geology*(52), 17-43.

Bridgman, P. (1923). The compressibility of thirty metals. *Proceedings of the American Academy of Arts and Science, 58*, 165-242.

Brinch Hansen, J. (1970). *Revised and extended formula for bearing capacity.* Danish Geotechnical Institute Copenhagen.

Broms, B. (1966). Methods of Calculating the Ultimate Bearing Capacity of Piles - A Summary. *Soils-Soils*(18-19), 21-32.

Broutman, L., & Sahu, S. (1972). A new theory to predict cumulative fatigue damage in fiberglass reinforced plastics. *Composite Materials: Testing and Design (Second Conference)*. ASTM STP 497 American Society for Testing and Materials.

Brown, E., & Hudson, J. (1974). Fatigue failure characteristics of some models of jointed rock. *Earthquake Eng. and Struct. Dyn., 2*(4), 379-86.

Brown, S. (1974). Repeated load testing of a granular material. *Journal of the Geotechnical Engineering Division, 100*, 825-841.

BS 1377: Part 8: 1990. (1990). *Methods of test for soils for civil engineering purposes — Part 8 Shear strength tests (effective stress).* London: British Standard Institution.

BSH. (2007). *Bundesamt für Seeschifffahrt und Hydrographie. Konstruktive Ausführung von Offshore - Windenergieanlagen.* BSH-Nr.7005.

Burdine, N. (1963). Rock Failure under Dynamic Loading Conditions. *Society of Petroleum Engineers, 3*(1), 1-8.

Butterfield, R., & Gottardi, G. (1994). A complete three-dimensional failure envelope for shallow footings on sand. *Geotechnique, 44*(1), 181-184.

Bye, A., Erbrich, C., Rognlien, B., & Tjelta, T. (1995). Geotechnical design of bucket foundations. *Offshore Technology Conference.* Houston, Texas.

Byrne, B. (2000). *Investigations of suction caissons in dense sand.* The University of Oxford.

Byrne, B., & Houlsby, G. (2001). Observations of footing behaviour on loose carbonate sands. *Geotechnique, 51*(5), 463-466.

Byrne, B., & Houlsby, G. (2002). Experimental investigations of the response of suction caissons to transient vertical loading. *ASCE Journal of Geotechnical and Geoenvironmental Engineering*.

Byrne, B., Houlsby, G., & Martin, C. (2002). Cyclic Loading of Shallow Foundations on Sand. *Proc. Int. Conf. on Phsical Modelling in Geotechnics (ICPMG).* St John's, Newfoundland.

Canelli, L., Ferrero, A., Migliazza, M., & Segalini, A. (2012). Mechanical behaviour of rock

discontinuities under seismic conditions. *Armonizing rock engineering and the enviroment.* Beijing.

Caquot, A., & Kérisel, J. (1953). Sur le terme de surface dans le calcul des fondations en milieu. *Third International conference on Soil Mechanics and Foundation Engineering*, (pp. 336–337). Zürich.

Carter, J., Booker, J., & Wroth, C. (1982). A Critical State Soil Model for Cyclic Loading. *Soil Mechanics – Transient and Cyclic Loads*, 219-252.

Casagrande, A. (1971, September). On Liquefaction phenomena. *Geotechnique, XXI(3)*, 197-202.

Cassidy, M. (1999). *The nonlinear dynamic analysis of jackup platforms subjected to random waves.* The Oxford University.

Castillo, E., & Fernández-Canteli, A. (2009). *A Unified Statistical Methodology for Modeling Fatigue Damage.* Springer Science & Business Media.

Castro, G. (1975). Liquefaction and Cyclic Mobility of Saturated Sands. *Journal of the Geotechnical Engineering Division, 101*(GT6), 551-569.

Castro, G., & Poulos, S. (1977). Factors affecting liquefaction and cyclic mobility. *J. Geotech. Eng. Div. Am. 8 Soc. Civ. Engrs., 103*, 501-516.

CEN. (2004). *EN 13286-7-Unbound and Hydraulically Bound Mixtures-Part 7: Cyclic Load Triaxial Test for Unbound Mixtures.* Brussels: CEN.

CEN ISO/TS 17892-2. (2004). *Geotechnical investigation and testing - laboratory testing of soil - Part 2: Determination of density of fine grained soil.* Brussles: European Committee for Standardization.

Chan, F. (1990). *Pavement deformation resistance of granular layers in pavements.* Nottingham: University of Nottingham for the degree of Doctor of Philosophy.

Chang, C., Zoback, M., & Khaksar, A. (2006). Empirical relations between rock strength and physical properties in sedimentary rocks. *Journal of Petroleum Science & Engineering, 51*, 223-237.

Chen, A., & Chen, W. (1975). Constitutive Relations for Concrete. *ASCE Journal of Engineering Mechanics, 101*(4), 465-481.

Chen, E., & Taylor, L. (1986). Fracture of brittle rock under dynamic loading conditions. *Fracture mechanics of ceramics*, 175-186.

Chow, F. (1997). *Investigations into the behaviour of displacement piles for offshore foundations.* Imperial College. University of London.

Coffin, J. (1954). A study of the Effects of Cyclic Thermal Stresses on a Ductile Metal. *76*, 931-950.

Collins, I., & Houlsby, G. (1997). Application of thermomechanical principles to the modelling of geotechnical materials. *Proc. Roy. Soc.*, 1975-2001.

Cornelissen, H., & Reinhardt, H. (1984). Uniaxial tensile fatigue failure of concrete under constant-amplitude and programme loading. *Mag. Conc. Res., 36*(129), 219-226.

Cornell, J., & Berger, R. (1987). Factors that influence the value of the coefficient of determination in simple linear and nonlinear regression models. *Phytopatology*(77), 63-70.

Corten, H., & Dolan, T. (1956). Cumulative fatigue damage. *Proc. Int. Conf. Fatigue of*

*Metals* (pp. 235-246). London: Institution of Mechanical Engineers.

Coyle, H., & Reese, L. (1966). Load Transfer for Axially Loaded Piles in Clay. *Journal Soil Mechanics Found. Div., 92*(SM2), 1-26.

Crossland, B. (1954). Proceedings of the Institution of Mechanical Engineers. *The effect of fluid pressure on the shear properties of metals, 168*, 935-946.

D4254-16, A. (2016). *Standard Test Methods for Minimum Index Density and Unit Weight of Soils and Calculation of Relative Density.* West Conshohocken, PA: ASTM International.

Dafalias, Y., & Herrmann, L. (1982). Bounding surface formulation of soil plasticity. *Soil mechanics–Transient and cyclic loads*.

Datta, M., Gulhati, S., & Rao, G. (1982). Engineering Behaviour of Carbonate Soil of India and Some Observations on Classification of Such Soils. *Geotechnical Properties, Behaviour, and Performance of Calcareous Soils, ASTM STP 777*, 113-140.

Day, R. (2001). *Soil Testing Manual: Procedures, Classification Data and Sampling Practises.* New York: McGraw-Hill Professional Publishing.

De Beer, E. (1970). Experimental determination of the shape factors and the bearing capacity. *Geotechnique, 20*, 387– 411.

DeAlba, P., Seed, H., & Chan, C. (1976). Sand Liquefaction in Large Scale Simple Shear Tests. *Journal of the Geotechnical Engineering Div., 102*(GT9), 909-927.

DIN 1054:2005-01. (2005). *Baugrund - Sicherheitsnachweise im Erd- und Grundbau. Normenausschuss Bauwesen im Deutschen Institut für Normung e.V.*

DIN 196-1. (2005). *Methods of testing cement - part 1: Determination of strength.* Deutsches Institut für Normung e. V.

Dingqing, L., & Selig, E. (1994). Resilient Modulus for Fine-Grained Subgrade Soils. *Journal of Geotechnical Engineering, 120*(6), 939-957.

DNV-OS-J101. (2013). *Design of offshore wind turbine structures.* Norway: Det Norske Veritas.

Dobereiner, L., & Freitas, M. (1986). Geotechnical properties of weak sandstones. *Geotechnique, 36*, 79-94.

Donald, I. (1956). Shear Strength Measurements in Unsaturated Non- Cohesive Soils With Negative Pore Pressures. *Proceedings of 2nd Australia-New Zealand Conference of Soil Mechanics and Foundation Engineering*, (pp. 200-205). Christchurch, New Zealand.

Dowling, N., & Begley, J. (1976). Fatigue Crack Growth During Plasticity and the J Integral. *ASTM STP 590*, 82-103.

Downs, D., & Chieruzzi, R. (1966). Transmission Tower Foundations. *J. Power Divn., 92*(2), 91-114.

Duncan, J., & Wright, S. (2005). *Soil Strength and Slope Stability* (1 ed.). Wiley.

EA-Pfähle. (2012). *Empfehlungen des Arbeitskreises "Pfähle".* Deutsche Gesellschaft für Geotechnik e.V. (Hrsg.).

Echtermeyer, A., Kensche, C., Bach, P., Poppen, M., Lilholt, H., Andersen, S., et al. (1996). Method to predict fatigue lifetimes of GRP wind turbine blades and comparison with experiments. *The 1996 European Union wind energy conference and exhibition.*

Göteborg, Sweden: Stephens and Associates.
El-Gammel, M. (1984). *Elastic stress and strain in cohesionless soils.* Civil Eng. dept. Leeds University.
EN 1999-1-3:2007/A1. (2011). *Eurocode 9: Design of aluminium structures - Part 1-3:Structures susceptible to fatigue.* Brussels: CEN.
EN 12390-2:2000. (2000). *Testing hardened concrete. Part 2: Making and curing specimens for strength tests.* Brussels: CEN.
EN 12859. (2012). *Gypsum blocks - definition, requirements and test methods.*
EN 1990:2002+A1 Eurocode 0. (1990). *Basis of structural design.* Brusselss: CEN.
EN 1991-2. (2003). *Eurocode 1: Actions on structures - Part 2: Traffic loads on bridges.* Brussels: CEN.
EN 1992-1-1:Eurocode 2. (2004). *Design of concrete structures - Part 1-1 : General rules and rules for buildings.* Brussles: CEN.
EN 1993-1-9:2006 Eurocode 3. (2006). *Design of steel structures – Part 1-9: Fatigue.* Brussels: CEN.
EN 1997-2 Eurocode 7. (2007). *Geotechnical design, Part 2: Ground investigation and testing.* Brussels: CEN.
EN 1998-5: Eurocode 8. (2004). *Design of structures for earthquake resistance – Part 5: Foundations, retaining structures and geotechnical aspects.* Brussels: CEN.
Erarslan, N., & Williams, D. (2012a). Investigating the Effect of Fatigue on Fracturing Resistance of Rocks. *Journal of Civil Engineering and Architecture, 6*(10), 1310-1318.
Erarslan, N., & Williams, D. (2012b). Mechanism of rock fatigue damage in terms of fracturing modes. *International Journal of Fatigue, 43*, 76–89.
Erken, A., & Ulker, C. (2006). Effect of cyclic loading on monotonic shear strength of fine-grained soils. *Engineering Geology, 89*(3-4), 243-257.
Fatemi, A., & Yang, L. (1998). Cumulative fatigue damage nad life prediction theories: a survey of the state of the art for homogeneous materials. *Int. J. Fatigue, 20*(1), 9-34.
Finn, W. (1988). Analysis of the response of soil-structure systems to cyclic loading. In E. Evgin (Ed.), *Proceedings on the Workshop of Constitutive Laws for the Analysis of Fill Retention Structures* (pp. 421-438). Department of Civil Engineering, University of Ottawa.
Finn, W., Lee, K., & Martin, G. (1977). An effective stress model for liquefaction. *Journal of the Geotechnical Engineering Division, 103*(GT6), 517-533.
(2003). FKM - Guideline Analytical strength assessment of components in mechanical engineering. 5th revised edition. In Forschungskuratorium Maschinenbau (Ed.). VDMA-Verlag.
Foreman, R., Peary, V., & Engle, R. (1967). Numerical Analysis of Crack Propagation in Cyclic - Loaded Structures. *Journal of Basic Engineering, 89*, 459-464.
Freudenthal, A., & Heller, R. (1959). On Stress Interaction in Fatigue and a Cumulative Damage Rule. *J. Aero-Space Science, 26*(7), 431-442.
Fugro. (2004). *Axial pile capacity design method for offshore driven piles in sand, P-1003.*
Gajan, S., & Kutter, B. (2009). Contact Interface Model for Shallow Foundations Subjected

to Combined Cyclic Loading. *Journal of Geotechnical and Geoenvironmental Engineering, 135*(3), 407-419.

Galjaard, P., Paute, J., & Dawson, A. (1996). Comparison and performance of repeated load triaxial test equipment for unbound granular materials. (A. Gomes Correia, Ed.) *Flexible Pavements*, 7-22.

Galloway, J., Harding, H., & Raithby, K. (1979). *Effects of Moisture Changes on Flexural and Fatigue Strength of Concrete.* Crowthorne, Transport and Road Research Laboratory.

Garnier, J. (2013). Advances in lateral cyclic loading design: contribution of the SOLCYP project. *Proceedings of TC 209 Workshop - Design for cyclic loading: piles and other foundations, 18 ICSMGE*, (pp. 59-68). Paris.

Gatelier, N., Pellet, F., & Loret, B. (2002). Mechanical damage of an anisotropic porous rock in cyclic triaxial tests. *International Journal of Rock Mechanics & Mining Sciences, 39*.

Gavin, K., Jardine, R., Karlsrud, K., & Lehane, B. (2015). The effects of pile ageing on the shaft capacity of offshore piles in sand. (V. Meyer, Ed.) *Frontiers in Offshore Geotechnics III, I*, 129-151.

Gerber, W. (1874). Calculation of the allowable stresses in iron structures. *Z. Bayer Archit Ing Ver, 6*(6), 101-110.

Glucklich, J. (1965). Static and Fatigue Fractures of Portland Cement Mortar in Flexure. *Proceedings, First International Conference on Fracture*, *2*, pp. 1343-1382.

Goder, D., Kalman, H., & Ullmann, A. (2002). Fatigue characteristics of granular materials. *Powder Technology, 122*(1), 19–25.

Goodin, E., Kallmeyer, A., & Kurath, P. (2004). Evaluation of Nonlinear Cumulative Damage Models for Assessing HCF/LCF Interactions in Multiaxial Loadings. *9th National Turbine Engine High Cycle Fatigue (HCF) Conference.* Pinehurst, NC.

Goodman, J. (1899). *Mechanics Applied to Engineering.* London: Longman, Green & Company.

Goto, S., & Tatsuoka, F. (1988). Effect of end conditions on triaxial compressive strength for cohesionless soil. In A. S. 977, *Advanced Triaxial Testing Soil Rock* (pp. 692-705).

Grabe, J., & Dührkop, J. (2008). Zum Tragverhalten von überwiegend horizontal belasteten Pfählen. *Tagungsband zur 30. Baugrundtagung 2008 der DGGT in Dortmund*, (pp. 143-150).

Grashuis, A., Dieterman, H., & Zorn, N. (1990). Calculation of cyclic response of laterally loaded piles. *Computers and Geotechnics, 10*(4), 287-305.

Grgic, D., & Giraud, A. (2014). The influence of different fluids on the static fatigue of a porous rock: Poro-mechanical coupling versus chemical effects. *Mechanics of Materials, 71*, 34-51.

Griffith, A. (1921). The phenomena of rupture and flow in solids. *Philosophical Transactions of the Royal Society of London, 221*, 163-198.

Griffith, A. (1924). Theory of rupture. *Proc. First Int. Cong. Applied Mech* (pp. 55-63). Delft - Technische Boekhandel and Drukkerij.

Gudehus, G., & Hettler, A. (1981). Cyclic and monotonous model test in sand. *Proc., 10th*

*ICSMFE*, *2*, pp. 211-214.
Gylltoft, K. (1983). *Fracture mechanics models for fatigue in concrete structures.* Luleå: Tekniska högskolan i Luleå.
Gylltoft, K., & Elfgren, L. (1977). *Utmattningshållfasthet för anläggningskonstruktioner: en inventering.* Stockholm: Statens råd för byggnadsforskning : Sv. byggtjänst.
Hahn, H., & Kim, R. (1976). Fatigue Behaviour of composite laminates. *Journal of Composite Materials, 10*, 156-180.
Haibach, E. (1970). Modified linear damage accumulation hypothesis accounting for a decreasing fatigue strength during increasing fatigue damage. *Lab. für Betriebsfestigkeit*.
Haibach, E. (1989). *Betriebsfestigkeit. Verfahren und Daten zur Bauteilberechnung.* Düsseldorf: VDI-Verlag.
Haimson, B. (1978). Effect of cyclic loading of rocks. *Dynamic geotechnical testing*, pp. 228-245.
Haimson, B., & Kim, C. (1972). Mechanical behaviour of rock under cyclic fatigue. In E. Cording (Ed.), *Stability of Rock Slopes, Proc. 13th Symp. Rock Mech.* (pp. 845-863). New York: ASCE.
Hall, C., & Hamilton, A. (2016). Porosities of building limestones: using the solid density to assess data quality. *Materials and Structures*.
Hilsdorf, H., & Kesler, C. (1966). Fatigue Strength of Concrete Under Varying Flexural Stresses. *Proceedings, American Concrete Institute, 63*, 1059-1075.
Hoek, E. (1994). Strength of rock and rock masses. *ISRM News Journal, 2*(2), 4-16.
Hoek, E. (2000). *Practical rock engineering, Course notes by Evert Hoek.* North Vancouver: Evert Hoek Consulting Engineer Inc.
Hoek, E., & Bieniawski, Z. (1965). Brittle fracture propagation in rock under compression. *Intern. J. Fracture Mech., 1*(3), 137-155.
Hoek, E., & Brown, E. (1980). Empirical strength criterion for rock masses. *J. Geotech. Engineering Div., 106*(GT9), 1032-1035.
Hoek, E., & Brown, E. (1988). The Hoek-Brown failure criterion - a 1988 update. *Proc. 15th Canadian Rock Mech. Symp* (pp. 31-38). Toronto: Civil Engineering Dept. University of Toronto.
Hoek, E., Marinos, P., & Benissi, M. (1998). Applicability of the Geological Strength Index (GSI) classification for very weak and sheared rock masses. The case of the Athens Schist Formation. *Bull. Engg. Geol. Env., 57*(2), 151-160.
Hoek, E., Wood, D., & Shah, S. (1992). A modified Hoek-Brown criterion for jointed rock masses. *Proc. rock characterization symp. Int. Soc. Rock Mech.: Eurock 92* (pp. 209-213). London: British Geotechnical Society.
Holmquist, D., & Matlock, H. (1976). Resistance-Displacement Relationships for Axially loaded Piles in Soft Clay. *Proc. 8th OTC Conf.*, *OTC 2474*, pp. 554-569. Houston.
Hordijk, D. (1991). *Local approach to fatigue of concrete.* Delft: The Delft University of Technology.
Horsrud, P. (2001). Estimating mechanical properties of shale from empirical correlations. *SPE Drill, 16*, 68-73.

Houlsby, G. (1999). A model for the variable stiffness of undrained clay. *Proc. Int. Symp. on Pre-Failure Deformation Characteristic of Geomaterials*, *99*, pp. 443-450. Torino.

Houlsby, G., Ibsen, L., & Byrne, B. (2005). Suction caissons for wind turbines. *Frontiers in Offshore Geotechnics*, 75-93.

Howe, R., & Owen, M. (1972). Cumulative Damage in Chopped Strand Mat/Polyester Resin Laminates. *8th International R. P. Conference.* Brighton: British Plastics Federation-.

Hu, L. (1959). Development of a triaxial stress testing machine and triaxial stress experiments. *Proc. Society Experimental Stress Analysis, 16*, (pp. 27-37).

Hudson, C. (1973). *A study of fatigue and fracture in 7075-T6 aluminium alloy in vacuum and air Environments.* NASA technical note.

Hwang, W., & Han, K. (1986). Fatigue modulus concept and life prediction. *Journal of Composite Materials, 20*, 154-165.

Ibrahim, A., & Schanz, T. (2015). Shear Strength and Collapsibility of Gypsiferous Soils. In *Engineering Geology for Society and Territory* (Vol. 2, pp. 1109-1115).

Ibsen, L. (1999). Cyclic Fatigue Model. *AAU Geotechnical Engineering Papers, ISSN 1398-6465 R9916, Soil Mechanics Paper No 34,*.

Ibsen, L., & Liingaard, M. (2005). Output-Only Modal Analysis Used on New Foundation Concept for Offshore Wind Turbine. *Proceedings of the 1st International Operational Modal Analysis Conference (IOMAC).* Copenhagen.

Idriss, I., & Boulanger, R. (2008). *Soil liquefaction during earthquakes.* Oakland: Earthquake Engineering Research Institute.

Idriss, I., Dobry, R., & Singh, R. (1978). Nonlinear behavior of soft clays during cyclic loading. *Journal of Geotechnical Engineering Division, 104*(12), 1427-1447.

Ingraffea, A., & Heuze, F. (1980). Finite element models for rock fracture mechanics. *Int. J. Numer. Anal. Meth. Geomech., 4*, 25-43.

International Standard IEC. (2005-2008). *61400-1. Wind Turbines - Part 1: Design Requirements.* International Electrotechnical Commission.

Ireland, H. (1957). Pulling Tests on Piles in Sand. *Proc. 4th Int. Conf. S.M. & F.E.*, *2*, pp. 43-54.

Ishihara, K. (1996). *Soil Behaviour in Earthquake Geotechnics.* Oxford Engineering Science Series.

Ishizuka, Y., Abe, T., & Kodama, J. (1990). Fatigue behaviour of granite under cyclic loading. In R. Brumer (Ed.), *ISRM international symposium—static and dynamic considerations in rock engineering*, (pp. 139-146). Swaziland.

ISRM. (1979). Suggested Methods for Determining Water Content, Porosity, Density, Absorption and Related Properties and Swelling and Slake-durability Index Properties. *International Journal of Rock Mechanics and Mininig Sciences and Geomechanics*, 141-156.

ISRM. (1983). Suggested Methods for Determining the Strength of Rock Materials in Triaxial Compression. *International Journal of Rock Mechanics and Mining Sciences and Geomechanics, 20*, 285-290.

ISRM. (1999). Draft ISRM suggested method for the complete stress–strain curve for intact rock in uniaxial compression. *International Journal of Rock Mechanics and Mining*

*Sciences, 36*(3), 279-289.

Iwan, W. (1967). On a class of models for the yielding behaviour of continuous and composite systems. *J. Appl. Mech., 34*(E3), 612-617.

Janssen, L., Lacal Arántegui, R., Brøndsted, P., Gimondo, P., Klimpel, A., Johansen, A., et al. (2012). *Scientific Assessment in Support of the Materials Roadmap Enabling Low Carbon Energy Technologies: Wind Energy.* JRC Scientific and Technical Reports, European Union.

Japan Road Association. (2002). *Design Specifications of Highway Bridges, Part V Seismic Design.* JRA.

Jardine, R. (1998). *Interim Report on Cyclic Loading Model and Synthetic Soil Profile for HSE Funded Pile Cyclic Loading Study.* Imperial College Consultants (ICON).

Jardine, R., & Chow, F. (1996). *New design methods for offshore piles.* London: Marine Technology Directorate.

Jardine, R., & Standing, J. (2000). *Pile Load Testing Performed for HSE Cyclic Loading Study at Dunkirk, France.*

Jardine, R., & Standing, J. (2012). Field axial cyclic loading experiments on piles driven in sand. *Soils and Foundations, 52*(4), 723-737.

Jardine, R., Chow, F., Overy, R., & Standing, J. (2005). *ICP Design methods for driven pile in sand and clays.* London: Thomas Telford Publishing.

Johnston, I. (1991). Geomechanics and the emergence of soft rock technology. *Australian Geomechanics*(21), 3-26.

Jong, U., & Chan, G. (1991). *A study on the Fatigue Failure Behaviour of Cheon-Ho Mt. Limestone Under Cyclic Loading.* Korea Atomic Energy Research Institute.

Joosse, P., van Delft, D., & Bach, P. (1994). Fatigue Design Curves compared to Test Data of Fiberglass Blade Material. *European Wind Energy Conference Proceedings*, *3*, pp. 720-726. Thessaloniki, Greece.

Jostad, H., Grimstad, G., Andersen, K., & Sivasithamparam, N. (2015). A FE procedure for calculation of cyclic behaviour of offshore foundations under partly drained conditions. In Meyer (Ed.), *Frontiers in Offshore Geotechnics III* (pp. 153-172). Oslo: Taylor & Francis Group.

Kaplan, M. (1961). Crack Propagation and Fracture of Concrete. *Proceedings, American Concrete Institute, 58*, 591-611.

Karlsrud, K., Clausen, C., & Aas, P. (2005). Bearing capacity of driven piles in clay, the NGI approach. *Proceedings of International Symposium on Frontiers in Offshore Geotechnics* (pp. 775 - 782). Perth: A.A. Balkema Publishers.

Karlsrud, K., Jensen, T., Wensaas Lied, E., Nowacki, F., & Simonsen, A. (2014). Significant ageing effects for axially loaded piles in sand and clay verified by new field load tests. *Proceedings of the Offshore Technology Conference.* Houston.

Karman, T. (1911). Festigkeitsversuche unter alleseitigern Druck. *Vereines Deutsch. Ing., 55*, 1749-1757.

Kazerani, T. (2011). *Micromechanical Study of Rock Fracture and Fragmentation under Dynamic Loads Using Discrete Element Method.* Lausanne: Ecole Polytechnique Federale de Lausanne.

Kempfert, H. (2009). Pfahlgründungen. In Grundbau Taschenbuch Teil 3. In *Gründungen und Geotechnische Bauwerke* (pp. 73-277).

Kempfert, H., Thomas, S., & Gebreselassie, B. (2010). Observation of pile-soil-interaction during cyclic axial loading using particle image velocimetry. *GeoShanghai 2010 International Conference* (pp. 67-72). Shanghai: ASCE.

Keverling Buisman, A. (1940). *Grondmechanica.* Delft, The Netherlands: Waltman.

Kim, D., & Ha, S. (2014). Effects of Particle Size on the Shear Behavior of Coarse Grained Soils Reinforced with Geogrid. *Materials, 7*, 963-979.

Kirsch, F., & Richter, T. (2010). Ein analytisch-empirischer Ansatz zur Bestimmung der Tragfähigkeit und der Verformungen von axial zyklisch belasteten Pfählen. *Veröff. Inst. Boden. Felsm., Heft 172*.

Kitamura, R., & Hidaka, M. (1988). Cyclic Loading Test on Sandy Soil by True Triaxial Testing Apparatus. *Proceedings of Ninth World Conference on Earthquake Engineering*, *III*, pp. 47-52. Tokyo-Kyoto, Japan.

Knaff, A. (2013). *Fatigue of Clay, Bachelor's thesis.* University of Luxembourg.

Kraft, L., Cox, W., & Verner, E. (1981). Pile Load Tests: Cyclic Loads and Varying Load Rates. *Jnl. Geot. Eng. Divn., 107*, 1-19.

Kramer, S. (1996). *Geotechnical Earthquake Engineering.* Upper Saddle River, N.J: Prentice-Hall.

Kranz, R. (1980). *The effects of confining pressure and stress difference on static fatigue of granite.* Palisades, New York: Columbia University.

Kwasniewski, M., & Takahashi, M. (2006). Behavior of a sandstone under axi- and asymmetric compressive stress conditions. In C. Leung, & Y. Zhou (Ed.), *Rock Mechanics in Underground Construction (proc. 4th Asian Rock Mech. Symp.* (p. 320). Singapore: World Scientific Publishing Co. Pte. Ltd.

Kwasniewski, M., & Takahashi, M. (2007). Effect of confining pressure, intermediate principal stress and minimum principal stress on the mechanical behaviour of a sandstone. In L. Ribeiro e Sousa, & et al. (Ed.), *Proceedings of the 11th Congress of the International for Rock Mechanics. I*, pp. 237-242. Lisbon: Tylor & Francis/Balkema.

Labuz, J., & Biolzi, L. (2007). Experiments with rock: remarks on strength and stability issues. *International Journal of Rock Mechanics and Mining Sciences 2007*(44), 525–37.

Lade, P., & Karimpour, H. (2015). Time effects in granular materials: From micro to macro behaviour. In Soga et al. (Ed.), *Proceedings of the TC105 ISSMGE International Symposium on Geomechanics from Micro to Macro* (pp. 1243-1248). Cambridge, UK: Taylor.

Lambe, T., & Whitman, R. (1969). *Soil Mechanics.* John & Sons, Inc.

Lamborn, M. (1986). *A Micromechanical Approach to Modelling Partly Saturated Soils, M.Sc. Thesis.* Texas: Texas A&M University.

Larson, M. (1998). A static fatigue constitutive law for joints in weak rock. *Mechanics of Jointed and Faulted Rock*(Mar.), 171-177.

Le, J., Manning, J., & Labuz, J. (2014). Scaling of fatigue crack growth in rock. *International*

*Journal of Rock Mechanics & Mining Sciences, 72*, 71-79.

LeBlanc, C., Houlsby, G., & Byrne, B. (2010). Response of stiff piles in sand to long-term cyclic lateral loading. *Geotechnique, 60*(2), 79-90.

Lee, J., & Rhee, C. (1992, March). A study on the Fatigue Failure Behaviour of Cheon-Ho Mt. Limestone Under Cyclic Loading. *Journal of the Korean Nuclear Society, 24*, 98-109.

Lee, K., & Albesia, A. (1974). Earthquake induced settlements in saturated sands. *J. of ASCE, 100*, 387-405.

Lehane, B. (1992). *Experimental investigations of pile behaviour using instrumented field piles.* University of London. Imperial College.

Lehane, B., & Jardine, R. (1994). Shaft capacity of driven piles in sand: a new design method. *Proc. 7th Int. Conf. on the Behaviour of Offshore Structures*, (pp. 23-36). Boston.

Lehane, B., Schneider, J., & Xu, X. (2005). The UWA-05 method for prediction of axial capacity of driven piles in sand. *Proc., Int. Symp. Frontiers Offshore Geomech* (pp. 683-689). Perth: ISFOG.

Lemaitre, J. (1985). Coupled Elasto-Plasticity and Damage Constitutive Equations. *Computer Methods in applied Mechanics and Engineering, 51*, 31-49.

Levy, N., Einav, I., & Hull, T. (2009). Cyclic shakedown of piles subjected to two-dimensional lateral loading. *International Journal for Numerical and Analytical Methods in Geomechanics, 33*, 1339–1361.

Li, H., Zhao, J., & Li, T. (1999). Triaxial compression tests on a granite at di?erent strain rates and confining pressures. *International Journal of Rock Mechanics and Mining Sciences, 36*, 1057-1063.

Li, N., Chen, W., Zhang, P., & Swoboda, G. (2001). The mechanical properties and a fatigue-damage model for jointed rock masses subjected to dynamic cyclical loading. *Int. J. of Rock Mechanics and Mining Sciences, 38*, 1071-1079.

Liang, C., Lippmann, H., & Najar, J. (1993). Effect of artificially induced vibrations on the prevention of coal mine bumps. *Rockbursts and Seismicity in Mines* (pp. 91-94). Rotterdam: Balkema.

Libertiny, G. (1967). Effect of hydrostatic pressure on the short life fatigue property of an alloy steel. *Proc. Inst. Of Mech. Engineers, 182*, 58-64.

Liu, E., & He, S. (2012). Effects of cyclic dynamic loading on the mechanical properties of intact rock samples under confining pressure conditions. *Engineering Geology, 120*(27), 81-91.

Liu, E., Huanhg, R., & He, S. (2012). Effects of Frequency on the Dynamic Properties of Intact Rock Samples Subjected to Cyclic Loading under Confining Pressure Conditions. *Rock Mech Rock Eng, 45*, 89–102.

Liu, J., Xie, H., Hou, Z., Yang, C., & Chen, L. (2014). Damage evolution of rock salt under cyclic loading in uniaxial tests. *Acta Geotechnica*, 153-160.

Liu, Y., Huang, M., & Li, S. (2013). Simplified analysis of cyclic degradation of axial bearing capacity for offshore wind pile foundations. *Rock and Soil Mechanics, 34*(9), 2655-2660.

Lloyd, J., Lott, J., & Kesler, C. (1968). *Fatigue of concrete.* University of Illinois at Urbana Champaign. University of Illinois at Urbana Champaign, College of Engineering. Engineering Experiment Station.

Lockner, D. (1998). A generalized law for brittle deformation of Westerly granite. *Journal of Geophysical Research, 103*(3), 5107-5123.

Long, J., & Vanneste, G. (1994). Effects of Cyclic Lateral Loads on Piles in Sand. *Journal of Geotechnical Engineering, 120*(1), 225-244.

Lowes, L. (1993). *Finite Element Modeling of Reinforced Concrete Beam-Column Bridge Connections.* Berkeley: University of California.

Lubliner, J., Oliver, J., Oller, S., & Oñate, E. (1989). A Plastic-Damage Model for Concrete. *International Journal of Solids and Structures, 25*(3), 299-326.

Luong, M. (1980). Stress-strain aspects of cohesionless soils under cyclic and transient loading. *International Symposium on Soil under Cyclic and transient Loading* (pp. 315-324). Rotterdam: Balkema.

Maekawa, K., Okamura, H., & Pimanmas, A. (2003). *Nonlinear mechanics of reinforced concrete.* London: Spon.

Malccot, Y., Daudeville, L., Dupray, F., Poinard, C., & Buzaud, E. (2010). Strength and damage of concrete under high triaxial loading. *European Journal of Environmental and Civil Engineering, 14*, 777-803.

Mandell, J., Reed, R., & Samborsky, D. (1992). *Fatigue of Fiberglass Wind Turbine Blade Materials.* Montana State University. Montana: Sandia National Laboratory contractor report: SAND92-7005`.

Manouchehrian, A., & Marji, M. (2012). Numerical analysis of confinement effect on crack propagation mechanism from a flaw in a pre-cracked rock under compression. *Acta Mechanica Sinica, 28*(5), 1389–1397.

Manson, S. (1953). Behaviour of Materials under Conditions of Thermal Stress. *Heat Transfer Symp.* University of Michigan, Engineering Research Inst.

Manson, S., & Hirschberg, M. (1964). Fatigue behaviour in strain cycling in the low- and intermediate cycle range. (J. Burke, N. Reed, & V. Weiss, Eds.) *Fatigue, an interdisciplinary approach*, 133.

Manson, S., Nachtigall, A., & Freche, J. (1961). Proceedings. *American Society for Testing and Materials, 61*, 679-703.

Mao, X. (2000). *The Behaviour of Three Calcareous Soils in Monotonic and Cyclic Loading.* University of Western Australia.

Marco, S., & Starkey, W. (1954). A concept of fatigue damage. *Trans ASME, 76*, 627-632.

Martin, C. (1994). *Physical and Numerical Modelling of Offshore Foundations Under Combined Loads.* The Oxford University.

Martin, C., & Houlsby, G. (2001). Combined loading of Spudcan foundations on clay: Laboraory tests. *Geotechnique, 50*(4), 325-338.

Martin, G., Finn, W., & Seed, H. (1975). Fundamentals of liquefaction under cyclic loading. *Journal of the Geotechnical Engineering Division ASCE*.

Masing, G. (1926). Eigenspannungen und Verfestigung beim Messing. *Proc 2nd Int. Cong. of App. Mech.*, (pp. 332-335).

Matasovic, N., & Vucetic, M. (1995, June 1). Generalized cyclic-degradation-pore Pressure Generation model for clays. *Journal of Geotechnical and Geoenvironmental Engineering, 121*(1).

Matlock, H., & Foo, S. (1979). Axial analysis of pile using a hysteretic and degrading soil model. *Proc. Conf. Num. Methods in Offshore Piling* (pp. 165-185). London, UK: I.C.E.

Matlock, H., Foo, S., & Bryant, L. (1978). Simulation of lateral pile behaviour. *Earthquake Engineering and Soil Dynamics*, 600-619.

Matsuishi, M., & Endo, T. (1968). Fatigue of metals subjected to varying stress. *Japan Soc. Mech. Engineering*.

Mazaras, J. (1984). *Application de la mécanique de l'endommagement au comportement non linéaire et à la rupture du béton de structure.* Paris: Université Paris 6.

McEvily, A. (1988). On Closure in Fatigue Crack Growth. *ASTM STP 982*, 35-43.

Meyerhof, G. (1953). The bearing capacity of foundations under eccentric and inclined loads. *Proc. III intl. Conf. on Soil Mechanics Found. Eng.*, *1*, pp. 440-445. Zürich, Switzerland.

Meyerhof, G. (1963). Some recent research on the bearing capacity of foundations. *Canadian, 1*(1), 16-26.

Meyerhof, G. (1976, March). Bearing Capacity and Settlement of Pile Foundations. *J. Geotech. Div., 102*(GT3), 197-228.

Michelis, P. (1985). Polyaxial yielding of granular rock. *J. Eng. Mech.*(111), 1049-1066.

Miner, M. (1945). Cumulative damage in fatigue. *In. Journal if applied mechanics, 12*(3), 159-164.

Mingming, H., Ning, L., Yunsheng, C., & Caihui, Z. (2015). Strength and Fatigue Properties of Sandstone under Dynamic Cyclic Loading. (S. De Rosa, Ed.) *Shock and Vibration*(Article ID 614549).

Mirzaghorbanali, A., Nemcik, J., & Aziz, N. (2013). Effects of Cyclic Loading on the Shear Behaviour of Infilled Rock Joints Under Constant Normal Stiffness Conditions. *Rock Mechanics and Rock Engineering, 47*(4), 1373-1391.

Mittag, J., & Richter, T. (2005). Beitrag zur Bemessung von vertikal zyklisch belasteten Pfählen, In: Festschrift zum 60. Geburtstag von Prof. Dr.-Ing. Hans-Georg Kempfert. *Heft 18 der Schriftenreihe Geotechnik Universität Kassel*.

Mogi, K. (1972). Effect of the triaixal stress system on fracture and flow of rocks. *Phys. Earth Planet. Interiors, 5*, 318-324.

Morrow, J. (1964). Fatigue Properties of Metals. *Meeting of Division 4 of the SAE Iron and Steel Technical Committee.*

Morrow, J. (1968). Fatigue Design Handbook. *Advances in Engineering, 4*, 21-29.

Mróz, Z. (1967). On the description of anisotropic workhardening. *J. Mech. Phys. Solids, 15*, 163-175.

Mu, B., & Shah, S. (2005). Fatigue behavior of concrete subjected to biaxial loading in the compression region. *Materials and Structures, 38*, 289-298.

Muir Wood, D. (1991). *Approaches to modelling the cyclic stress-strain response of soils.* Blackie and Son Ltd, Glasgow and London, Van Nostrand Reihnhold, New York.

Murdock, J. (1965). *A critical Review of Research on Fatigue of Plain Concrete.* University of Illinois. Urbana, Illinois: Engineering Experiment Station Bulletin No. 475.

Murthy, V. (2002). *Principles and Practises of Soil Mechanics and Foundation Engineering.*

Nasseri, M., Grasselli, G., & Mohanty, B. (2007). Experimental relationship between fracture toughness and fracture roughness in anisotropic granitic rocks. *Rock Mechanics: Meeting Society's Challenges and Demands - Eberhardt, Stead & Morrison (eds)*, 617-624.

Niazi, F., & Mayne, P. (2013). Cone Penetration Test Based Direct Methods for Evaluating Static Axial Capacity of Single Piles. *Geotech Geol Eng, 31*, 979–1009.

Nielsen, S., Shajarati, A., Sorensen, K., & Ibsen, L. (2012). *Behaviour of Dense Frederikshavn Sand During Cyclic Loading.* Department of Civil Engineering. Aalborg: Aalborg University.

Niemunis, A., Wichtmann, T., & Triantafyllidis, T. (2005). *A high-cycle accumulation model for sand.* Ruhr-University Bochum, Institute of Soil Mechanics and Foundation Engineering.

Niemunis, A., Wichtmann, T., & Triantafyllidis, T. (2006). Long term deformations in soils due to cyclic loading. *Modern Trends in Geomechanics, Springer Proceedings in Physics, 106*, 427-462.

Nijssen, R., Krause, O., & Philippidis, T. (2004). *Benchmark of lifetime prediction methodologies.* Optimat Blades Technical Report.

Norén-Cosgriff, K., Jostad, H., & Madshus, C. (2015). Idealized load composition for determination of cyclic undrained degradation of soils. In Meyer (Ed.), *Frontiers in Offshore Geotechnics III* (pp. 1097-1102). Oslo: Taylor & Francis Group.

O'Brien, T., & Reifsnider, K. (1981). Fatigue damage evaluation through stiffness measurements in boron-epoxy laminates. *Journal of Composite Materials, 15*, 55-70.

Oh, B. (1986). Fatigue analysis of plain concrete in flexure. *J. Struct. Eng., 112*, 273-288.

Ohnaka, M., & Mogi, K. (1982). Frequency characteristic of acoustic emission in rocks under uniaxial compression and its relation to the fracturing process to failure. *Journal of Geophysical Research, 87*(B5), 3873–3884.

Oliveira, D., Lourenço, P., & Roca, P. (2006). Cyclic behaviour of stone and brick masonry under uniaxial compressive loading. *Materials and Structures, 39*(2), 247-257.

O'Neill, M., & Murchison, J. (1983). *An Evaluation of p-y Relationships in Sands, A Report to the American Petroleum Institute.* Department of Civil Engineering: University of Houston-University Park.

O'Reilly, M. (1991). Cyclic load testing of soils. In M. O'Reilly, & S. Brown, *Cyclic loading of soils: from theory to design* (pp. 70-121). London: Blackie.

O'Reilly, M., & Brown, S. (1991). *Cyclic Loading of Soils: from theory to design.* Glasgow and London: Blackie and Son Ltd.

Palmgren, A. (1924, April). Die Lebensdauer von Kugellagern (Life Length of Roller Bearings. In German). *Zeitschrift des Vereines Deutscher Ingenieure (VDI Zeitschrift), 68*(14), 339-341.

Paris, P., Gomez, M., & Anderson, W. (1961). A rational analytic theory of fatigue. *The Trend in Engineering, 13*, 9-14.

Paterson, M. (1958). Experimental deformation and faulting in Wombeyan marble. *Geol Soc Am Bull, 69*, 465-476.

Patiño, H., Soriano, A., & González, J. (2013). Failure of a soft cohesive soil subjected to combined static and cyclic loading. *Soils and Foundations, 53*(6), 910-922.

Pecker, A. (2007). *Soil Behaviour under Cyclic Loading.* Palaiseau, France: Soil Mechanics Laboratory, Ecole Polytechnique.

Peng, R., Ju, Y., Xie, H., & Li, L. (2011). Energy conversion and damage evolution of rocks under cyclic loading conditions. In Kwasniewski, Li, & Takahashi, *True Triaxial testing of Rocks* (pp. 331-341). CRC Press.

Peralta, P., & Achmus, M. (2010). An experimental investigation of piles in sand subjected to lateral cyclic loads. *7th International Conference on Physical Modelling in Geotechnics*, *2*, pp. 985-990. Zurich.

Peterson, R. (1988). Interpretation of Triaxial Compression Test Results on Partially Saturated Soils. *Advanced Triaxial Testing of Soil and Rock, ASTM STP 977*, 512-538.

Philippidis, T., & Passipoularidis, V. (2006). Residual strength after fatigue in composites: Theory vs. experiment. *International Journal of Fatigue, 29*, 2104-2116.

Plona, T., & Cook, J. (1995). Effects of stress cycles on static and dynamic Young's moduli in Castlegate sandstone. (S. Daemen, Ed.) *Rock Mechanics*, 155-160.

PMB Engineering. (1988). *PAR: Pile Analysis Routines, Theoretical and User's Manuals.* San Francisco: PMB Engineering Inc.

Poinard, C., Malecot, Y., & Daudeville, L. (2010). Damage of concrete in a very high stress state: experimental investigation. *Materials and Structures, 43*, 15-29.

Post, N., Bausano, J., Case, S., & Lesko, J. (2006). Modeling the remaining strength of structural composite materials subjected to fatigue. *International Journal of Fatigue, 28*, 1100-1108.

Post, N., Case, S., & Lesko, J. (2008). Modeling the variable amplitude fatigue of composite materials: A review and evaluation of the art for spectrum loading. *International Journal of Fatigue, 30*, 2064-2086.

Poulos, H. (1979). Development of an Analysis for Cyclic Axial Loading of Piles. *Proceedings, 3rd International Conference Numerical Methods in Geomechanics*, *1.4*, pp. 1513-1530. Aachen.

Poulos, H. (1981). Cyclic axial response of single pile. *J. Geotechnical Engineering, 107*(1), 41-58.

Poulos, H. (1982). *Influence of cyclic loading on axial pile response.* Sydney: University of Sydney, School of Civil and Mining Engineering.

Poulos, H. (1987). Analysis of residual stress effects in piles. *J. Geotech. Eng., 113*(3), 216-229.

Poulos, H., & Davis, E. (1974). *Elastic solutions for Soil and Rock Mechanics.* John Wiley & Sons Inc.

Poulos, H., & Jansen, R. (1989). Liquefaction Related Phenomena. In *Advance Dam Engineering for Design, Construction, and Rehabilitation* (pp. 292–297). Van Nostrand Reinhold.

Poulos, H., Carter, J., & Small, J. (2001). Foundations and retaining structures: research and

practice. *Proc. 15th Int. Conf. Soil Mech. Foundation Eng.*, *4*, pp. 2527-2606. Istanbul.

Prandtl, L. (1920). Über die Härte plastischer Körper. *Nachr. Ges. Wiss. Goettingen, Math.-Phys.*, 74–85.

Puech, A. (2013). Advances in axial cyclic pile design, Contribution of the SOLCYP project. *Proceedings of TC 209 Workshop 18th ICSMGE.* Paris.

Puech, A., Benzaria, O., Thorel, L., Garnier, J., Foray, P., Silva, M., et al. (2013). Cyclic stability diagrams for piles in sands. *Proceedings 18th ICSMGE*, (pp. 85-88). Paris.

Pugno, N., Ciavarella, M., Cornetti, P., & Carpinteri, A. (n.d.). A generalized Paris's law for fatigue crack growth.

Pyke, R. (1973). *Settlement and liquefaction of sands under multi directional loading.* Berkeley: University of California.

Pyke, R. (1979). Nonlinear soil models for irregular cyclic loadings. *Journal of the Geotechnical Engineering Division, 105*(GT6), 715-726.

Pytlik, R., & Van Baars, S. (2014). Fatigue of geomaterials. *Computer Methods and Recent Advances in Geomechanics* (p. 88). Kyoto, Japan: CRC Press/Balkema.

Pytlik, R., & Van Baars, S. (2015). Laboratory tests on Dutch limestone (Mergel). In W. Schubert, & A. Kluckner (Ed.), *Future Development of Rock Mechanics - Proceedings of the ISRM Regional Symposium EUROCK 2015 & 64th Geomechanics Colloquium* (pp. 439-444). Salzburg, Austria: Austrian Society for Geomechanics.

Pytlik, R., & Van Baars, S. (2015, July). Triaxiaalproeven op Limburgse mergel leveren verassende resultaten. *Geotechniek*, 10-13.

Rajashree, S., & Sundaravadivelu, R. (1996). Degradation model for one-way cyclic lateral load on piles in soft clay. *Comput. Geotech., 19*(4), 289-300.

Randolph, M. (2009). Offshore Design Approaches and Model Tests for Sub-Failure Cyclic Loading of Foundations. In C. Di Prisco, & D. Muir Wood, *Mechanical behaviour of soils under environmentally induced cyclic loads* (pp. 441-480). Udine: CISM.

Randolph, M., & Gouvernec, S. (2011). *Offshore Geotechnical Engineering* (1. Edition ed.). Spon Press.

Randolph, M., & Wroth, C. (1978). Analysis of vertical deformation of vertically loaded piles. *J. Geotech. Eng. Div., 104*(2), 1465-1488.

Randolph, M., Carter, J., & Wroth, C. (1979). Driven piles in clay - the effects of installation and subsequent consolidation. *Geotechnique, 29*(4), 361-393.

Randolph, M., Dolwin, J., & Beck, R. (1994). Design of driven piles in sand. *Geotechnique, 44*(3), 427-448.

Ray, S., Sarkar, M., & Singh, T. (1999). Effect of cyclic loading and strain rate on the mechanical behaviour of sandstone. *International Journal of Rock Mechanics and Mining Sciences*, 543-549.

Reese, L., Cox, W., & Koop, F. (1974). Analysis of Laterally Loaded Piles in Sand. *Proceedings of the Sixth Annual Offshore Technology Conference.* Houston.

Reifsnider, K., & Stinchcomb, W. (1986). A critical Element Model of the Residual Strength and Life of Fatigue-Loaded Composite Coupons. *Composite Materials: Fatigue and Fracture*, 298-303.

Reissner, H. (1924). Zum Erddruckproblem. In C. Biezeno, & J. Burgers (Ed.), *Proc., 1st Int. Congress for Applied Mechanics*, (pp. 295-311). Delft, The Netherlands.

Resende, L., & Martin, J. (1987). Closure of Formulation of Drucker-Prager Cap Model. *J. Eng. Mech.*, 1257-1259.

Rimoy, S., Jardine, R., & Standing, J. (2013). Displacement response to axial cycling of piles driven in sand. *Geotechnical Engineering, 165*(GE1), 1 – 16.

Roscoe, K., & Burland, J. (1968). On the generalised stress-strain behaviour of 'wet' clay. (J. Heyman, & F. Leckie, Eds.) *Engineering Plasticity*, 535-609.

Roscoe, K., & Schofield, A. (1957, January). The stability of short pier foundations on sand, discussion. *British Welding Journal*, 12-18.

Rücker, W. (2007). Offshore wind energy plants: Problems and possible solutions. *Proceedings of the EVACES 2007*, (pp. 55-72). Porto.

Salciarini, D., & Tamagnini, C. (2009). A hypoplastic macroelement model for shallow foundations under monotonic and cyclic loads. *Acta Geotechnica*.

Salim, M., & Mohamed, Z. (2012). Cyclic Loading Effect on the Uniaxial Compressive Strength of Weathered Rock. *6th Symposium on Advances in Science and Technology.* Kuala Lumpur.

Sangrey, D., Henkel, D., & Esrig, M. (1969). The effective stress response of a saturated clay soil to repeated loading. *Can. Geotech. J., 3*, 241-252.

Sarfaraz Khabbaz, R. (2012). *Fatigue Life Prediction of Adhesively-Bonded Fiber-Reinforced Polymer Structural Joints under Spectrum Loading Patterns.* EPFL, École Polytechnique Federale De Lausanne.

Sawicki, A. (1987). An engineering model for compaction of sand under cyclic loading. *Engineering Transactions, 35*(4), 677–693.

Schaff, J., & Davidson, B. (1997a). Life Prediction methodology for composite structures. Part I - Constant amplitude and two-stress level fatigue. *Journal of Composite Materials, 31*(2), 128-157.

Schaff, J., & Davidson, B. (1997b). Life Prediction methodology for composite structures. Part II - Spectrum fatigue. *Journal of Composite Materials, 31*(2), 158-181.

Schofield, A., & Wroth, C. (1968). *Critical State Soil Mechanics.* McGraw-Hill.

Schwarz, P. (2002). *Beitrag zum Tragverhalten von Verpresspfahlen mit kleinem Durchmesser unter axialer zyklischer Belastung* (Vol. 33). Lehrstuhl und Prufamt fur Bodenmechanik und Felsmechanik der Technischen Universitat Munchen.

Seed, H., & Lee, K. (1966). Liquefaction of saturated sands during cyclic loading. *Journal of Soil Mechanics and Foundation Engineering, 92*(SM6), 105-134.

Seed, H., Martin, P., & Lysmer, J. (1976). Pore water pressure changes during soil liquefaction. *Journal of the Geotechnical Engineering Division, 102*(GT4), 323-346.

Sendeckyj, G. (1981). Fitting Models to Composite Materials Fitting Data, Test methods and Design Allowables for Fibrous Composites. In A. S. materials, *ASTM STP 734, in C. C. Chamis* (pp. 245-260).

Shajarati, A., Sorensen, K., Nielsen, S., & Ibsen, L. (2012). *Manual for Cyclic Triaxial Test.* Aalborg University.

Shanley, F. (1953). *Fatigue Analysis of Aircraft Structures.* ASTIA.

Silver, M., & Seed, H. (1971). Deformation characteristics of sand under cyclic loading. *J.Soil Mech. & Found. Div., 97*(No.SM8), 1081-1098.

Singh, S. (2011). Fatigue Strength of Hybrid Steel-Polypropylene Fibrous Concrete Beams in Flexure. *The Twelfth East Asia-Pacific Conference on Structural Engineering and Construction. 14*, pp. 2446-2452. Elsevier.

Slutter, R., & Ekberg, C. (1958). Static and Fatigue Tests on Prestressed Concrete Railway Slabs. *American Railway Engineering Association, 60*(544), 3-50.

Soderberg, C. (1930). Fatigue of safety and working stress. *Transactions of the American Society of Mechanical Engineers, 52 (Part APM-52-2)*, 13-28.

SOLCYP. (2013). Design for cyclic loading: piles and other foundations. In A. Puech (Ed.), *Proceedings of TC 209 Workshop 18th ICSMGE - Paris, 4 September 2013.* Paris: ISSMGE Technical Committee TC 209 – Offshore Geotechnics.

Sowa, V. (1970). Pulling Capacity of Concrete Cast in Situ Bored Piles. *Can. Geot. Jnl., 7*, 482-493.

Sridhanya, K., Rajagopal, K., & Lakshmana Rao, C. (2009, April). Modeling of Degradation of Clayey Soils under Repeated Loading. *Indian Geotechnical Journal, 39*(2), 139-152.

Steenfelt, J., Randolph, M., & Wroth, C. (1981). Model Tests on Instrumented Piles Jacked into Clay. *Proc. 10th Int. Conf. S.M. & F.E.*, *2*, pp. 857-864. Stockholm.

Strohmeyer, C. (1914). The determination of fatigue limits under alternating stress conditions. *Proceedings of the Royal Society of London*, *90*, pp. 411-425. London.

Stüssi, F. (1955). Die Theorie der Dauerfestigkeit und die Versuche von August Wöhler. *TKVSB, 13*.

Suiker, A. (2002). *The mechanical behaviour of ballasted railway tracks.* Delft, The Netherlands: Delft University of Technology.

Sukumar, N., Chopp, D., & Moran, B. (2003). Extended fininte element method and fast marching method for three-dimensional fatigue crack propagation. *Eng. Fract. Mech., 70*, 29-28.

Swane, I., & Poulos, H. (1985). Shakedown Analysis Of A Laterally Loaded Pile Tested In Stiff Clay. *Civ. Eng. Trans. I.E. Aust.*, *27 (3)*, pp. 275-280. Perth, Western Australia.

Tavakoli, H., Shafiee, A., & Jafari, M. (2008). Effect of cyclic loading on undrained behaviour of compacted sand/clay mixtures. *The 14th World Conference on Earthquake Engineering.* Beijing.

Terzaghi, K. (1943). *Theoretical Soil Mechanics.* New York: John Wiley & Sons.

Thiers, G., & Seed, H. (1969). Vibration Effects of Earthquake on Soils and Foundations. *American Society for Testing and Materials*, 3-56.

Tsuha, C., Foray, P., Jardine, R., & et al. (2012). Behaviour of displacement piles in sand under cyclic axial loading. In *Soils and Foundations* (Vol. 52, pp. 393-410).

UK DEn. (1990). *Offshore Installations, Guidance on Design.* London: HMSO Construction, and Certification, Department of Energy.

Vahdatirad, M., Bayat, M., Andersen, L., & Ibsen, L. (2012). An improved asymptotic sampling approach for stochastic finite element stiffness of a laterally loaded monopile. *9th International Conference on Testing and Design Methods for Deep*

*Foundations.*
Van Baars, S. (1996). *Discrete element analysis of granular materials.* Delft, The Netherlands: Delft University of Technology.
Van Delft, D., de Winkel, G., & Joosse, P. (1997). Fatigue behaviour of fibreglass wind turbine blade material under variable amplitude loading. *AIAA/ASME Wind Energy Symposium, no. AIAA-97-0951*, (pp. 180-188). Reno, Nevada.
Van Eekelen, H. (1977). Single-parameter models for progressive weakining of soils by cyclic loading. *Geotechnique, 27*(3), 357-368.
Van Eekelen, H., & Potts, D. (1978). The behaviour of Drammen Clay under cyclic loading. *Geotechnique, 28*, 173-196.
Van Leeuwen, J., & Siemens, A. (1979). Miner's rule with respect to plain concrete. *Heron, 24*(1).
Van Weele, A. (1979). Pile Bearing Capacity Under Cyclic Loading Compared with that Under Static Loading. *Proc. 2nd Int. Conf. Beh. Off. Structures*, (pp. 475-488). London.
Viana da Fonseca, A., Rios, S., Amaral, M., & Panico, F. (2013). Fatigue Cyclic Tests on Artificially Cemented Soil. *Geotechnical Testing Journal, 36*(2), 1-9.
Voyiadjis, G., & Abu-Lebdeh, T. (1994). Plasticity Model for Concrete Using the Bounding Surface Concept. *Internation Journal of Plasticity, 10*(1), 1-22.
Vyalov, S. (1978). *Rheologic Principles of Soil Mechanics (in Russian).* Moscov: Vysshaya Shkola.
Waagaard, K. (1981). *Fatigue strength of offshore concrete structures.* COSMAR.
Wadsworth, N., & Hutchings, J. (1958). The effect of atmospheric corrosion on metal fatigue. *Philosophical Magazine, 3*(34), 1154.
Weibull, W. (1949). A statistical report of fatigue failure in solids. *Transactions, 27*.
Werkmeister, S. (2003). *Permanent deformation behaviour of unbound granular materials.* Dresden: University of Technology.
White, D., & Lehane, B. (2004). Friction fatigue on displacement piles in sand. *Géotechnique, 54*(10), 645–658.
Whitney, J. (1981). Fatigue characterisation of composite materials. In *Fatigue of fibrous composite material* (Vol. 723, pp. 133-151). ASTM STP.
Whitney, P. (2001). Fatigue Failure of the De Havilland Comet I. In D. Jones, *Failure Analysis Case Studies II* (pp. 185-192). Elsevier Science Ltd.
Wichtmann, T., & Triantafyllidis, T. (2012). Behaviour of Granular Soils Under Environmentally Induced Cyclic Loads. In *Mechanical Behaviour of Soils Under Environmentally Induced Cyclic Loads* (Vol. 534, pp. 1-136). CISM Courses and Lectures.
Wöhler, A. (1870). über die Festigkeits-Versuche mit Eisen und Stahl. *Zeitschrift für Bauwesen, 20*, 73-106.
Xiao, J., Ding, D., Jiang, F., & Xu, G. (2009). Fatigue damage variable and evolution of rock subjected to cyclic loading. *International Journal of Rock Mechanics and Mining Sciences*.
Xu, D., & Geng, N. (1985). The variation law of rock strength with increase of intermediate

principal stress (in Chinese). *Acta Mechanics Solida Sinica, 7*(1), 72–80.

Yamashita, S., Sugimoto, F., Imai, T., Namsrai, D., Yamauchi, M., & Kamoshida, N. (1999). The relationship between the failure process of the creep or fatigue test and the conventional compression test on rock. In G. Vouille, & P. Berest (Ed.), *ISRM ninth international congress on rock mechanics*, (pp. 699-702). Paris.

Yang, Z., Jardine, R., Zhu, B., Foray, P., & Tsuha, C. (2010). Sand grain crushing and interface shearing during displacement pile installation in sand. *Geotechnique, 6*, 469-482.

Yao, W., & Himmel, N. (1999). Statistical analysis of data from truncated fatigue life and corresponding residual strength experiments for polymer matrix composites. *International Journal of Fatigue, 21*, 581-585.

Yasuhara, Y., Hyde, A., Toyata, N., & Murakami, S. (1997). Cyclic stiffness of plastic silt with an initial drained shear stress. *Proc. Geotechnique Symp.p. In print(SIP) on Prefailure Deformation Behavior of Geomaterials, R. J.Jardine et al., eds.*, (pp. 373-382). London.

Yazdani, S., & Schreyer, H. (1988). An anisotropic damage model with dilatation for concrete. *Mech. Meter., 7*, 231-244.

Yoshida, N., Yasuda, S., Kiku, H., Masuda, T., & Finn, W. (1994). Behavior of sand after liquefaction. *Proc., 5th U.S.-Japan Workshop on Earthquake Resistant Design of Lifeline Facilities and Countermeasures Against Soil Liquefaction*, (pp. 181-198). Salt Lake City.

Youd, T. (1972). Compaction of sand by repeated shear straining. *Journal of the Soil Mechanics and Foundations Division, 97*(7), 709-725.

Yu, H. (2006). *Plasticity and Geotechnics.* Springer.

Yu, H., Khong, C., & Wang, J. (2007). A unified plasticity model for cyclic behaviour of clay and sand. *Mechanics research communications, 34*(2), 97-114.

Zafar, S., & Rao, K. (2010). Assessment of cyclic triaxial behaviour of Shiwalik sandstone. *International Journal of Research in Engineering & Technology*.

Zambelli, C., di Prisco, C., & Imposimato, S. (2004). A cyclic elasto-viscoplastic constitutive model: theoretical discussion and validation. In T. Triantafyllidis, *Cyclic Behaviour of Soils and Liquefaction Phenomena* (pp. 99-106). Balkema.

Zhao, J. (2000). Applicability of Mohr-Coulomb and Hoek-Brown strength criteria to the dynamic strength of brittle rock. *International Journal of Rock Mechanics and Mining Sciences, 37*, 1115-1121.

Zhenyu, T., & Haihong, M. (1990). Technical note: an experimental study and analysis of the behaviour of rock under cyclic loading. *Int. J. Rock Mech. Min. Sci., 27*(1), 51-56.

Zhu, M., & Michalowski, R. (2005). Shape Factors for Limit Loads on Square and Rectangular Footings. *Journal of Geotechnical and Geoenvironmental Engineering, 131*(2), 223-231.

Zienkiewicz, O., & Mróz, Z. (1984). Generalised plasticity formulation and applications to geomechanics. In C. Desai, & R. Gallagher, *Mechanics of Engineering Materials* (p. Chapter 33). Chichester: John Wiley & Sons.

# LIST OF SYMBOLS

*Bearing capacity*

| | |
|---|---|
| $\delta$ | - angle of the wall friction |
| $\gamma$ | - volumetric weight |
| $\gamma_t$, $\gamma_b$, $\gamma_s$ | - partial factors |
| $\xi_1$, $\xi_2$ | - correlation factors |
| $\phi$ | - friction angle |
| $c$ | - cohesion |
| $d$ | - diameter of the shaft at base level |
| $i_c$, $i_q$, $i_\gamma$ | - correction factors |
| $n$ | - total factor of safety |
| $p$ | - ultimate bearing capacity |
| $q$ | - side load |
| $q_0$ | - is the average effective overburden pressure |
| $s_c$ | - shape factor |
| $s_q$ | - shape factor |
| $s_\gamma$ | - shape factor |
| $A_b$ | - base area of pile |
| $B$ | - total width of the loaded strip |
| $K_s$ | - average lateral earth pressure coefficient |
| $N_c$, $N_q$, $N_\gamma$ | - dimensionless bearing capacity factors |
| $R_a$ | - working load |
| $R_b$ | - base resistance |
| $R_{b;k}$ | - characteristic values of the base resistance |
| $R_{c;k}$ | - characteristic compressive resistance |
| $R_{c;m(mean)}$ | - mean characteristic compressive resistance |
| $R_{c;m(min)}$ | - minimum characteristic compressive resistance |
| $R_{c;d}$ | - design compressive resistance |
| $R_{b;k}$ | - characteristic values of the shaft resistance |
| $R_s$ | - shaft resistance |

*Stresses & strains*

| | |
|---|---|
| $\delta$ | - tangent angle of failure line in p-q diagram |
| $\varepsilon$ | - strain |
| $\varepsilon_{ap}$ | - amplitude of plastic cyclic strain |
| $\varepsilon_e$ | - elastic strain |
| $\varepsilon_p$ | - plastic strain |
| $\varepsilon_t$ | - total strain |
| $\sigma$ | - stress |
| $\sigma_1$ | - maximum principal stress |
| $\sigma_2$ | - medium principal stress |

$\sigma_3$ - minimum principal stress
$\sigma_c$ - intercept in $\sigma_3$ - $\sigma_1$ space
$\sigma_d$ - deviatoric stress
$\sigma_{d,max}$ - maximum deviatoric stress
$\Delta\sigma$ - stress range
$\tau$ - shear stress
$\tau_0$ - shear stress based on the linear regression for static tests
$b$ - ordinate in a p – q diagram
$p$ - the average value of the minor and major principal stresses
$q$ - the difference of the major and minor principal stresses
$A$ - cross-section area of a sample
$E$ - Young's modulus
$E_{av}$ - average Young's modulus (measured at 10%-80% of ultimate strength)
$E_{sec}$ - Young's modulus measured from zero stress to a certain fixed percentage of the ultimate strength
$E_{tan}$ - Young's modulus measured at 50 % of ultimate strength
$F$ - load
$S_{sy}$ - yield strength in shear
$S_y$ - yield strength in uniaxial tension

*Cyclic loading & Fatigue*

$\alpha,\beta$ - remaining shear strength curve parameters
$\sigma_a$ - cyclic stress amplitude
$\sigma_e$, $S_e$ - endurance limit (fatigue limit)
$\sigma_{eff}$ - effective alternating stress
$\sigma_f$ - true fracture stress
$\sigma_{cyc}$ - cyclic stress
$\sigma_{d,cyc}$ - cyclic deviatoric stress
$\sigma_m$ - cyclic mean stress
$\sigma_{max}$ - maximum cyclic stress
$\sigma_{min}$ - minimum cyclic stress
$\sigma_u$ - ultimate stress
$\sigma_y$ - yield stress
$c_0$ - cohesion based on the linear regression for static tests
$c_{rem}$ - remaining cohesion
$\tau_{cyc}$ - cyclic shear stress
$\tau_{rem}$ - remaining shear strength
$i$ - cyclic stress ratio
$f$ - frequency of cyclic loading
$n$ - applied number of cycles
$z_i$ - part of life spent at cyclic stress ratio $i$
$D$ - damage parameter

$D_{L,d}$ - safe design damage value
$F_{cyc}$ - cyclic force
FDF - fatigue design factor
$N$ - number of cycles to failure (fatigue life)
$N_{rem}$ - remaining number of cycles to failure
$R$ - stress ratio
$S$ - fatigue strength
$S_0$ - static (initial) strength
$S_{rem}$ - remaining strength

*Others*

$\rho$ - density of material
$\rho_d$ - average density of material
$\rho_{min}$ - minimum density of material
$\rho_{max}$ - maximum density of material
$\rho_p$ - density of the particles
$a$ - crack length
c/s - cement to sand ratio
$d$ - sample diameter
$e$ - void ratio
$h$ - sample height
$m$ - material constant
$n$ - porosity
$A$ - area of the sample
$C$ - material constant
$C_c$ - coefficient of curvature
$C_u$ - uniformity coefficient
$D_{50}$ - average grain size
$K$ - stress intensity factor
$K_{max}$ - maximum stress intensity factor
$K_{min}$ - minimum stress intensity factor

*Statistics*

$\mu$ - mean of normal distribution
*a,b,c, A,B, C, D, F,G* - regression coefficients
$p$ - probability of failure
$r^2$ - coefficient of determination
*std* - standard deviation of normal distribution
$s_{all}$ - standard deviation of all points
$s_{est}$ - standard error of estimate
$N_{eq}$ - equivalent number of cycles
$S_i$ - random sample

# APPENDICES

# A. LABORATORY TEST RESULTS

## a) Data presentation convention - comparison

Below a comparison based on the laboratory tests results are presented. For each type of data presentation convention a linear regression can be applied and the Mohr-Coulomb shear strength parameters can be obtained. Due to sensitivity of number of data point and data spread different coefficient of determination (and different accuracy of the results) can be obtained. The influence of some parameters on the linear regression was discussed by Cornell & Berger (1987). They advised to keep in mind that multiple observations of $Y$ at each $X$ have a reducing effect on the $r^2$; therefore, $r^2$ should not be relied on as the sole model-fitting criterion. The selected range of $X$ should be as large as possible, with the assurance that the relationship between $Y$ and $X$ is linear over the range. The slope $\delta$ (the higher the slope, the smaller the $r^2$) also has an impact on the $r^2$.

From the Figure A.1, Figure A.2 and Figure A.3 it can be seen that the most accurate prediction of the friction angle $\phi$ and cohesion $c$ can be obtained from the $p$-$q$ plots.

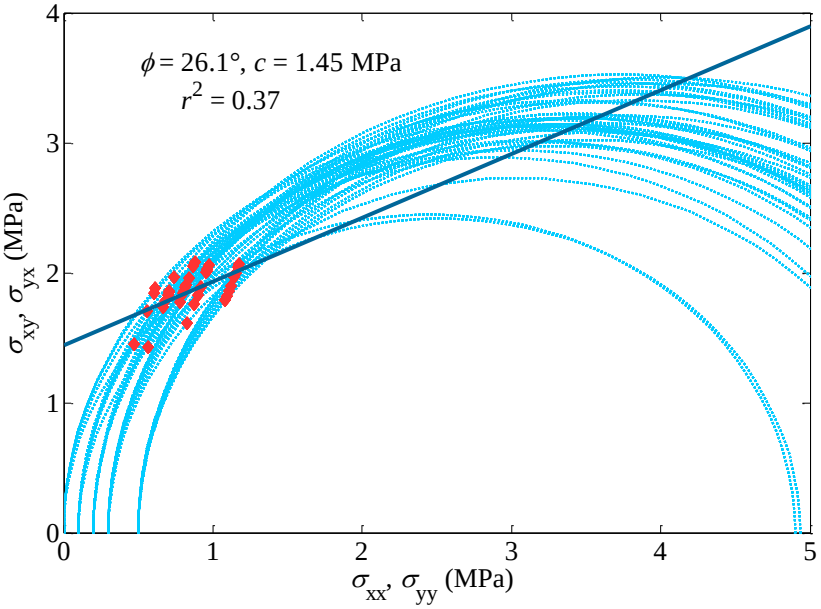


*Figure A.1. $\sigma_{zz}$,$\sigma_{xx}$ – $\tau_{zx}$,$\tau_{xz}$ – Mohr circles for artificial gypsum*

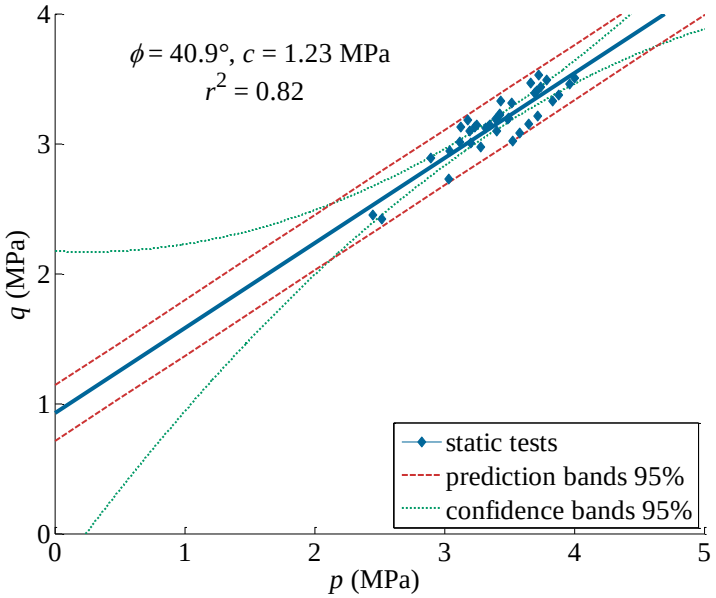


*Figure A.2. p-q plot for artificial gypsum*

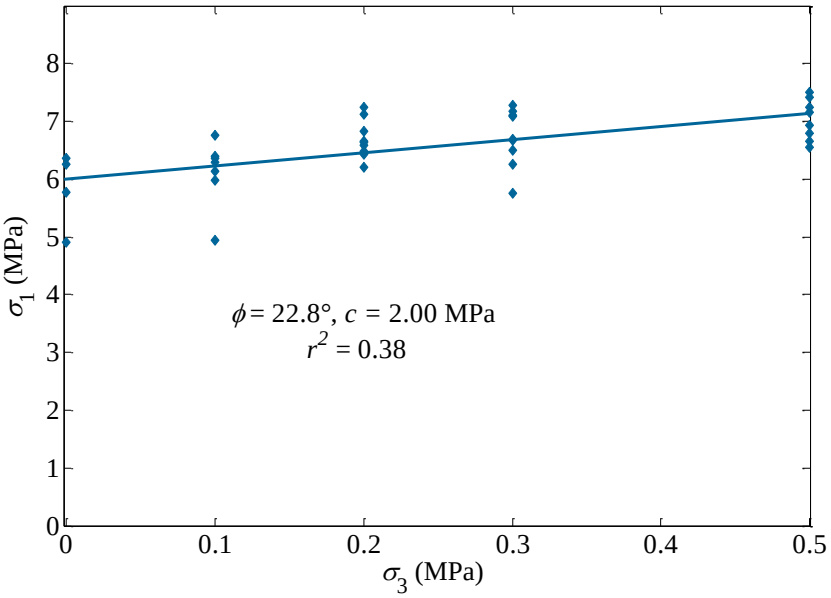


*Figure A.3. $\sigma_3$ - $\sigma_1$ plot for artificial gypsum*

### b) Static data & normal distribution

First static, triaxial tests were performed on cylindrical samples. All the tests were conducted in dry conditions, and the samples had natural moisture. The static tests were run until failure the number maximum peak load was measured ($p$, $q$). The failure was determined as load for which the strains are increasing and the stresses cannot reach the cyclic stresses. The densities for all samples investigated in static tests are also presented. Additionally the ratio of the laboratory tests to the calculated interpolated failure curve is given ($\tau/\tau_0$). The results are presented below.

*Artificial gypsum – static triaxial tests*

*Table A-1. Artificial gypsum static test results*

| | $F_{max}$ (N) | $\sigma_3$ (MPa) | $p$ (MPa) | $q$ (MPa) | $\tau/\tau_0$ (-) | $\rho_d$ = (g/cm$^3$) | behaviour | Type of fracture |
|---|---|---|---|---|---|---|---|---|
| Test 1 | 7484 | 0.10 | 3.43 | 3.33 | 1.14 | 0.99 | brittle | Cone & Split |
| Test 2 | 7186 | 0.10 | 3.19 | 3.09 | 1.06 | 1.01 | brittle-ductile | Cone & Split |
| Test 3 | 6919 | 0.10 | 3.04 | 2.94 | 1.00 | 0.97 | brittle | Cone & Split |
| Test 4 | 7713 | 0.20 | 3.51 | 3.31 | 1.05 | 0.99 | brittle-ductile | Cone & Split |
| Test 5 | 6972 | 0.20 | 3.20 | 3.00 | 0.95 | 0.99 | ductile | Cone & Split |
| Test 6 | 7410 | 0.20 | 3.42 | 3.22 | 1.02 | 1.00 | ductile | Cone & Split |
| Test 7 | 7972 | 0.30 | 3.79 | 3.49 | 1.02 | 1.00 | brittle-ductile | Cone & Split |
| Test 8 | 6914 | 0.30 | 3.28 | 2.98 | 0.87 | 0.99 | ductile | Cone & Split |
| Test 9 | 7040 | 0.30 | 3.40 | 3.10 | 0.91 | 1.00 | brittle | Cone & Split |
| Test 10 | 7191 | 0.10 | 3.23 | 3.13 | 1.07 | 1.00 | brittle-ductile | Cone & Split |
| Test 11 | 7196 | 0.10 | 3.25 | 3.15 | 1.07 | 1.00 | brittle-ductile | Cone & Split |
| Test 12 | 8065 | 0.20 | 3.72 | 3.52 | 1.11 | 1.00 | brittle-ductile | Cone & Split |
| Test 13 | 7992 | 0.20 | 3.66 | 3.46 | 1.09 | 0.99 | brittle-ductile | Cone & Split |
| Test 14 | 7332 | 0.30 | 3.49 | 3.19 | 0.94 | 0.99 | brittle-ductile | Cone & Split |
| Test 15 | 7797 | 0.30 | 3.71 | 3.41 | 1.00 | 0.99 | brittle-ductile | Cone & Split |
| Test 16 | 7793 | 0.30 | 3.69 | 3.39 | 0.99 | 0.98 | ductile | Cone & Split |
| Test 17 | 7783 | 0.30 | 3.74 | 3.44 | 1.01 | 0.99 | ductile | Cone & Split |
| Test 18 | 7937 | 0.50 | 4.00 | 3.50 | 0.90 | 0.99 | ductile | Cone |
| Test 19 | 7845 | 0.50 | 3.96 | 3.46 | 0.89 | 1.00 | ductile | Cone |
| Test 20 | 7671 | 0.50 | 3.83 | 3.33 | 0.86 | 1.00 | brittle-ductile | Shear |
| Test 21 | 7299 | 0.20 | 3.39 | 3.19 | 1.01 | 0.99 | brittle | Cone & Split |
| Test 22 | 6985 | 0.20 | 3.34 | 3.14 | 0.99 | 1.01 | ductile | Cone & Split |
| Test 23 | 7061 | 0.20 | 3.32 | 3.12 | 0.98 | 1.00 | brittle-ductile | Cone & Split |
| Test 24 | 7262 | 0.20 | 3.43 | 3.23 | 1.02 | 0.99 | brittle-ductile | Cone & Split |
| Test 25 | 6770 | 0.50 | 3.52 | 3.02 | 0.78 | 1.00 | ductile | Cone & Split |
| Test 26 | 5435 | 0.10 | 2.52 | 2.42 | 0.83 | 1.00 | brittle | Cone & Split |
| Test 27 | 6907 | 0.50 | 3.58 | 3.08 | 0.79 | 1.02 | brittle-ductile | Cone & Split |
| Test 28 | 7247 | 0.50 | 3.71 | 3.21 | 0.83 | 1.02 | brittle-ductile | Cone & Split |
| Test 29 | 7177 | 0.00 | 3.18 | 3.18 | 1.18 | 1.01 | brittle | Cone & Split |
| Test 30 | 6736 | 0.00 | 2.89 | 2.89 | 1.07 | 0.98 | brittle | Cone & Split |
| Test 31 | 7340 | 0.50 | 3.65 | 3.15 | 0.81 | 0.98 | ductile | Cone & Split |
| Test 32 | 6364 | 0.30 | 3.03 | 2.73 | 0.80 | 0.98 | ductile | Cone & Split |
| Test 33 | 7441 | 0.30 | 3.50 | 3.20 | 0.94 | 0.99 | ductile | Cone & Split |
| Test 34 | 7855 | 0.50 | 3.87 | 3.37 | 0.87 | 1.00 | ductile | Cone & Split |
| Test 35 | 7018 | 0.10 | 3.11 | 3.01 | 1.03 | 1.01 | brittle-ductile | Cone & Split |
| Test 36 | 5704 | 0.00 | 2.45 | 2.45 | 0.91 | 1.01 | brittle | Cone & Split |
| Test 37 | 7276 | 0.00 | 3.13 | 3.13 | 1.16 | 1.02 | brittle | Cone & Split |

Only samples 1, 3, 10, 11, 25, 27, 29 and 30 had small flaws on the surface after core drilling.

A bigger flaw on the surface was present only on sample 24. Defect in the core after triaxial tests were found only in samples no 9, 25, 27, 32 and 33.

The cumulative empirical and standard normal distribution of cohesion is presented in Figure A.4. Both, the empirical (based on the measure data) and the standard normal cumulative density functions are very similar. The Kolmogorov-Smirnov tests give value 0, so the test does not reject the null hypothesis at the 5% significance level. (i.e., there is no difference between data and a normal data set). The data is normally distributed (however, the probability is low: 41%) Test for normality showed that the results are approximately symmetric (skewness = -0.368, where for -0.5 to 0.5 the distribution is assumed to be symmetric) and no conclusion about the kurtosis can be given because the value is between −2 and +2 (the kurtosis is -0.85, where the kurtosis of the normal distribution is 0). Thus, it can be assumed that the cohesion is normally distributed. The coefficient of variation is low and equals 11.4%.

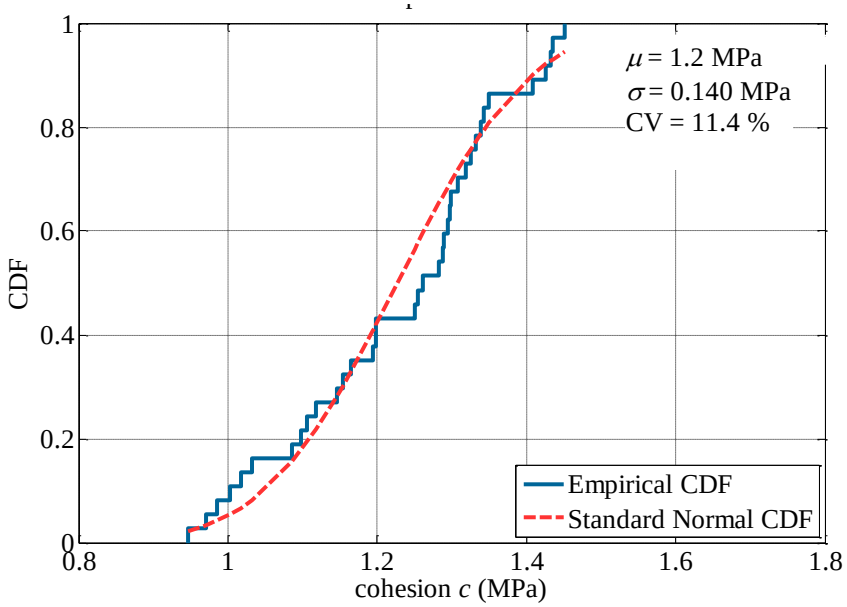


*Figure A.4. The cumulative empirical and normal distribution of cohesion for artificial gypsum*

The bootstrap method

The bootstrapping statistical technique was used to draw a large number of observations with replacement from the original data to create a bootstrap sample (resample), and calculate the mean for this resample and standard deviation. This procedure is repeated many times (e.g. 1000). The values of mean and standard deviation can show if there is a difference of quantifying the random variability.

Nearly all the estimates for friction angle $\phi$ lie on the interval 40.4° ±3.3° (Figure A.5) and $c$ = 1.25 ±0.25 MPa for cohesion (Figure A.6). Whereas the friction angle $\phi$ is very-well constrained, the cohesion $c$ shows larger scatter. The true values as used to simulate the laboratory data set are $\phi$= 40.4° for the slope and $c$ = 1.25 MPa for the intercept with the y-

axis, whereas the coefficients calculated using the linear regression were $\phi = 40.7°$ and $c = 1.24$ MPa, respectively. It can be seen that the values are very close to each other.

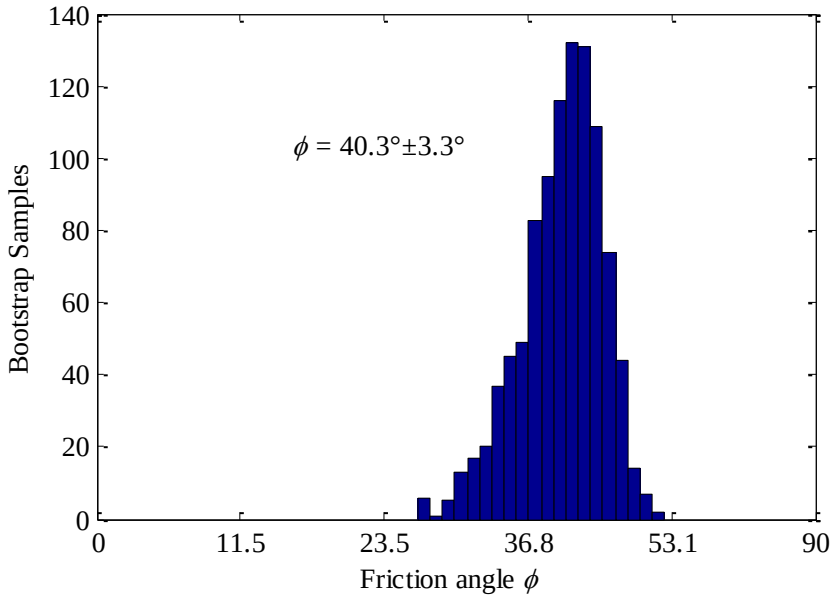


*Figure A.5. Histogram of the friction angle ϕ regression coefficient as estimated from bootstrap resampling*

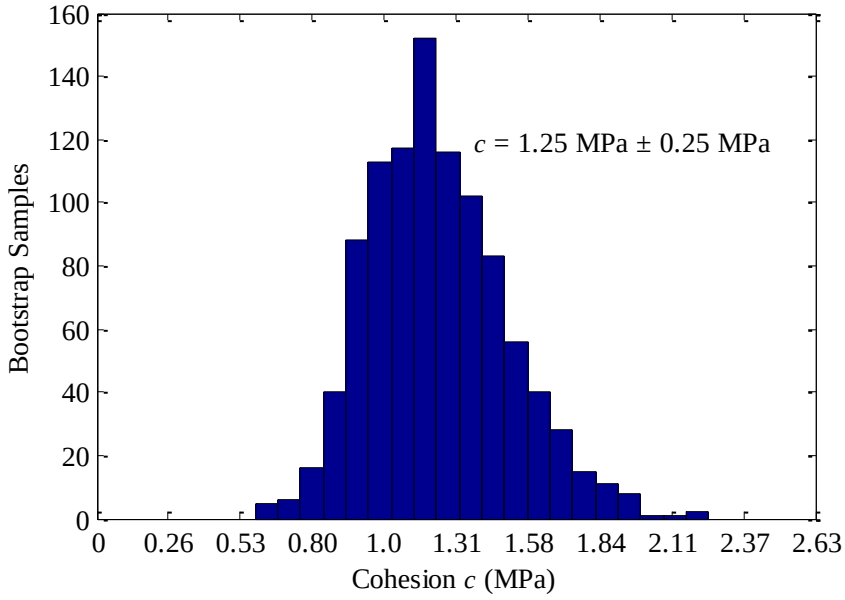


*Figure A.6. Histogram of the cohesion c regression coefficient as estimated from bootstrap resampling*

*Mortar – static triaxial tests*

*Table A-2. Mortar static test results (1 week, cement/sand 0.5, beach sand)*

| | $F_{max}$ (N) | $\sigma_3$ (MPa) | $p$ (MPa) | $q$ (MPa) | $\tau/\tau_0$ (-) | $\rho_d$ = (g/cm$^3$) | behaviour |
|---|---|---|---|---|---|---|---|
| Test 1 | 3555 | 0.10 | 1.68 | 1.58 | 0.91 | 1.92 | brittle |
| Test 2 | 4200 | 0.30 | 2.11 | 1.81 | 0.80 | 1.90 | brittle-ductile |
| Test 3 | 5212 | 0.50 | 2.71 | 2.21 | 0.79 | 1.85 | brittle ductile |
| Test 4 | 4416 | 0.00 | 1.90 | 1.90 | 1.29 | 1.93 | brittle |
| Test 5 | 5860 | 0.25 | 2.77 | 2.52 | 1.18 | 1.88 | brittle |
| Test 6 | 9727 | 1.00 | 5.20 | 4.20 | 1.02 | 1.93 | brittle-ductile |
| Test 7 | 3422 | 0.00 | 1.48 | 1.48 | 1.01 | 1.91 | brittle |
| Test 8 | 4555 | 0.30 | 2.28 | 1.98 | 0.87 | 1.87 | brittle |
| Test 9 | 8845 | 1.00 | 4.86 | 3.86 | 0.93 | 1.90 | brittle-ductile |
| Test 10 | 6799 | 0.30 | 3.28 | 2.98 | 1.31 | 1.92 | brittle-ductile |
| Test 11 | 3676 | 0.00 | 1.61 | 1.61 | 1.10 | 1.86 | brittle |

*Table A-3. Mortar static test results (1 week, cement/sand 1.5, beach sand)*

| | $F_{max}$ (N) | $\sigma_3$ (MPa) | $p$ (MPa) | $q$ (MPa) | $\tau/\tau_0$ (-) | $\rho_d$ = (g/cm$^3$) | behaviour |
|---|---|---|---|---|---|---|---|
| Test 1 | 16355 | 0.00 | 7.28 | 7.28 | 0.94 | 1.71 | brittle |
| Test 2 | 19676 | 0.10 | 8.57 | 8.47 | 1.06 | 1.76 | brittle |
| Test 3 | 20496 | 0.30 | 9.01 | 8.71 | 1.03 | 1.70 | brittle |
| Test 4 | 21384 | 0.50 | 9.68 | 9.18 | 1.03 | 1.75 | brittle |
| Test 5 | 22225 | 1.00 | 10.58 | 9.58 | 0.95 | 1.73 | brittle-ductile |

*Table A-4. Mortar static test results (1 week, cement/sand 1.0, beach sand)*

| | $F_{max}$ (N) | $\sigma_3$ (MPa) | $p$ (MPa) | $q$ (MPa) | $\tau/\tau_0$ (-) | $\rho_d$ = (g/cm$^3$) | behaviour |
|---|---|---|---|---|---|---|---|
| Test 1 | 10490 | 0.00 | 4.67 | 4.67 | 0.98 | 1.80 | brittle |
| Test 2 | 10717 | 0.10 | 4.71 | 4.61 | 0.93 | 1.77 | brittle |
| Test 3 | 13259 | 0.30 | 5.93 | 5.63 | 1.05 | 1.81 | brittle |
| Test 4 | 13917 | 0.50 | 6.48 | 5.98 | 1.03 | 1.80 | brittle |
| Test 5 | 14725 | 1.00 | 7.34 | 6.34 | 0.93 | 1.80 | brittle-ductile |
| Test 6 | 15533 | 0.30 | 6.12 | 5.82 | 1.08 | 1.83 | brittle |

*Table A-5. Mortar static test results (1 month, cement/sand 1.0, coarse sand)*

| | $F_{max}$ (N) | $\sigma_3$ (MPa) | $p$ (MPa) | $q$ (MPa) | $\tau/\tau_0$ (-) | $\rho_d$ = (g/cm$^3$) | behaviour |
|---|---|---|---|---|---|---|---|
| Test 1 | 10339 | 0.00 | 4.56 | 4.56 | 1.14 | 1.89 | brittle |
| Test 2 | 10511 | 0.10 | 4.73 | 4.63 | 1.06 | 1.90 | brittle |
| Test 3 | 12196 | 0.20 | 5.58 | 5.38 | 1.14 | 1.86 | brittle |
| Test 4 | 12329 | 0.30 | 5.74 | 5.44 | 1.07 | 1.84 | brittle |
| Test 5 | 9599 | 0.50 | 4.73 | 4.23 | 0.73 | 1.88 | brittle-ductile |
| Test 6 | 16782 | 1.00 | 8.40 | 7.40 | 0.98 | 1.90 | brittle-ductile |
| Test 7 | 12918 | 0.50 | 6.19 | 5.69 | 0.98 | 1.85 | brittle |

The cumulative empirical and standard normal distribution of cohesion for mortar (1 month, c/s = 1.0) is presented in Figure A.4. Both, the empirical (based on the measure data) and the standard normal cumulative density functions are very similar. The Kolmogorov-Smirnov tests give value 0, so the test does not reject the null hypothesis at the 5% significance level. (i.e., there is no difference between data and a normal data set). The data is normally distributed (the probability is high: 89%) Test for normality showed that the results are approximately symmetric (skewness = -0.18, where for -0.5 to 0.5 the distribution is assumed to be symmetric) and no conclusion about the kurtosis can be given because the value is between −2 and +2 (the kurtosis is -1.4, where the kurtosis of the normal distribution is 0). Thus, it can be assumed that the cohesion is normally distributed. The coefficient of variation is low and equals 7.1%. For other mortar set of samples (different curing time and c/s ratio) the results are similar.

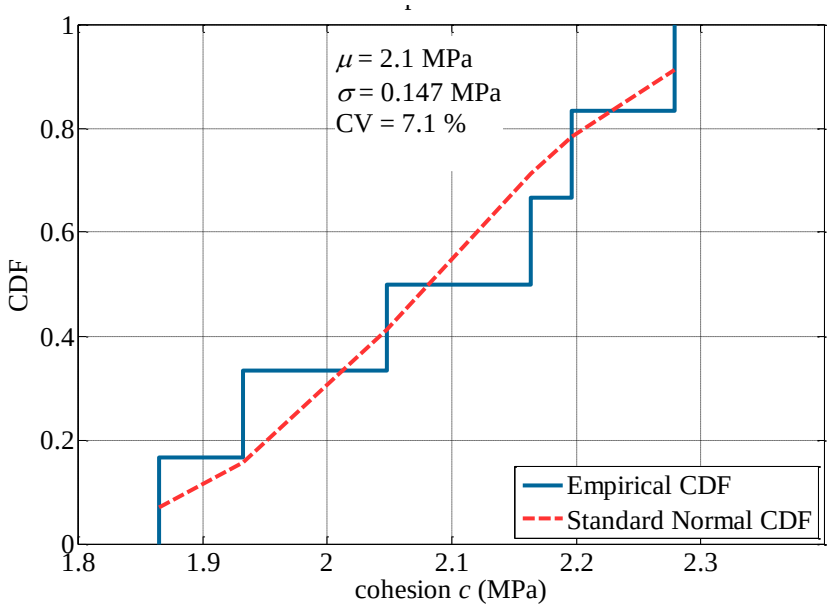


*Figure A.7. The cumulative empirical and normal distribution of cohesion for mortar (1 month, c/s=1.0)*

*Limestone – static triaxial tests*

*Table A-6. Limestone (vertical samples)*

| | $F_{max}$ (N) | $\sigma_3$ (MPa) | $p$ (MPa) | $q$ (MPa) | $\tau/\tau_0$ (-) | $\rho_d$ = (g/cm$^3$) | behaviour |
|---|---|---|---|---|---|---|---|
| Test 1 | 315 | 0.00 | 0.15 | 0.15 | 1.91 | 1.25 | brittle |
| Test 2 | 881 | 0.15 | 0.60 | 0.45 | 0.99 | 1.29 | brittle-ductile |
| Test 3 | 1473 | 0.30 | 1.02 | 0.71 | 0.86 | 1.30 | ductile |
| Test 4 | 736 | 0.05 | 0.41 | 0.35 | 1.61 | 1.34 | brittle |

*Table A-7. Limestone(horizontal samples)*

| | $F_{max}$ (N) | $\sigma_3$ (MPa) | $p$ (MPa) | $q$ (MPa) | $\tau/\tau_0$ (-) | $\rho_d$ = (g/cm$^3$) | behaviour |
|---|---|---|---|---|---|---|---|
| Test 1 | 421 | 0.05 | 0.27 | 0.22 | 1.10 | 1.46 | brittle |
| Test 2 | 549 | 0.11 | 0.44 | 0.33 | 0.99 | 1.43 | ductile |
| Test 3 | 656 | 0.16 | 0.54 | 0.39 | 0.87 | 1.45 | ductile |
| Test 4 | 1269 | 0.30 | 0.90 | 0.60 | 0.76 | 1.28 | ductile |
| Test 5 | 232 | 0.06 | 0.16 | 0.10 | 0.46 | 1.34 | brittle |
| Test 6 | 170 | 0.00 | 0.08 | 0.08 | 1.10 | 1.37 | brittle |

*Crumbled limestone – static triaxial tests*

*Table A-8. Crumbled limestone*

| | $F_{max}$ (N) | $\sigma_3$ (MPa) | $p$ (MPa) | $q$ (MPa) | $\tau/\tau_0$ (-) | behaviour |
|---|---|---|---|---|---|---|
| Test 1 | 677 | 0.10 | 0.40 | 0.30 | 1.03 | ductile |
| Test 2 | 1722 | 0.30 | 1.06 | 0.76 | 0.87 | ductile |
| Test 3 | 1182 | 0.20 | 0.72 | 0.52 | 0.92 | ductile |
| Test 4 | 347 | 0.05 | 0.21 | 0.15 | 1.01 | ductile |
| Test 5 | 921 | 0.15 | 0.56 | 0.41 | 0.92 | ductile |
| Test 6 | 2430 | 0.49 | 1.56 | 1.07 | 0.77 | ductile |

*Norm sand – static triaxial tests*

*Table A-9. Norm sand*

| | $F_{max}$ (N) | $\sigma_3$ (MPa) | $p$ (MPa) | $q$ (MPa) | $\tau/\tau_0$ (-) | behaviour |
|---|---|---|---|---|---|---|
| Test 1 | 269 | 0.06 | 0.17 | 0.12 | 0.96 | ductile |
| Test 2 | 423 | 0.11 | 0.29 | 0.19 | 0.78 | ductile |
| Test 3 | 865 | 0.21 | 0.59 | 0.38 | 0.84 | ductile |
| Test 4 | 1081 | 0.30 | 0.77 | 0.48 | 0.73 | ductile |

*Beach sand – static triaxial tests*

*Table A-10. Beach sand*

| | $F_{max}$ (N) | $\sigma_3$ (MPa) | $p$ (MPa) | $q$ (MPa) | $\tau/\tau_0$ (-) | behaviour |
|---|---|---|---|---|---|---|
| Test 1 | 574 | 0.12 | 0.37 | 0.25 | 0.95 | ductile |
| Test 2 | 1398 | 0.35 | 0.97 | 0.62 | 0.76 | ductile |
| Test 3 | 2116 | 0.52 | 1.45 | 0.93 | 0.78 | ductile |

*Coarse sand – static triaxial tests*

*Table A-11. Coarse sand*

| | $F_{max}$ (N) | $\sigma_3$ (MPa) | $p$ (MPa) | $q$ (MPa) | $\tau/\tau_0$ (-) | behaviour |
|---|---|---|---|---|---|---|
| Test 1 | 531 | 0.10 | 0.33 | 0.23 | 0.92 | ductile |
| Test 2 | 1416 | 0.30 | 0.92 | 0.62 | 0.81 | ductile |
| Test 3 | 2303 | 0.50 | 1.52 | 1.02 | 0.80 | ductile |

**c) S-N curve**

In tables below cyclic test results used to create the S-N curves can be found. All the tests were conducted in dry conditions, and the samples had natural moisture. The cyclic tests were

run until failure for a given cyclic stress ratio $\tau_{cyc}/\tau_0$ and the number of cycles until failure $N$ was counted. The failure was determined as load for which the strains are increasing and the stresses cannot reach the cyclic stresses.

*S-N curve for artificial gypsum – cyclic triaxial tests*

*Table A-12.Tests for S-N curve for artificial gypsum*

| | $\sigma_3$ (MPa) | $N$ | $\tau_{cyc}/\tau_0$ | behaviour | Type of fracture | surface defects |
|---|---|---|---|---|---|---|
| Test 1 | 0.10 | 167 | 0.95 | ductile | Cone & Split | small flaws |
| Test 2 | 0.10 | 132 | 0.95 | ductile | Cone & Split | small flaws |
| Test 3 | 0.10 | 2 | 0.95 | ductile | Cone & Split | big flaws |
| Test 4 | 0.10 | 159 | 0.95 | ductile | Cone & Split | small flaws |
| Test 5 | 0.10 | 170 | 0.95 | ductile | Cone & Split | small flaws |
| Test 6 | 0.10 | 7 | 0.95 | ductile | Cone & Split | one big flaw |
| Test 7 | 0.10 | 172 | 0.95 | ductile | Cone & Split | one small flaw |
| Test 8 | 0.30 | 68 | 0.80 | ductile | Cone & Split | 3 small flaws |
| Test 9 | 0.30 | 140 | 0.80 | ductile | Cone & Split | |
| Test 10 | 0.30 | 17 | 0.80 | ductile | Cone & Split | small flaws |
| Test 11 | 0.30 | 165 | 0.80 | ductile | Cone & Split | |
| Test 12 | 0.30 | 4 | 0.80 | ductile | Cone & Split | |
| Test 13 | 0.30 | 262 | 0.80 | ductile | Cone & Split | |
| Test 14 | 0.30 | 120 | 0.70 | ductile | Cone & Split | one flaw |
| Test 15 | 0.30 | 135 | 0.80 | ductile | Cone & Split | few flaws |
| Test 16 | 0.30 | 166 | 0.80 | ductile | Cone & Split | many flaws |
| Test 17 | 0.50 | 174 | 0.70 | ductile | Cone & Split | |
| Test 18 | 0.20 | 15 | 0.90 | ductile | Cone & Split | |
| Test 19 | 0.10 | 53 | 0.90 | ductile | Cone & Split | |
| Test 20 | 0.30 | 50 | 0.90 | ductile | Cone & Split | two flaws |
| Test 21 | 0.30 | 20 | 0.90 | ductile | Cone & Split | |
| Test 22 | 0.30 | 47 | 0.90 | ductile | Cone & Split | |
| Test 23 | 0.30 | 9 | 0.90 | ductile | Cone & Split | |
| Test 24 | 0.30 | 50 | 0.90 | ductile | Cone & Split | |
| Test 25 | 0.50 | 14 | 0.90 | ductile | Cone & Split | |
| Test 26 | 0.50 | 8 | 0.90 | ductile | Cone & Split | two flaws |
| Test 27 | 0.10 | 30 | 0.70 | ductile | Cone & Split | one flaw |
| Test 28 | 0.30 | 21 | 0.70 | brittle | Cone & Split | two small flows |
| Test 29 | 0.30 | 37 | 0.70 | brittle | Cone & Split | one small flaw |
| Test 30 | 0.10 | 176 | 0.80 | ductile | Cone & Split | |
| Test 31 | 0.10 | 855 | 0.80 | ductile | Cone & Split | |
| Test 32 | 0.10 | 945 | 0.80 | ductile | Cone & Split | |
| Test 33 | 0.10 | 331 | 0.80 | ductile | Cone & Split | |
| Test 34 | 0.30 | 182 | 0.80 | ductile | Cone & Split | |
| Test 35 | 0.30 | 343 | 0.80 | No data | Cone & Split | |
| Test 36 | 0.10 | 177 | 0.60 | No data | Cone & Split | |
| Test 37 | 0.50 | 635 | 0.60 | ductile | Cone & Split | |
| Test 38 | 0.50 | 374 | 0.40 | ductile | Cone & Split | |
| Test 39 | 0.10 | 622 | 0.80 | brittle-ductile | Cone & Split | |
| Test 40 | 0.30 | 1275 | 0.80 | brittle-ductile | Cone & Split | |
| Test 41 | 0.30 | 876 | 0.80 | brittle-ductile | Cone & Split | |
| Test 42 | 0.50 | 228 | 0.60 | brittle | Cone & Split | |

| | | | | | |
|---|---|---|---|---|---|
| Test 43 | 0.30 | 291 | 0.60 | ductile | Cone & Split |
| Test 44 | 0.30 | 3256 | 0.60 | ductile | Cone & Split |
| Test 45 | 0.10 | 510 | 0.40 | ductile | Cone & Split |
| Test 46 | 0.10 | 705 | 0.40 | ductile | Cone & Split |
| Test 47 | 0.10 | 3682 | 0.80 | ductile | Cone & Split |
| Test 48 | 0.10 | 5951 | 0.60 | ductile | Cone & Split |
| Test 49 | 0.10 | 1271 | 0.90 | brittle | Cone & Split |
| Test 50 | 0.10 | 11341 | 0.40 | ductile | Cone & Split |

Defect in the core after triaxial tests were found only in samples number 3, 4, 6, 10, 12, 14, 15, 17, 20, 22, 23, 24, and 28.

*S-N curve for mortar – cyclic triaxial tests*

*Table A-13.Tests for S-N curve for mortar (1 week, cement/sand 0.5)*

| | $\sigma_3$ (MPa) | $N$ | $\tau_{cyc}/\tau_0$ | behaviour |
|---|---|---|---|---|
| Test 1 | 0.30 | 97 | 0.8 | brittle |
| Test 2 | 0.30 | 654 | 0.8 | brittle |
| Test 3 | 0.30 | 2 | 0.8 | brittle-ductile |
| Test 4 | 0.10 | 89 | 0.8 | brittle |
| Test 5 | 0.00 | 5 | 0.8 | brittle |
| Test 6 | 0.30 | 829 | 0.8 | brittle |
| Test 7 | 0.10 | 2183 | 0.6 | brittle |
| Test 8 | 0.10 | 1363 | 0.8 | brittle |
| Test 9 | 0.50 | 4342 | 0.8 | brittle |

*Table A-14.Tests for S-N curve for mortar (1 week, cement/sand 1.0)*

| | $\sigma_3$ (MPa) | $N$ | $\tau_{cyc}/\tau_0$ | behaviour |
|---|---|---|---|---|
| Test 1 | 0.10 | 9 | 0.8 | brittle |
| Test 2 | 0.50 | 19 | 0.8 | brittle |
| Test 3 | 0.10 | 127 | 0.8 | brittle |
| Test 4 | 0.10 | 523 | 0.8 | brittle |

*Table A-15.Tests for S-N curve for mortar (1 month, cement/sand 1.0)*

| | $\sigma_3$ (MPa) | $N$ | $\tau_{cyc}/\tau_0$ | behaviour |
|---|---|---|---|---|
| Test 1 | 0.10 | 332 | 0.80 | brittle |
| Test 2 | 0.10 | 42369 | 0.80 | brittle |
| Test 3 | 0.30 | 12484 | 0.80 | brittle |
| Test 4 | 0.30 | 12 | 0.80 | brittle-ductile |
| Test 5 | 0.10 | 193 | 0.80 | brittle |
| Test 6 | 0.30 | 839 | 0.60 | brittle |
| Test 7 | 0.10 | 5920 | 0.80 | brittle |
| Test 8 | 0.10 | 4353 | 0.60 | brittle |

**d) The remaining shear strength curve data points**

In tables below cyclic test results used to create the remaining shear strength curves can be

found. All the tests were conducted in dry conditions, and the samples had natural moisture. The cyclic tests were run for a given number of cycles $N$ and then in the final cycle until the failure the maximum remaining strength ($p$ and $q$) was measured. The ratio of cyclic loading to a static strength for the same confining pressure is given as a ratio $\tau_{cyc}/\tau_0$.

*Artificial gypsum – cyclic triaxial tests*

*Table A-16.Tests for remaining shear strength curve for artificial gypsum*

| | $\tau_{cyc}/\tau_0$ | $N$ | $\sigma_3$ (MPa) | $p$ (MPa) | $q$ (MPa) | behaviour | Type of fracture |
|---|---|---|---|---|---|---|---|
| Test 1 | 0.80 | 10 | 0.30 | 3.30 | 3.00 | | cone & split |
| Test 2 | 0.80 | 10 | 0.10 | 3.30 | 3.20 | ductile | cone & split |
| Test 3 | 0.80 | 10 | 0.50 | 4.13 | 3.63 | ductile | cone & split |
| Test 4 | 0.80 | 100 | 0.10 | 2.88 | 2.78 | ductile | cone & split |
| Test 5 | 0.80 | 100 | 0.30 | 2.92 | 2.62 | ductile | cone & split |
| Test 6 | 0.80 | 100 | 0.10 | 2.85 | 2.75 | ductile | cone & split |
| Test 7 | 0.80 | 100 | 0.30 | 3.41 | 3.11 | ductile | cone & split |
| Test 8 | 0.80 | 100 | 0.10 | 2.89 | 2.79 | ductile | cone & split |
| Test 9 | 0.80 | 100 | 0.50 | 3.87 | 3.37 | ductile | cone & split |
| Test 10 | 0.80 | 100 | 0.50 | 3.63 | 3.13 | ductile | cone & split |
| Test 11 | 0.80 | 1000 | 0.10 | 2.16 | 2.06 | ductile | cone & split |
| Test 12 | 0.80 | 1000 | 0.30 | 2.77 | 2.47 | brittle | cone & split |
| Test 13 | 0.80 | 1000 | 0.50 | 3.41 | 2.91 | brittle | cone & split |
| Test 14 | 0.60 | 10 | 0.10 | 3.22 | 3.12 | ductile | cone & split |
| Test 15 | 0.60 | 10 | 0.30 | 3.31 | 3.01 | ductile | cone & split |
| Test 16 | 0.60 | 10 | 0.50 | 4.06 | 3.56 | ductile | cone & split |
| Test 17 | 0.60 | 100 | 0.30 | 3.06 | 2.76 | ductile | cone & split |
| Test 18 | 0.60 | 100 | 0.50 | 3.74 | 3.24 | ductile | cone & split |
| Test 19 | 0.60 | 100 | 0.10 | 2.79 | 2.69 | ductile | cone & split |
| Test 20 | 0.60 | 100 | 0.30 | 3.06 | 2.76 | brittle | cone & split |
| Test 21 | 0.60 | 100 | 0.10 | 3.21 | 3.11 | ductile | cone & split |
| Test 22 | 0.60 | 1000 | 0.10 | 3.06 | 2.96 | ductile | cone & split |
| Test 23 | 0.60 | 1000 | 0.30 | 2.61 | 2.31 | ductile | cone & split |
| Test 24 | 0.60 | 1000 | 0.30 | 2.34 | 2.04 | ductile | cone & split |
| Test 25 | 0.60 | 1000 | 0.50 | 2.96 | 2.46 | ductile | cone & split |
| Test 26 | 0.60 | 1000 | 0.10 | 2.49 | 2.39 | brittle | cone & split |
| Test 27 | 0.40 | 10 | 0.10 | 3.48 | 3.38 | ductile | cone & split |
| Test 28 | 0.40 | 10 | 0.30 | 3.22 | 2.92 | ductile | cone & split |
| Test 29 | 0.40 | 10 | 0.50 | 3.68 | 3.18 | brittle-ductile | cone & split |
| Test 30 | 0.40 | 100 | 0.10 | 2.67 | 2.57 | ductile | cone & split |
| Test 31 | 0.40 | 100 | 0.30 | 3.01 | 2.71 | ductile | cone & split |
| Test 32 | 0.40 | 100 | 0.50 | 3.40 | 2.90 | ductile | cone & split |
| Test 33 | 0.40 | 100 | 0.10 | 2.91 | 2.81 | ductile | cone & split |
| Test 34 | 0.40 | 100 | 0.30 | 3.24 | 2.94 | ductile | cone & split |
| Test 35 | 0.40 | 1000 | 0.10 | 3.14 | 3.04 | ductile | cone & split |
| Test 36 | 0.40 | 1000 | 0.30 | 2.94 | 2.64 | ductile | cone & split |
| Test 37 | 0.40 | 1000 | 0.50 | 2.91 | 2.41 | ductile | cone & split |
| Test 38 | 0.40 | 1000 | 0.10 | 2.64 | 2.54 | ductile | cone & split |
| Test 39 | 0.40 | 1000 | 0.10 | 3.05 | 2.95 | brittle | cone & split |
| Test 40 | 0.40 | 1000 | 0.30 | 2.81 | 2.51 | No data | cone & split |

| | | | | | | | |
|---|---|---|---|---|---|---|---|
| Test 41 | 0.40 | 10000 | 0.30 | 2.49 | 2.19 | ductile | cone & split |
| Test 42 | 0.40 | 10000 | 0.10 | 2.20 | 2.10 | ductile | cone & split |
| Test 43 | 0.20 | 100000 | 0.10 | 1.53 | 1.43 | brittle | cone & split |
| Test 44 | 0.20 | 100000 | 0.50 | 2.59 | 2.09 | brittle | cone & split |

## *Mortar – cyclic triaxial tests*

*Table A-17.Tests for remaining shear strength curve for mortar (1 week, cement/sand ratio = 0.5)*

| | $\tau_{cyc}/\tau_0$ | $N$ | $\sigma_3$ (MPa) | $p$ (MPa) | $q$ (MPa) | behaviour |
|---|---|---|---|---|---|---|
| Test 1 | 0.60 | 100 | 0.10 | 1.50 | 1.40 | brittle-ductile |
| Test 2 | 0.60 | 100 | 0.30 | 1.97 | 1.67 | ductile |
| Test 3 | 0.60 | 100 | 0.50 | 2.93 | 2.43 | ductile |
| Test 4 | 0.80 | 100 | 0.10 | 2.54 | 2.44 | brittle |
| Test 5 | 0.80 | 100 | 0.50 | 3.80 | 3.30 | ductile |
| Test 6 | 0.80 | 100 | 0.30 | 2.35 | 2.05 | ductile |
| Test 7 | 0.80 | 100 | 0.30 | 2.69 | 2.39 | brittle-ductile |
| Test 8 | 0.80 | 100 | 0.00 | 1.78 | 1.78 | brittle |
| Test 9 | 0.40 | 1000 | 0.50 | 2.63 | 2.13 | ductile |
| Test 10 | 0.40 | 1000 | 0.10 | 1.06 | 0.96 | brittle-ductile |
| Test 11 | 0.40 | 1000 | 0.30 | 1.77 | 1.47 | brittle |
| Test 12 | 0.60 | 1000 | 0.30 | 2.21 | 1.91 | brittle-ductile |
| Test 13 | 0.60 | 1000 | 0.10 | 1.76 | 1.66 | brittle |
| Test 14 | 0.60 | 1000 | 0.50 | 2.68 | 2.18 | brittle-ductile |
| Test 15 | 0.80 | 1000 | 0.50 | 3.15 | 2.65 | ductile |
| Test 16 | 0.40 | 10000 | 0.30 | 1.70 | 1.40 | brittle |
| Test 17 | 0.40 | 10000 | 0.10 | 1.25 | 1.15 | brittle |
| Test 18 | 0.60 | 10000 | 0.30 | 2.24 | 1.94 | brittle |
| Test 19 | 0.60 | 10000 | 0.50 | 3.05 | 2.55 | brittle |

*Table A-18.Tests for remaining shear strength curve for mortar (1 week, cement/sand ratio = 1.0)*

| | $\tau_{cyc}/\tau_0$ | $N$ | $\sigma_3$ (MPa) | $p$ (MPa) | $q$ (MPa) | behaviour |
|---|---|---|---|---|---|---|
| Test 1 | 0.80 | 100 | 0.10 | 4.38 | 4.28 | brittle |
| Test 2 | 0.80 | 100 | 0.30 | 5.90 | 5.60 | brittle |
| Test 3 | 0.60 | 100 | 0.10 | 5.01 | 4.91 | brittle |
| Test 4 | 0.60 | 100 | 0.50 | 6.20 | 5.70 | brittle |
| Test 5 | 0.40 | 100 | 0.10 | 5.25 | 5.15 | brittle |
| Test 6 | 0.40 | 100 | 0.50 | 5.77 | 5.27 | brittle |
| Test 7 | 0.80 | 1000 | 0.30 | 5.93 | 5.63 | brittle |
| Test 8 | 0.60 | 1000 | 0.10 | 4.38 | 4.28 | brittle |
| Test 9 | 0.60 | 1000 | 0.30 | 5.93 | 5.63 | brittle |
| Test 10 | 0.40 | 1000 | 0.10 | 3.63 | 3.53 | brittle |
| Test 11 | 0.40 | 1000 | 0.50 | 6.02 | 5.52 | brittle-ductile |
| Test 12 | 0.80 | 10000 | 0.50 | 9.80 | 9.30 | brittle |
| Test 13 | 0.60 | 10000 | 0.10 | 7.05 | 6.95 | brittle |
| Test 14 | 0.60 | 10000 | 0.50 | 5.95 | 5.45 | brittle-ductile |
| Test 15 | 0.40 | 10000 | 0.50 | 5.04 | 4.54 | brittle-ductile |
| Test 16 | 0.40 | 10000 | 0.10 | 5.01 | 4.91 | brittle |

*Table A-19.Tests for remaining shear strength curve for mortar (1 month, cement/sand ratio = 1.0)*

| | $\tau_{cyc}/\tau_0$ | $N$ | $\sigma_3$ (MPa) | $p$ (MPa) | $q$ (MPa) | behaviour |
|---|---|---|---|---|---|---|
| Test 1 | 0.80 | 100 | 0.1 | 4.11 | 4.08 | brittle |
| Test 2 | 0.60 | 100 | 0.1 | 3.53 | 3.43 | brittle |
| Test 3 | 0.60 | 100 | 0.3 | 4.06 | 3.76 | brittle-ductile |
| Test 4 | 0.80 | 1000 | 0.30 | 5.34 | 5.04 | brittle |
| Test 5 | 0.80 | 1000 | 0.10 | 4.08 | 3.98 | brittle |
| Test 6 | 0.80 | 1000 | 0.50 | 6.24 | 5.74 | brittle |
| Test 7 | 0.40 | 1000 | 0.10 | 4.12 | 4.02 | brittle |
| Test 8 | 0.40 | 1000 | 0.50 | 5.33 | 4.83 | ductile-brittle |
| Test 9 | 0.80 | 10000 | 0.30 | 5.94 | 5.64 | brittle |
| Test 10 | 0.80 | 10000 | 0.00 | 5.24 | 5.24 | brittle |
| Test 11 | 0.80 | 10000 | 0.50 | 7.64 | 7.14 | brittle |
| Test 12 | 0.60 | 10000 | 0.10 | 4.46 | 4.36 | brittle |
| Test 13 | 0.60 | 100000 | 0.10 | 6.35 | 6.25 | brittle |
| Test 14 | 0.60 | 100000 | 0.30 | 6.89 | 6.59 | brittle |

*Limestone – cyclic triaxial tests*

*Table A-20.Tests for remaining shear strength curve for limestone*

| | $\tau_{cyc}/\tau_0$ | $N$ | $\sigma_3$ (MPa) | $p$ (MPa) | $q$ (MPa) | behaviour |
|---|---|---|---|---|---|---|
| Test 1 | 0.80 | 10 | 0.05 | 0.27 | 0.22 | ductile |
| Test 2 | 0.80 | 10 | 0.30 | 0.92 | 0.61 | ductile |
| Test 3 | 0.80 | 100 | 0.05 | 0.27 | 0.23 | ductile |
| Test 4 | 0.80 | 100 | 0.30 | 1.09 | 0.78 | ductile |
| Test 5 | 0.80 | 100 | 0.15 | 0.60 | 0.45 | ductile |
| Test 6 | 0.60 | 100 | 0.05 | 0.29 | 0.24 | ductile |
| Test 7 | 0.60 | 100 | 0.15 | 0.63 | 0.47 | ductile |
| Test 8 | 0.80 | 1000 | 0.05 | 0.36 | 0.29 | ductile |
| Test 9 | 0.80 | 1000 | 0.05 | 0.42 | 0.37 | ductile |
| Test 10 | 0.80 | 1000 | 0.15 | 0.58 | 0.42 | ductile |

*Crumbled limestone – cyclic triaxial tests*

*Table A-21.Tests for remaining shear strength curve for crumbled limestone*

| | $\tau_{cyc}/\tau_0$ | $N$ | $\sigma_3$ (MPa) | $p$ (MPa) | $q$ (MPa) | behaviour |
|---|---|---|---|---|---|---|
| Test 1 | 0.80 | 1000 | 0.10 | 0.43 | 0.34 | ductile |
| Test 2 | 0.80 | 1000 | 0.30 | 1.10 | 0.83 | ductile |
| Test 3 | 0.80 | 1000 | 0.05 | 0.29 | 0.23 | ductile |
| Test 4 | 0.80 | 1000 | 0.20 | 0.85 | 0.64 | ductile |
| Test 5 | 0.80 | 10000 | 0.20 | 0.93 | 0.73 | ductile |
| Test 6 | 0.80 | 10000 | 0.10 | 0.55 | 0.46 | ductile |
| Test 7 | 0.80 | 10000 | 0.30 | 1.37 | 1.07 | brittle-ductile |

*Norm sand – cyclic triaxial tests*

*Table A-22.Tests for remaining shear strength curve for norm sand*

| | $\tau_{cyc}/\tau_0$ | $N$ | $\sigma_3$ (MPa) | $p$ (MPa) | $q$ (MPa) | behaviour |
|---|---|---|---|---|---|---|
| Test 1 | 0.80 | 1000 | 0.20 | 0.59 | 0.39 | ductile |

| | | | | | | |
|---|---|---|---|---|---|---|
| Test 2 | 0.80 | 1000 | 0.05 | 0.18 | 0.13 | ductile |
| Test 3 | 0.80 | 1000 | 0.10 | 0.32 | 0.22 | ductile |
| Test 4 | 0.80 | 1000 | 0.30 | 0.85 | 0.56 | ductile |
| Test 5 | 0.80 | 10000 | 0.30 | 0.88 | 0.58 | ductile |
| Test 6 | 0.80 | 10000 | 0.10 | 0.35 | 0.25 | ductile |
| Test 7 | 0.80 | 100000 | 0.10 | 0.37 | 0.27 | brittle |

*Beach sand – cyclic triaxial tests*

*Table A-23.Tests for remaining shear strength curve for beach sand*

| | $\tau_{cyc}/\tau_0$ | $N$ | $\sigma_3$ (MPa) | $p$ (MPa) | $q$ (MPa) | behaviour |
|---|---|---|---|---|---|---|
| Test 1 | 0.80 | 100 | 0.10 | 0.32 | 0.22 | ductile |
| Test 2 | 0.80 | 100 | 0.30 | 0.92 | 0.62 | ductile |
| Test 3 | 0.80 | 1000 | 0.10 | 0.31 | 0.21 | ductile |
| Test 4 | 0.80 | 1000 | 0.30 | 0.95 | 0.65 | ductile |
| Test 5 | 0.80 | 10000 | 0.30 | 1.02 | 0.72 | ductile |
| Test 6 | 0.80 | 10000 | 0.10 | 0.37 | 0.27 | ductile |

*Coarse sand – cyclic triaxial tests*

*Table A-24.Tests for remaining shear strength curve for coarse sand*

| | $\tau_{cyc}/\tau_0$ | $N$ | $\sigma_3$ (MPa) | $p$ (MPa) | $q$ (MPa) | behaviour |
|---|---|---|---|---|---|---|
| Test 1 | 0.80 | 1000 | 0.10 | 0.38 | 0.28 | ductile |
| Test 2 | 0.80 | 1000 | 0.30 | 0.91 | 0.61 | ductile |
| Test 3 | 0.80 | 10000 | 0.10 | 0.40 | 0.30 | ductile |
| Test 4 | 0.80 | 10000 | 0.30 | 0.98 | 0.68 | ductile |
| Test 5 | 0.40 | 10000 | 0.10 | 0.32 | 0.22 | ductile |
| Test 6 | 0.40 | 10000 | 0.30 | 0.91 | 0.61 | ductile |
| Test 7 | 0.40 | 1000 | 0.10 | 0.33 | 0.23 | ductile |
| Test 8 | 0.40 | 1000 | 0.30 | 0.90 | 0.60 | ductile |

**e) Hoek-Brown failure criterion for limestone**

The tests on crumbled limestone showed that the Mohr-Coulomb failure criterion might be inaccurate for weak rocks. Since Mohr-Coulomb failure criterion is not accurate for small stresses, the best solution might be to reduce the cohesion of the limestone, or to use another failure criterion to model the strength of this soft limestone. Therefore, the Hoek-Brown failure criterion (Hoek & Brown, 1980), (Hoek & Brown, 1988), (Hoek, Wood, & Shah, 1992), (Hoek, 2000) has been investigated. Hoek et al. (1998) extended the range of the Geological Strength Index (GSI) down to 5 to include extremely poor quality schistose rock masses (grade: $R_0$ for extremely weak rock, when UCS = 0.25 – 1 MPa). For excellent to fair quality rock masses, the original Hoek-Brown criterion is used, while for poor and extremely poor masses, the modified criterion (1992) with zero tensile strength is applied.

The Hoek-Brown failure criterion defined this limestone as an extremely weak rock due to the uniaxial compressive strength ($UCS$) = 292 kPa (in Hoek-Brown indicated as $\sigma_{ci}$). The Hoek-Brown parameter $m_i$ = 7 was taken from Hoek & Brown (1988) for sedimentary

carbonate rock. From all methods (Hoek & Brown, 1980, modified HB from 1988, HB model based on RMR and GSI methods etc.) of estimating the values of $m_b$, $s$ and in some cases $a$ (see Table A-25 and Figure A.8) the failure line could not fit the laboratory data. It must be mentioned, however, that Bieniawski's RMR is difficult to be applied for very poor quality rock masses and also that the relationship between RMR and $m$ and $s$ is no longer linear in these very low ranges. As the cohesion $c$ is very low and the friction angle $\phi$ of the limestone is very high, the inclination of the failure line is much higher than the predicted by the HB model.

*Table A-25.Hoek-Brown model parameters*

| Model | | $m_b$ | $m_b/m_i$ | $s$ | $a$ |
|---|---|---|---|---|---|
| (Hoek & Brown, 1980) | $\sigma_1 = \sigma_3 + \sigma_{ci}\sqrt{\frac{m_b\sigma_3}{\sigma_{ci}} + s}$ | 7 | - | 1 | 0.5 |
| (Hoek, Wood, & Shah, 1992)[1)] | $\sigma_1 = \sigma_3 + \sigma_{ci}\left(\frac{m_b\sigma_3}{\sigma_{ci}}\right)^a$ | 0.007[1)] | 0.001 | 0[1)] | 0.65[1)] |
| GSI, (Hoek, 1994)[2)] | $\sigma_1 = \sigma_3 + \sigma_{ci}\left(\frac{m_b\sigma_3}{\sigma_{ci}} + s\right)^a$ | 0.037[2)] | - | 1.05[2)] | 0.62[2)] |
| RMR, (Hoek & Brown, 1988)[3)] | $\sigma_1 = \sigma_3 + \sigma_{ci}\sqrt{\frac{m_b\sigma_3}{\sigma_{ci}} + s}$ | 0.26[3)] | - | 3.63[3)] | - |
| Best fit[4)] | $\sigma_1 = \sigma_3 + \sigma_{ci}\left(\frac{m_b\sigma_3}{\sigma_{ci}} + s\right)^a$ | 5.41 | - | 0.82 | 0.84 |
| Best fit based on original HB equation[5)] | $\sigma_1 = \sigma_3 + \sigma_{ci}\sqrt{\frac{m_b\sigma_3}{\sigma_{ci}} + s}$ | 21.81 | - | 1 | 0.5 |

1) For modified Hoek-Brown there is no tension, thus $s = 0$, $m_b$ and $a$ are constants for crushed rock,
   $m_b/m_i = 0.001$ based on surface condition and structure
   $a = 0.65$ very poor surface condition were taken
2) For GSI = 5 values of $m_b$, $s$ and $a$ were calculated as:
   $\frac{m_b}{m_i} = exp\left(\frac{GSI-100}{28-14D}\right)$
   $s = exp\left(\frac{GSI-100}{9-3D}\right)$
   $a = \frac{1}{2} + \frac{1}{6}\left(e^{-GSI/15} - e^{-20/3}\right)$
   where $D = 0.7$ excavation of soft rock by ripping and dozing and the degree of damage to the slope is less (mechanical excavation)
3) For RMR=8 calculated as summation for carbonate rocks of fair quality rock mass 5 for spacing of discontinuities and 3 for RQD=8, the values of $m_b$ and $s$ were calculated from:
   $\frac{m_b}{m_i} = exp\left(\frac{RMR-100}{14}\right)$
   $s = exp\left(\frac{RMR-100}{6}\right)$
4) Best fit parameters were obtained in nonlinear regression of the Hoek (1994) formulation
5) Best fit parameters were obtained in nonlinear regression of the original Hoek & Brown (1980) formulation

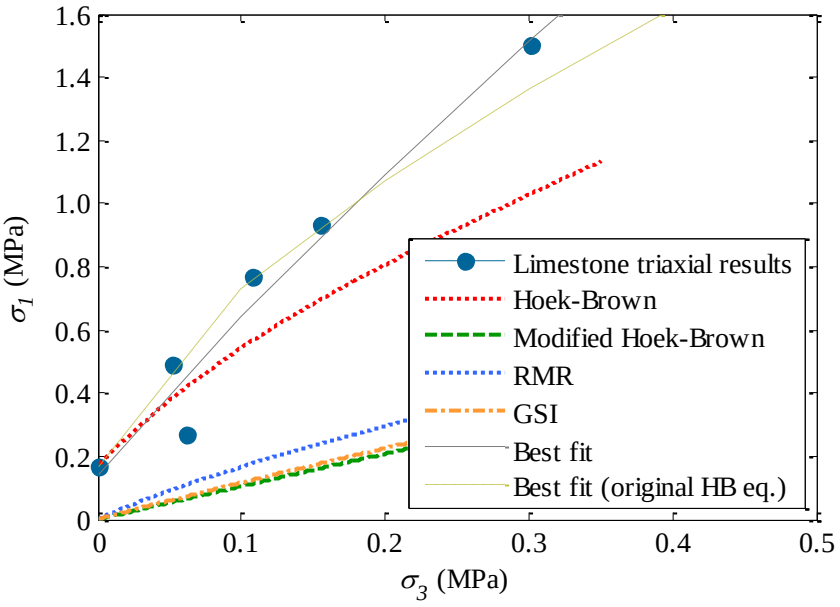


*Figure A.8. Hoek-Brown models for limestone*

Although the HB model predicts correctly the low tensile strength, it does not predict accurately the $\sigma_1$ - $\sigma_3$ relationship for higher confining pressures $\sigma_3 > 0$. The recalculated equivalent cohesion and friction angle did not correspond to the ones calculated with the M-C theory. Therefore, only Hoek-Brown parameters taken arbitrarily could fit the laboratory data (best fit method, Figure A.8), which limits the main advantage of the Hoek-Brown method – the simple parameterisation of the model. There is also an extension of Hoek-Brown model for layered rocks, but this was not used as it requires many other parameters and extensive laboratory data obtaining, making that particular approach useless for basic strength estimation.

The information presented above indicates that the Hoek-Brown failure criterion is also not enough accurate to describe extremely weak rocks like limestone. Therefore, the simple two-parameter Mohr-Coulomb criterion, although it does not model the limestone's strength behaviour for low confining pressures very well, is still the most reasonable failure model.

## B. FACTORS AFFECTING THE RESULTS OF ARTIFICIAL GYPSUM

### a) Imperfections in artificial gypsum

It was noticed that some cyclic tests finished at very early stage, after only few cycles has been applied. In some samples, air bubbles (Figure B.9 and Figure B.10) were found on the shear plane surface, and probably lowered the strength of the sample and caused prematurely fail (Figure B.11). The presence of imperfections induces more stress concentration effect, causing the crack resistance to be much lower than for the material without such a bubbles.

*Figure B.9. Air bubbles on the surface of the sample*

*Figure B.10. Air bubbles inside the tested sample*

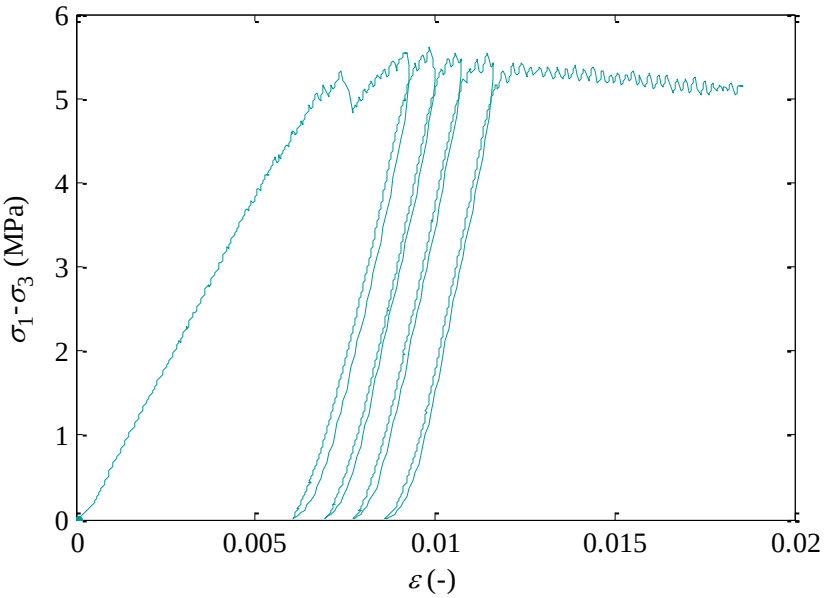


*Figure B.11. Stress-strain plot of prematurely failed artificial gypsum due to air bubbles*

**b) Water content**

*Crumbled limestone*

To investigate the impact of water on the shear strength, several tests were carried out for saturated and crumbled limestone with natural moisture. The results were very surprising (Figure B.12 and Table B-26). A significant cohesion reduction and small friction angle increase was found. It was expected that strength parameter (cohesion) will increase due to suction, as was presented by researcher: Donald (1956), Lamborn (1986), and Peterson (1988). Peterson gave the following strength equation:

$$\tau = c' + (\sigma - u)\, tan\, \phi' + C_\psi \qquad B\text{-}1$$

where $C_\psi$ is an apparent cohesion due to suction. The apparent cohesion due to suction, $C_\psi$, depends on the water content of the soil.

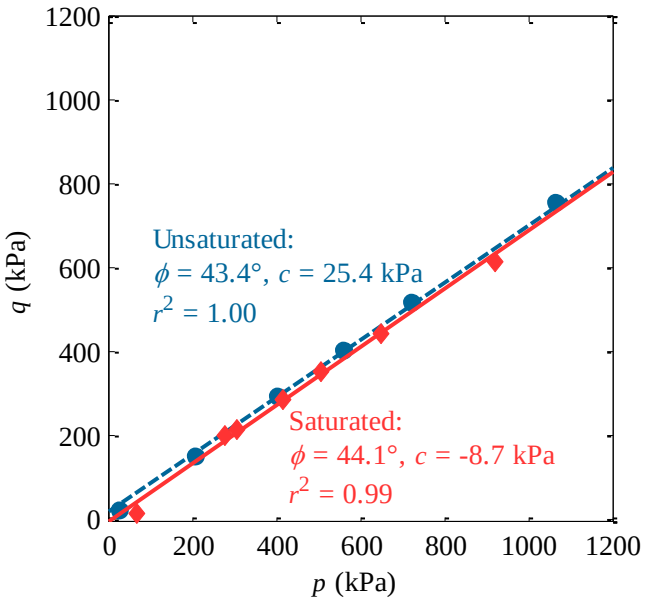


*Figure B.12. Mohr Coulomb failure envelope for dry and fully saturated crumbled limestone*

*Table B-26.Shear strength parameters from triaxial tests for saturated crumbled limestone*

| Saturation: | | 0% | 100% |
|---|---|---|---|
| $\phi$ | (°) | 43.4 (44.8) | 44.1 (43.3) |
| $c$ | (kPa) | 25.4 (0) | -8.7 (0.0) |
| tensile strength | (kPa) | 21.9 (0) | -7.3 (0.0) |

It was found from laboratory tests on sand, that there is no suction and the water has a negative effect on the Mohr-Coulomb strength parameters. For the purpose of the research, it was assumed that the saturation does not have significant effect on the triaxial tests for sand.

It should be noticed that there is no formulation to account for water suction on rocks. Experiments show that the strength of silicate rocks can drop by as much as 30% due to saturation (Dobereiner & Freitas, 1986).

The water impact on the fatigue life of geomaterials can have significant effects. Grgic & Giruad (2014) stated that the increase in microcracking damage is mainly due to the poro-mechanical coupling. They showed that the time-dependent strength and the time to failure increase while the dilatant volumetric deformation decreases as the chemical influence of the interstitial fluid decreases, i.e., the rock is weaker in the presence of water. At a microscopic scale, capillary suction implies negative liquid pressure in pores and microcraks. This negative liquid pressure applies tensile forces on crack planes thus inducing a decrease in the stress intensity factor as does confining pressure. More, tests are required to investigate the water presence and fatigue life dependency.

### c) Mortar – curing time

The curing time of mortar can have a big impact on the cyclic strength results. For static tests,

the cohesion $c$ (constant friction angle $\phi$ was assumed) increased of about 25% for tests done after 3 weeks comparing with the tests done after 1 week (Figure B.13 and Table B-27). This could have a significant meaning in case of long cyclic tests.

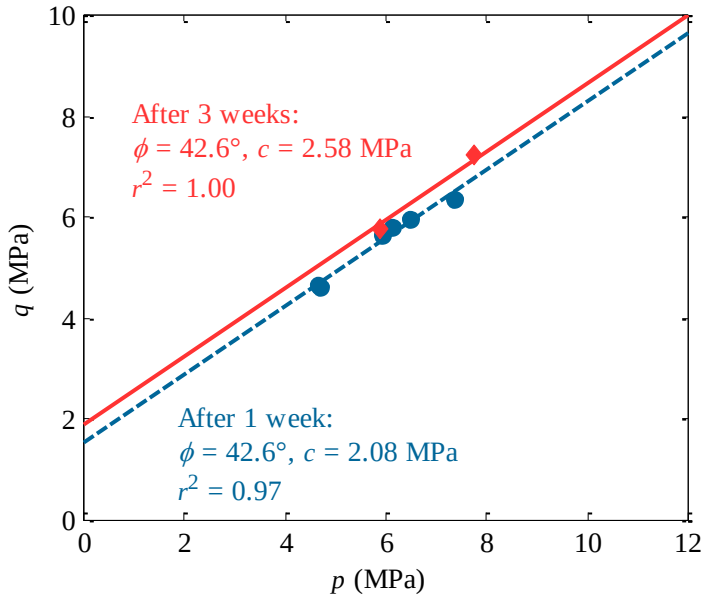


*Figure B.13. Stress point for static triaxial tests on mortar after 1 and 3 weeks*

*Table B-27.Strength parameters after 1 and 3 weeks (constant friction angle assumed)*

| | 1 week | 3 weeks | 3 weeks / 1 week |
|---|---|---|---|
| $\phi$ (°) | 42.6 | 42.6 | Const. $\phi$ |
| $c$ (MPa) | 2.08 | 2.58 | 125% |

## C. FATIGUE OF CONCRETE

*Introduction*

Many concrete structures such as highway, bridges, railroad, airport pavements, and marine structures are subjected to cyclic loading. Fatigue of concrete can be, however, interesting for two other reasons. One is that the foundations, which transmit the cyclic loadings directly into the ground, are often made from concrete and the second reason is that concrete and rocks are similar materials and their strength can be represented accurately by Mohr-Coulomb failure criterion.

Basically, concrete is a solid material and consists of three components: the cement matrix, the aggregate and the interface between the matrix and aggregate. The internal structure is similar to rocks, which are also solid aggregate of one or more minerals or mineraloids. Concrete, same as rock, as a conglomerate, contain many flaws and pre-cracked aggregates from which cracks may initiate, and concrete lacks of complete bonds between aggregate and matrix. Because of this, the strength of concrete is widely scattered. This information can be helpful to describe and prepare tests for fatigue tests of rocks and soils

*Cyclic loading on concrete structures*

Even though, during the lifetime of a bridge, road or rail, traffic and environmental loadings will produce large numbers of repetitive loading cycles, fatigue in concrete was recognised rather late in comparison to steel. Therefore the mechanism of fatigue failure in concrete is not fully understood yet.

The mechanism associated with fatigue-crack propagation in brittle materials, is quite distinct from those commonly encountered in ductile materials (e.g. metals). This is caused by microvoids and microcracks which were formed during shrinking and hardening period in concrete. Due to cyclic loading these microcracks propagate - at the beginning the growth of cracks is very slow but at the end of the fatigue life in both concrete and steel rapidly accelerates. In concrete the crack-growth rate is much more sensitive to the applied stress intensity than in metals, thus the crack growth in concrete is much faster than in steel and the fatigue life of concrete is much shorter than of metals. Because concrete as a composite materials is much less homogeneous than steel the failure in concrete does not require any phase of crack initiation. It is known that the weakest zone in concrete is the cement-matrix part and fracture of concrete occurs through the paste with very few failures occurring through the sand particles (Lloyd, Lott, & Kesler, 1968). Murdock (1965) has prepared a comprehensive and critical review of research conducted in the area of concrete fatigue. He noted that the fatigue of concrete can be studied from two points of views: fundamental (micromechanical) and empirical one (e.g. S-N curves).

The first use of fracture mechanics with mortar and concrete was made by Kaplan (1961).

Glucklich (1965) extended fracture mechanics to mortar under repeated loading. Cyclic loading on stones and brick masonry was conducted by Oliveira et al. (2006). Recently a lot of models have been proposed based on theory of elasticity e.g. (Ahmad & Shah, 1982), plasticity e.g. (Chen & Chen, 1975), Abu-Lebdeh & Voyiadjis (1993) and Voyiadjis & Abu-Lebdeh (1994), damage theory e.g. (Lemaitre, 1985), Mazaras (1984), elastic-plastic-damage models e.g. Lubliner et al., (1989), Maekawa et al. (2003). Numerical modelling was conducted by e.g. (Lowes, 1993).

*Fracture mechanics for concrete*

Some of the experimental investigations on fatigue crack propagation in concrete have been already carried out e.g. (Bazant & Oh, 1983). Bazant & Xu (1991) confirmed that Paris law can be applied in concrete. The behaviour of concrete under strain control cyclic loading was studied by Bahn & Hsu (1998). Resende & Martin (1987), Yazdani & Schreyer (1988), Mu & Shah (2005) stated that it is possible to predict the fatigue life of the airport concrete pavement by conducting the fatigue test over just a few cycles. Although the basic concepts of fracture mechanics appear rational in nature, the application of the method to a concrete requires many approximations. This approach makes application of results difficult (Lloyd, Lott, & Kesler, 1968).

*Description of concrete in standards*

The description for concrete fatigue is given in *Eurocode 2-2 – Design of concrete structures*. A detailed description of concrete fatigue is also given in e.g. ACI – American Concrete Institute (2005), VBB1995 – Dutch Code – Concrete bridges, etc.

The Eurocode 2 suggests checking the resistance of concrete for both for concrete and for steel and the calculation shall be based on the assumption of cracked cross sections neglecting the tensile strength of concrete but satisfying compatibility of strains. The Eurocode 2 suggests using techniques applied in steel fatigue to fatigue in concrete.

The loading factor is usually 1.0. This implies that calculations on fatigue have to be completed on serviceability limit state. Material factors are different for different codes, and they range from 1.2 for VBB 1995 (Dutch Code) to 1.5 EC2/2 (Euro Code 2).

The Miner's hypothesis, which is very useful in metals fatigue, is probably valid with some limitations for concrete materials. Hilsdorf & Kesler (1966) showed, however, that the Miner's assumption of linear accumulation of fatigue damage in concrete is false. It was already investigated that concrete does not possess endurance limit, and even small cyclic loadings shorten its fatigue life (ACI Committee 215R, 2005). This is probably due to lack of strain hardening in concrete (Gylltoft, 1983).

*Parameters influencing fatigue life of concrete*

A large number of parameters are known to influence fatigue behaviour of concrete. These

include:

- Concrete properties (cement content, water-to-cement ratio etc.),
- Curing conditions,
- Specimen size,
- Aggregate type and quality,
- Moisture condition, e.g. Gylltoft & Elfgren (1977), Galloway et al. (1979),
- Age of concrete,
- Environmental effects, e.g. humidity: Van Leeuwen & Siemens (1979) and Waagaard (1981), temperature etc.,
- Stress range, e.g. Hilsdorf & Kesler (1966),
- Rate of loading,
- Creep effect, e.g. Slutter & Ekberg (1958),
- Rest effect between cycles, e.g. Lloyd et al. (1968), Murdock (1965),
- Load frequency, e.g. Awad 1971, Spark 1973, Awad 1974, Hordijk (1991),
- Load history,
- Stress reversal,
- Confining pressure,
- Etc.